

Searching for the Pliocene: Southern Exposures

Robert E. Reynolds, editor



California State University Desert Studies Center
The 2012 Desert Research Symposium

April 2012

Table of contents

Searching for the Pliocene: Field trip guide to the southern exposures

| | |
|--|-----|
| Field trip day 1 | 5 |
| <i>Robert E. Reynolds, editor</i> | |
| Field trip day 2 | 19 |
| <i>George T. Jefferson, David Lynch, L. K. Murray, and R. E. Reynolds</i> | |
| Basin thickness variations at the junction of the Eastern California Shear Zone and the San Bernardino Mountains, California: how thick could the Pliocene section be? | 31 |
| <i>Victoria Langenheim, Tammy L. Surko, Phillip A. Armstrong, Jonathan C. Matti</i> | |
| The morphology and anatomy of a Miocene long-runout landslide, Old Dad Mountain, California: implications for rock avalanche mechanics | 38 |
| <i>Kim M. Bishop</i> | |
| The discovery of the California Blue Mine | 44 |
| <i>Rick Kennedy</i> | |
| Geomorphic evolution of the Morongo Valley, California | 45 |
| <i>Frank Jordan, Jr.</i> | |
| New records of fish from northern exposures of the Imperial Formation of Riverside County, California .. | 53 |
| <i>Mark A. Roeder</i> | |
| Shell rubble beds of the mollusk <i>Thylacodes</i> (Gastropoda: Vermetidae) in the upper Miocene Imperial Formation near Whitewater, Riverside County, California, previously called the “worm tube bed.” | 65 |
| <i>Patrick I. LaFollette</i> | |
| The desert fan palm: a recent invader in the American Southwest | 69 |
| <i>James W. Cornett</i> | |
| San Andreas fault geomorphology and slip rate in the Indio Hills, Riverside County, California | 72 |
| <i>David K. Lynch</i> | |
| The Pliocene fossil record of Anza-Borrego Desert State Park, western Salton Trough, California | 77 |
| <i>G.T. Jefferson, L.K. Murray, and S.D. Keeley</i> | |
| Earliest delivery of sediment from the Colorado River to the Salton Trough at 5.3 Ma: evidence from Split Mountain Gorge | 88 |
| <i>Rebecca Dorsey</i> | |
| Before the big chill—a quick look at global climate in the Pliocene, Earth’s last sustained warm period ... | 94 |
| <i>Richard (Tony) VanCuren</i> | |
| Searching for a pupfish migration route—back to the Pliocene? | 99 |
| <i>Jeffrey Knott</i> | |
| Thermal tolerances for the desert pupfish (<i>Cyprinodon macularius</i>): a case for rapid evolution | 101 |
| <i>Allan A. Schoenherr</i> | |
| The dazed and confused identity of Agassiz’s land tortoise, <i>Gopherus agassizii</i> (Testudines, Testudinidae), the new desert tortoise, <i>Gopherus morafkai</i>, and consequences for conservation | 103 |
| <i>R.W. Murphy, K.H. Berry, T. Edwards, A.E. Leviton, A. Lathrop, and J.D. Riedle</i> | |

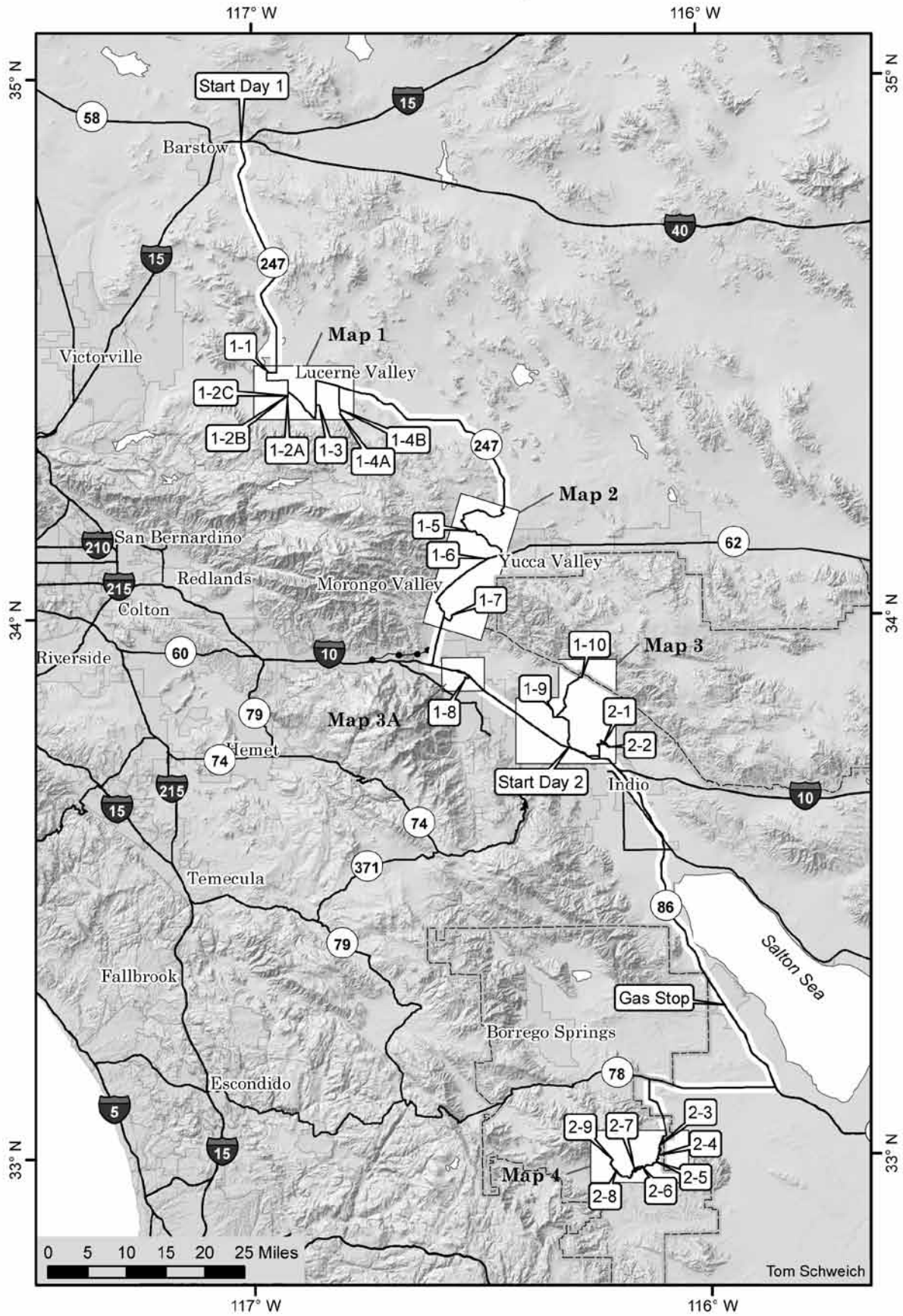
| | |
|---|------------|
| What do we know about the effects of climate change, especially global warming, on desert tortoises? | 105 |
| <i>Jeff Lovich</i> | |
| Desert reptiles and climate change: winners and losers in a warming world | 108 |
| <i>Cameron W. Barrows</i> | |
| Age, stratigraphy, depositional environment and vertebrate ichnology of the Pliocene Copper Canyon Formation, Death Valley, California | 114 |
| <i>Torrey Nyborg, Paul Buccheim, and Kevin E. Nick</i> | |
| Review of proboscideans from the Middle Miocene Barstow Formation of California | 125 |
| <i>Don L. Lofgren, Abby Hess, Drew Silver, and Peter Liskanich</i> | |
| A near-complete skull of <i>Castor canadensis</i> from the badlands of El Golfo de Santa Clara, Sonora, Mexico | 135 |
| <i>Carrie M. Howard and Christopher A. Shaw</i> | |
| Ichnites in the Bouse Formation, Amboy, San Bernardino County, California | 136 |
| <i>Robert E. Reynolds</i> | |
| Was it washed in? New evidence for the genesis of Pleistocene fossil vertebrate remains in the Mojave Desert of southern California | 140 |
| <i>J. D. Stewart, Michael Williams, Marjorie Hakel, and Scott Musick</i> | |
| Quaternary offset of the Cady fault, eastern California shear zone, southern California | 144 |
| <i>K. M. Schmidt and V. E. Langenheim</i> | |
| Reynoldsite, a new mineral from the Blue Bell claims, California and the Red Lead mine, Tasmania | 151 |
| <i>Anthony R. Kampf, Stuart J. Mills, Robert M. Housley, Ralph S. Bottrill, and Uwe Kolitsch</i> | |
| Early Neogene cat tracks from California and Utah | 153 |
| <i>Robert E. Reynolds and Andrew R. C. Milner</i> | |
| Fumaroles exposed by the dropping Salton Sea level | 160 |
| <i>David K. Lynch, Kenneth W. Hudnut, and Paul M. Adams</i> | |
| The Oro Copia Mine, Orocopia Mountains, Riverside County, California | 169 |
| <i>Larry Vredenburg</i> | |
| Sites I would like to see: moonshine still sites in the California Desert | 172 |
| <i>Frederick W. Lange</i> | |
| Abstracts of proceedings—The 2012 Desert Studies Symposium | 178 |
| <i>Robert E. Reynolds, compiler</i> | |

Front cover: Willis Palms

Back cover: Mission Creek fan

Title page: Curtis Palms

Index Map



Searching for the Pliocene: field trip guide to the southern exposures

Day 1

Robert E. Reynolds

Redlands, California, rreynolds220@verizon.net

INTRODUCTION—Recognition that glacial cycles occupied the last ~1 Ma of the Pliocene has led to a redefinition of the beginning of the Pleistocene Epoch, changing the beginning of the Pleistocene from 1.8 Ma to 2.6 Ma. The Pliocene is now defined as between 5.3 and 2.6 Ma (Finney, 2011). Even though shortened, the Pliocene was eventful, and these events can be seen in the southern deserts. Global climatic events, such as gradual cooling and drying and the start of polar ice caps, and altered ocean currents from the closing of the Isthmus of Panama, are overprinted by regional events, such as the rise of the Transverse Ranges and the resulting rain shadow that created the Mojave Desert climate. This period saw the inception of the Eastern California Shear Zone and development of strike-slip faults that cut across most of the Mojave Desert. Many of the Mojave Desert's coarse gravel deposits have been assigned to the Pliocene. We will visit sediments that herald and record Pliocene tectonism and pluvial events.

Early on Day 1, we will visit the Old Woman Sandstone, dated by fossil mammals to the late Pliocene. These rocks provides early Pleistocene constraints on the rise of the San Bernardino Mountains. Lucerne Valley also contains the Blackhawk landslide, perhaps triggered by the Helendale fault and/or glacial cycles. Stops on both days will feature outcrops where we can compare textures of landslides, fanglomerates, and conglomerates.

Late on Day 1 we will visit faults that are responsible for the topography of the modern eastern San Bernardino Mountains. The Miocene precursor of the San Andreas fault system may have assisted in the opening of the Gulf of California, allowing the incursion of the Miocene–Pliocene marine Imperial Formation.

Convene at the Desert Studies Center in Zzyzx; proceed north toward I-15.

Enter I-15 westbound.

Continue past Afton Road.

Pass under Minneola Road and through the California Agricultural Inspection Station.

Continue past Ghost Town Road (gas available).

Continue past the exit for Old Hwy 58.

Continue past the East Main Street exit.

EXIT I-15 at Barstow Road. The Mojave River Valley Museum is two blocks north.

0.0 (0.0) Stop at signal. Re-set odometer. TURN LEFT (south) onto Barstow Road (Highway 247).

3.5 (3.5) Reach the summit (entrance to a landfill) of the Lenwood Anticline on western Daggett Ridge and enter Stoddard Valley. Gravels exposed in the road cuts are probably Pliocene in age. They underlie fine-grained deposits that farther to the northwest contain an early Pleistocene ash bed (Cox et al, 2002).

4.5 (1.0) Cross the Lenwood Fault at the north base of Daggett Ridge, a ridge developed by compression along a left bend in the Lenwood Fault.

4.9 (0.4) Continue past a right turn (west) to Stoddard Road

5.9 (1.0) Continue past a left turn leading to the Peach Spring Tuff (18.8 Ma; Miller et al, 2010) and the early Miocene Barstow Formation of Daggett Ridge. We will next encounter middle Miocene sediments at Pioneertown. Proceed south on Highway 247.

9.1 (3.2) Pass the Slash-X Café.

10.1 (1.0) Continue past a left turn to Stoddard Wash and Meridian gates.

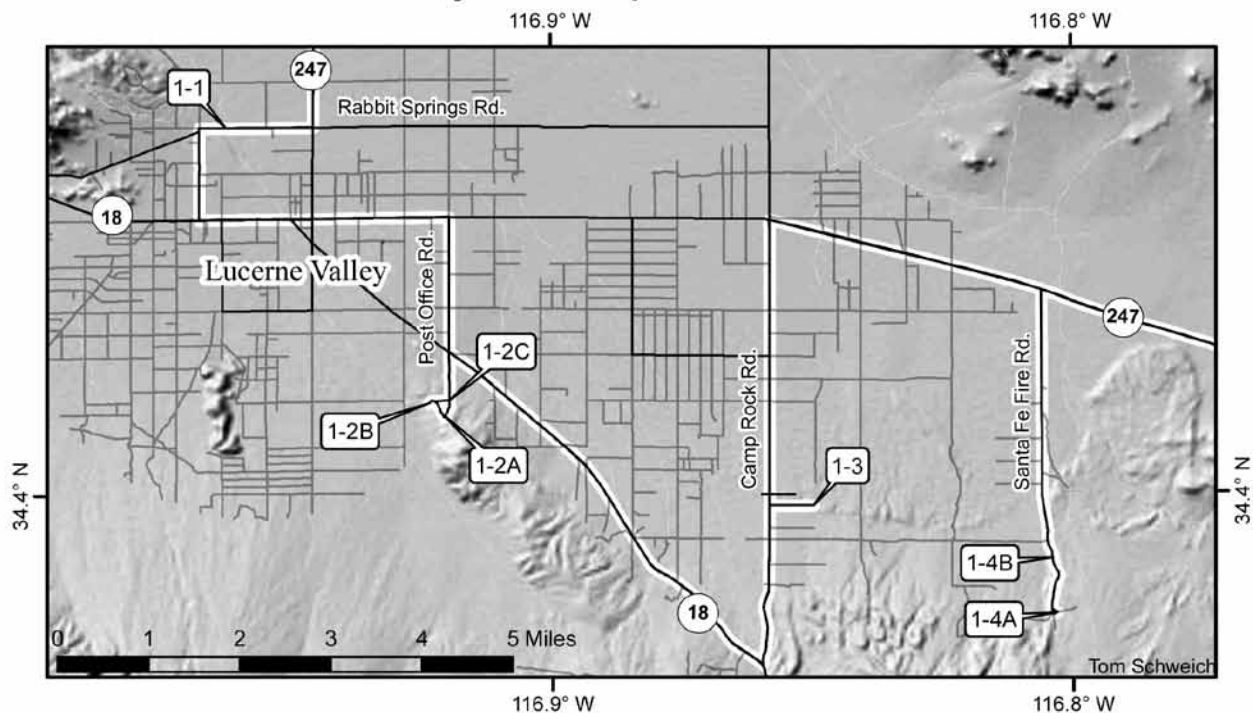
13.0 (2.9) View (2:00) of a ridge with granitic boulders that remain from exhumation of the pre-Miocene erosional surface (Oberlander, 1972).

17.2 (4.2) Cross the summit of Barstow Road at Goat Mountain Pass (el. 4148'), the junction of Stoddard Ridge (Jurassic Sidewinder volcanics), and the West Ord Mountains (Jurassic-Cretaceous granitic rocks). We are leaving the Mojave River drainage system and entering the internally drained Lucerne Valley basin. Highway 247 bears southwest. Drive downhill between Jurassic/ Cretaceous quartz monzonite outcrops.

Sidewinder Mountain (2:00) is supported by metamorphosed Jurassic volcanic rocks.

21.3 (4.1) Barstow Road bears southeast.

Day 1, Stops 1 to 4B



26.1 (4.8) Slow for a complex junction at Peterman Hill; proceed south on Highway 247.

26.9 (0.8) Continue past Northside Road. We are at the northern margin of the Pleistocene/Holocene playa of Lucerne Lake. Extensive Pleistocene lacustrine sediments are mapped on its southeastern margin (Bortugno and Spittler, 1986). The Lucerne drainage basin covers more than 250 square miles between the Helendale fault (west) and the Lenwood fault (east).

31.4 (4.5) Gobar Road. Slow; prepare for right turn.

31.8 (0.4) TURN RIGHT (west) at Rabbit Springs Road.

32.8 (1.0) **STOP 1-1: HELENDALE FAULT SCARP AT RABBIT SPRINGS.** Notice silts and groundwater discharge along the Helendale fault scarp. The Pleistocene age of the spring discharge is reinforced by the presence of a fossil horse femur (*Equus* sp. lg.). Plastic, non-brittle deformation of soils along the scarp are described (Bryan, 2004).

The Helendale fault, a dextral fault in the Eastern California Shear Zone, separates shallower basement (approximately 300 m depth) east of the fault beneath Lucerne Valley from deeper basement (approximately 550 m or more) west of the fault. The thickest part of the basin fill is generally located near the San Bernardino Mountains and the basin shallows northward (Langenheim, et al, 2012).

We are at the approximate midpoint of the Helendale fault as it strikes southeast to its terminus near Baldwin Lake in the San Bernardino Mountains. The fault passes the source of the Blackhawk landslide and an earthquake on

the fault has been suggested as the cause of mountain-side collapse (Shreve, 1968, 1987). The right-lateral strike-slip characteristics of the Helendale fault and the development of Lucerne Valley as a thrust-loaded depressed lowland have been presented (Aksoy et al, 1986).

33.1 (0.3) Stop at Kendall. TURN LEFT (south). The north frontal fault scarp can be seen at the heads of alluvial fans along the north base of the San Bernardino Mountains (Langenheim, et al, 2012).

34.1 (1.0) Stop at Highway 18. TURN LEFT (east). This is a daytime headlight highway. There is an opportunity to fill gas tanks ahead.

35.1 (1.0) Proceed through the five-point intersection of Hwys 18 and 247.

35.3 (0.2) Stop at Barstow Road (Hwy 247). Proceed east.

35.6 (0.3) Continue past Allen Way; prepare to turn right into Community Center.

35.7 (0.1) TURN RIGHT into Pioneer Park Community Center. Carpool if necessary.

36.3 (0.6) Pass Meridian Road. We are due north of the monument set at the Base Line and Meridian station by Henry Washington on Mount San Bernardino, December, 1852 (Laurie, 1967).

Prepare for a right turn in one-half mile.

36.8 (0.5) TURN RIGHT (south) on Post Office Road.

37.3 (0.5) View southwest (2:00) of the North Frontal fault (Langenheim, et al, 2012). Tan Old Woman Sandstone (OWS=Tertiary Lacustrine Sediments [Tl] of Powell and Matti, 2000) in the foreground is uplifted along the Helendale fault.

37.8 (0.5) Cross Foothill Road.

38.3 (0.5) Stop at Hwy 18, watch for cross traffic, and proceed south on Post Office Road.

38.8 (0.5) At this complex intersection, a graded road enters from the right (west) and three roads lie ahead to south. Proceed south on the central fork that ascends the ridge.

39.0 (0.2) PARK at overview.

STOP 1-2A: OLD WOMAN SANDSTONE. View northwest of gravel pit exposing OWS and Quaternary alluvium. To the southeast is granitic basement exposing an exhumed pre-Miocene erosional surface. The OWS has three facies: at the first stops we will examine western facies outcrops of silty arkosic sandstone with brown to gray paleosols containing pedogenic carbonate. Chocolate colored playa silts are present in central facies outcrops two miles east southeast.

The OWS was deposited in a southward-deepening? depocenter similar to the depocenter containing the Phelan Peak Formation (Weldon, 1985), the latter at the northeast edge of the San Gabriel Mountains. The Phelan Peak Formation (4.2–1.5 Ma) was deposited at a time overlapping that of the 3.0–2.5 Ma OWS along the north flank of the San Bernardino Mountains. The OWS was deposited from Pitzer Buttes (western facies; this locality) east to Old Woman Springs (eastern facies). As compression along the San Andreas fault caused the eastern Transverse Ranges (San Gabriel and San Bernardino mountains) to rise, packages of sediments developed along the north margin. These typically include, from lowest and oldest:

- A. Arkosic sandstone shed southwesterly from sources northeasterly on the Mojave Block. Pulses of deposition were intermittent, allowing paleosols and pedogenic carbonate to form.
- B. Fluvial and playal sediments suggesting that southwest drainage systems were being blocked.
- C. Coarse sands and conglomerates being shed northward over the playa facies. The playa facies moved northward as the Transverse Ranges increased in height and continued the northward shedding of coarse debris. Many of these north-vergent sheets of conglomerate



The central facies of the Old Woman Sandstone is capped by caliche-cemented Paleozoic limestone clasts shed northward from the rising San Bernardino Mountains.

contain high percentages of carbonate rock, and have been re-cemented by carbonate-rich ground water to form resistant layers on the north slope of the mountains. Mountain uplift caused anticlinal folds to form along east-west axes in the layers of debris (Stop 1-3).

Three facies of the Old Woman Sandstone (OWS) have been described (Sadler, 1982). The western facies (here) contains non-vesicular basalt clasts and light and dark colored Sidewinder series metamorphosed Jurassic volcanics at its base. The basalt clasts are derived from the east or east southeast (see mp. 67.6), while the metavolcanic clasts are derived from the north (Sidewinder, Ord, Rodman mountains). There are no clasts present from sources in the San Bernardino Mountains. The vertebrate fossils (rabbits, rodents and horses) indicate an age of late Pliocene for the western facies of the OWS (3.0–2.5 Ma; May and Repenning, 1982).

The central facies (southeast), the type section of the OWS (Richmond, 1960; Shreve, 1968; Dibblee, 1964, 1967), contains basalt clasts at its base derived from easterly sources and clasts from a terrane containing sources of monzonite, migmatite, and gneiss. Vertebrate fossils (rabbits, gophers and woodrats), along with magnetostratigraphic correlations, indicate an age of late Pliocene (3.0–2.0 Ma; May and Repenning, 1982).

The eastern facies of the OWS crops out south of Old Woman Springs. This fine-grained facies overlies Miocene basalts and contains sparse basalt cobbles near its top. All of the facies, western, central and eastern, interfinger with and are overlain by sandstone carrying distinctive clasts of Paleozoic limestone from sources in the San Bernardino Mountains. The overlying clast suite also includes well-rounded cobbles of quartzite from the Oro Grande

area that have been shed southward during the middle Miocene and recycled northward as the San Bernardino Mountains rose.

The clast suite here and in other facies of the OWS is characteristic of the Mojave Desert, and therefore, the deposit predates development of the thrust-faulted north flank of the San Bernardino Mountains (Reynolds and Kooser, 1986). The massive mountains south of us, reaching elevations over 11,000 feet, apparently rose in less than 2 million years. In the San Timoteo Formation at El Casco, clasts from the San Bernardino Mountains appear in the section about 1.5 Ma (Albright, 1999). In Cajon Pass, the Older Alluvium is the coarsest deposit, indicating the steepest and highest time of uplift. The base of the Old Alluvium contains the Brunhes/Matuyama reversal at 780,000 years (Weldon, 1985). The San Bernardino Mountains may have gained their maximum height only half a million years ago!

Drive northwest down the ridge to a graded road.

39.1 (0.1) TURN LEFT (west) on the graded road.

39.2 (0.1) **STOP 1-2B: WESTERN FACIES OF OLD WOMAN SANDSTONE.** PARK in a cleared area and examine the gray paleosol with diffuse to nodular pedogenic carbonate. Walk north to see exposures of tan arkose with brown paleosols. This is the western facies of the OWS. Fossil mammals (May and Repenning, 1982) provide an age range of 3.0–2.5 Ma (late Pliocene). This means that mountain uplift did not start until the earliest Pleistocene. Red-brown paleosols with slump fractures filled with caliche are Holocene in age.

The Magnetic Polarity Time Scale (MPTS) for the Gauss–Matuyama MPTS intervals between 3.5 and 2.0 Ma contain six reversal events (Berggren, W. A., et al, 1995; Hehn, V. N., et al, 1996), suggesting that further studies of magneto- and biostratigraphy would greatly help to refine the lithostratigraphic record present in the western and central facies of the OWS.



Western facies of the Old Woman Sandstone at Stop 1-2B.

DRIVE EAST to a complex intersection.

39.5 (0.3) **STOP 1-2C: LOWER OLD WOMAN SANDSTONE.** Park at a complex intersection and walk south along the wash road to a cut exposing the base of the section in the OWS western facies. Look for metavolcanic and basalt clasts that have a source north and east in the Mojave Desert. Quartzite clasts from Oro Grande were deposited on the range top in the Miocene–Pliocene Crowder Formation, and have been recycled northward into overlying Pleistocene sediments (Sadler and Reeder, 1983).

Return to complex intersection and retrace to Hwy 18.

40.0 (0.5) Stop at Hwy 18. TURN RIGHT (southeast) toward Cushenbury Grade. We are driving parallel to the trace of the Helendale fault (Rabbit Spring–Box S fault of Vaughn, 1922). The Mitsubishi Cement Corporation's Cushenbury Quarry is ahead to the south. The raw material from the quarry is Mississippian Bird Springs limestone of late Paleozoic age. The Bird Springs has an older, gray "lower grade" unit with high concentrations of iron, alumina and silica. The younger, white, "high grade" marbles have very low levels of iron, silica, and alumina.

Mitsubishi Cement's Cushenbury Quarry provides calcium carbonate raw materials for the Cushenbury Cement Plant, a dry process plant originally constructed in 1957. The most recent renovation was completed in 1982 with the construction of a pre-heater / pre-calciner kiln rated at 5,000 tons per day. Ancillary resources imported to the plant to produce cement include: iron, alumina, silica and gypsum. Primary energy resource is coal; the plant also burns waste tires as a fuel additive. —Austin Marshall

40.9 (0.9) Continue past Aliento Avenue.

41.2 (0.3) Continue past Midway Avenue.

42.0 (0.8) The low hills to the right are Old Woman Sandstone.

42.8 (0.8) Continue past Richard Road.

44.7 (1.9) Prepare for a left turn.

44.8 (2.1) TURN LEFT (north) on Camp Rock Road. For the next .75 mile, the ridge on the right is composed of very old Pleistocene fan deposits (Qvof; Powell and Matti, 2000) with advanced soils. Camp Rock Road is not shown on 1921 maps (Thompson, 1929). Today, it runs north through the Ord Mountain mining district through Daggett and to Camp Rock in the Calico Mountains, from which it apparently received its name (Schoffstall, 2010).

In 1930, Gilbert H. Tegelberg, Sr. homesteaded on the west 1/2 section 26, T. 4N, R.1E, SBBM, in Lucerne Valley. A wagon road ran the full mile length of the property. The road ran north from what is now Highway 247 and Highway 18. He did not want his property split, and with the help of other homesteaders, cleared the brush for five miles by hand. He drove the first track on it with his 1925 Chevy. He named it Terry Road in honor of the first homesteader in the area, and the first school bus driver in the valley. During World War II the county changed the name to Camp Rock Road.

In August 1932 there was a cloudburst above Camp Rock Road, which cut a six foot deep ditch. County Supervisor Arthur L. Doran answered "it will be taken care of immediately." The horse drawn grader at the Pioneer Park Community Center Museum is the one used to fill up the ditch and grade the road. Signed Gilbert H. Tegelberg, Jr.. Dated 8/26/94

45.7 (0.9) Continue past Cheshire Road.

46.2 (0.5) Continue past Bauer Road.

46.6 (0.4) TURN RIGHT on an unnamed road 0.1 miles before (south of) Rosewood Street.

47.1 (0.5). **STOP 1-3: ANTICLINE.** Park on top of the hill to look eastward along an anticlinal fold developed as a pressure ridge during the early Pleistocene thrusting that uplifted the northern margin of the San Bernardino Mountains. In the immediate foreground, the Conglomerate of Cushenbury Springs (QTs: clasts of gray limestone, white marble, brown and white quartzite, coarse, non-vesicular basalt) overlies OWS, the latter exposed through a window of erosion. White caliche indicates that the surface developed a Pleistocene soil horizon. This anticline extends two miles east toward the Blackhawk landslide (Qols; Powell and Matti, 2000). RETRACE to Camp Rock Road.

47.7 (0.6) Stop; TURN RIGHT (north) onto paved Camp Rock Road.

47.8 (0.1) Continue past Rosewood Street.

48.9 (1.1) Continue past Arroyo Road.

49.3 (0.4) Continue past Sutter Road.

49.8 (0.5) Continue past Foothill Road.

50.8 (1.0) Stop at Hwy 127/Old Woman Springs Road. TURN RIGHT (east).

52.9 (2.1) Continue past Donaldson Road.

53.8 (0.9) Prepare to turn right on Santa Fe Fire Road.

53.9 (0.1) TURN RIGHT on Santa Fe Fire Road.

54.1 (0.2) Pass Foothill Road. The northern toe of the Blackhawk landslide can be seen to the east southeast.

55.1 (1.0) Continue past a graded road to the right.

55.6 (0.5) SLOW for dip. Pass an abandoned homestead on the right.

56.1 (0.5) Look to the west to a light colored low hill that marks the trace of the east-trending anticline axis (from Stop 1-3) composed of caliche-cemented sandstone carrying Paleozoic limestone clasts. At its east end, anticline development apparently involved middle Pleistocene and early Late Pleistocene sediments (Qmof and Qoc: Powell and Matti, 2000). The central facies of the Old Woman Sandstone is located two miles west. The Blackhawk landslide is on the immediate east side of road.

56.4 (0.3) DIP— SLOW! Santa Fe Fire Road (Route 3205) encounters the west flank of the Blackhawk landslide.

56.7 (0.3) BEAR LEFT (east) on Route 3205 at the junction. PARK and walk south to low hill.

STOP 1-4A: WEST FLANK BLACKHAWK LANDSLIDE. We are near the middle of the Blackhawk landslide, debris from which extends 3 miles north and 1.6 miles south (total 4.6 miles). The deposit at this point is 1.3 miles wide, but reaches a width of 1.9 miles farther north. The Blackhawk landslide sits more than seven miles from its northern tip, near Hwy 247, to its source farther south up Blackhawk Canyon, on the east side of the Helendale fault (Stout, 1982).

The Blackhawk landslide consists of thoroughly brecciated Paleozoic limestone, sandstone, and granite. Legend states that miners following silver veins in the limestone dug downward until they found sand and crushed desert bushes. Rock avalanche breccia is derived chiefly from metamorphosed Paleozoic carbonate strata and subordinately from Pliocene conglomeratic sandstone and granitic rocks. The underlying range front thrust fault separating the limestone from the sandstone has been displaced and disrupted as part of the landslide mass.

Cemented carbonate breccia is overlain in swales on the landslide surface by an Av horizon of loess-like, vesicular calcareous silt as thick as 6 cm. The Blackhawk landslide event is dated to greater than 17,400 ybp, based on ¹⁴C dates on gastropod shells in a playa on top of the landslide (Stout, 1982). This period of the late Pleistocene is near the Wisconsin Glacial Maximum (18,000 ybp). It is possible that increased moisture, weight of snow pack, and activity on the Helendale fault in the source area triggered this massive slope failure. The degree of cementation of the surface of the landslide may indicate a much older age, and the presence of incised colluvial aprons on the flanks of the landslide indicates that the age of the slide predates

Old Quaternary deposits (Qoc2 and Qoc1; Powell and Matti, 2000).

The Pleistocene Blackhawk landslide covers parts of the older Silver Reef rock avalanche mass farther east (Woodford and Harris, 1928; Shreve, 1958, 1968, 1987). The Silver Reef landslide was emplaced earlier in the Pleistocene. The Blackhawk landslide is a classic example of a sturzstrom—a landslide type characterized by having great horizontal movement when compared to its initial vertical drop. In many cases the horizontal displacement is 20 times greater than the vertical distance. Sturzstroms are similar to glaciers, mudslides, and lava flows in that they flow across land with low apparent friction. It has been noted that their mobility increases with increasing volume (Shaller and Shaller, 1996). The kinetic energy in a sturzstrom is much higher than in a typical landslide. Once moving, it can ride over nearly any terrain. Its momentum can even carry it up small hills (Hsu, 1975). Sturzstrom deposits have been recognized on Mars, Venus, Io, Callisto, and Phobos. One leading model that explains the mechanics of movement involves “acoustic fluidization.” In this model, vibrations caused by the sound of the slide reduce the overall friction present in the slide and allow it to travel much greater distances (Collins, n.d.). Another theory involves air pockets forming under the slide and providing a cushion that the slide rides over to generate its long run out distances (Shreve 1958, 1968, 1987), although the merit of this theory has been called into question by the presence of sturzstroms on solar system bodies such as on the moon and Phobos, which lack atmospheres.

Not to be confused with sturzstroms or landslides, the slopes to the east are composed of north-dipping sheets of well cemented early Pleistocene fan deposits with clasts of gray metamorphosed limestone set in well cemented sandy matrix. Debris flow deposits are massive and unsorted with angular pebble- to cobble-sized clasts. (Powell and Matti, 2000).

If interested, passengers can walk north through gullies to examine landslide debris and rejoin vehicles 0.2 miles north.

Return to vehicles; RETRACE toward Highway 247.

Retrace toward HWY 127

57.3 (0.6) **STOP 1-4B: BLACKHAWK LANDSLIDE.** A road cut exposes the internal structure of the Blackhawk landslide. PARK far right and examine the south cut with pink Paleozoic limestone breccia and a VW-size clast of arkosic sandstone. The north cut shows angular light and dark gray Paleozoic limestone covered by a drape of rounded limestone clasts from Holocene alluvium. Proceed north.

57.4 (0.1) Dip—use caution.

58.4 (1.0) Continue past a homestead on the left. Slow for dip.

60.0 (1.6) Continue past the intersection with Foothill Road.

60.2 (0.2) Stop at paved Hwy 247 (Old Woman Springs Road). Watch for cross traffic. TURN RIGHT (east) onto Hwy 247.

61.2 (1.0) Continue past Santa Fe Road. Gravel piles mark cuts that expose the north toe of the Blackhawk landslide.

62.9 (1.7) The view south shows the Silver Reef landslide on the east side of the Blackhawk landslide.

66.3 (3.4) Pass through a road cut in Older Pleistocene Alluvium in the scarp of Old Woman Springs fault.

66.8 (0.5) Continue past Bessemer Mine Road (the road to Johnson Valley OHV recreational area). This road crosses the Lenwood, Johnson Valley, and Emerson faults. Activity on the latter two during the 1991 Landers quake produced major vertical and right-lateral offsets (Reynolds, 1992).

67.6 (0.8) Old Woman Springs is on the right. In 1917, it was a cattle camp owned by A. R. Swarthout, and water flowed at 125 gallons/minute from a tunnel in basalt to a 160 ft³ reservoir, and then to 9 acres of alfalfa (Thompson, 1929). Black basalt dated at 6.0 Ma (two unpub K-Ar dates, Jan Morton, written commun. to D. M. Miller, 2012) underlies a small outcrop of eastern facies of the “Old Woman Sandstone” (not visible). The Old Woman Springs fault scarp (inactive during Landers quake; Reynolds, 1992) is exposed for five miles and to the southeast merges with the North Frontal Thrust system (Langenheim, this vol., Fig. 1) beyond which it cuts the crystalline rocks of the San Bernardino Mountains.

70.9 (3.3) Continue past Lafton Road. East (left) of Hwy 247, a low hill marks the trace of the Lenwood fault, inactive during the Landers 1991 earthquake (Reynolds, 1992).

71.6 (0.7) View south (3:00) of the Old Woman Springs fault cutting older alluvial fans of the San Bernardino Mountains.

74.6 (3.0) Continue past Big Horn Road.

76.2 (1.6) Continue past Valle Vista Road.

76.9 (0.7) Continue past Rock Corral Road.

82.3 (5.4) Continue past Bodick Road. To the east, on Kickapoo Road between Bodick and Linn Roads, ruptures on the Kickapoo fault and farther east on the Homestead Valley fault demolished houses during the 7.6 Mw 1991 Landers earthquake (Reynolds, 1992).

85.3 (3.0) Continue past Linn Road.

86.9 (1.6) Continue past New Dixie Mine Road. Ruby Mountain to the right (west) may be one of the vents for local basalt flows. It is an alkaline basalt (basanite) intrusion and flow complex of late Miocene age (6-10 Ma) (Neville, 1986). The local termination of alkaline basalt volcanism near the San Bernardino Mountains appears to coincide with estimates of the beginning of transpressional tectonics for the region (Sadler and Reeder, 1983). Basalt from this source can be recognized by entrained megacrysts formed in the mantle of the chromediopside group, including kaersutite (Wilshire and Shervais, 1975).

87.6 (0.7) Continue past Reche Road. This was the epicenter of the June 28, 1991 Landers 7.6 Mw earthquake. Hills to the east are made up of metamorphosed sedimentary rocks (pre Cretaceous gneiss) and crossed by Cretaceous pegmatites that have recently produced topaz, gem quality aquamarine beryl, and unusual metallic oxides (Kennedy, 2012).

87.9 (0.3) Drop into wash.

89.2 (1.3) Continue past Hondo Road.

89.6 (0.4) Enter Flamingo Heights/

92.5 (2.9) Drop downhill into Pipes Canyon and prepare to turn right.

92.8 (0.3) TURN RIGHT onto Pipes Canyon Road.

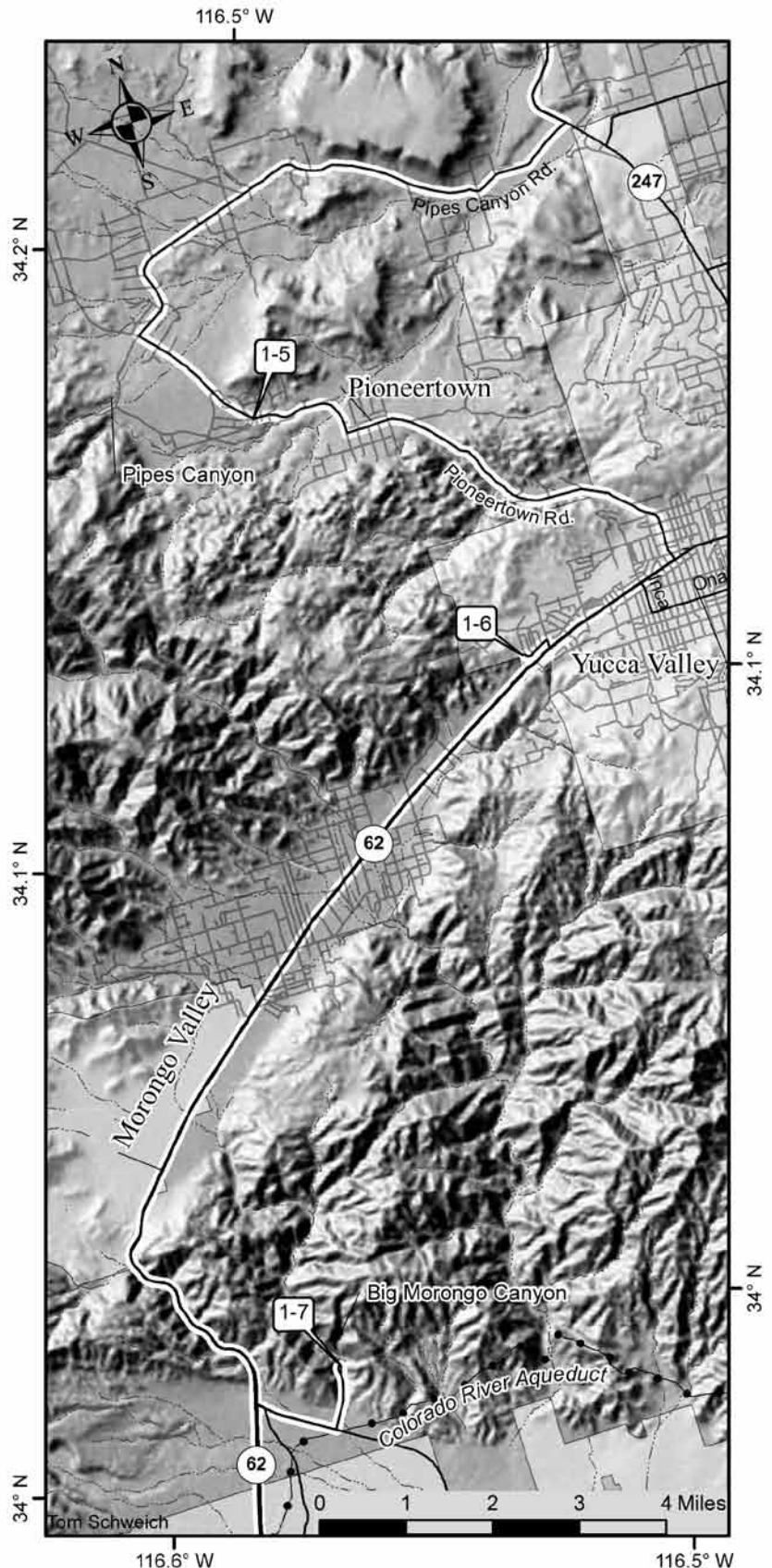
94.1 (1.3) Coarse Quaternary stream cobbles exposed in the south bank of Pipes Wash (right) overlie tan Pioneer-town sandstone. Pipes Wash and Chapar-rosa Wash join here. They drain easterly, then northerly along the Homestead Valley fault, to empty into Emerson Lake basin.

94.7 (0.6) The dark varnish on the basalt scree at 2:00 on the slopes of Flat Top Mountain suggests that this debris may have been stable since Pleistocene times.

95.1 (0.4) About eight individual flow units make up the stacked basalt to the left at 1:00.

96.0 (0.9) To the left at 9:00, note the crude columnar jointing in basalts

Day 1, Stops 5 to 7



overlying a middle Tertiary erosional surface that developed on granitic rocks.

98.7 (2.7) Cross Pipes Wash. Water rises to the surface as a result of shallow granitic bedrock between the volcanic tablelands.

98.9 (0.2) Black Hill, to the southeast, is a mesa of stacked Pioneertown basalt flows.

99.5 (0.6) Stop at Pioneer Town Road. TURN LEFT and proceed south. The basalts flowed easterly over a gently undulating surface and are thickest to the southeast.

101.0 (1.5) Prepare to pull right

101.1 (0.1) **STOP 1-5: OVERVIEW OF PIONEER TOWN SEDIMENTS AND BASALT FLOWS.** PARK at Keys Road (junction with Yucca Trail). Ahead and to the right are the dark Pioneertown basalts and white patches of Tertiary sediments. The Pioneertown basalts cover an area of approximately 22 km² and may reach a thickness of 60 m. The pile is made up of individual flow units three to seven m thick, each capped by a terminal vesiculated or amygdoloidal top. Eight or nine individual flow units have been observed in the thickest portion of the pile. These basalts are alkali olivine in composition (Neville, 1983); potassium/argon dates for similar flows range from 6.9 to 9.3 Ma (Morton, p.c. 1985, cited in Reynolds and Kooser, 1986; Peterson, 1976; Oberlander, 1972). The basalts overlie and are interbedded with Tertiary arkose deposits and overlie granitic basement. In some places, Tertiary soil horizons on Cretaceous granitic rocks are preserved beneath the flows (Oberlander, 1972). The basalts are correlative, in terms of age and petrogenesis, with other alkaline volcanics found in the Mojave Desert, such as Cima Dome, Amboy Crater, Dish Hill, and Pisgah Crater (Neville, 1983; Neville et al, 1985).

Tertiary sediments are rare in the eastern San Bernardino Mountains. This section has been referred to as Old Woman Sandstone by Dibblee (1967b), but the difference in clast lithologies and the age of the overlying basalts indicate that their age and source differ significantly from the Old Woman Sandstone. Similarly, lithology and stratigraphy distinguish this arkose from the Santa Ana Sandstone. Fragmentary vertebrate fossils of antelope and proboscideans suggest a mid-Miocene Clarendonian North American Land Mammal Age (12–10 Ma) for the lower silty sediments, time-correlative with the middle portion of the Crowder Formation in Cajon Pass (Reynolds et al, 2008).

Easterly, in cuts for building pads, you can see, from lowest: (1) brown silty sands with paleosols representing low energy deposition; (2) arkosic sands representing higher energy deposition; (3) vertical faults offsetting the sedimentary section downward to the east; (4) a possible erosional surface and soil which may have formed prior to basalt flows; and (5) 6.9–9.3 Ma basalts laid down on



Parry's beargrass (*Nolina parryi* S. Watson). Photo courtesy Stan Shebs.

undulating topography and with interfingering arkose (Sadler, 1982; Morton, p.c. 1985). The apparent flow direction was roughly northeast to east, and the basalt flows are thickest to the southeast.

The Pioneertown area sits at a biologic crossroad between the Transverse Ranges and the Mojave Desert at an elevation of 4,300 feet. Desert wash plant communities and Joshua tree woodlands give way to piñons and junipers of higher elevations. Here the California juniper (*Juniperus californica* Carrière) takes the place of the Utah juniper (*J. osteosperma* (Torr.) Little) of the eastern Mojave. While much of this area burned in the 2006 Sawtooth Complex fire, we should be able to see a few of the showy Parry's beargrass (*Nolina parryi* S. Watson). An apparent case of convergent evolution, the beargrasses have many visible traits similar to the yuccas and agaves. Therefore, for many years they were placed in the Agave family. As knowledge of the genetic relationships among plants rapidly advanced, it became apparent that they were quite different genetically from the yuccas and agaves. Consequently, the beargrasses were placed in a succession of several other families until, at least for now in California, we place them in the Butchers-Broom Family (Ruscaceae) (Tom Schweich).

PROCEED EAST on Pioneertown Road.

102.2 (1.1) Cross Chaparrosa Wash.

102.4 (0.2) Slow, TURN LEFT (east) into Pioneertown. Pioneertown was built as a set for western movies. It was named by Dick Curtis, an actor, on Labor Day 1947 (Gudde, 1974).

103.3 (0.9) TURN RIGHT (south) at the east end of Pioneertown toward a rocky granitic ridge known as Sawtooths. During the early Tertiary, granitic basement rocks were deeply weathered along joint sets (Oberlander, 1972). Recent erosion has exposed this boulder terrain in the Sawtooths.

104.6 (1.3) Enter Water Canyon, developed along the trace of the Water Canyon fault. The fluvial sediments exposed below the terrace on the right are undisturbed by faulting.

105.5 (1.9) Sunnyslope Road. Cross the most northern suspected trace of the Pinto Mountain fault as mapped by Dibblee (1967a). The left lateral Pinto Mountain fault is the southern margin of the Mojave Desert geomorphic province. The Mojave Desert to the north is characterized mostly by northwest-striking right lateral faults. The Little San Bernardino Mountains to the south make up the eastern portion of the Transverse Range geomorphic province. During the 1991 Landers earthquake, ruptures on the Kickapoo fault crossed the Pinto Mountain fault into the Transverse Range Province.

106.0 (0.5) Stop sign at Yucca Trail. Proceed. We have just crossed the suspected southern trace of the Pinto Mountain fault (Dibblee, 1967b).

106.1 (0.1) Traffic signal at Hwy 62 in Joshua Tree. TURN RIGHT (west) toward Yucca Valley and Morongo Valley.

106.8 (0.7) Traffic signal at Kickapoo Trail.

107.3 (0.5) Traffic signal at Camino del Cielo.

107.6 (0.3) Pass Piñon Street. A trip south on Piñon and west on Navajo would lead to steeply dipping arkosic sediments with paleosols, similar in appearance to the Pioneertown section. These are unconformably overlain by shallow-dipping quartzite fanglomerate with a possible source in the San Bernardino Mountains. The unconformably overlying fanglomerate has a high percentage of basalt clasts containing the ultramafic mantle xenolith kaersutite, with a possible source at Ruby Mountain (Grimes, 1986). This sequence suggests that left lateral strike-slip movement along the Pinto Mountain fault may have separated sections of the Pioneertown sequence, modifying topography to allow development of drainage systems to the south. This would be a reversal from the east-draining systems of the late Miocene through Quaternary.

107.8 (0.2) TURN RIGHT on Fairway Drive.

107.9 (0.1) TURN LEFT (west) immediately on Rockaway Avenue and bear right (north) through a turn.

108.3 (0.4) **STOP 1-6: MORONGO VALLEY (GRIMES MEMORIAL STOP)**. Gerald James Grimes (1947–2011) was an engineering geologist and a founding member of the Inland Geological Society. His 1987 M.S. thesis was “Geology at the Convergence of the Pinto Mountain fault and Morongo Valley fault, southern California.”

PARK and walk west uphill to a water tank. View west shows Morongo Valley graben bounded on the north by the Pinto Mountain fault and on the south by the Morongo Valley fault. The Pinto Mountain fault trends westerly and cannot be mapped west of the north branch of the San Andreas fault. The Morongo Valley fault is crossed by antecedent streams that form Little Morongo Canyon and Big Morongo Canyon (Jordan, 2012).

The mapped trace of the Morongo Valley fault is 1,000 feet (300 meters) south, along the toe of the northwest-facing slope of the Little San Bernardino. Two mapped traces of the main Pinto Mountain fault are about 2,000 feet (600 meters) northwest of the stop, running along the toe of the southeast-facing slope of the Big San Bernardino's. A branch of the Pinto Mountain fault is located 1,250 feet (380 meters) east of the tank, crossing through the housing tract, near the intersection of Rockaway Avenue and Whitney Avenue. This splay of the Pinto Mountain fault and the Morongo Valley fault are included within Alquist–Priolo Zones, but the main traces of the Pinto Mountain fault north of the site are *not* included within an A–P Zone.

Review of digital aerial photography (Google Earth, Bing 3D, World Wind) suggests that additional splays of the Pinto Mountain fault bracket both the north and south sides of the water tank. An additional branch of the Morongo Valley fault is also identifiable running along the northwest side of Highway 62. Several northwest-trending lineaments suggest that branches of northwest-striking faulting traverse the canyon just west of the water tank, as well as just east of Rockaway Avenue. These northwest-striking faults appear to be part of the larger Helendale–Pipes Canyon fault zone. A branch of the Mission Creek fault offsets gneiss, truncating the southwest end of the valley. The Morongo Valley fault actually continues along a northwest-facing scarp. A southeast-dipping branch of the Morongo Valley fault is expected to accommodate normal movement along most of the northwest edge of the valley. Both branches of the Morongo Valley fault cross the block of gneiss out to the Mission Creek fault. The Pinto Mtn. fault continues west of Yucca Valley intersecting the Mill Creek fault (Jordan, this vol.; Figs. 1-8).

In addition to the faulting, large, deep-seated landslides bracket both sides of the valley, forming the flanks of both the Little and Big San Bernardino Mountains. The four major drainages within the valley enigmatically cross the valley floor perpendicular to its long axis, rather than flowing along its long axis to the topographical low

point at the southern end of the valley. These four drainages are antecedent to formation of the valley. Landslides within these drainages, northwest of the valley, provide the source materials for the debris flows that make up the alluvial fans of the valley floor. Flow within these drainages has been sufficient to incise the surrounding mountains and maintain flow paths through the Little San Bernardino Mountains out to Desert Hot Springs. The expected flow rates of these drainages during the Holocene epoch suggest that the slip rate along the Morongo Valley fault is very low. The symmetry of the valley suggests that the slip rates along the southern and northern branches of the Morongo Valley fault zone are similar, probably on the order of 0.5 millimeter per year or less —Frank Jordan

RETRACE to Hwy 62.

108.8 (0.5) STOP at Hwy 62 on Fairway Drive. TURN LEFT (west). Drop into Morongo Valley.

109.7 (0.9) To the north, vegetation lineament, changes of rock color and left -lateral bends in canyons mark the trace of the Pinto Mountain fault as it passes west, beyond our view, to terminate at the North Branch of the San Andreas fault.

112.0 (2.3) Little Morongo Road and flood channel. We are north of the green riparian habitat of little Morongo Canyon.

115.7 (3.7) At least 254 species of birds have been recorded from Big Morongo Canyon Preserve at Covington Park. Several rare or unusual species nest here, and other species are abundant during spring and fall migration seasons. The preserve is internationally recognized for abundance of bird species and has been designated as one of the United States' Important Bird Areas.

116.3 (0.6) Traffic signal at Senilis Road in Morongo.

116.8 (0.5) SR 62 heads south as a steep and winding route.

119.4 (2.6) Cross the trace of the Mission Creek Branch of the San Andreas fault at the base of the San Bernardino Mountains. Mount San Jacinto, ahead, reaches an elevation of 10,787 feet.

119.8 (0.4) TURN LEFT (east) on North Indian Canyon Boulevard toward Desert Hot Springs. The Indio Hills are visible at 1:00.

120.7 (0.9) TURN LEFT (north) before reaching the "Dip" sign. A dirt track crosses a gas line marked by yellow signs and heads northerly into Big Morongo Canyon.

121.1 (0.4) Proceed through cross roads. The west slope contains conglomerate with cabin-size boulders. The east canyon wall is made up of fault-sliced green and gray metamorphic rocks. The scarp of the Mission Creek Branch of the San Andreas fault system forms the southern margin of the Little San Bernardino Mountains. Proceed northeasterly along the wash bottom.

121.5 (0.4) **STOP 1-7: MORONGO REVERSE FAULT.** PARK at the s bend in the canyon before reaching the preserve fence. The Morongo reverse fault thrusts gneissic basement rocks over Tertiary conglomerate (Dibblee, 1967a). Proctor (1968) suggested it was an inactive western extension of the Dillon shear zone. Walk 1000 feet south and examine large boulders of gneiss supported by the conglomerate. RETRACE south to North Indian Canyon Boulevard.

121.9 (0.4) Exit the canyon at trace of Mission Creek Branch of the Coachella Valley Segment (CVS of SAF, Matti and Morton, 1993) of the San Andreas fault.

122.2 (0.3) Stop at the pavement. TURN RIGHT onto North Indian Canyon Boulevard. Dissected Pleistocene deposits of the Mission Creek fan lie ahead.

123.2 (1.0) Stop at the traffic signal. TURN LEFT (south) onto Hwy 62.

123.9 (0.7) Cross Mission Creek.

124.6 (0.7) Mission Creek Road. The underground Colorado River Aqueduct is marked by a tall gravel berm that crosses from east to west.

126.3 (1.7) Continue past Pierson Blvd.

127.3 (1.0) Low hills ahead and to the southeast mark the scarp of the Banning Branch of the Coachella Valley Segment of the San Andreas fault (Banning Branch).



Dissected Pleistocene deposits of Mission Creek fan (see MP 122.2)

During the last 125,000 years, stresses on the Mission Creek CVS of SAF (Mission Creek) has been transferred to the Banning Branch (Matti and Morton, 1993) producing a through-going structure. The Banning Branch appears to have a Holocene slip rate of 25 mm/yr (Hardin and Matti, 1989), and to have generated 3 km of right slip in the last 125,000 years (Matti et al, 1983; Matti and Morton, 1993). The two branches join as a single structure to the southeast in the vicinity of Curtis Palms (Stop 2-1).

127.9 (0.6) Pass the scarp of the Banning Branch at 10:00.

128.7 (0.8) Continue past Dillon Road to the east. Prepare to enter I-10.

129.3 (0.6) Stay in the right lane to enter Interstate 10 east, toward Indio.

129.9 (0.6) ENTER I-10 eastbound.

132.9 (3.0) EXIT I-10 at Indian Canyon Drive.

133.3 (0.4) Stop sign. TURN LEFT (east) on Garnet Ave.

133.5 (0.2) Stop at the intersection of North Indian Drive and Garnet Ave. Proceed straight east on Garnet Avenue between I-10 (north) and Garnet Hill (south).

134.4 (0.9) Garnet Avenue divides and becomes dirt— stay right.

134.7 (0.3) Dip! Continue on lower frontage road.

135.2 (0.5) Cross a wash and prepare to turn right (south).

135.3 (0.1) TURN RIGHT (south) and proceed across a wash.

135.5 (0.2) Stay right past a left turn. The preferred road swings westerly around the southeast tip of Garnet Hill.

135.7 (0.2) Road forks ahead, BEAR LEFT. Proceed across pole line road.

135.9 (0.2) Proceed northwest at the reverse junction.

136.0 (0.1) STOP 1-8: IMPERIAL FORMATION SECTION AT GARNET HILL. PARK. We are 600 feet above sea level, and the six million year old sediments immediately to the north contain marine mollusks. To the west, Mount San Jacinto rises to 10,787 feet. The topographic relations suggest significant tectonic change in the last six million years.

Outcrops from the “northern” exposures of the Imperial Formation (Cabazon [Lion Canyon, Powell, 1985; 1986; 1988]; White-water [Super Creek, Powell, 1985; 1986; 1988], and Garnet Hill) are considered Miocene in age (Powell, 1986,1988; McDougall et al, 1994; Rymer et al, 1994). Outcrops from the “southern” exposures are considered Pliocene

in age (Mount, 1974; Johnson et al, 1983; Opdyke et al, 1977, Jefferson and Lindsay, 2006) and include those at Ocotillo Wells [=San Felipe Hills (see Powell, 1993)], Superstition Mountain, Fish Creek–Vallecito Wash area, southern Coyote Mountain, Yuha Buttes, and northern Cucupa Mountains, east of Mexicali, Mexico (Ingle, 1974). One major exception to this north-south division are the four Imperial Formation exposures in the Indio Hills: 1) just west of Willis Palms Oasis; 2) near the mouth of Pushawalla Canyon; 3) a mile east of the north end of Washington Street; and 4) in the northwest Indio Hills, where the fauna appears to be Pliocene (Powell, 1986; Powell, et al, 2011).

The section ahead includes brown silty lacustrine sand low in the section that contains a white ash dated between 8.0 and 7.6 Ma (Rymer et al, 1994; Powell, 1995). The lacustrine sands are overlain by the marine Imperial Formation, a gray conglomerate in a light gray silty sandy matrix which contains oysters and other marine fossils. Boulders contain borings from pelecypods. Although the clasts in the Imperial are very large, and the deposit is thick, it probably cannot be considered a sturzstrom. The boulders are from mixed rock types, sub- to well-rounded and matrix supported. In contrast, a sturzstrom such as the Blackhawk landslide has angular, jigsaw-fitting, monolithologic clasts supported by pulverized fines of the same material. When we enter Split Mountain Gorge (Day 2, Stop 2-4) compare this conglomerate to the Elephant Trees Conglomerate and nearby sturzstrom. Walk north to a northwest-trending gully. Walk east to a north-trending gully.

A. Evidence for the lacustrine environment of deposition is based on the presence of groups of nonmarine microfossils. (Rymer et al, 1994, 1995).

B. Miocene molluscan bivalves (oysters, scallops, clams and boring clams), gastropods,



The coarse marine Imperial Formation at Garnet Hill overlies olive-colored lacustrine silts (see Stop 1-8).

barnacles, and echinoderms serve as evidence for the marine environment of the Imperial Formation. The invertebrates reinforce a shallow subtidal environment with well-rounded rocks that can be seen in outcrop (Powell, 1995).

C. Two low hills to the south are remains of an anticline with a south-trending axis. Garnet Hill to the north is a west-trending anticline. The different orientation of fold axes and the “hummocky weathering” ground between the fold axes marks the trace of the Garnet Hill fault (Rogers, 1965).

D. We are on the south side of the Banning Branch of the SAF which places Miocene Garnet Hill Imperial Formation outcrops in a right-lateral offset relationship to Miocene Imperial Formation outcrops including the Super Creek deposits (northwest). Imperial Formation deposits at Willis Palms (Stop 1-9, east) and Travertine Point are Pliocene in age and represent different facies than the Miocene deposits.

RETRACE along Garnet Avenue to the intersection with North Indian Canyon Drive.

136.7 (0.7) Garnet Avenue (dirt section). Proceed northwest on south side of I-10.

137.5 (0.8) Dirt road turns to pavement.

138.3 (0.8) Intersection. Proceed west on Garnet Avenue.

138.5 (0.2) Stop, TURN RIGHT and enter I-10 east bound toward Indio.

141.4 (2.9) Continue past Palm Drive and Gene Autry Trail.

144.7 (3.3) Continue past Date Palm Drive.



Mollusk borings in marble from Garnet Hill (Stop 1-8).

148.1 (3.4) Continue past the exit for Bob Hope and Ramon Road. Services available.

149.7 (1.6) Continue past Monterey Avenue.

152.1 (2.4) Continue past Cook Street.

155.7 (3.6) EXIT at Washington Street. Stay in the left lane for a turn.

155.9 (0.2) Stop at Washington Street and TURN LEFT (north) over I-10.

156.0 (0.1) Traffic signal at Varner; proceed north.

156.1 (0.1) Traffic signal at Market Place; proceed north.

156.5 (0.4) Traffic signal at Dell Webb Blvd south.

157.4 (0.9) Traffic signal at Dell Webb Blvd north.

158.3 (0.9) Washington bends left (northwest).

159.3 (1.0) Washington Street bends west.

159.9 (0.6) Continue past Thousand Palms Canyon Road. Washington Street is now called Ramon Road.

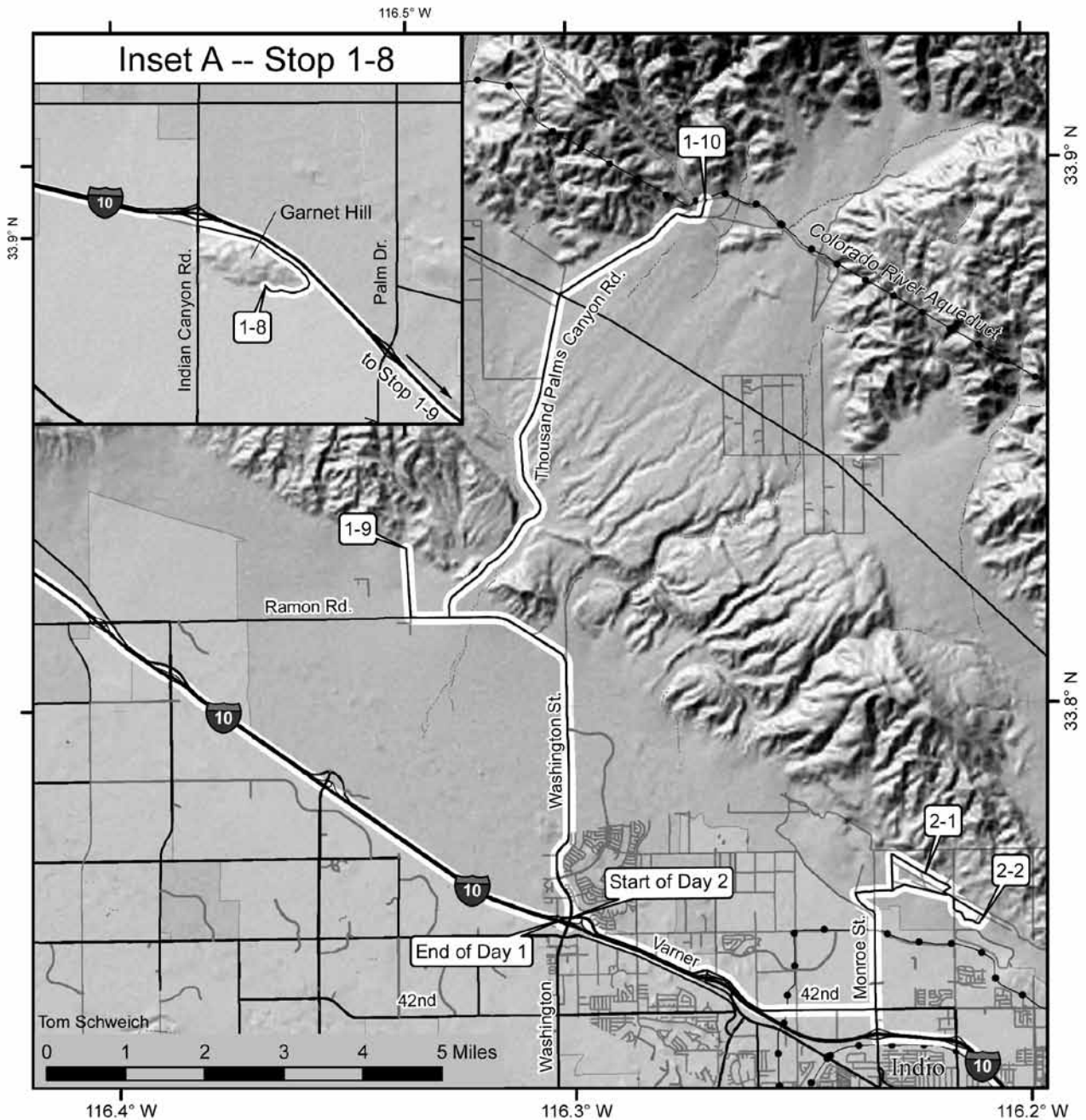
160.4 (0.5) TURN RIGHT on Baxley Road before you reach the geodesic dome.

161.3 (0.9) **STOP 1-9: WILLIS PALMS OUTCROP OF THE IMPERIAL FORMATION.** Walk 900 feet east to the easternmost outcrop of tan, silty Imperial Formation. Dense accumulations of oysters (*Dendostrea vespertina*) suggest a Pliocene marine environment, although the valves are disarticulated, and may have been concentrated in this bed from an original source nearby. *D. vespertina* is one of the most common taxa from the Yuha and Camels Head members of the Deguynos Formation, and suggests correlation between Willis Palms and the Fish Creek exposures (4.49 to 4.25 Ma). This locality differs from Garnet Hill, in that fossils are Pliocene, there are no apparent underlying lacustrine sediments, and that the fossiliferous silty sand, does not contain coarse clasts. This exposure is between the Banning Branch (south) and Mission Creek Branch (north) of the SAF.



Fossil oysters (*Dendostrea vespertina*) from the Imperial Formation at Willis Palms. See Stop 1-9.

Day 1, Stops 8 to 10, Day 2, Stops 1 and 2



Fringe-Toed Lizard Preserve at Willis Palms, just west of 1000 Palms Canyon Road. Fringe-toed lizards are sand specialists that live in windblown sand dunes and sand ramps. The lizard gets its name from elongated scales (fringes) on their hind toes. These fringes allow them to move rapidly across the sand surfaces. There are also fringes on the external ear and backward orientated nasal openings to prevent sand from entering these structures. The shape of the head allows the lizard to dive into the sand and “sand swim” below the sand surface, “disappearing” from potential predators. Predators include snakes, shrikes, and whip-tailed lizards. Fringe-toed lizards are active during the warmer months

(March–October). Reproduction occurs April through May with eggs laid in the sand. No parental care is known. The species is omnivorous, eating small insects and some plant material. Their ranges are associated with creosote bush.

The Coachella Valley Fringe toed lizard (*Uma inornata*) is found in the sand dunes within the Coachella Valley. The lizards was listed as threaten by the federal government and endangered by the State of California in 1980. The U.S. Fish and Wildlife Service set aside about 12,000 acres of critical habitat. The 3,709 acres Coachella Valley National Wildlife Refuge was established in 1985 to

protect the lizard and other species. The Coachella Valley Preserve is 16,405 acres of fringe-toed lizard windblown sand habitat adjacent to the refuge and is managed by Nature Conservancy, Bureau of Land Management, California Department of Parks and Recreation, California Department of Fish and Game, U.S. Fish and Wildlife Service, and the Center for National Land Management.

The Coachella Preserve is located about 10 miles east of Palm Springs. It is also the home of Thousand Palm Oasis. A portion of the Preserve is located just west of Thousand Palms Canyon Road at Willis Palms. (See also: Barrows, C. W. 1997.) (—William Presch)

RETRACE to Ramon Road.

162.2 (0.8) Stop at Ramon Road. TURN LEFT (east).

162.7 (0.5) TURN LEFT (north) on Thousand Palms Canyon Road.

163.1 (0.4) We cross the scarp of Banning Branch of the SAF as we enter the Indio Hills. The Indio Hills are a pressure ridge between the Mission Creek and Banning branches of the San Andreas fault. The ridge is about 20 miles long and up to 4 miles wide, trending west-northwest. The loosely consolidated Miocene–Pliocene–Pleistocene deposits consist of sandstone, conglomerate, shale, siltstone with minor limestone, efflorescent evaporite minerals, and sedimentary breccia. The hills are surrounded by fans of Pliocene to Holocene alluvium with terrace, lake, and marine deposits, with many clasts of gneiss and diorite from sources in the Little San Bernardino Mountains to the north and east. Subsurface water flows south to the Salton Sea.

164.2 (1.1) Drop into a wash. Cross the scarp of Mission Creek Branch. Cottonwood trees and dark green vegetation extends east across wash along the trace of the fault.

164.8 (0.6) Proceed past the entrance to Thousand Palms oasis.

167.4 (2.6) Stop at Dillon Road. Watch for cross traffic. Proceed across Dillon Road and travel northeast on Thousand Palms Canyon Road toward Fan Hill.

169.4 (2.0) Proceed across Fan Canyon Wash.

169.8 (0.4) **STOP 1-10: COLORADO RIVER AQUEDUCT.** Construction of the aqueduct near Thousand Palms began in 1933 and was completed in 1935. Tunnels and pipes carry Colorado River water 110 miles to this point and then an additional 70 miles westerly to Lake Mathews (Los Angeles Department of Water and Power, n.d.)

The Colorado River has a Pleistocene and Holocene record of filling lakes in the Salton Trough (Li, 2003). Before the aqueduct was built, the Colorado River flooded annually, and in 1905, it breached a farmer-cut irrigation canal. The water flowed into the Imperial Valley for 2 years and

created the 35-mile long, 9 to 12-mile wide Salton Sea. The Boulder Canyon Project Act of 1929 provided for building dams and hydroelectric plants along the Colorado River. Over a period of 50 years, 18 major dams and diversions were built to provide each state in the watershed with its share. As a preventative measure to drought, Diamond Valley Lake near Hemet was built in the 1990s and holds enough water for 8.4 million people. Retrace to Dillon Road.

171.6 (0.8) Dillon Road. Stop, then proceed south on 1000 Palms Canyon Road to Thousand Palms Preserve and Ramon Road. We have crossed the Mission Creek and Banning branches of the SAF.

174.2 (2.6) Entrance to Thousand Palms Preserve. Continue south on Thousand Palms Canyon Road.

174.4 (0.2) Cross the Mission Creek branch of the SAF. Continue south.

175.8 (1.4) Cross the Banning branch of the SAF. Willis Palms is visible one-quarter mile to the west.

176.2 (0.4) Stop at Ramon Road. TURN LEFT (east).

177.4 (1.2) View left (northeast) of Hidden Palms on the Banning Branch of SAF and the distant Horseshoe Palms on the Mission Creek Branch of SAF. At Biskra Palms just west of Curtis Palm and the Granite Construction Co quarry, the two branches of the San Andreas fault join and continue to the southeast.

177.8 (0.4) Ramon Road turns south and is re-named Washington Street.

179.7 (0.9) North Del Web Boulevard is on the left.

180.6 (1.9) Traffic signal at South Del Web Boulevard.

180.9 (0.3) Traffic signal at Market Place Blvd. Prepare to turn left.

181.1 (0.2) **Stop** at Varner Road before reaching Interstate 10.

END OF DAY 1. Services available (gas, food, motels) by travelling south to Indio or west on I-10 to Ramon Road.

Day 2

George T. Jefferson,¹ David Lynch,² L. K. Murray,¹ and R. E. Reynolds³

¹California Department of Parks and Recreation, Colorado Desert District Stout Research Center, Anza-Borrego Desert State Park®, Borrego Springs, CA 92004

²USGS and Thule Scientific

³Redlands, CA, rreynolds220@verizon.net

On Day 2, we will see approximately 3 million years of continuous stratigraphic section starting with early Pliocene Imperial Formation marine deposits in the base of the Deguynos Formation (ca. 5.1 Ma; Figure 1). The entire marine depositional record lasts from about 6.3 to 4.25 Ma. The first evidence of terrestrial input is at ca. 5.3 Ma, within the top of the Latrania Formation, with discussions of clast assemblages from an ancestral Colorado River (Dorsey, 2012; Gastill et al., 1996) and from the ancestral Gila River (Kimbrough et al., 2011).

Our route will traverse the marine prodelta, delta front, and near shore marine delta; respectively the Mud Hills, Yuha, and Camels Head members of the Deguynos Formation (see Jefferson et al., 2012). The latter part of the route covers the transition to terrestrial deltaic deposits of the 4.2 to 2.4 Ma Arroyo Diablo Formation and the lateral equivalent fluvial Olla Formation of the lower Palm Spring Group. The route will visit excellent outcrops where we can compare and contrast textures of landslides, fanglomerates and conglomerates.

0.0 (0.0) Convene north of I-10 at Washington Street and Varner Road in the Stater Brothers parking lot north of the Arco gas station. Proceed east on Varner Road.

0.1 (0.1) Continue past the Washington St. freeway ramp.

0.3 (0.2) Continue past Desert Cities Drive/Newcastle.

0.5 (0.2) Traffic signal at Fifties Way. TURN LEFT, proceed 300 feet, then TURN RIGHT on Avenue 40 and proceed east.

0.9 (0.4) Traffic signal at Adams.

1.9 (1.0) Traffic signal at Jefferson Street.

2.9 (1.0) Traffic signal at Madison Street.

3.4 (0.5) Traffic signal at Sun City Boulevard.

4.4 (1.0) Traffic signal at Jefferson Street.

4.9 (0.5) Stop. TURN LEFT (north) on Monroe Street

5.0 (0.1) Monroe bears left and ascends a berm.

5.4 (0.4) TURN RIGHT (east) on the dirt road before reaching the Granite Construction gate.

Signs indicate “Coachella Valley Mounted Rangers” and “Metate Ranch.”

5.9 (0.5) TURN LEFT (north) at the fence corner and drive to a dirt power line road crossing diagonally. Pass six immense solar panels on the Granite Construction property. The prominent line of palm trees (Curtis Palms) and enhanced vegetation ahead marks the surface trace of the San Andreas Fault (SAF) along the foot of the Indio Hills. This vegetation lineament is the result of subsurface ground water ponding to the surface because it cannot easily cross the fault plane due to clay-like fault gouge.

6.4 (0.5) TURN RIGHT (southeast) on the power line road and drive between power line towers.

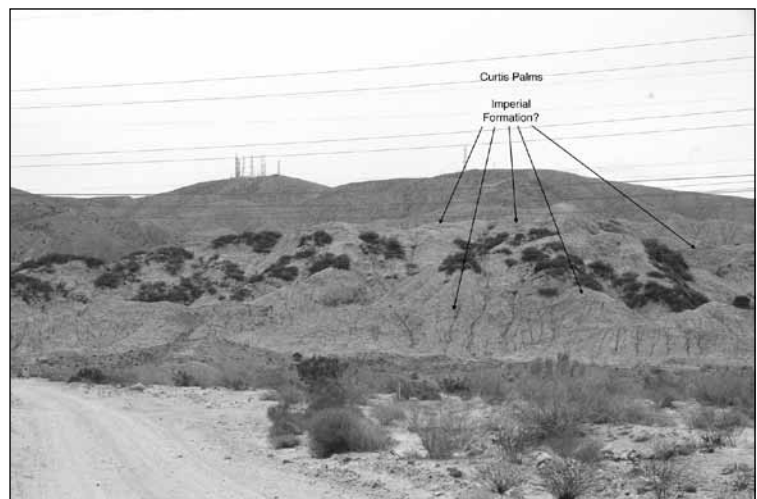
6.9 (0.5) **STOP 2-1: SAN ANDREAS FAULT.** Here are examples of offset channels, shutter ridges, soil color and texture changes, and slope breaks marking the SAF. The prominent lineament of vegetation includes California fan palms (*Washingtonia filifera*; Cornett, 2012). Whitish alkaline evaporite deposits contain thenardite and other minerals. The 1979 Imperial Valley earthquake (Mw = 6.6) on the Imperial fault south of here reactivated the SAF in the Indio Hills and other places further south. Continue easterly on dirt road.

7.2 (0.3) Complex intersection with sign post. TURN SHARP RIGHT (south) past the hill. Cross the SAF where the road jogs right at a faint vegetation line.

7.3 (0.1) TURN LEFT (east) on a prominent dirt road. Take the RIGHT FORK between fenced pump stations.

7.9 (0.6) At a three-point intersection, take the RIGHT FORK (south) and follow the curving dirt road 0.1 miles into a prominent vegetation line.

8.0 (0.1) **STOP 2-2: SAN ANDREAS FAULT VEGETATION.** This line of vegetation has a sharp southern boundary on the SAF. Looking north we see more scrubby vegetation than we do south of the fault, suggesting that ground



Imperial Formation along the San Andreas Fault at Curtis Palms. See MP 5.9

water ponds against the fault. CONTINUE SOUTH 250 ft to a dirt road.

8.1 (0.1) TURN RIGHT (west)

8.2 (0.1) TURN RIGHT (north) and continue 0.16 miles to the on which road we entered.

8.3 (0.1) TURN LEFT (west) on pump station road and cross the SAF. Return (northwest) to the south fence line of the Granite Construction Co.

8.7 (0.4) BEAR LEFT (west) just past the pump station at x intersection toward the Granite Construction Co.

9.3 (0.6) BEAR LEFT at left fork.

9.5 (0.2) Fence corner, proceed west to Monroe St.

9.9 (0.4) Stop at paved Monroe Street. TURN LEFT (south) and proceed south on Monroe St toward I-10.

10.5 (0.6) Cross Avenue 40.

11.5 (1.0) Stop at Avenue 42. Proceed south over I-10.

11.8 (0.3) TURN LEFT onto the eastbound I-10 onramp. The surrounding surface area is approximately at sea level. According to Flanagan (2010):

- The Salton Basin, or Salton Trough, is the largest area of dry land below sea level in the Western Hemisphere, over 2000 square miles.

- The lowest elevation of the sediment floor of the Salton Sea is 277 feet below sea level, five feet higher than the floor of Death Valley at Badwater. This low point is covered by the Salton Sea, the largest lake in California (surface elevation 230 feet below sea level; average size 15 miles by 35 miles with a maximum depth of about 50 feet).

- Birding at the Salton Sea can put you in touch with over 400 documented species.

- The Salton Basin is one of the most seismically active areas in North America. This earthquake activity comes from continual movement along the San Andreas fault system. At the same time, the East Pacific Rise is separating the Californias (Baja Peninsula and portions of California west of the San Andreas fault) from the mainland of Mexico. The San Andreas and the East Pacific Rise are part of the same system, which starts south near the Antarctic and continues to Cape Mendocino in northern California.

- Multiple columns of steam rising across the Imperial Valley Geothermal Area mark 10 generating plants with a combined capacity of 327 megawatts of electricity.

- Over the past 6.3 million years, the Colorado and Gila River systems have transported sediments eroded from the Colorado Plateau, carved from the Grand Canyon and stripped from the southern two-thirds of Arizona, depositing them all into the Salton Trough. The total stack of sediments exceeds 20,000 feet at the deepest point in the basin.

- The badlands of the Anza-Borrego Desert on the western edge of the basin are internationally known for their fossil flora and fauna buried within a continuous record of sediments deposited between 8 and 1 million years ago.

- Imperial County is one of the top 10 agricultural counties in the U. S.

12.7 (0.9) Continue past Jackson Street.

13.9 (1.2) Continue past Golf City Parkway.

14.4 (0.5) STAY RIGHT as I-10 bears easterly toward Blythe

14.6 (0.2) BEAR SOUTH onto State Route (SR) 86S toward Brawley and El Centro.

17.6 (3.0) Traffic signal at 50th Street.

17.9 (0.3) Traffic signal at 52nd Street.

23.9 (6.0) Signal at 62nd Avenue. **OPTIONAL TRIP:** Drive 8.4 miles west to the west end of 62nd Avenue. Climb the berm to view the Martinez Mountain landslide (Baldwin, 1986), which is less than half the surface area of that of the Blackhawk landslide in Lucerne Valley.

24.3 (0.4) Cross over the Union Pacific tracks west of Mecca.

25.9 (1.6) Continue past the junction of 66th Street (Hwy 195) running east to SR 111, Niland, and the Salton Sea Recreational Area.

27.0 (1.1) Cross over the Whitewater River channel that leads south to the river delta. Hwy 86S is 200 below sea level. Since leaving Monroe Street, we have dropped 200 feet in elevation. Since the last maximum elevation of the Salton Sea 300 years ago, the Whitewater River channel has deepened and delta prograded toward the current level of the Salton Sea.

33.4 (6.4) Continue past 81st Street.

34.9 (1.5) Continue past Lincoln Street.

36.2 (1.3) Continue past 85th Street.

36.6 (0.4) Continue past 86th Street. **Travertine Point** is at 1:00. Tufa layers on boulders at Travertine Point record Pleistocene and Holocene maximum lake stands of Lake

Cahuilla dating from $17,590 \pm 280$ ybp to $7,205 \pm 120$ ybp (Turner and Reynolds, 1977; Li, 2003, Jefferson and Lindsay, 2008). The base of the outcrop is 100 feet below AMSL, while the top is 50 above AMSL. Petroglyphs incised in tufa date to 9,000 ybp (Turner and Reynolds, 1977).

Fossils from the marine Imperial Formation occur in an outcrop at the west end of the Travertine Ridge. Forty-four invertebrate taxa, including one coral, 40 mollusks (30 bivalves and 10 gastropods), and three echinoids are reported. The Travertine Point outcrop is midway between Imperial Formation exposures north of Palm Springs and at Fish Creek Wash. The Travertine Point fauna is inferred to have lived in subtropical to tropical waters at littoral to inner sublittoral (<50 m) water depths. Coral and molluscan species from the outcrop indicate a Pliocene age (Powell, 2008).

Recessional shoreline terraces of Pleistocene Lake Cahuilla can be seen on the east-facing slopes for about a mile south of Travertine Point.

34.3 (1.7) Continue past Desert Shores Drive. A Lake Cahuilla shoreline can be seen to the right (west).

36.8 (2.5) Continue past Brawley Avenue at Salton Sea Beach. To the west is Wonderstone Wash and Rainbow Rock, a hot spring sinter deposit that contains gold (Hillemeier et al, 1991, 1992; Van Buskirk and McKibben, 1993).

38.0 (1.2) Continue past Norm Niver Road (gas available).

40.4 (2.4) Continue past Treadwell Boulevard.

42.3 (1.9) Continue past North Marina Boulevard.

44.3 (2.0) STOP at Salton City, the east access to Borrego Springs (SR S22). **Fill vehicles with gas.** No gas will be available for the next 120+ miles. CONTINUE SOUTH on SR 86S.

45.3 (1.0) Continue past Harvard Avenue.

45.8 (0.5) Cross Arroyo Salada.

46.6 (0.8) Road to Salton Sea Airport. We are 135 feet below sea level.

47.3 (0.7) Tule Wash. About a mile west, several springs surface in the wash, probably associated with the San Felipe fault.

48.4 (0.7) We are at sea level. Notice the bluffs consisting of Pleistocene Lake Cahuilla deposits to the west.

54.3 (5.9) TURN RIGHT (west) on SR 78 toward Ocotillo Wells. Ahead, the highway crosses silts from Lake Cahuilla below the 40 foot high shoreline. These silts cover Plio-Pleistocene fluvial sediments of the Borrego and/or Brawley formations.

54.8 (0.5) Note copice dunes held in place by creosote (*Larrea tridentata*) and cat claw acacia (*Acacia greggii*).

58.4 (3.6) Artesian springs at Flowing Wells are three miles north.

60.6 (2.2) Sea level. A break in slope marks the high shoreline of Lake Cahuilla at elevation +40 ft one-half mile ahead on the right (north) side of the road. Look for shoreline terraces and beach bars.

61.4 (0.8) Cross Pole Line Road and under a powerline.

62.4 (1.0) Cross Tarantula Wash.

64.6 (2.2) Continue past the right turn at the paved road to the OHV camping area.

65.1 (0.5) Continue past the Blue Inn Café and then San Felipe Creek.

66.5 (1.4) Continue past Payne Road, with OHV camping left and right. Open camps are available from Payne Road west to County Line Road (0.7 miles).

67.2 (0.7) San Diego County line.

68.7 (1.5) Los Puertecitos historical marker is on the left (south). Named "The Little Pass" by de Anza, his expedition camped here on Monday, December 18, 1775, while en route through Borrego Valley to Coyote Canyon.

70.2 (1.5) Slow; prepare to turn left across oncoming traffic.

70.4 (0.2) TURN LEFT (south) on Split Mountain Road in Ocotillo Wells. Services (gas, markets, motels) are 35 miles northwest in Borrego Springs. PROCEED from Ocotillo Wells on Split Mountain Road to Fish Creek Wash dirt road.

70.9 (0.5) The Split Mountain Store is on the left.

73.0 (2.1) The road bends southeast and becomes Old Kane Springs Road.

74.1 (1.1) BEAR RIGHT (south) on Split Mountain Road.

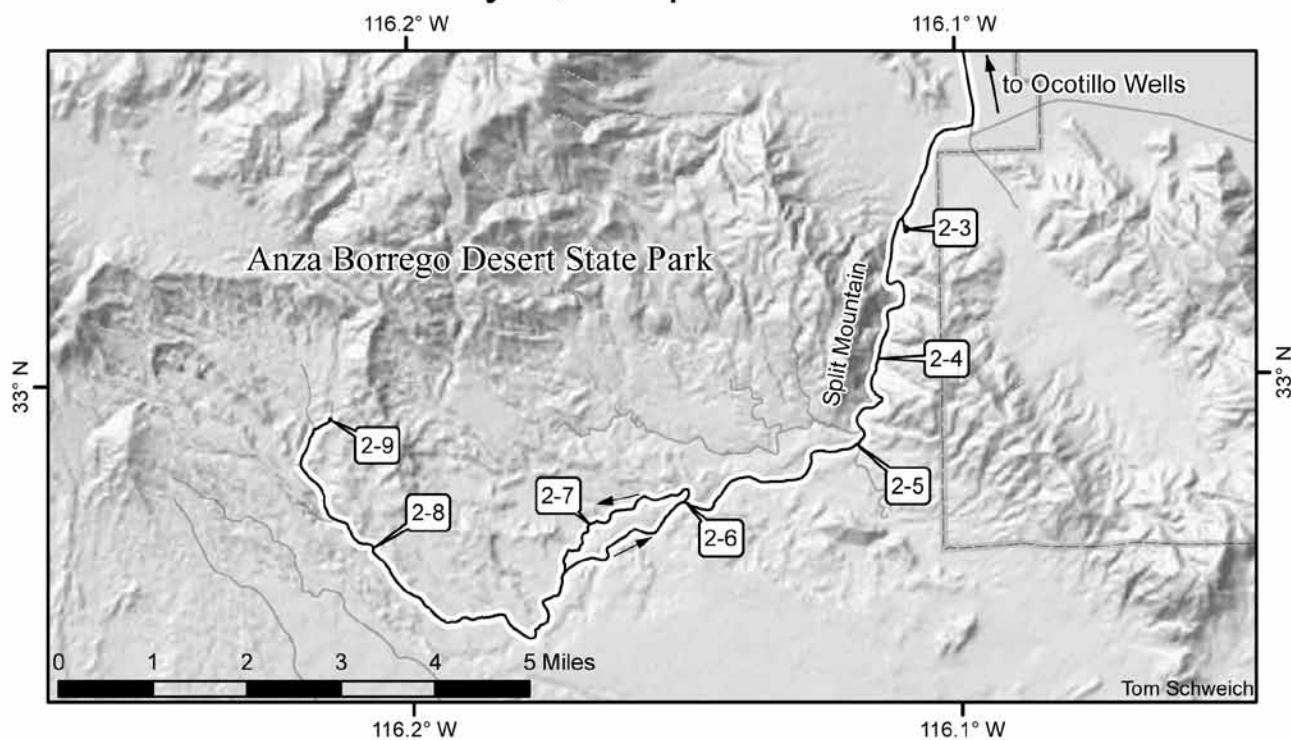
76.0 (1.9) Enter Anza-Borrego Desert State Park (ABDSP).

76.2 (0.2) Continue past a right (west) turn to the Elephant Tree area. Information on this site and other interesting hikes is available at the ABDSP Visitor Center in Borrego Springs.

78.4 (2.2) TURN RIGHT (southwest) onto the Fish Creek Wash dirt road.

Split Mountain Road dead ends at the US Gypsum mine (visible ahead and to the east from the Fish Creek Campground). The hills to the north of Fish Creek Wash road, and west of the south end of the pavement on Split Mountain Road, were mined for celestine during WWII (Durrell, 1953).

Day 2, Stops 3 to 9



The clastic marine late Miocene Latrania Formation and underlying Fish Creek Gypsum compose the base of the Imperial Group (Figure 1). The base of the Fish Creek Gypsum overlies crystalline basement rock east of the mine, interfingers with the top of the Elephant Trees Conglomerate near Fish Creek Campground, is in part separated from the Elephant Trees Conglomerate by a sturzstrom, and is laterally equivalent to the base of the near shore Latrania Formation (Stop 2-4). The approximately 80 m-thick gypsum has been interpreted as a sabkha-like deposit (Dean, 1996) but it essentially lacks calcite, and otherwise has a distinctive metallic trace element and temperature signal of a geothermal vent (Peterson and Jefferson 1997). The gypsum yields marine nanoplankton and other microfossils (Dean, 1996). It is 90% pure, and has been mined since 1920s. The celestine deposit is lens-shaped within the base Latrania Formation. Elsewhere, the base of the Latrania Formation yields a diverse tropical invertebrate fauna with east Atlantic and Caribbean Ocean affinities (Démeré and Rugh 2006).

Vegetation is quite sparse in the Fish Creek and Split Mountain Gorge because of the normally low rainfall in southernmost California exacerbated by a rain shadow cast by the Peninsular Ranges to the west. Plants found here are mostly denizens of the Colorado Desert, and most of them are found in washes, canyons, and rock fractures where the shape of the land concentrates water. Larger shrubs in the washes are likely to be creosote bush (*Larrea tridentata* (DC.) Coville) and palo verde, of which there are two species in the area (*Parkinsonia aculeata* L.

and *P. florida* (Benth. ex A. Gray) S. Watson). Among the more showy plants will be the ocotillo (*Fouquieria splendens* Engelm.) with long, wand-like branches tipped with red flowers. There are a few elephant trees (*Bursera microphylla* A. Gray) in the Fish Creek/Vallecito Creek basin, but their greater concentration is at the “Elephant Tree Area” to the northeast. In the driest areas, and often on desert pavement, small plants with a little rosette of oval leaves and many-branched stems with tiny white flowers are likely one of many species of buckwheat (*Eriogonum* sp.). Dense stands of *Agave deserti* occur in Olla Wash at 1,500 feet elevation along our route. —Tom Schweich

79.8 (1.4) PARK to the right in Fish Creek Campground. Restrooms are available in the campground.

00 (00): STOP 2-3: FISH CREEK CAMPGROUND.

Regroup at the Fish Creek Campground entrance road in Fish Creek Wash at 09:30a, **reset trip odometers to zero**. Proceed up Fish Creek Wash for a 30 mile round trip. Four-wheel-drive and high clearance vehicles are highly recommended. Bring lunches and water. We will return down Fish Creek Wash, so car pooling also is highly recommended. Parking is permitted within one car length of the main dirt road. Please note that collecting specimens of any kind is prohibited within the State Park.

This part of the second day of the Desert Symposium field trip traverses the Pliocene part of the Fish Creek/Vallecito Creek Basin 5 km-thick stratigraphic section. Starting in the late Miocene at 6.3 Ma, these deposits record the

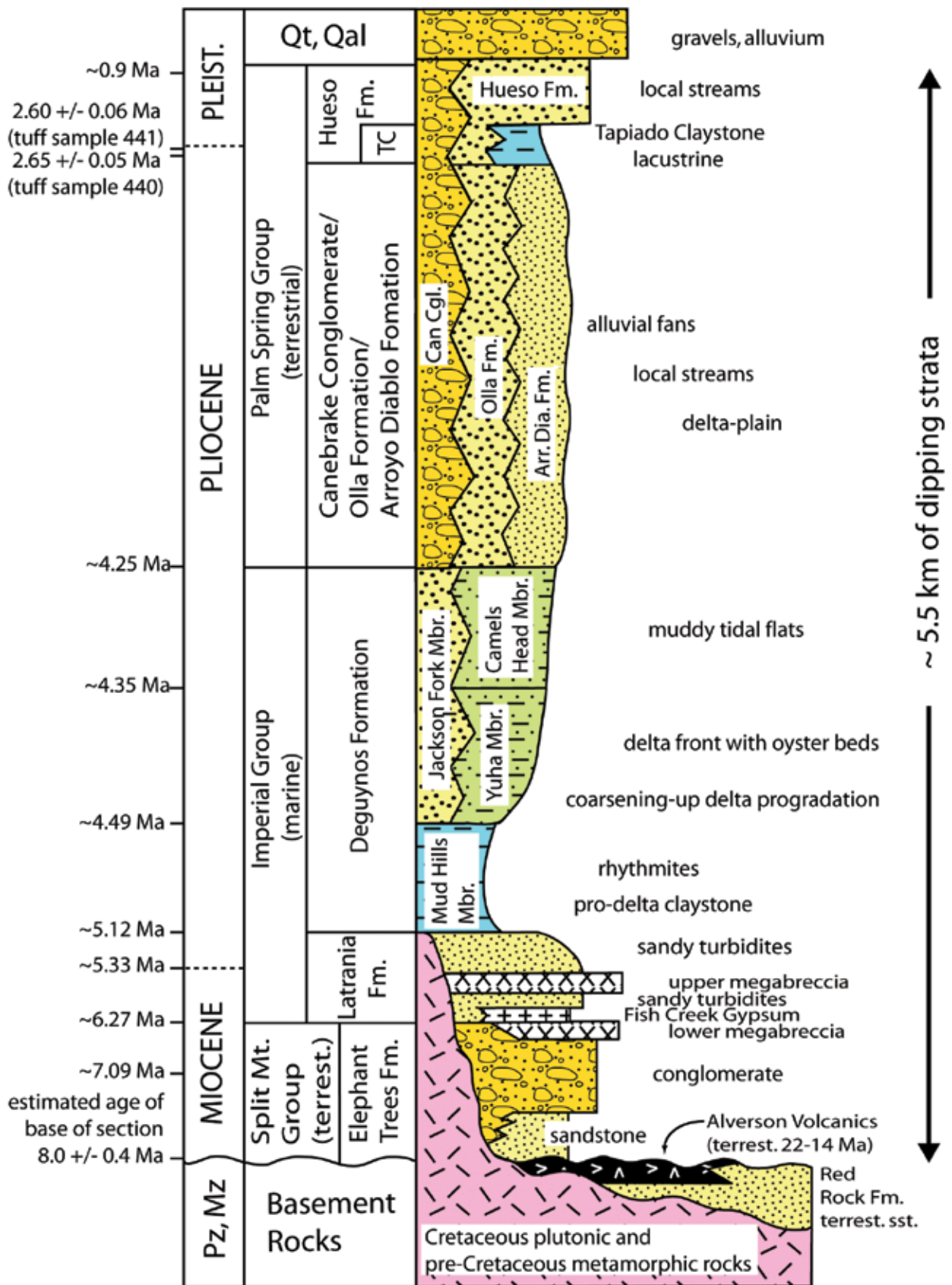


Figure 1. Generalized stratigraphic column for the Vallecito Creek/Fish Creek stratigraphic section (modified from Dorsey, 2006, fig. 5.3; Dorsey et al., 2011, fig. 5).

opening of the Salton Trough, filling by the ancestral Gulf of California, and deposition of the Colorado River delta across the Salton Trough. The stratigraphic units visited in route fall within in the upper part of the Imperial Group and lower part of the Palm Spring Groups (Figure 1). Nomenclature for these deposits is presently under revision (G. Jefferson and C. Powell, pers. comm.). That used herein follows Jefferson and Lindsay (2006), where the lower and upper parts of the Imperial Formation have been designated the Latrania and Deguynos formations respectively and placed within the Imperial, elevated to group rank by Winker and Kidwell (1996). The Palm Spring Group and its subordinate formations are defined by Cassiliano (2002). For an historical summary and correlation of stratigraphic nomina see Remeika (1998) and Lindsay and Jefferson (2006). The stratigraphic section is summarized in Figure 1. Also see Winker and Kidwell (1996) and Dorsey et al. (2006, 2011) for a discussion of the regional geology.

The trip covers over 3 million years of continuous stratigraphic section starting with late Miocene deposits in the base of the Latrania Formation at ca. 6.3 Ma (Figure 1). The entire marine depositional record lasts from about 6.3 to 4.25 Ma. The first evidence of terrestrial input from the ancestral Gila River (Kimbrough et al., 2011) (originally thought to represent the Colorado River; Gastill et al., 1996) is at ca. 5.3 Ma, within the top of the Latrania Formation. The route will traverse the marine prodelta, delta front, and near shore marine delta; respectively the Mud Hills, Yuha, and Camels Head members of the Deguynos Formation (see Jefferson et al., 2012). The latter part of the route covers the transition to terrestrial deltaic deposits of the 4.2 to 2.4 Ma Arroyo Diablo Formation and the lateral equivalent fluvial Olla Formation of the lower Palm Spring Group.

Continue southwest along Fish Creek Wash into Split Mountain Gorge. Note alternating very coarse conglomerates and well-sorted sands of Elephant Trees Conglomerate. Compare the clasts to those that we saw in the Imperial at Garnet Hill (Stop 1–8).

1.2 (1.2) In route at mile 1.2 are excellent exposures of the reddish-brown, poorly sorted matrix and clast-supported boulder Elephant Trees Conglomerate along the west (right) side of Split Mountain Gorge. The Elephant Trees Conglomerate is cut by the antecedent Fish Creek drainage which runs north through the Gorge, following the north-south Split Mountain Fault that is perpendicular to the axis of the Split

Mountain anticline. This erosion exposes the conglomerate, primarily debris flows and fanglomerates, in the core of the fold. The conglomerate is about 8 to 6.5 Ma, and coarsens upward. The largely fluvial sandstone base to this unit was previously correlated with the early Miocene, 22 Ma, “Red Rock” formation that crops out several km to the south. Locally a lower megabreccia or sturzstrom (Abbott 1996) separates the top of this unit from the base of the Latrania at mile 2.9. The sturzstrom crops out along the east (left) side of the canyon. Note the very large, house-sized clasts in this medium-gray, very poorly sorted megabreccia.

1.6 (0.4) The sturzstrom dips from eastern ridge top to canyon floor ahead.

1.9 (0.3) **STOP 2-4: LOWER STURZSTROM AND THE BASE OF THE LATRANIA FORMATION** (Figure 1). PARK on the LEFT side of the road.

The most spectacular of all mass movements occur when... rapidly moving debris flows travel far and kill in great numbers. Specifically, rock falls with volumes in excess of one million cubic meters may flow horizontally up to 25 times farther than their vertical fall and reach speeds up to 280 km/hr, running up and over sizable hills in their paths. For example, tin 1970 in Peru, a 230 meter-high hill was overrun by an earthquake-triggered, high-speed mass burying 18,000 people beneath a 30 meter-thick mass of debris.

Heim described events following the disaster in Elm, Switzerland, September, 1881,



Sturzstrom at Stop 2-4

where a 10 million m³ dry mass dropped 600 m, and flowed 2.2 km, moving at 180 km/hr. Eye witnesses [indicated] a dry mass flowed like a “torrential flood” or “boiling stew.”... The shattered pieces of bedrock lay in a jigsaw-puzzle fabric where broken pieces could mentally be placed back together...

Heim coined a new name—*sturzstrom* [German] from *sturz* = fall & *strom* = stream. These events are flows, not slides (Abbott, 1996; see also Hsu, 1975).

The base of the Latrania Formation of the Imperial Group is exposed on the east (left) side of canyon as Here these locally derived pale-olive, silty sandstones and siltstones lap onto the top of the lower megabreccia (*sturzstrom*) and over the Fish Creek Gypsum. The gypsum is seen pinching out between these units several hundred meters to the southeast. An invertebrate ichnite-rich, near-shore facies of the Latrania is not present in these exposures, but crops out above the Elephant Trees Conglomerate about 1 km to the northwest along strike from the Fish Creek Campground.

2.0 (0.1) For the next 0.3 miles along Fish Creek Wash (both sides of canyon) are exposures of turbidites in the middle and upper Latrania Formation. These relatively deep water marine turbidites are moderately sorted, medium-grained, pale brown sandstones and siltstones that are locally derived and devoid of Colorado or Gila River transported clastic materials. They have been variously called the Lycium and/or Wind Caves members of the Latrania Formation (see Winker and Kidwell, 1966), yield marine microfossils, and contain invertebrate ichnites. A second, upper megabreccia occurs within the top of the Latrania at the upper end of Split Mountain Gorge.

2.6 (0.5) The first evidence of the ancestral river deposits (from either the Gila River [Gastill et al., 1996; Kimbrough et al., 2011] or the Colorado River [Dorsey et al. 2007; Dorsey, 2012]) or other speculative river systems, are located in this outcrop. These pale gray-brown, fine to medium-grained sandstones within the top of the Latrania Formation and below the Mud Hills member of the Deguynos Formation, yield the first evidence of river transported clastics. The quartz-rich sands typically contain fine grains of magnetite, and are better sorted and rounded than the locally derived sediments (turbidites?). They typically lack appreciable amounts of locally derived biotite, which is present in the underlying sediments that crop out immediately down section. These fluviially derived sediments contain a distinctive zircon signature compared to deposits of the lower Latrania Formation (Kimbrough et al., 2011; Dorsey, 2012). Based on magnetostratigraphy (Dorsey et al. 2007), this event occurs ca. 5.3 Ma (Figure 1).

2.8 (0.2) STAY LEFT where the wash bends to the left and widens, near the intersection with North Fish Creek Wash located to the right side of the main wash. In this time period (5–4.5 Ma), elsewhere in Imperial and San Bernardino counties, Desert Symposium trips (2007, 2008, 2011) visited exposures of the Lawlor Tuff (4.83 Ma). This dated ash has yet to be recognized in the Fish Creek/Vallecito Creek Basin sequence.

3.0 (0.2) **STOP 2-5: MUD HILLS MEMBER OF THE DEGUYNOS FORMATION** (Figure 1). PARK on either side of the road. The 400 m-thick Mud Hills member includes all but the top-most beds of the prominent strike ridge or “flat iron” seen to the southwest called the Elephant Knees. Deposited in relatively deep water, this medium olive-colored, very fine-grained, well-sorted marine claystone largely predates progradation of the ancestral Colorado River delta front to the west across the Salton Trough. It yields a small, primarily molluscan invertebrate assemblage, bony fish and the deep water shark *Squalus* (M. Roeder pers. comm.; McDougall, 2008; Jefferson et al. 2012).

3.1 (0.1) Pass Fossil Reef dune rehabilitation area on left.

3.8 (0.7) Excellent exposures of Colorado River delta rhythmites are present for the next half-mile along both sides of Fish Creek Wash. These ca. 10 cm-thick cyclic packages of fine-grained sandstone, silty sandstone, and siltstone deposits occur in the top of the Mud Hills member of the Deguynos Formation. They represent delta front sediments and range from 4.49 to 4.4 Ma. The physical drivers for this depositional phenomenon (climatic, tidal, or other) and the duration of a single cycle are presently undetermined (Lynch and Adams, 2009).

5.5 (1.7) **STOP 2-6: YUHA MEMBER OF DEGUYNOS FORMATION** (Figure 1). PARK on the LEFT side of the road at junction. Tempestite coquinas exposed in the wash are primarily composed of mixed single valves of *Dendostrea vespertina*, *Anomia subcostata*, and *Argopecten deserti* (Deméré and Rugh 2006; Jefferson et al., 2012). The deposits are lens-shaped and have a short outcrop pattern along strike. This, and taphonomy of the bivalve taxa, suggest high-energy erosion of estuarine materials and re-deposition into channels on the distal marine delta plain or upper delta front. The 600 m-thick primarily pale yellowish-olive silty sandstone and medium brown shell coquina member records upward shallowing water depths. Jefferson et al. (2012) tentatively correlate the upper part of the Yuha member with marine deposits at Willis Palms.

TURN RIGHT (north) into Loop Wash.

6.0 (0.5) The next mile exposes the 600 m-thick Camels Head member. The ca. 4.4 to 4.25 Ma Camels Head member of the upper-most Deguynos Formation records the transition from the marine to the continental delta plane. It represents near shore mudflat and beach deposits.

Note the interbedded pale yellow, pink, and grayish brown silty claystones and sandstones through this part of the section, in comparison to the pale yellowish-olive silty sandstone and medium brown shell coquinas of the Yuha member.

6.9 (0.9) **STOP 2-7: ARROYO DIABLO FORMATION** (Figure 1). PARK on either side of the road. The 4.25 to 2.8 Ma old Arroyo Diablo Formation is primarily composed of pale reddish to pale yellowish-brown, moderately well-sorted sandstones, and in some exposures, consists of fining upward sand-silt sequences. The 2.5 km-thick unit represents the terrestrial delta plane and interfingers with locally derived fluvial deposits of the Olla Formation (Stop 2-8) along the basin margin. A variety of different shapes of sandstone concretions and fossil woods typify this unit. The fossil wood assemblage contains taxa whose modern relatives occupy lowlands and coastal areas, and suggests up to 62 cm of annual precipitation (Remeika, 2006). Fossil vertebrates include an elephant-like gomphothere, camels, and the horse *Dinohippus* (Jefferson et al., 2012). The ancestral Colorado River extends its delta across the ancestral Gulf during Arroyo Diablo time, isolating the Salton Trough to the north about 3.9 Ma ago. To the north, the Arroyo Diablo Formation interfingers with pale reddish claystones and siltstones of the lacustrine and playa deposits of the Borrego Formation. The Borrego Formation is not exposed in the Fish Creek Basin. To the south, deltaic deposits spilled into the ancestral Gulf of California as they do today.

BEAR LEFT to the upper intersection of Loop Wash and Fish Creek Wash.

7.7 (0.8) TURN RIGHT (west) into Fish Creek Wash. Do not re-enter Loop Wash when returning down Fish Creek Wash at the end of the tour.

8.2 (0.5) Note fluvial and deltaic sands, and channels cut through the sandstone.

10.8 (2.6) **STOP 2-8: OLLA FORMATION** (Figure 1). PARK on the RIGHT side of the road and walk to top of the right bank of the wash. In the Fish Creek exposures, the Olla Formation dates from approximately 4.25 to 2.8 myr (Dorsey et al. 2011). Here the formation interfingers basinward with the pale reddish to pale yellowish-brown, moderately well-sorted sandstones of the Arroyo Diablo Formation. Toward the basin margin it interfingers with the Canebrake Conglomerate (Stop 2-9), and at its base with the basin margin Jackson Fork member of the Deguynos Formation. Winker (1987; Winker and Kidwell, 1996) described the Olla Formation in Fish Creek Basin as composed of locally derived fluvial sandstones and siltstones interbedded with Arroyo Diablo Formation-like Colorado River sediments. The formation produces a rich and diverse fossil vertebrate assemblage (Mroz et al., 2011; Jefferson et al., 2012).

In northern ABDSP, the 620 m-thick Olla Formation is composed of pale brown fluvial channel sandstones (3+ m-thick cross-bedding) that are interbedded with pale olive overbank sandy and silty claystones (Mroz et al., 2011). Tongues of Arroyo Diablo Formation-like sediments appear only in the uppermost part of the unit where it also interfingers with lacustrine claystones of the Borrego Formation. Lacking absolute dates, precise correlation of these rocks with the type Olla Formation in the Fish Creek Basin is uncertain (Mroz et al., 2011). However, current directions in the Fish Creek Wash exposures are from the north and northwest (Winker, 1987), and in the Truckhaven Rocks current directions are from the northwest (Mroz et al., 2011). During Olla time, the mouth of the ancestral Colorado River was located east of ABDSP. These observations suggest that the Olla Formation at Truckhaven Rocks may represent an additional and significant fluvial sediment source distinct from the ancestral Colorado and Gila Rivers and local sources in the Peninsular Range.

11.5 (0.7) STAY RIGHT—avoid Sandstone Canyon.

11.7 (0.2) BEAR RIGHT past Olla Wash.

12.7 (1.0) **STOP 2-9: OLLA FORMATION AND CANEBRAKE CONGLOMERATE** (Figure 1). Drive a short distance past this stop, TURN AROUND and PARK on the RIGHT side of the wash. Walk a short distance down the wash to a saddle on southeast side for overview

The Olla Formation interfingers on the basin margin with the pale brown, poorly sorted coarse-grained sandstones and conglomerates of the Canebrake Conglomerate. To the north the Canebrake Conglomerate on the skyline is composed of granitic and metamorphic rocks (present in wash) shed from the Vallecito Mountains (Kairouz, 2005). To the south and southeast the Olla Formation, pale olive, thin-bedded silty sandstone, is seen interfingering with the pink-colored Arroyo Diablo Formation-like well-sorted, medium to coarse-grained sandstones.

RETRACE 13 miles east and north back through Split Mountain Gorge to Split Mountain Road.

13.2 (0.5) BEAR LEFT past Olla Wash.

13.9 (0.7) BEAR LEFT past Sandstone Canyon.

16.7 (2.8) Continue past Arroyo Seco del Diablo

17.6 (0.9) Proceed northeast on Fish Creek Wash. Do not enter Loop Wash.

19.4 (1.8) BEAR RIGHT past Loop Wash entrance. Proceed northeast in Fish Creek Wash.

24.7 (5.3) Leave Split Mountain Gorge and pass Fish Creek Camp.

26.2 (1.5) Split Mountain Road (paved).

30.5 (4.3) SLOW for left bend in road.

34.5 (1.0) SLOW for right bend in road.

36.2 (1.7) Ocotillo Wells, the intersection of SR-78 and Split Mountain Road.

End Day 2 There are several route options to either return home or continue your visit in ABDSP.

1. **Exit trip east** (right turn) on SR-78 to SR-86 north (left turn) to I-10 west (left turn) and Riverside and Los Angeles counties, and north (right turn) on I-15 to San Bernardino County, or I-10 east (right turn) to Arizona. A south (right turn) on SR-86 south to I-8 returns to Yuma (left turn) or San Diego (right turn).

2. **Exit trip west** (left turn) on SR-78 to SR-67 in Ramona into San Diego County, and I-8.

3. **Visitor Center** To visit the ABDSP Visitor Center (closes at 05:00p), exit trip west (left turn) on SR-78 to Borrego Springs Road (right turn 6.7 miles) to Borrego Springs, at traffic circle go west (left turn) on SR-22, Palm Canyon Drive, the Colorado Desert District Stout Research Center, State Park Visitor Center and Palm Canyon Campground (developed, reservation required).

4. From the Visitor Center continue on SR-22 west (left turn) to S-2 west (right turn) to SR-79 west (right turn) to Temecula and north (right turn) on I-15 to SR-91 west (left turn) into Orange and Los Angeles Counties. Or you can travel east on SR-22 to SR-86 (see above).

ACKNOWLEDGMENTS—We thank Dave Miller, USGS, for consistent and consistent guidance, and appreciate the encouragement of R. Powell & J. Matti. We had helpful road log and field discussions with K. Bishop, D. Lynch, A. Marshall, T. Schweich, E. Wilson, P. LaFollette, M. Roeder, and W. Presch. The maps that Tom Schweich produced for this and other Desert Symposium volume are exceptional!

Literature Cited

- Abbott, P.L. 1996. Why sturzstroms? In *Sturzstroms and Detachment Faults Anza-Borrego Desert State Park California*, P.L. Abbott and D.C. Seymour, ed. South Coast Geological Society Annual Field Trip Guide Book Number 24, p. 164.
- Aksoy, R., P. M. Sadler, and S. Biehler. 1986. Gravity anomalies over sedimentary basins on the Helendale Fault trend, in *Geology around the margins of the eastern San Bernardino Mountains*, M. A. Kooser and R. E. Reynolds, ed. Redlands, Inland Geological Society, p 121-128.
- Albright, L. B. 1999. Magnetostratigraphy and biochronology of the San Timoteo Badlands, southern California, with implications for local Pliocene–Pleistocene tectonic and depositional patterns. *GSA Bulletin*; September 1999; v. 111; no. 9; p. 1265–1293.
- Baldwin, J. 1986. Martinez Mountain rock avalanche, in *Geology of the Imperial Valley, California*, P. D. Guptil, E. M. Gath, and R. M. Ruff, ed. South Coast Geological Society, Annual Field Trip Guidebook, 14, p. 37-48.
- Barrows, C. W. 1997. Habitat relationships of the Coachella Valley fringe-toed lizard (*Uma inornata*). *The Southwestern Naturalist* 42, p. 218-223
- Berggren, W. A., D. V. Kent, C. C. Swisher, and M. P. Aubry. 1995. A revised Cenozoic geochronology and chronostratigraphy, in *Geochronology, time scales and global stratigraphic correlation*, ed. W. A. Berggren, D. V. Kent, M. P. Aubry, and J. Hardenbol, J. Society for Sedimentary Geology (SEPM) Special Publication 54, p. 129–212.
- Bryan, K. A. 2004. Non-brittle fault deformation in trench exposure at the Helendale Fault, in: *Breaking Up*, R. E. Reynolds, ed. Cal State Fullerton Desert Symposium 2004, p. 51-54.
- Cassiliano, M. L. 2002. Revision of the stratigraphic nomenclature of the Plio-Pleistocene Palm Spring Group (new rank), Anza-Borrego Desert, southern California. *Proceedings of the San Diego Society of Natural History* 38, p. 1-30.
- Collins, G. S. and H. J. Melosh. n.d. Acoustic fluidization and the extraordinary mobility of sturzstroms. Lunar and Planetary Lab., University of Arizona, Tucson, <http://amcg.ese.ic.ac.uk/~gsc/publications/abstracts/lpsc03b.pdf>
- Dean, M. 1996. Neogene Fish Creek Gypsum and Associated Stratigraphy and Paleontology, Southwestern Salton Trough, California. In *Sturzstroms and Detachment Faults, Anza-Borrego Desert State Park, California*, P.L. Abbott and D.C. Seymour, ed. South Coast Geological Society, Annual Field Trip Guide Book No. 24, p. 123-148.
- Deméré, T. A., and N.S. Rugh. 2006. Invertebrates of the Imperial Sea. In *The Fossil Treasures of the Anza-Borrego Desert*, G.T. Jefferson and L. Lindsay, ed. Sunbelt Publications, San Diego, California, p. 43-69.
- Dibblee, T.W. Jr. 1964. Geological map of the Rodman Mountains quadrangle, San Bernardino County, California. U.S. Geological Survey Miscellaneous Geological Investigations Map, I430; scale 1:62,500.
- _____. 1967a. Geologic map of the Morongo Valley quadrangle, San Bernardino County, California. U.S. Geological Survey Miscellaneous Geologic Investigations Map I517.
- _____. 1967b. Geologic map of the Joshua Tree quadrangle, San Bernardino and Riverside counties, California. U.S. Geological Survey Miscellaneous Geologic Investigations Map I-516, 1:62,500.
- _____. 1967d. Geologic map of the Old Woman Springs quadrangle, San Bernardino County, California. U.S. Geological Survey Misc. Geological Investigations Map I516.
- _____. 1981. Geologic map of the Banning quadrangle, California, in *Geologic quadrangle maps of the San Jacinto Mountains and vicinity, California*, A.R. Brown, ed. Santa Ana, South Coast Geological Society geologic map SCGS-2, scale 1:62,500.
- _____. 1981. Geology of the San Jacinto Mountains and adjacent areas, in *Geology of the San Jacinto Mountains*, A.R. Brown and R.W. Ruff, ed. Santa Ana, South Coast Geological Society Annual Field Trip Guidebook 9, p. 1-47.
- _____. 1982. Geology of the San Bernardino Mountains, southern California, in *Geology and mineral wealth of the California Transverse Ranges*, D.L. Fife and J.A. Minch, ed. Santa Ana, South Coast Geological Society, p. 149-169.
- _____. 1992. Geology and inferred tectonics of the Pinto Mountain Fault, eastern Transverse Ranges, California, in *Deformation associated with the Neogene Eastern California Shear Zone, southeastern California and southwestern Arizona*, S.M. Richards, ed. Redlands, San Bernardino County Museums Special Publication 921, p. 2831.

- Dorsey, R. J. 2006. Stratigraphy, tectonics, and basin evolution in the Anza-Borrego Desert region. In *The Fossil Treasures of the Anza-Borrego Desert*, G.T. Jefferson and L. Lindsay, ed. Sunbelt Publications, San Diego, California, p. 89-104.
- Dorsey, R.J. 2012. Earliest delivery of sediment from the Colorado River to the Salton Trough at 5.3 Ma: Evidence from Split Mountain Gorge. California State University, Desert Studies Consortium, this volume.
- Dorsey, R. J., A.L. Fluette, B. A. Housen, K. A. McDougall, S. U. Janecke, G. J. Axen, and C. Shirvell. 2006. Chronology of Late Miocene to Early Pliocene Sedimentation at Split Mt. Gorge, Western Salton Trough: Implications for Development of the Pacific-North America Plate Boundary. Poster presented at RCL-Cortez Workshop: "Lithospheric Rupture in the Gulf of California - Salton Trough Region," Ensenada (Mexico), January 9-13, 2006.
- Dorsey, R.J., A. Fluette, K. McDougall, B. A. Housen, S. Janecke, G.J. Axen, and C. R. Shirvell. 2007. Chronology of Miocene-Pliocene deposits at Split Mountain Gorge, southern California: a record of regional tectonics and Colorado River evolution. *Geology* 35(1) p. 57-60.
- Dorsey, R.J., B. A. Housen, S. U. Janecke, C. M. Fanning, and A. L. F. Spears. 2011. Stratigraphic record of basin development within the San Andreas fault system: Late Cenozoic Fish Creek-Vallecito basin, southern California. *Geological Society of America Bulletin* 123(5, 6), p. 771-793.
- Durrell, C. 1953. Celestite deposits near Ocotillo, San Diego County, California. California Division of Mines and Geology Special Report 32, p. 5-7.
- Flanagan, Pat. 2010. Down Home Learning, Desert Report, June, 2010, Desert Protective Council.
- Gastil, R. G., D. L. Krummenacher, and P. L. Abbott. 1996. Arrival of the Colorado River in the Salton Trough defined by magnetic susceptibility. In *Sturzstroms and Detachment Faults Anza-Borrego Desert State Park California*, P. L. Abbott and D. C. Seymour, ed. South Coast Geological Society Annual Field Trip Guide Book Number 24, p. 203-208.
- Grimes, G. 1986. Sediments adjacent to a portion of the Pinto Mountain Fault in the Yuca Valley area of San Bernardino County, California, in *Geology around the margins of the eastern San Bernardino Mountains*, M. A. Kooser and R. E. Reynolds, ed. Inland Geological Society, p.75-76.
- Gudde, E. G. 1974. *California Place Names*. Berkeley, University of California Press.
- Hardin, J. W., and J. C. Matti. 1989. Holocene and Late Pleistocene slip rates on the San Andreas Fault in Yucaipa, California, using displaced alluvial-fan deposits and soil chronology. *GSA Bulletin* vol. 101, p. 1107-1117.
- Hehn, V. N., B. J. MacFadden, L. B. Albright, and M. O. Woodburne. 1996. Magnetic polarity, stratigraphy and possible differential tectonic rotation of the Miocene-Pliocene mammal-bearing San Timoteo Badlands, southern California. *Earth and Planetary Science Letters*, v. 141, p. 35-49.
- Hillemeier, F. L., M. D. Johnson, and R. R. Kern. 1991. Introduction to the Salton Trough rift. In *The diversity of mineral and energy sources in southern California*, M. A. McKibben, ed. Society of Economic Geologists Guidebook Series, 12, p. 139-155.
- Hillemeier, F. L., M. D. Johnson, and R. R. Kern. 1992. Geology, alteration and mineralogy of the Modoc Hot Spring gold prospect, Imperial County, California. In *Salton Trough gold deposits*, SEM-AIME fall field trip, p. 139-155.
- Hsu, K.J. 1975. Catastrophic debris streams (sturzstroms) generated by rockfalls. *Geological Society of America Bulletin* vol. 86 (1), p. 129-140.
- Ingle, J. C. 1974. Paleobathymetric history of Neogene marine sediments, northern Gulf of California, in *Geology of Peninsular California; A guidebook for the 49th annual meeting of the Pacific Section, AAPG-SEG-SEPM*, p. 121-138.
- Jefferson, G. T., and L. Lindsay, ed. 2006. *The Fossil Treasures of the Anza-Borrego Desert*. Sunbelt Publications, San Diego, California.
- Jefferson, G. T., and L. Lindsay. 2008. The Lake Cahuilla high shoreline and a stable overflow path elevation, southeastern California and northeastern Baja California. In *Trough to Trough*, R.E. Reynolds, ed. The 2008 Desert Symposium Field Guide and Proceedings, California State University, Desert Studies Consortium and LSA Associates, Inc., p. 107-109.
- Jefferson, G. T., L. K. Murray, and S. D. Keeley. 2012. The Pliocene fossil record of Anza-Borrego Desert State Park, western Salton Trough, California (this volume).
- Johnson, N.M., C. B. Officer, N. D. Opdyke, G. D. Woodward, P. K. Zeitler, and E. H. Lindsay. 1983. Rates of late Cenozoic tectonism in the Vallecito-Fish Creek basin, western Imperial Valley, California: *Geology*, vol. 11, p. 664-667.
- Kimbrough, D. L., M. Grove, G. E. Gehrels, J. B. Mahoney, R. J. Dorsey, K. A. Howard, P. K. House, P. A. Peartree, K. Flessa. 2011. Detrital zircon record of Colorado River integration into the Salton Trough, origin and evolution of the Colorado River System II symposium, USGS Flagstaff, Arizona, May 24-26, 2010, USGS Open-File Report.
- Kairouz, M. E. 2005. Geology of the Whale Peak region of the Vallecito Mountains: Emphasis on the kinematics and timing of the West Salton Detachment Fault, southern California. Master of Science Thesis, Department of Geology, University of California Los Angeles, 156 p.
- Laurie, B. D. 1967. Washington Monument Resurvey Expedition. San Bernardino County Museum Association *Quarterly*, vol. 14 (3, 4), p. 1-48.
- Li, H-C. 2003. A 20-kyr climatic and hydrologic history of Salton Basin, California recorded by geochemical proxies in lacustrine deposits. In *Land of Lost Lakes*, the 2003 Desert Symposium Field Trip, R. E. Reynolds, ed. California State University, Desert Studies Consortium in association with LSA Associates, Inc, p. 57-60.
- Lindsay, L., and G. T. Jefferson. 2006. Appendix Table 4: Stratigraphic names correlation table. In *The Fossil Treasures of the Anza-Borrego Desert*, G. T. Jefferson and L. Lindsay, ed. Sunbelt Publications, San Diego, California.
- Los Angeles Department of Water and Power, n.d. The Colorado River Aqueduct. <http://wsoweb.ladwp.com/Aqueduct/historyoflaa/coloradoriver.htm> accessed 3/31/12.
- Lynch, D. K., and P. M. Adams. 2009. Fish Creek rhythmites and aperiodic temporal sedimentation. In *Landscape Evolution at an Active Plate Margin, The 2009 Desert Symposium Field Guide and Proceedings*, R. E. Reynolds and D. R. Jessey, ed. California State University Desert Studies Consortium and LSA Associates, Inc., p. 159-164.
- McDougall, K., C. L. Powell II, J. C. Matti, and R. Z. Poore. 1994. The Imperial Formation and the opening of the ancestral Gulf of California [abs.]. *Geological Society of America Abstracts with Programs*, vol. 26, p. 71.
- May, S. R., and C. A. Repenning. 1982. New evidence for the age of the Old Woman Sandstone, Mojave Desert, California, in,

- Guidebook*, J. D. Cooper, ed. Geological Society of America, Cordilleran Section Meeting, Anaheim, California, 1982, p. 93-96.
- McDougall, K. 2008. Late Neogene marine incursions and the ancestral Gulf of California. Geological Society of America *Special Paper* 439:353-371.
- Mount, J. D. 1974. Molluscan evidence for the age of the Imperial Formation, southern California. *Abstracts of Program*, Annual Meeting, Southern California Academy of Sciences, p. 29.
- Mroz, A., G.T. Jefferson, and L.K. Murray 2011. Deferred Maintenance Program project report #158280 July 2011: Truckhaven Rocks. Document on File, Department of Parks and Recreation Natural Resources Division, Sacramento, and Colorado Desert District Stout Research Center Library, Borrego Springs, 26 p.
- Murray, L. K. 2008. Effects of taxonomic and locality inaccuracies on biostratigraphy and biochronology of the Hueso and Tapiado formations in the Vallecito Creek-Fish Creek section, Anza-Borrego Desert, California. PhD Dissertation, Department of Geology, University of Texas, Austin, 531 p.
- Neville, S.L. 1983. Late Miocene alkaline volcanism, south-central Mojave Desert and northeast San Bernardino Mountains, California. University of California, Riverside, M.S. thesis.
- Neville, S. L. 1986. Late Miocene alkaline volcanism, Ruby Mountain, San Bernardino County, California, in *Geology around the margins of the eastern San Bernardino Mountains*, M. A. Kooser and R. E. Reynolds, ed. Redlands, Inland Geological Society, p 95-100.
- Neville, S.L., P. Schiffman, and P. Sadler. 1985. Ultramafic inclusions in late Miocene alkaline basalts from Fry and Ruby Mountains, San Bernardino County, California. *American Mineralogist*, vol. 70, p. 668-677.
- Oberlander, T.M. 1972. Morphogenesis of granitic boulder slopes in the Mojave Desert, California. *Journal of Geology*, vol. 80, p. 119.
- Opdyke, N. D., E. H. Lindsay, N. M. Johnson, and T. Downs. 1977. The paleomagnetism and magnetic polarity stratigraphy of the mammal-bearing section of Anza Borrego State Park, California. *Quaternary Geology*, vol. 7, no. 3, p. 316-329.
- Peterson, D. G. Jr., and G. T. Jefferson. 1997. Submarine hydrothermal venting, a reevaluation of the source of the Fish Creek Gypsum, Imperial County, California. In *Memories, Minerals, Fossils, and Dust, Abstracts from Proceedings of the 1997 Desert Research Symposium*, San Bernardino County Museum Association Quarterly 44(1), p. 37-38.
- Peterson, R.M. 1976. Patterns of Quaternary denudation and deposition of Pipes Wash (Mojave Desert), California. University of California, Riverside, Ph.D. thesis.
- Powell, C.L. II. 1985. Bivalve molluscan paleoecology of northern exposures of the marine Neogene Imperial Formation in Riverside County, California. *Annual Report Western Society of Malacologists* 7, p. 29-32.
- _____. 1986. Stratigraphy and bivalve molluscan paleontology of the Neogene Imperial Formation in Riverside County, California. San Jose State University, M.S. thesis.
- _____. 1988. The Miocene and Pliocene Imperial Formation of southern California and its molluscan fauna; an overview: Annual Report Western Society of Malacologists 20, p. 11-18.
- _____. 1993. Macrofossils from the Imperial Formation in the Ocotillo Wells State Vehicle Recreation area, Imperial and San Diego Counties, California: U. S. Geological Survey _____. 1995. Paleontology and significance of the Imperial Formation at Garnet Hill, Riverside County, California, , USGS Open-File Report 95-489, p. 1-10.
- _____. 2008. Pliocene Invertebrates from the Travertine Point Outcrop of the Imperial Formation, Imperial County, California: U.S. Geological Survey *Scientific Investigations Report* 2008-5155, 25 p.
- Powell, C. L. II, M. A. Roeder, and K. McDougall. 2011. A preliminary report on the paleontology of the Imperial Formation (ancestral Gulf of California; Pliocene) in the Indio Hills, Riverside County, southern California. *CalPaleo 2011 Abstracts with Program*, p. 22.
- Powell, R. E., and J. C. Matti. 2000. Geologic map and digital database of the Cougar Buttes 7.5' quadrangle, San Bernardino County, California. United States Geological Survey open-file report 00-175.
- Proctor, R. J. 1958. Geology of the Desert Hot Springs area, Little San Bernardino Mountains, California. M.S. thesis, University of California, Los Angeles.
- Reynolds, R. E. 1992. Landers: Earthquakes and aftershocks. San Bernardino County Museum Association *Quarterly*, vol. 40(1), p. 1-72.
- Remeika, P. 1998. Marine invertebrate paleontology and stratigraphy of the Vallecito-Fish Creek Basin: a historic review, synthesis, and revision. In *Geology and Hydrothermal Resources of the Imperial and Mexicali Valleys*, L. Lindsay and W. G. Hample, ed. San Diego Association of Geologists Annual Field Trip Guidebook 1998, pp. 59-92.
- Remeika, P. 2006. Ancestral woodlands of the Colorado River delta plain. In *Fossil Treasures of the Anza-Borrego Desert*, G. T. Jefferson and L. Lindsay, ed. Sunbelt Publications, San Diego, California, p. 75-87.
- Reynolds, R. E., and M. A. Kooser, 1986. Field trip road log, in *Geology around the margins of the eastern San Bernardino Mountains*, M. A. Kooser and R. E. Reynolds, ed. Redlands, Inland Geological Society, p. 7-51.
- Reynolds, R.E., R. L. Reynolds, and E. H. Lindsay. 2008. Biostratigraphy of the Miocene Crowder Formation, Cajon Pass, southwestern Mojave Desert, California, in *Geology and vertebrate paleontology of western and southern North America*, X. Wang and L. G. Barnes, ed. Contributions in honor of David P. Whistler, Natural History Museum of Los Angeles County Science Series 41, pp.237-253.
- Rogers, T.H. 1965. Geologic map of California, Santa Ana sheet, scale 1:250,000. California Division of Mines and Geology.
- Rymer, M. J., A. M. Sarna-Wojcicki, C. L. Powell, and J. A. Barron. 1994. Stratigraphic evidence for late Miocene opening of the Salton Trough in southern California. *Abstracts with Programs*, Geological Society of America, Cordilleran Section, v. 26, no. 2, p. 87.
- Rymer, M. J., C. L. Powell II, A. M. Sarna-Wojcicki, and J. A. Barron., 1995. Late Miocene stratigraphic and paleogeographic setting of Garnet Hill in the northwestern Salton Trough, southern California. *American Association of Petroleum Geologists Bulletin*, vol. 79, no. 4, p. 596.
- Sadler, P. M. 1982. Provenance and structure of late Cenozoic sediments in the northeast San Bernardino Mountains. GSA Cordilleran Section *Volume and Guidebook*, p. 83-92.
- Sadler, P.M., and W. A. Reeder. 1983. Upper Cenozoic, quartzite-bearing gravels of the San Bernardino Mountains, Southern California: Recycling and mixing as a result of transpressional uplift, in *Tectonics and Sedimentation along Faults of the San Andreas System*, D. W. Anderson and M. J. Rymer,

- ed. Pacific Section, Society of Economic Palaeontologists and Mineralogists, p. 45-57.
- Schoffstall, P. A. 2010. *Mojave Desert Dictionary*. Barstow, Mojave River Valley Museum, p. 257.
- Shaller, P. J. and A. S. Shaller. 1996, Review of proposed mechanisms for sturzstroms (long-runout landslides), in *Sturzstroms and Detachment Faults, Anza-Borrego Desert State Park, California*, P. L. Abbott and S. D. Seymour, ed. Santa Ana, South Coast Geological Society, p. 185-202.
- Shreve, R. L. 1958. Geology and mechanics of the Blackhawk landslide. Pasadena, California Institute of Technology, unpublished Ph.D. thesis.
- Shreve, R. L. 1968. The Blackhawk landslide. Geological Society of America *Special Paper* 108, 47 p.
- _____. 1987. Blackhawk landslide, southwestern San Bernardino County, California, in *Centennial Field Guide Volume 1*, M. L. Hill, ed. Cordilleran Section, Boulder, Colorado, Geological Society of America, p. 109-114.
- Stout, M. L. 1977. Radiocarbon dating of landslides in southern California. *California Geology*, vol. 30, p. 99-105.
- Topozada, T. R. 1993. The Landers–Big Bear earthquake sequence and its felt effects. *California Geology*, vol. 46(1), p. 3-9.
- Treiman, J. A. 1992a. Eureka Peak and related faults: Joshua Tree South and Yucca Valley South quadrangles, San Bernardino and Riverside counties, California. California Division of Mines and Geology, *Fault Evaluation Report* FER-230, 15 p.
- _____. 1992b. Eureka Peak and Burnt Mountain faults, two “new” faults in Yucca Valley, San Bernardino County, California, in *Landers Earthquake of June 28, 1992, San Bernardino County, California, Field Trip Guidebook*, D. B. Ebersold, ed. Southern California Section, Association of Engineering Geologists 1992 Annual Field Trip, p. 19-22.
- Turner, W. G., and R. E. Reynolds. 1977. Dating the Salton Sea petroglyphs. *Science News*, 111 (February).
- Umbarger, K. E. 1992. Geology and petrology of the Spy Mountain region, Landers quadrangle, San Bernardino County, California. California State University, Los Angeles, MS thesis.
- Van Buskirk, M. C., and M. A. McKibben. 1993. The Modoc Fossil Hot Spring Deposit. San Bernardino County Museum Association *Special Publication* 93(1), p. 81.
- Vaughan, F.E., 1922. Geology of the San Bernardino Mountains north of San Gorgonio Pass. University of California Publications in Geological Sciences, 13:319-411.
- Vaughn, F. E. 1922. Geology of the San Bernardino Mountains north of San Gorgonio Pass. University California Dept. Geology, *Bulletin*, vol. 13, no. 9, p. 397.
- Wilshire, H. G., and J. W. Shervais. 1975. Al-augite and Cr-diopside ultramafic xenoliths in basaltic rocks from the western United States, in *Physics and Chemistry of the Earth*, 9, L. H. Aherns et al, ed. Pergamon, New York, p. 257-272.
- Winker, C. D. 1987. Neogene stratigraphy of the Fish Creek–Vallecito section, southern California: implications for early history of the northern Gulf of California and Colorado delta. Ph.D. Dissertation, Department of Geosciences, University of Arizona, Tucson, 494 p.
- Winker, C. D., and S. M. Kidwell. 1996. Stratigraphy of a marine rift basin: Neogene of the western Salton Trough, California. In *Field Conference Guide*, P. L. Abbott and J. D. Cooper, ed. Pacific Section of American Association of Petroleum Geologists, GB 73, Pacific Section Society of Economic Paleontologists and Mineralogists, Book 80, p. 295-336.
- Wright, L. A., R. M. Stewart, T. E. Gay Jr. and G. C. Hazenbush. 1953. Mines and mineral deposits of San Bernardino County, California. *California Journal of Mines and Geology*, vol. 49, p. 49-192.

Basin thickness variations at the junction of the Eastern California Shear Zone and the San Bernardino Mountains, California: how thick could the Pliocene section be?

Victoria Langenheim,¹ Tammy L. Surko,² Phillip A. Armstrong,³ and Jonathan C. Matti⁴

¹United States Geological Survey (USGS), Menlo Park, CA

²Dominion Resources, Inc., Clarksburg, WV

³Department of Geological Sciences, California State University, Fullerton, CA

⁴United States Geological Survey (USGS), Tucson, AZ

ABSTRACT—We estimate the thickness of Neogene basin fill along the junction of the Eastern California Shear Zone and the North Frontal thrust system of the San Bernardino Mountains using gravity data with geologic and well log constraints. The geometry of the basin fill is of interest for groundwater assessment and location of potential faults, as well as providing an upper bound on the thickness of any potential, buried Pliocene sediments. Nearly one thousand new gravity measurements were collected along the North Frontal thrust system from Hesperia to Johnson Valley. Three-dimensional inverse modeling of the new and existing gravity data shows that Neogene deposits are segmented into basins along the range front of the San Bernardino Mountains. The Helendale fault, a dextral fault in the Eastern California Shear Zone, separates shallower basement (approximately 300 m depth) beneath Lucerne Valley east of the fault from deeper basement (approximately 550 m or more) west of the fault. The thickest part of the basin fill is generally located near the San Bernardino Mountains and the basin shallows northward. The amount of throw on the North Frontal thrust appears to decrease eastward, as the gravity gradient associated with the fault diminishes in amplitude. The thickness of basin fill away from the North Frontal system and east of the Helendale fault is less than 100 to 200 m, except for local pockets generally developed along strike-slip faults of the Eastern California Shear Zone and local east-west oriented depressions associated with folding of the basin fill.

Introduction

The thickness of Neogene basin fill is of interest to not only geologists who wish to understand the tectonic and landscape evolution of Southern California but also those interested in the availability of groundwater and in estimating shaking hazard along the urban fringes of southern California, where population growth has been rapid. In particular, where can one expect to find deep Neogene basin fill along the junction between the San Bernardino Mountains, a range that began uplift in the late Pliocene (e.g., Cox and others, 2003), and the Eastern California Shear Zone, a strike-slip system that initiated during the Miocene (fig. 1)? Much of the sedimentary record during this crucial time along this junction is not exposed and is limited to scattered outcrops south of Hesperia and east of Lucerne Valley (fig. 2). In this paper we use inversion of gravity data to ascertain the configuration of the Neogene basin fill and to provide an upper bound on the extent of Pliocene sediments along the

North Frontal thrust and its intersection with faults of the Eastern California Shear Zone.

Basin geometry should reflect interactions of strike-slip and thrust faults. Thrust faults can load the crust, forming downwarps that lie outboard of and parallel to the thrust fault. Strike-slip faults produce basins that are generally isolated to releasing stepovers, yet the intersection of northwest-trending dextral faults with an east-west striking thrust domain should produce alternating basins and uplifts along that interface, depending on whether the strike-slip faults extend across and into the thrust domain and on the relative timing of faulting.

This area is well suited to analysis of gravity data for understanding the Neogene basin geometry. Gravity data reflect crustal density variations, and one of the most significant density contrasts is that between dense pre-Cenozoic basement and less dense Neogene basin fill. Older Cenozoic sedimentary rocks often are of intermediate density and can complicate inversion of the gravity data. In the San Bernardino Mountains and adjacent

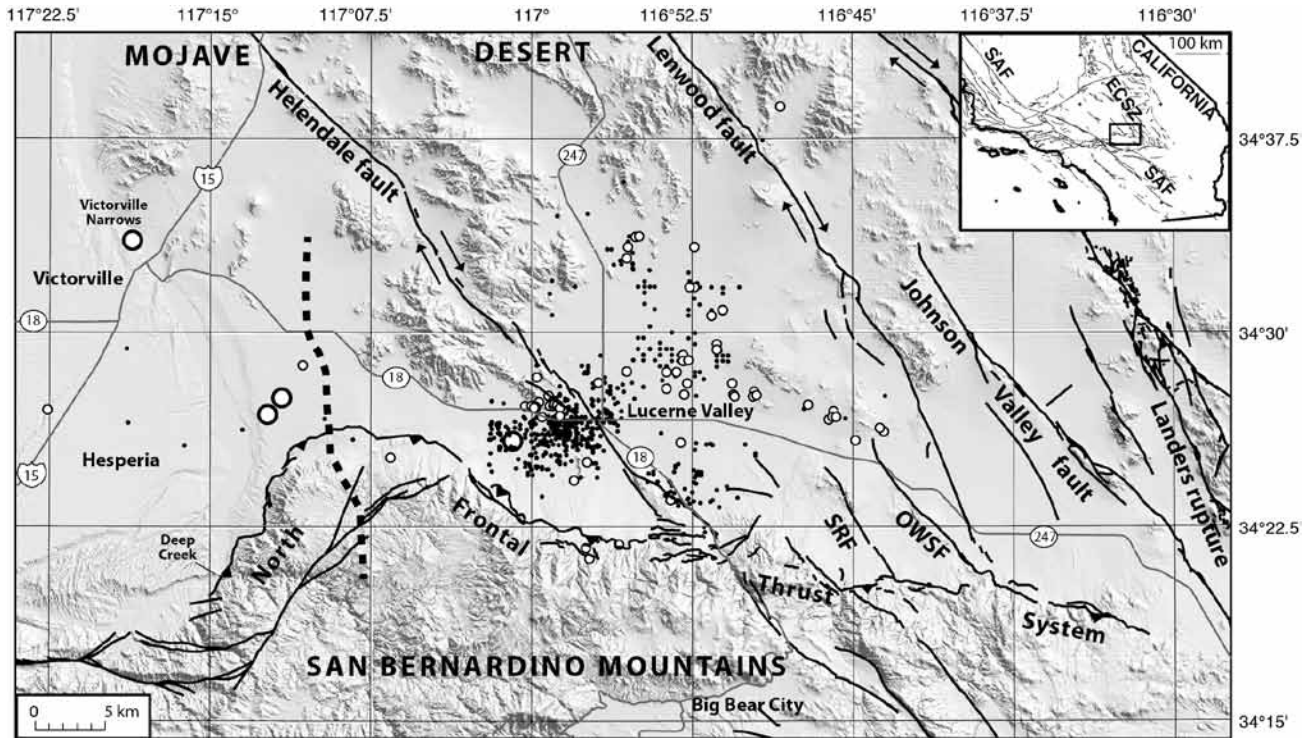


Figure 1. Shaded-relief topographic map of study area. Black lines, Quaternary faults from Jennings and Bryant (2010). Small solid black circles, water wells that did not penetrate basement; small and large open circles, water and oil wells, respectively, that did penetrate basement; dashed black line, seismic reflection profile of Li and others (1992). Abbreviations: OWSF, Old Woman Springs fault; SRF, Silver Reef fault. Abbreviations in inset: ECSZ, Eastern California Shear Zone; SAF, San Andreas fault.

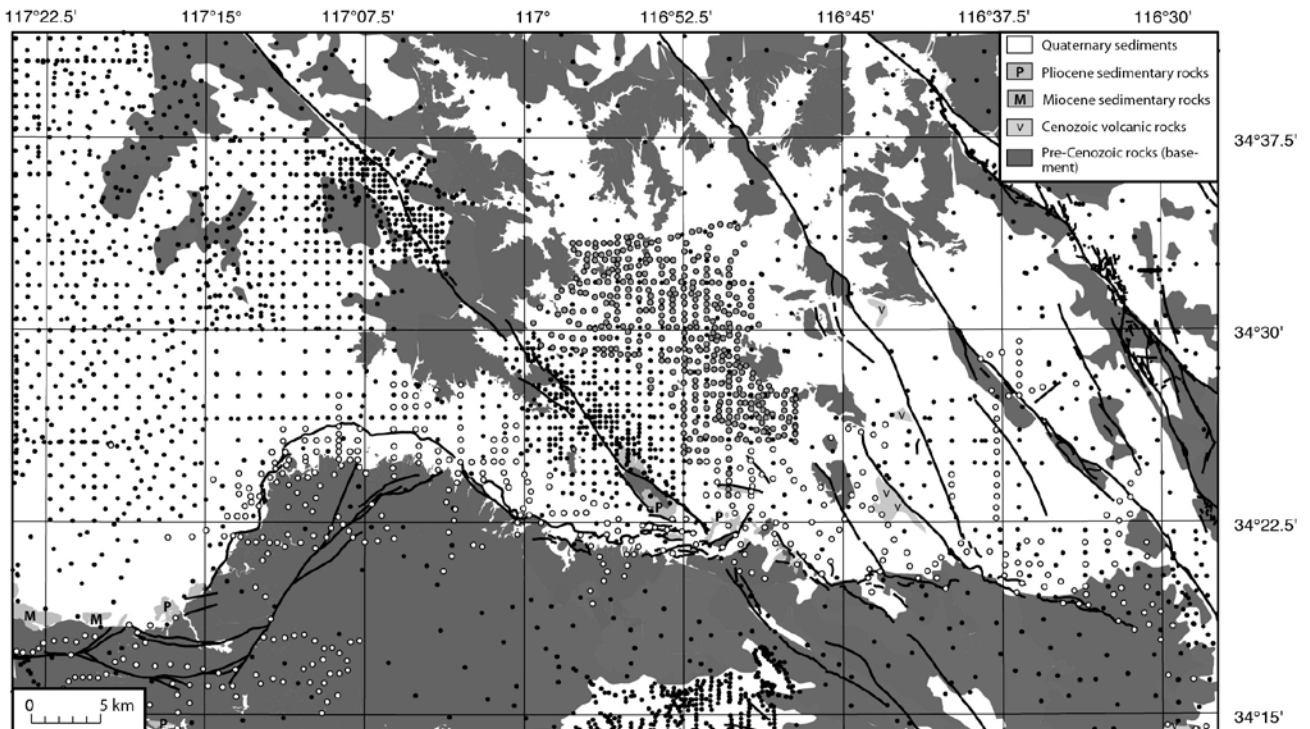


Figure 2. Simplified geologic map with gravity measurement locations. Small black circles, previously published data; gray circles from Surko (2006); black-rimmed white circles, unpublished data from U.S. Geological Survey. Faults from Jennings and Bryant (2010).

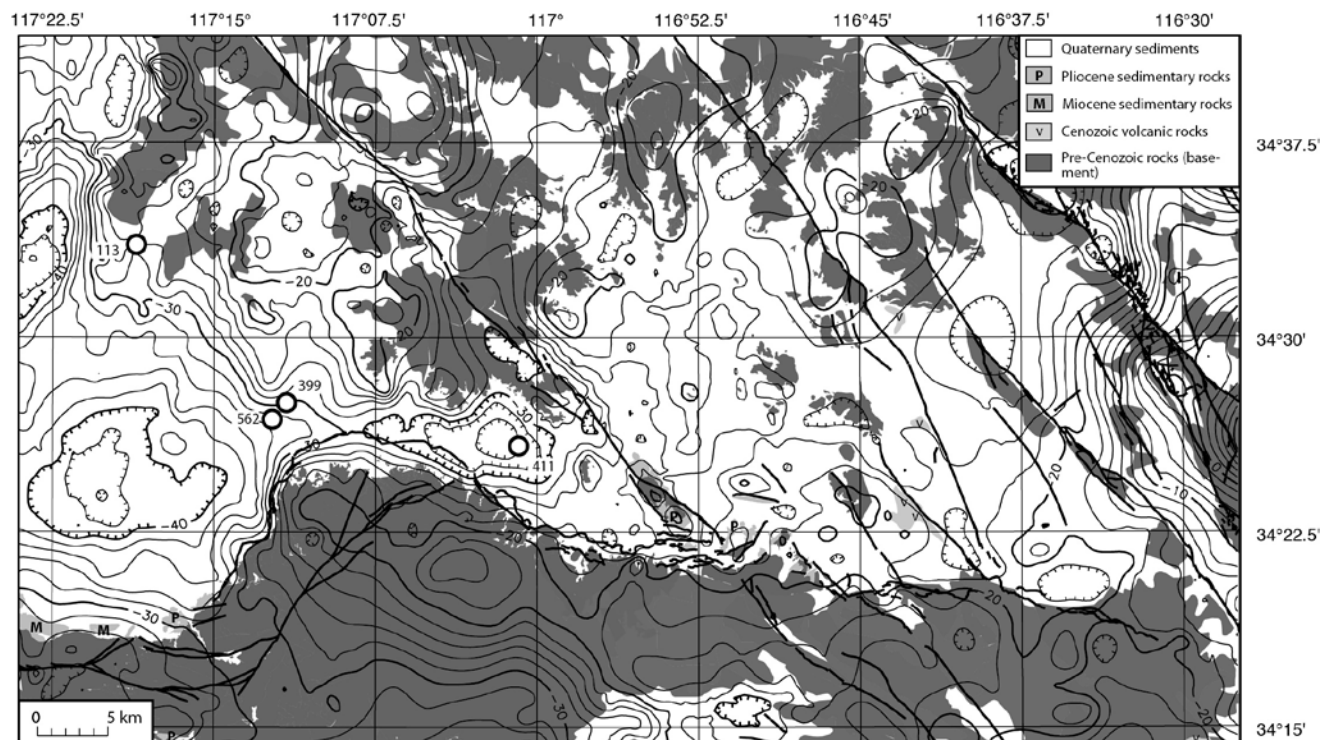


Figure 3. Isostatic residual gravity contours superposed on simplified geologic map. Contour interval, 2 mGal. Large black-rimmed circles, oil wells that did penetrate basement. Numbers next to circles are reported depth to basement in meters.

Mojave Desert, a significant erosion surface, capped locally by Miocene basalt, was carved into the Mesozoic and older crystalline basement rocks (Oberlander, 1972; Spotila and Sieh, 2000), suggesting that the potential complication in the gravity analysis arising from older Cenozoic rocks is low to nonexistent.

This study refines earlier work that used gravity data and borehole information to map the configuration of Cenozoic fill (Mabey, 1960; Aksoy, 1986; Subsurface Surveys, 1990; Spotila and Sieh, 2000). In particular, this study benefits from nearly one thousand new gravity measurements that bracket the North Frontal thrust system and from a 3-dimensional inversion method (Jachens and Moring, 1990) that utilizes gravity and geology, and is modified to include constraints from drill-hole data.

Data Sets

Gravity

As part of a master's thesis, 455 gravity measurements were collected in Lucerne Valley to support groundwater investigations (Surko, 2006). Data were also collected at 533 new sites by the U.S. Geological Survey along the northern range front of the San Bernardino Mountains. These new data supplemented data that were compiled from published sources (Biehler and others, 1988, Aksoy, 1986, Subsurface Surveys, 1990). Gravity data were reduced to isostatic anomalies using a reduction density of $2,670 \text{ kg/m}^3$ and included earth-tide, instrument drift, free-air, Bouguer, latitude, curvature, and terrain

corrections (e.g. Telford and others, 1976). An isostatic correction using a sea-level crustal thickness of 25 km and a mantle-crust density contrast of 400 kg/m^3 was applied to the gravity data to remove the long-wavelength gravitational effect of isostatic compensation of the crust due to topographic loading. The data were gridded at a spacing of 300 m, roughly the spacing of measurements within Lucerne Valley, using a minimum curvature algorithm (Briggs, 1974). The resulting gravity field is termed the isostatic residual gravity anomaly and reflects density variations in the upper and middle crust (fig. 3).

Geology

Geologic data from several sources were compiled for this study. Digital compilations of mapping at a scale of 1:24,000 or 1:62,500 were available for several of the quadrangles in the Mojave Desert part of the study area (Dibblee, 1960, 1964a, 1964b, 1964c; Sadler, 1982; Powell and Matti, 2000; Miller and Matti, 2001). In areas not covered by this scale of mapping, we used digital data from the San Bernardino 1:100,000-scale quadrangle (Morton and Miller, 2003) and from the statewide compilation at a scale of 1:750,000 (Jennings and others, 1977). These geologic data were used primarily to delineate the Neogene deposits from the basement rocks.

Wells

As described by Surko (2006), well logs were collected that contain well depth data, lithologic data, and well construction information from the California Department of Water Resources and the Division of Oil and Gas. A majority of the logs were from Lucerne Valley because

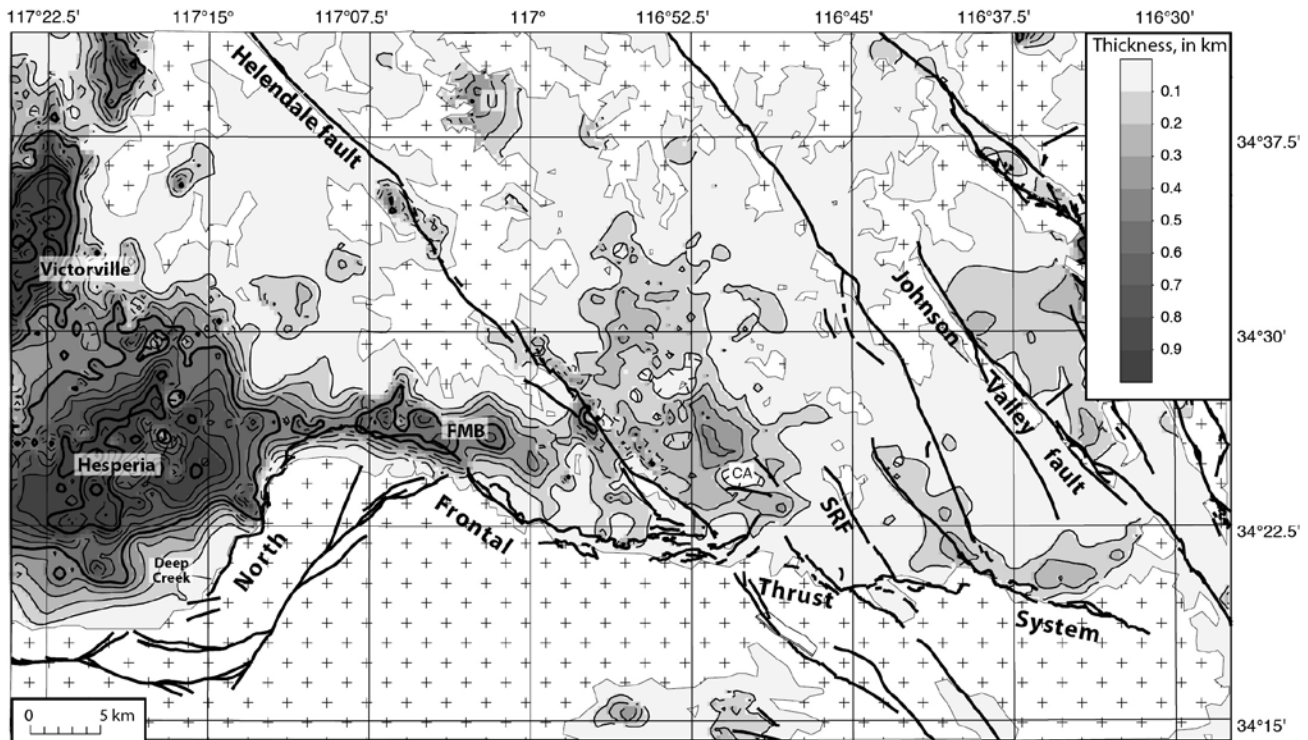


Figure 4. Thickness of Neogene basin deposits. Contour intervals, 100 m and 500 m. CA, Coyote Anticline; FMB, Fifteenmile basin; SRF, Silver Reef fault. U, basin configuration not constrained by measurements on basement.

this area was the focus of the study by Surko (2006). The wells, located by township, range, section and tract, are generally located to within 200 m of their true locations. Of the 2,465 well logs that were collected, we used 78 that penetrated basement as constraints for the inversion (fig. 1). As a quality check, we also compared the inversion results with 637 wells that did not apparently penetrate basement (fig. 1). We note the inherent uncertainty in picking the depth at which the well encountered competent bedrock from the logs due to (1) the absence of actual samples to examine, (2) descriptions by drillers who are not geologists, and (3) the significant weathering of the granitic basement (up to 15 m in Lucerne Valley according to Powell and Matti, 2000).

Gravity Field

The gravity field of the study area reflects the large density contrast between the dense basement complex and lower density basin fill, but also density variations within the basement complex. Gravity values measured on basement in the far eastern part of the study area (east of the Johnson Valley fault) reach values of nearly +10 mGal (attributed to a mostly concealed, voluminous body of Jurassic hornblende diorite; Langenheim and Jachens, 2002), whereas values measured on basement comprised of more felsic composition elsewhere (such as Mesozoic monzogranite and granitic rocks; Morton and Miller, 2003) are generally 20 or even 30 mGal lower. Gravity lows are associated with thick Neogene basin fill west of the Helendale fault and are supported by oil well logs that indicate several hundred meters of fill (California Division

of Oil, Gas, and Geothermal Resources, 1982; fig. 3). East of the Helendale fault, the gravity field is fairly flat. A broad, low-amplitude north-trending gravity high bisects Lucerne Valley; the highest values coincide with a small outcrop of basement (granodiorite and gneiss; Dibblee, 1964a). Steep gravity gradients mark the North Frontal thrust system from about 117°15' W east to 117°W. East of 117°W, the gravity gradient becomes diffuse, suggesting less vertical offset or, alternatively, shallower dip on the fault.

Inversion Method

The thickness of the Neogene basin deposits was estimated using the method of Jachens and Moring (1990), modified slightly to permit inclusion of constraints at points where the thickness of the Neogene deposits is known from direct observations in boreholes. An initial estimate of the 'basin gravity anomaly' is made by passing a smooth surface through the gravity values at stations measured where the basement rocks crop out (initial estimate of the 'basement gravity field') and subtracting this from the isostatic residual gravity field. This represents only the initial estimate because the gravity values at points on basement complex that lie close to the basin deposits are influenced by the lower density Neogene basin deposits and are therefore lower than they would be if those deposits were not present. To compensate for this effect, the initial 'basin gravity anomaly' is used to calculate an initial estimate of the thickness of the basin deposits, and the gravity effect of these basin deposits is calculated at all of the basement gravity stations. A second estimate of the

'basement gravity field' is then made by passing a smooth surface through the basement gravity values corrected by the basin effect and the process is repeated to produce a second estimate of the thickness of the basin deposits. This process is repeated until further steps do not result in significant changes to the modeled thickness of the basin deposits, usually in five or six steps.

The 'basin gravity anomaly' was converted to sediment thickness using an assumed density contrast between the sedimentary deposits and the underlying basement complex that varies with depth. We assume a density contrast of -740 kg/m^3 for the upper 60 m, a contrast of -380 kg/m^3 from 60 to 1200 m depth, and a contrast of -270 kg/m^3 below 1200 m. This density-depth relationship was modified from that derived for the Basin and Range (Jachens and Moring, 1990) by comparing the 'basin gravity anomaly' with the thickness of the basin deposits identified at various drill holes that penetrated basement. The reasonableness of this selection of density contrasts was further tested by examining the 'basement gravity field' for any indications of local anomalies at the sites where wells penetrated the basement complex and the solution was forced to honor those data.

Results

The gravity inversion resulted in a calculated thickness of the Neogene basin fill that ranges from 0 m in those areas with exposed basement rocks to more than 1 km in the Hesperia and Victorville areas (fig. 4). Different density-depth functions may change the overall thickness estimates, but will not change the shape of the basin-basement contact. See, for example, the discussion of 8 different inversions for the Lucerne Valley area by Surko (2006).

The basin configuration that results from the gravity inversion indicates deep basins (as much as 1 km) beneath the Hesperia and Victorville areas, with shallower basins to the east (fig. 4). The Victorville basin has a north-northeast trend; its geometry and distance from the North Frontal thrust suggest that its basin structure is not related to the North Frontal thrust. The considerable width of the Hesperia basin is in stark contrast to the basins to the east; the depth and width of this basin probably reflect a pre-Pliocene history, as suggested by exposures of thick Miocene sediments along the southern margin of the basin (fig. 2). Lucerne Valley is underlain by a broad, but fairly shallow, northwest-trending basin ($<400 \text{ m}$). Thicker basin fill is located near the North Frontal thrust, with significantly thinner basin fill (<100 to 200 m) east of Lucerne Valley.

The calculated thickness of the basin deposits at places where a well penetrated the entire thickness of the basin deposits agrees with the observed thickness within an average of $7 \pm 21 \text{ m}$, which is expected because the solution was constrained to honor these values. The lack of perfect agreement reflects spatial averaging. Another

measure of the reliability of the solution can be obtained by comparing the calculated thicknesses with the total well depths at those wells that did not penetrate the basement rocks. For these wells, the calculated thickness of the basin deposits is generally greater than the total well depth, as it should be. For about 10% of the wells, the predicted basin thickness is less than that encountered in the well; most of those wells are located within a grid cell of the basement-basin contact.

The inversion assumes no lateral density variations within the basin deposits. Studies of basin fill found in drill holes in Lucerne Valley and the area of Victorville and Hesperia indicate that grain size and thus density may vary laterally with distance from the range front. Fine-grained lake deposits during the Pliocene were nestled against the range front; in response to uplift of the San Bernardino Mountains, the lakes moved northward (Powell and Matti, 2000; Cox and others, 2003). Coarser sediments are expected near the range front and may be denser than the density-depth function. Basin thickness may be underestimated in these areas.

Our estimate of basin thickness is slightly lower than that predicted by a seismic-reflection profile (490 m versus $\sim 550 \text{ m}$; Li and others, 1992; thick dashed line in fig. 1). Part of this may be due to lateral variations in the basin fill or the inability of the inversion method to account for faults that dip beneath basement rocks (such as the North Frontal thrust). The basin thickness, however, appears to be slightly underestimated along the length of the profile, rather than in the immediate vicinity of the thrust. Another more likely explanation is that the density contrasts used in the inversion may be slightly too high or the average velocity used to convert time to depth (2.75 km/s ; Li and others, 1992) may be too high.

The basin inversion reinforces the importance of the Helendale fault, which separates significantly thicker basin fill in the Hesperia and Fifteenmile basins from thinner fill in Lucerne Valley and areas to the east (fig. 4). Spotila and Anderson (2004) suggested that the Helendale fault marks a change in faulting style along the North Frontal thrust system, from thrusting to the west and strike slip to the east. The gravity inversion shows that the Helendale fault also is characterized by at least two areally small, but fairly deep ($\sim 500 \text{ m}$), basins formed within right steps in the fault zone. Conversely, where the Helendale fault intersects the North Frontal thrust system, basement shallows abruptly, likely within a left step within the Helendale fault, as proposed by Matti and others (1998).

The basin inversion also highlights the effects of the interaction of the North frontal thrust system with other faults of the Eastern California Shear Zone. The east-west trough of basin fill along the thrust system is not the same thickness everywhere. Variations in thickness are also located where the Old Woman Springs and Johnson Valley fault intersect the thrust.

The southern edge of the thick deposits associated with the Fifteenmile basin (fig. 4) coincides with a salient of

the North Frontal thrust (where the fault trace is concave southward). Thick deposits wrap around the mountain front to the west and south. At about latitude of 34°22.5' the abrupt thickening of basin fill deviates west from the mountain front. The shallow bench of subsurface basement coincides with dissected topography and drainage associated with Deep Creek (fig. 1). Similarly, east of the salient, the southern edge of the basin deviates from the fault trace and has a more easterly strike. We suggest that the deviations of the basin edge from the thrust fault traces may indicate concealed strands of the thrust or folding associated with the North Frontal thrust. We note, however, that west of the salient, the bench could also be associated with an earlier, Miocene episode of southward-directed thrusting documented by Meisling and Weldon (1989). It is not clear from their cross sections how this would produce the shallow basement bench. In Lucerne Valley, the basin inversion shows pockets of thicker sediment that bound the Coyote anticline (CA in fig. 4), cored by a north-verging thrust and representing northward propagation of the deformation front away from the North Frontal thrust (Pearce and others, 2004).

Other insights from the basin inversion include the nature of the eastern edge of the Lucerne Valley basin, which is nearly straight with a trend of 325°. The eastern edge of the basin fill beneath Lucerne Valley may be bounded by an extension of the Silver Reef fault, as suggested by Surko (2006). The extension of the fault is loosely supported by lineaments in unpublished aeromagnetic data. For the Hesperia basin, a deep, north-northwest-trending trough in the basement surface may represent an erosional channel 3 to 4 km north of the present-day outlet of Deep Creek. If the trough is a channel, its location is surprising because the ancestral Deep Creek drainage is considered the principal tributary of the ancestral Mojave River during the late Pliocene and early Pleistocene (Cox and others, 2003) and is deeply entrenched into the bedrock of the San Bernardino Mountains. If the trough represents a paleochannel, gradient considerations along the Mojave River argue for a pre-Pliocene age or for considerable uplift of the Victorville Narrows and/or subsidence of the Deep Creek area (~700 to 800 m) since the Pliocene. Alternatively, the trough may represent a local structural complication arising from an inferred bifurcation of the thrust and intersection with a northwest-trending fault mapped in the basement (Morton and Miller, 2003). Additional gravity data south of Deep Creek would help ascertain if there is a deep channel issuing from the present-day Deep Creek outlet.

The gravity inversion provides the shape of the Neogene basins along the junction of the North Frontal thrust system and the faults of the Eastern California Shear Zone. Downwarping of the basement surface along the North Frontal thrust can explain the east-west elongate basins; these basins appear to be segmented where dextral faults, such as the Helendale, Old Woman Springs, and Johnson Valley faults, intersect the thrust. These

results cannot differentiate between the ages of the basin fill. We, however, suggest that the inversion gives an upper bound on the thickness of Pliocene sediments in this area.

ACKNOWLEDGMENTS—We thank Dave Miller, Noah Athens, and Mike Sawlan for their comments and suggestions that improved the manuscript.

References

- Aksoy, R., 1986, Geological and Geophysical Investigations along the Helendale Fault Zone in the southern Mojave Desert, California: University of California, Riverside, 96 p.
- Biehler, Shawn, Tang, R.W., Ponce, D.A., and Oliver, H.W., 1988, Bouguer gravity map of the San Bernardino quadrangle, California, California Division of Mines and Geology, scale 1:250,000.
- Briggs, I.C., 1974, Machine contouring using minimum curvature: *Geophysics*, v. 39, p. 39-48.
- California Division of Oil, Gas, and Geothermal Resources, 1982, Oil and Gas Prospect Wells Drilled in California Through 1980: California Division of Oil, Gas and Geothermal Resources Report TR01, 258 p.
- Cox, B.F., Hillhouse, J.W., and Owen, L.A., 2003, Pliocene and Pleistocene evolution of the Mojave River and associated development of the Transverse Ranges and Mojave Desert, based on stratigraphy studies and mapping of landforms and sediments near Victorville, California: Geological Society of America Special Paper 368, p. 1-42.
- Dibblee, T. W. Jr., 1960, Geologic Map of the Apple Valley Quadrangle, San Bernardino County, California: United States Geological Survey.
- Dibblee, T. W. Jr., 1964a, Geologic Map of the Lucerne Valley Quadrangle, San Bernardino County, California: U.S. Geological Survey Miscellaneous Geologic Investigations Map I-426, scale 1:62,500.
- Dibblee, T. W. Jr., 1964b, Geologic Map of the Ord Mountains Quadrangle, San Bernardino County, California: U.S. Geological Survey Miscellaneous Geologic Investigations Map I-427, scale 1:62,500.
- Dibblee, T. W. Jr., 1964c, Geological Map of the Rodman Mountains Quadrangle, San Bernardino County, California: U.S. Geological Survey Miscellaneous Geologic Investigations Map I-430, scale 1:62,500.
- Jachens, R.C., and B.C. Moring, 1990, Maps of the thickness of Cenozoic deposits and the isostatic gravity over basement for Nevada, U.S. Geological Survey Open-File Report 90-404, 15 p.
- Jennings, C.W., and Bryant, W.A., comps., 2010, Fault activity map of California: California Geological Survey Geologic Data Map no. 6, map scale 1:750,000.
- Jennings, C.W., Strand, R.G., and Rogers, T.H., 1977, Geologic map of California: Calif. Div. Mines Geol. Map 14, scale 1:750,000.
- Langenheim, V.E., and Jachens, R.C., 2002, The Emerson Lake body: A link between the Landers and Hector Mines earthquakes, southern California, as inferred from gravity and magnetic anomalies: *Bulletin of the Seismological Society of America*, v. 92, p. 1606-1620.
- Li, Y-G., Henry, T.L., and Leary, P.C., 1992, Seismic reflection constraints on the structure of the crust beneath the San Bernardino Mountains, Transverse Ranges, southern California: *Journal of Geophysical Research*, v. 97, p. 8817-8830.

- Mabey, D.R., 1960, Gravity survey of the western Mojave Desert, California: U.S. Geological Survey Professional Paper 316-D, p. 51-73.
- Matti, J.C., Powell, R.E., and Miller, F.K., 1998, The San Bernardino Mountains of southern California: A Quaternary fold-, thrust-, and tear-fault belt: Geological Society of America Abstracts with Program, v. 30, no., 5, p. 53.
- Meisling, K.E., and Weldon, R.J., 1989, Late Cenozoic tectonics of the northwestern San Bernardino Mountains, southern California: Geological Society of America Bulletin v. 101, p. 106-128.
- Miller, F. K., and Matti, J. C., 2001, Geologic Map of the Fifteen-mile Valley 7.5' Quadrangle, San Bernardino County, California, U.S. Geological Survey Open-File Report 01-132, scale 1:24,000. Available at <http://geopubs.wr.usgs.gov/open-file/of01-132/>.
- Morton, D. M., and Miller, F. K., 2003, Preliminary geologic map of the San Bernardino 30' x 60' quadrangle, California: United States Geological Survey Open-File Report 03-0293, 190 p. Available at <http://pubs.usgs.gov/of/2003/of03-293/>.
- Oberlander, T.M., 1972, Morphogenesis of granitic boulder slopes in the Mojave Desert, California: Journal of Geology, v. 80, p. 1-20.
- Pearce, S.A., Pazzaglia, F.J., and Eppes, M.C., 2004, Ephemeral stream response to growing folds: Geological Society of America Bulletin, v. 116, p. 1223-1239.
- Powell, R. E., and Matti, J. C., 2000, Geologic map and digital database of the Cougar Buttes 7.5' Quadrangle, San Bernardino County, California: United States Geologic Survey Open-File Report 00-175, 34 p. Available at <http://geopubs.wr.usgs.gov/open-file/of00-175/>.
- Sadler, P.M., 1982, Geologic map of the Old Woman Springs 7.5' quadrangle: California Division of Mines and Geology, Plate K, scale 1:24,000.
- Spotila, J. A., and Anderson, K. B., 2004, Fault interaction at the junction of the Transverse Ranges and Eastern California shear zone: a case study of intersecting faults: Tectonophysics, v. 379, no. 1-4, p. 43-60.
- Spotila, J.A., and Sieh, Kerry, 2000, Architecture of transpressional thrust faulting in the San Bernardino Mountains, southern California, from deformation of a deeply weathered surface: Tectonics, v. 19, p. 589-615.
- Subsurface Surveys, 1990, Inventory of groundwater stored in the Mojave River basins: Unpublished report, prepared for the Mojave Water Agency, Apple Valley, California, 47 p. (Subsurface Surveys, Inc., 215 South Highway 101, Suite 203, Solana Beach, CA 92075 USA).
- Surko, T.L., 2006, Gravity survey of the Lucerne Valley groundwater basin: Implications for basin structure and geometry: Master's thesis, California State University, Fullerton, 298 p.
- Telford, W.M., Geldart, L.O., Sheriff, R.E., and Keyes, D.A., 1976, Applied Geophysics: New York, Cambridge University Press, 960 p.

The morphology and anatomy of a Miocene long-runout landslide, Old Dad Mountain, California: implications for rock avalanche mechanics

Kim M. Bishop

Department of Geosciences and Environment, California State University, Los Angeles

Abstract—The Old Dad Mountain area 25 km southeast of Baker, California, exposes an erosionally dissected Miocene terrestrial sedimentary sequence with intercalated megabreccia composed of Paleozoic carbonate. The megabreccia is interpreted to be long-runout rock avalanche deposits. Near the base of the sequence, the stratigraphically lowest megabreccia is exposed a distance of 5 km parallel to bedding. Near the center of the deposit is a hummock 1 km wide and 250 m thick that consists of mostly non-brecciated carbonate, except in the lowest 1 to 3 meters, which is thoroughly brecciated. North and south of the hummock, the megabreccia consists of 10 to 30 m thick deposits that extend approximately 1.5 km northwest and southeast from the hummock. Unlike the hummock, these “wings” of the deposit are brecciated throughout. The geometry of the megabreccia argues against the granular flow model to explain the low apparent friction of rock avalanche landslides. The geometry also argues against the trapped air cushion model.

Introduction

Long-runout rock avalanches, also commonly referred to as sturzstroms, are catastrophic landslides that travel much further than predicted by normal rock-on-rock frictional sliding (Hsu, 1975). The coefficient of friction for rock sliding based on laboratory experiments is typically at or near 0.6. For long-runout rock avalanches, apparent coefficient values typically range between 0.4 and 0.1 (Melosh, 1987). Numerous models have been proposed to explain the low rock avalanche apparent friction values, but no consensus has been reached. The anatomy of a long-runout rock avalanche deposit at Old Dad Mountain, eastern California (Fig. 1) appears to provide insights to understanding the low friction mechanics of rock avalanches.

Miocene sedimentary sequence and interbedded breccia

The Old Dad Mountain area in the eastern Mojave Desert, California exposes a Miocene terrestrial sedimentary and volcanic sequence predominantly consisting of poorly exposed

fanglomerate. Interbedded within the fanglomerate deposits are lesser volumes of volcanic flows, tuffs, lacustrine sediments, and beds of matrix poor breccia (Dunne, 1977), commonly referred to as megabreccia (Longwell, 1951). The Miocene sequence, resting nonconformably on Proterozoic metamorphic rocks, is faulted, tilted, and erosionally dissected. Age of the sequence is constrained from the presence of the 18-19 Ma Peach Springs Tuff

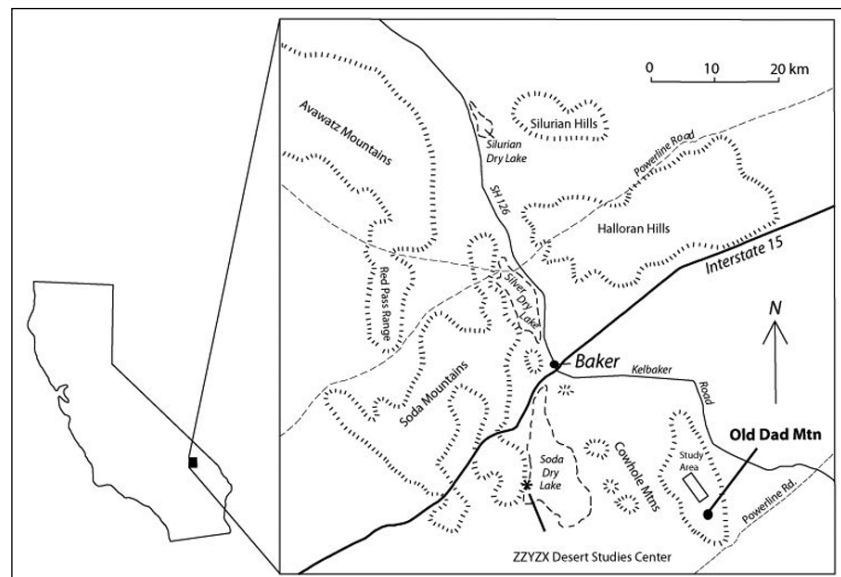


Figure 1. Location map showing Old Dad Mountain area.

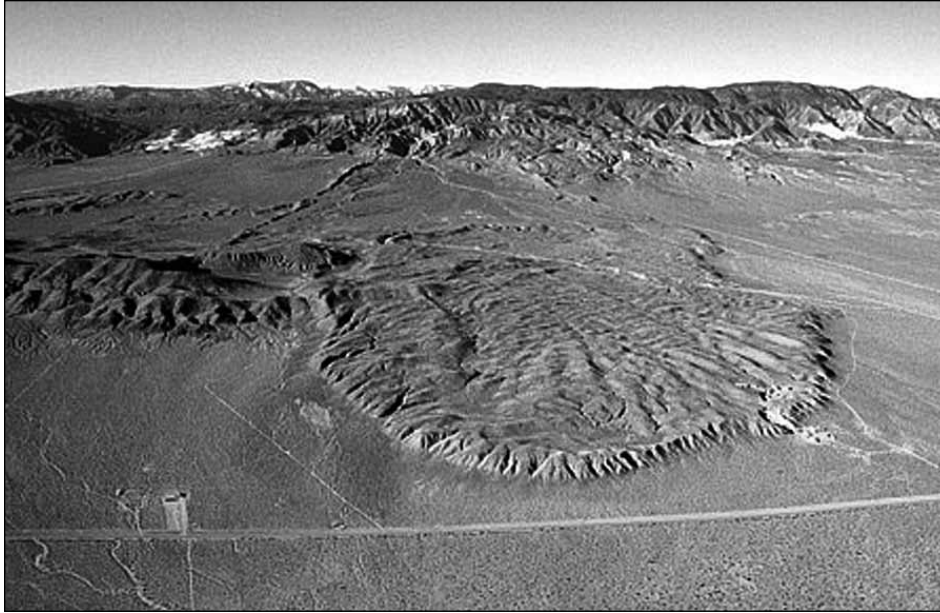


Figure 2. Photo of the Blackhawk landslide. View is to the south with the San Bernardino Mtns. in the background. The landslide runout distance across the relatively flat plain is 8 km and the width of the landslide is 3 km. Photo by Kerry Sieh.

in the lower part of the sequence (Skirvner, 1990). Basin deposition occurred during a period of crustal extension that is mostly understood from study of the contemporary Shadow Valley basin in the Halloran Hills and Kingston Range area 40 km to the north (Friedmann, 1997; Bishop, 1994).

The source area for the clastic detritus of the Miocene sequence is interpreted to be eastward. Direct evidence of transport directions from sedimentologic structures such as cross-bedding and clast imbrication is lacking. However, several lines of evidence suggest an easterly source. First, clasts from the Teutonia batholithic and Delfonte volcanic rock, both of which form basement rock exposed to the east but not to the west, are present within the sequence. Second, the age, structure, and sedimentologic characteristics of the sequence are similar to the Shadow Valley basin sequence exposed 30 km to the north in the Halloran Hills and Kingston Range area. Abundant evidence from the Shadow Valley basin sequence indicates derivation from a highland to the east in the vicinity of the present day Clark and Mescal Ranges (Bishop, 1994).

The megabreccia units within the sedimentary sequence at Old Dad Mountain are interpreted to be rock avalanche deposits on the basis of their morphologic and lithologic characteristics. The most important of these characteristics are overall sheet-like depositional form,

large clast-to-matrix ratio, jigsaw breccias textures, and preservation of source-rock stratigraphy. Each of these characteristics are prominent in rock avalanche deposits (Shaller and Shaller, 1996). An excellent example of a geologically young long-runout rock avalanche that displays all of these characteristics is the Pleistocene Blackhawk landslide (Shreve, 1968) in the southern Mojave Desert (Fig. 2).

The breccia deposits at Old Dad Mountain mostly consist of clasts no larger than 20 centimeters diameter. Breccia clasts consist predominantly of Paleozoic carbonate with a few scattered intrusive igneous clasts. The carbonate clasts

generally are buff to gray, the same colors as the Paleozoic carbonate sedimentary source rock from which they were derived. The breccia exhibits bands of clasts with the same color, which reflects the color banding that existed in the bedrock source from which the breccia was derived. The color banding indicates the breccia clasts did not mix with one another during landslide emplacement, rather the source rock from which the landslides were derived was shattered and the clasts thusly created only slightly displaced from their initial relative position to one another throughout the emplacement process.

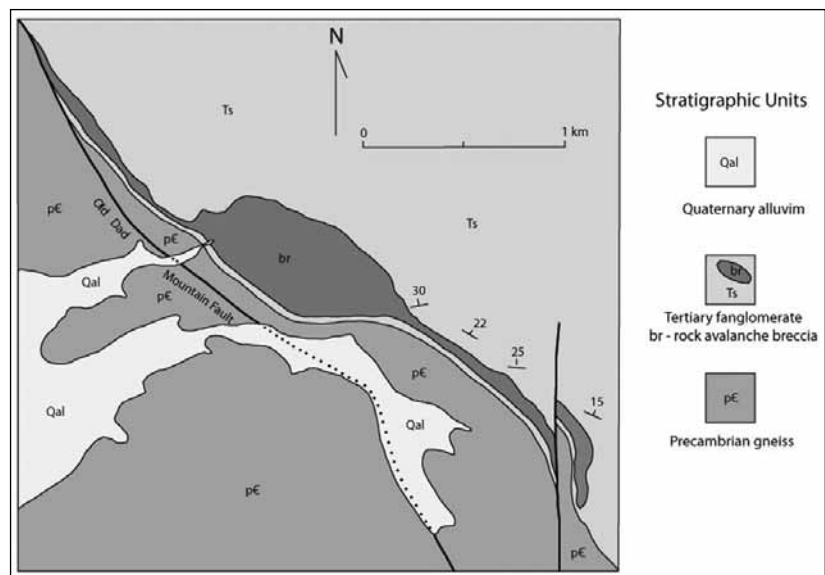


Figure 3. Geologic map of the study area containing rock avalanche breccia interbedded within Miocene sedimentary deposits at Old Dad Mountain.



Figure 4. Photo of the Miocene rock avalanche deposit taken from near the summit of Old Dad Mountain with view toward the northeast. The hummock and southern sheet-like wing of the rock avalanche are well-exposed in the photo.

This “preservation of stratigraphy” has been noted as an important characteristic of brecciated rock avalanche deposits (Shaller and Shaller, 1996; Hsu, 1975; Shreve, 1968). The subject of this paper is the stratigraphically lowest megabreccia deposit, which rests only a few meters above the base of the Miocene sequence (Fig. 3). The reason for focusing on this deposit is that it displays classic features of a long-runout rock avalanches such as those present in the Blackhawk landslide, but also has a distinctive hummock—a type of feature often not found in rock avalanche deposits. Furthermore, erosion dissection has exposed the internal structure of the rock avalanche.

Rock avalanche morphology and anatomy

Outcrops at Old Dad Mountain present an excellent exposure of the morphology and internal structure of the stratigraphically lowest rock avalanche deposit (Fig. 4). As exposed, the deposit is 4 km wide and has a sheet-like form that contains a distinct hummock near the center. A cross-section of the rock avalanche deposit with a reconstructed profile perpendicular to bedding is presented in Figure 5.

The hummock in the center of the deposit is 1 km wide and has a relatively uniform stratigraphic thickness of approximately 250 m. The significantly thinner “wings” that extend from the hummock to the north and south (Fig. 3) are each about 1.5 km long and generally 30 to 60 m thick (Fig. 5). The south wing appears to be cut by the Old Dad Mountain fault (Fig. 3) such that its original length was likely longer.

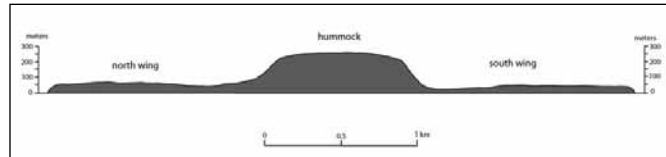


Figure 5. Cross-section of the rock avalanche deposit. Rendering shows the rock avalanche profile drawn with the base restored to horizontal.

Within the megabreccia deposit, the breccia fabric contrasts sharply in the hummock and the thinner wings. The carbonate rock comprising the hummock is mostly non-brecciated (Fig. 6), although localized pockets of breccia up to a few meters across are present. Throughout the wings north and south of the hummock, however, the deposit is everywhere brecciated with breccia clasts generally from 5 to 15 cm in diameter (Fig. 7). Although the hummock is mostly non-brecciated, the basal 1 to 3 m



Figure 6. Photo from the hummock illustrating the predominately non-brecciated character of the hummock rock. Note hammer for scale.



Figure 7. Photo of brecciated wing rock representative of the brecciated nature of the north and south wing rock. Photo taken of breccia in the north wing. Note hammer for scale.

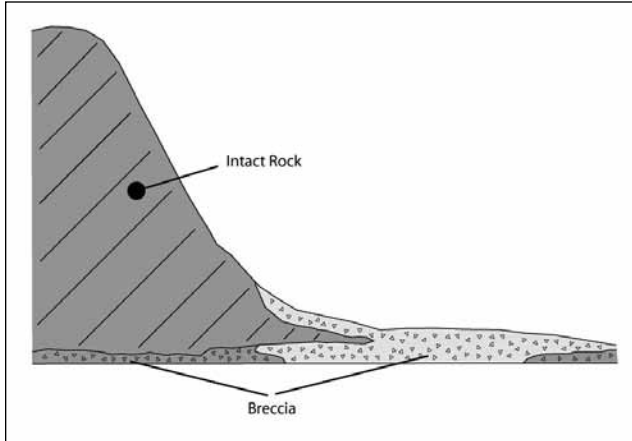


Figure 8. Drawing depicting the transitional nature of the hummock/wing rock from non-brecciated hummock rock to brecciated wing rock. The drawing illustrates that color characteristics of the Paleozoic carbonate interfingers within the transition of the hummock and south wing and indicates that there is no shear zone separating the hummock rock from the wing rock.

of the hummock rock consists entirely of breccia similar to that of the wings.

Study of the transition zone between the hummock and the thin wings extending from the hummock reveals that the zone is transitional from the non-brecciated hummock rock to the thoroughly brecciated wings. Carbonate lithologies of the carbonate within the hummock and those of the adjacent wing material are the same. Furthermore, color-banding in the hummock and the wings interfingers in the transition zone between the two areas (Fig. 8) The importance of this observation is that it indicates there was no significant, if any, shear deformation between the hummock material and the brecciated wing material during emplacement of the avalanche.

Given that the rock avalanche is interpreted to have been derived from the east and to have traveled nearly due west, the erosional cross-section exposed at Old Dad Mountain is believed to be essentially perpendicular to its travel direction. A hypothetical reconstruction based on the deposit outcrop is presented in Figure 9.

Significance of morphology and anatomy

Rock avalanches are catastrophic events during which the landslide is emplaced at velocities of 100 to 300 km/hr (Hsu, 1975). Two well-known deposits are the Blackhawk landslide, approximately 15,000 years old, and the 1881 Elm landslide, Switzerland. Both of these landslides are thoroughly brecciated, sheet-like deposits with clast sizes similar to those present in the wings of the Old Dad Mountain deposit. In contrast to the deposit at Old Dad Mountain, the two deposits lack any significant hummocks. (Shreve, 1968; Heim, 1932).

It is clear that both the Blackhawk and Elm landslides attained their sheet morphology during emplacement. Based on the report by Heim (1932), the bedrock block

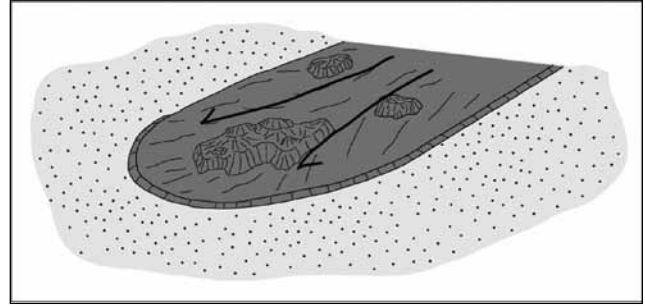


Figure 9. Conceptual diagram of the rock avalanche deposit illustrating the hummock surrounded by the sheet-like portion of the rock avalanche.

that broke loose to form the Elm rock avalanche had a map area of approximately 0.06 km². The area of the final deposit was .45 km², indicating that the landslide mass at its source was on average 7 times thicker than the final deposit. Similarly, the 15 km² Blackhawk landslide deposit was derived from Blackhawk Mountain in an area that measures approximately 2 km², indicating that the source block was on average 7.5 times thicker than the final deposit. The discrepancy between the thicknesses of the source block and final deposits for both the Elm and Blackhawk rock avalanches indicate that the long-runout masses spread horizontally during emplacement. Attenuation owing to horizontal spreading illustrated by the Blackhawk and Elm deposits is a characteristic of rock avalanches (Shaller and Shaller, 1996).

A long-standing controversy regarding rock avalanches is the mechanics by which the landslides attain runout distances that are much greater than predicted by the typical rock-on-rock coefficient of friction determined from laboratory experiments. In attempting to explain the long-runout distances under the assumption that one mechanical process predominates in most or all rock avalanches that causes these the apparent low friction, researchers have proposed two basic categories of models. One proposes that the rock avalanches undergo bulk flow (Campbell et al., 1989; Davies, 1982; Heim, 1932), in which the rock fragments throughout the mass are analogous to the molecules in a dense gas or a fluid (Shaller and Shaller, 1996). In these models, the bulk flow process causes the low apparent friction. The second category of models proposes that some type of basal lubrication decreased sliding friction. Types of proposed lubrication include compressed air (Shreve, 1959), elevated pore water pressure (Johnson, 1978), melted rock (Erismann, 1979), dynamic fragmentation in a zone of basal comminution (Davies et al., 2006), and granular flow within a strongly dilated, high dispersive pressure zone at the base of the rock avalanche (Straub, 1996).

The geometry and internal structure of the rock avalanche at Old Dad Mountain with its large hummock provides evidence to help evaluate whether the bulk flow or basal lubrication models are more likely to be correct.

The presence of the intact rock within the hummock above a basal layer of breccia 1 to 3 meters thick indicates that bulk fluid flow of the rock avalanche mass is not necessary for the apparent low friction behavior. Whatever process operates within rock avalanche breccia to create a low apparent friction of emplacement must have been confined to the basal few meters of the hummock part of the deposit at Old Dad Mountain. The evidence suggests that some sort of basal lubrication rather than bulk flow kinematics operated within the rock avalanche hummock.

As described previously, the gradational nature of the transition zone from the hummock to the wings indicates that the hummock and wing were emplaced without shearing occurring between the moving hummock and wing breccias. This, in turn, requires that the two areas moved in tandem at the same velocities. Given that the low friction process for emplacement of the hummock operated at the base, it is inferred that the same process must have operated in the basal zone of the landslide wings. If a different mechanical process operated in the wings to create low apparent friction, it seems likely that the coefficient of friction would have been somewhat different between the hummock area and the wings, which in turn almost certainly would have caused a difference in emplacement velocities between the hummock and the wings. Velocity differences would have resulted in shearing along a vertical plane between the two areas, which again, the evidence shows did not occur. The simplest explanation is that the same basal zone lubrication process acted in the hummock area and the thinner attenuated wings.

In addition to providing evidence that basal lubrication explains low friction and the concomitant long runout of rock avalanches, the Old Dad Mountain deposit characteristics provides some evidence for the efficacy of the different basal lubrication models. The compressed air cushion model proposed by Shreve (1968) for the Blackhawk landslide does not seem reasonable for the Old Dad Mountain landslide. Given the considerable difference between the thickness of the hummock and the wing areas of the landslide, it would be expected that the difference would create much greater air pressure below the hummock than below the wings. Presumably the air below the hummock would have rapidly flowed laterally and allowed the base of the hummock to contact the substrate surface. The increased friction from such contact would have slowed the hummock area down, which would have created a difference in velocities between the hummock and wing areas. Again, the evidence indicates the hummock and wing areas moved at the same velocity. A similar argument can be raised against the elevated pore water pressure model, although one might counter-argue that dispersal of differential pore water pressure could be retarded by low permeability.

Summary

Rock avalanches are rapidly emplaced landslides that behave with low apparent coefficients of friction. A rock avalanche deposit at Old Dad Mountain contains a large hummock bordered by thin, sheet-like areas (wings) of breccia that took on the sheet-like geometry during landslide emplacement. The hummock and wings were emplaced without significant, if any, differential movement between them. This, in turn, suggests that whatever process acted to create a low apparent coefficient of friction, one of the main characteristics of rock avalanches, was confined to the basal zone. Models that suggest bulk fluid flow as the cause of low friction are not compatible with the geometry of the Old Dad Mountain deposit. Furthermore, of the various basal lubrication models, the air cushion model does not seem compatible with the deposit. With less certainty, the elevated pore water pressure model also does not seem compatible. Given that the base of the hummock is brecciated, the preferred model by me is that strong dispersive stress created by highly energized particles at the base of the rock avalanche explains the low apparent friction.

ACKNOWLEDGEMENTS—The author is grateful for helpful reviews of the manuscript by Nate Onderdonk and Andre Ellis. Appreciation also goes to the ZZYX Desert Studies Center for accommodations during the field study.

References

- Bishop, K.M., 1994, Mesozoic and Cenozoic extensional tectonics of the Halloran and eastern Hills, eastern San Bernardino County, California (unpublished Ph.D. thesis), University of Southern California, Los Angeles, California, 251 p.
- Campbell, C.S., Cleary, P.W., and Hopkins, M., 1995, Large-scale landslide simulations: global deformation, velocities, and basal friction: *Journal of Geophysical Research*, v. 100, p. 8267-8283.
- Davies, T.R., McSaveney, M.J., and Beetham, R.D., 2006, Rapid block glides: slide-surface fragmentation in New Zealand's Waikaemoana landslide: *Quarterly Journal of Engineering Geology and Hydrogeology*, v. 39, p. 115-129.
- Davies, T.R.H., 1982, Spreading of rock avalanche debris by mechanical fluidization: *Rock Mechanics*, v. 15, p. 15-46.
- Dunne, G.C., 1977, Geology and structural evolution of Old Dad Mountain, Mojave Desert, California: *Geological Society of America Bulletin*, v. 88, p. 737-748.
- Erismann, T.H., 1979, Mechanisms of large landslides: *Rock Mechanics*, v. 12, p. 15-46.
- Friedmann, S.J., 1999, Sedimentology and stratigraphy of the Shadow Valley basin, eastern Mojave Desert, California, in Wright, L.A., ed., *Tertiary Basins and Volcanism of the Death Valley Region*: Geological Society of America, Special Paper, v. 333, p. 213-243.
- Heim, A., 1932, *Bergsturz und menschenleben*: Fretz & Wasmuth, A.G., Zurich, 218 p. (English translation by Skermer, N.A., 1991: BiTech Publishers, Vancouver, British Columbia).

- Hsu, K.J., 1975, Catastrophic debris streams (sturzstroms) generated by rockfalls: Geological Society of America Bulletin, v. 86, p. 129-140.
- Johnson, B., 1978, Blackhawk landslide, California, U.S.A., in Voight, B., ed., Rockslides and Avalanches, v. 1: Elsevier Publishing Company, New York, p. 481-504.
- Longwell, C. R., 1951, Megabreccia developed down-slope from large faults: American Journal of Science, v. 249, p. 343-355.
- Melosh, H. J., 1987, The mechanics of large rock avalanches: Geological Society of America Reviews in Engineering Geology, v. VII, p. 41-49.
- Shaller, P. J. and Shaller, A.S., 1996, Review of proposed mechanisms for Sturzstroms (long-runout landslides), in Abbott, P.L. and Seymour, D.C., Sturzstroms and Detachment Faults, Anza-Borrego Desert State Park, California: South Coast Geological Society, Inc., Santa Ana, CA, p. 185-202.
- Shreve, R.L., 1968, The Blackhawk landslide: Geological Society of America, Special Paper 108, 47 p.
- Straub, S., 1996, Self-organization in the rapid flow of granular material: evidence for a major flow mechanism: Geol Rundsch., v. 85, p. 85-91.

The discovery of the California Blue Mine

Rick Kennedy

Earth's Treasures, rick@earthstreasures.com

It was a fall spring day in Yucca Valley and Dave Schmidt had no idea he was about to discover some of the finest aquamarine ever found in California. As he was getting ready to leave, with his metal detector packed in his quad, he called out to his wife, Liz, "Hey honey, I'm off to go find you emeralds and rubies!" What he was really thinking was more along the lines of bullets and bottle caps. Dave didn't go into the mountains to go mineral collecting, he was looking for good sites to metal-detect.

Dave had far more than a layman's knowledge of rocks and minerals, being friends with some of the members of the Orcutt Mineral Society, so it was natural for him to be checking out the rocks as he rode around, looking for places to detect. As he got deeper into a canyon, he decided to go up to an outcrop he had noticed before.

There was something different about the outcrop—it was much whiter than anything else around. He rode as close as he could and then walked, taking time to look at some of the float on the hillside. There were large microcline feldspar crystals, and sheets of biotite and quartz. Although he did not know it at the time, Dave had stumbled onto a pegmatite!

When he made it up to the outcrop, he saw evidence that others had dug here before. A couple of test pits didn't seem very extensive, but some of the pieces of the pegmatite had blue hexagonal crystals. He dug and brought back some samples. He was pretty sure he had just found aquamarine! He contacted a friend in the

Minerals of the California Blue Mine

| | |
|----------------------------|--|
| Quartz var. smokey | SiO_2 |
| Beryl, var. aquamarine | $\text{Be}_3\text{Al}_2\text{Si}_6\text{O}_{18}$ |
| Topaz | $\text{Al}_2\text{SiO}_4(\text{F},\text{OH})_2$ |
| Albite, var. cleavelandite | $\text{NaAlSi}_3\text{O}_8$ |
| Microcline feldspar | KAlSi_3O_8 |
| Fluorite (green) | CaF_2 |
| Apatite (pink) | $\text{Ca}_5(\text{PO}_4)_3(\text{Cl})$ |
| Muscovite | $\text{KAl}_2(\text{Si}_3\text{Al})\text{O}_{10}(\text{OH},\text{F})$ |
| Biotite | $\text{K}(\text{Mg}, \text{Fe})_3(\text{Al}, \text{Fe})\text{Si}_3\text{O}_{10}(\text{OH},\text{F})$ |
| Phlogopite | $\text{KMg}_3\text{Si}_3\text{AlO}_{10}(\text{F},\text{OH})$ |
| Pseudorutile | $\text{Fe}_2\text{Ti}_3\text{O}_9$ |
| Wodginite | $\text{MnSnTa}_2\text{O}_8$ |
| Danalite | $\text{Fe}_4\text{Be}_3(\text{SiO}_4)_3\text{S}$ |

OMS, Ralph Bishop, who confirmed that the mineral was beryl, variety aquamarine. Ralph also got Dave in touch with geologist Mike Hunerlach. Both were very enthusiastic about Dave's find and have been very helpful ever since.

Armed with this new knowledge, Dave and Liz filed a claim on the area, calling it the California Blue Mine. Over time, he exposed several pockets by hand! The list of recovered species includes many excellent specimens of aquamarine, topaz, quartz, orthoclase feldspar, cleavelandite, and fluorite. Excellent crystals of aquamarine and topaz are perched on lustrous cleavelandite and smokey quartz. The metallic oxides pseudorutile and wodginite

are rare, and the black crystal of danalite is unusually large for this rare mineral. A web search did not reveal any other California localities for these three minerals.

Having worked with Dave at the mine, I can personally attest to his work ethic. It may have been a bit of luck mixed with a good general knowledge of rocks and minerals that got him there, but it was hard work that won him the results he has had up to this point. This discovery has taught the author a few things. First, no matter what you are doing, be open and observant. You never know what you will find. Second, there are still new finds to be made in California. Last, hard work prevails where all else fails. .



Geomorphic evolution of the Morongo Valley, California

Frank Jordan, Jr.

John R. Byerly, Inc., Bloomington, California 92316, geo.jordan@gmail.com

Introduction

Morongo Valley is an enigmatic northeast-southwest oriented (N55E) basin located at the boundary between the (Big) San Bernardino Mountains and the Little San Bernardino Mountains in the central portion of southern California. Morongo Valley appears to represent a classic down-dropped graben bounded by normal faults. The northeast terminus of the basin is anchored to the southeast corner of the Mojave Desert. The southwest end of the basin is truncated by a northwest-trending ridge. Normally considered to start at the southwest edge of the Town of Yucca Valley, geomorphologically, the northeast portion of the valley rightfully includes the western portion of the Town, up to around Avalon Avenue. The northeast trend of the valley is almost perpendicular to the northwest strike of the Mission Creek and Mill Creek Branches of the San Andreas fault. The presence of a unique *tensional* graben **within** the combined terranes of the overall *compressional* Big and Little San Bernardino Mountains presents a dilemma best addressed using the tool of geomorphology.

Geology and faulting

The geology and faulting of the Morongo Valley area have been previously mapped by Riley and Moyle (1960), Dibblee (1967a, 1967b, 1968b), Hope (1969), Proctor (1973), Baird *et al.* (1974), Ehlig (1977), Farley (1979), Marcus (1982), Clark *et al.* (1984), Grimes (1986, 1987), Matti *et al.* (1982a, 1982b, 1985, 1992), Jennings (1974, 1977, 1992, 1994), Jennings *et al.* (2010), Jennings and Bryant (2010), Bryant (2005), Rogers (1969), Bortugno and Spittler (1986), Ziony and Jones (1989), Hopson (1998), Plesch and Shaw (2002), Plesch *et al.* (2007), Morton and Miller (2003a, 2003b, 2006). Grimes (1987) provided detailed mapping of a portion of the Morongo Valley fault zone as part of his Master's Thesis at Cal State University, Los Angeles.

The valley is mapped as asymmetrically bounded by the Morongo Valley fault on the southeast and the Pinto Mountain fault on the northwest. The Morongo Valley fault is mapped as the bounding fault along the southeast margin of the valley. The fault strikes N55E, parallel to the valley itself. Grimes (1987) mapped the fault as extending into the southwestern portion of Yucca Valley. The fault displays primarily normal offset (Grimes, 1987). The Pinto Mountain fault strikes east-west between Yucca Valley and Twentynine Palms (Bader and Moyle, 1960; Dibblee, 1967a, 1967b, 1968b; Lewis, 1972; Hatheway,

1975; Hopson, 1998). At the northeast end of the Morongo Valley, the fault is mapped striking approximately N65W and is shown as the bounding fault along the northwest edge of Morongo Valley. Midway through Morongo Valley, the Pinto Mountain fault is mapped as entering the foothills of the Big San Bernardino Mountains with a more westerly strike. The fault is mapped as truncated by the Mill Creek Branch of the San Andreas fault on the previous geologic maps. The State of California, County of San Bernardino, and Town of Yucca Valley recognize portions of both faults as potentially active faults and includes traces of the faults within Alquist-Priolo Earthquake Fault Zones (California Division of Mines and Geology, 1974a, 1974b, 1993a, 1993b), County Fault Hazard Zones (San Bernardino County, 1989, 2003), and Town Fault Hazard Zones (1995).

At the Rockaway Avenue water tank stop, the mapped trace of the Morongo Valley fault is located about 1,000 feet (300 meters) south of the stop, along the southeast edge of Highway 62 and the toe of northwest-facing slope of the Little San Bernardino's (Bryant, 2005; USGS, 2007, 2008a; Frankel *et al.* 2002). The mapped traces of the main Pinto Mountain fault are located about 2,000 feet (600 meters) northwest of the stop, running along the toe of southeast-facing slope of the Big San Bernardino's (Bryant, 2005; USGS, 2007, 2008a; Frankel *et al.* 2002). The USGS and CGS disagree over the actual location of the main trace of the fault in this area. Both agree, though, that a branch of the fault is located approximately 1,250 feet (380 meters) east of the tank, crossing through the housing tract east of the tank, near the intersection of Rockaway Avenue and Whitney Avenue. Both this splay of the Pinto Mountain fault and the Morongo Valley fault are included within Alquist-Priolo Earthquake Fault Zones by CGS (California Division of Mines and Geology, 1974a, 1993a, 1993b). Curiously, the main traces of the Pinto Mountain fault north of the site, as mapped by CGS and the USGS, are not included within Alquist-Priolo Fault Zones. The western portion of the fault zone, west of Yucca Valley, is also excluded from the State's Alquist-Priolo Fault Zone mapping.

In addition to the three recognized branches of the Morongo Valley and Pinto Mountain faults, review of digital aerial photography available through Google Earth Pro (2012), Microsoft's Bing 3D (2011), and NASA's World Wind (2011) suggests that additional splays of the Pinto Mountain fault bracket both the north and south sides of the water tank. Review of the aerial photography



Figure 1: View of Morongo Valley (Google Earth Pro, 2012)

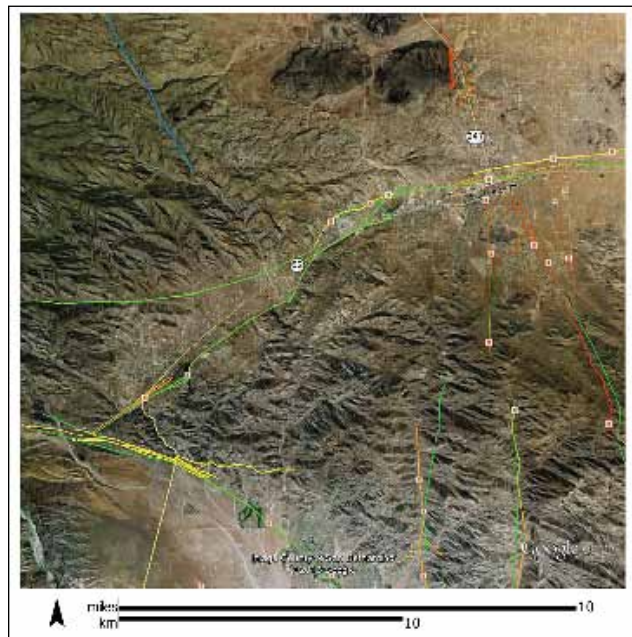


Figure 2: View of Morongo Valley. (Google Earth Pro, 2012)

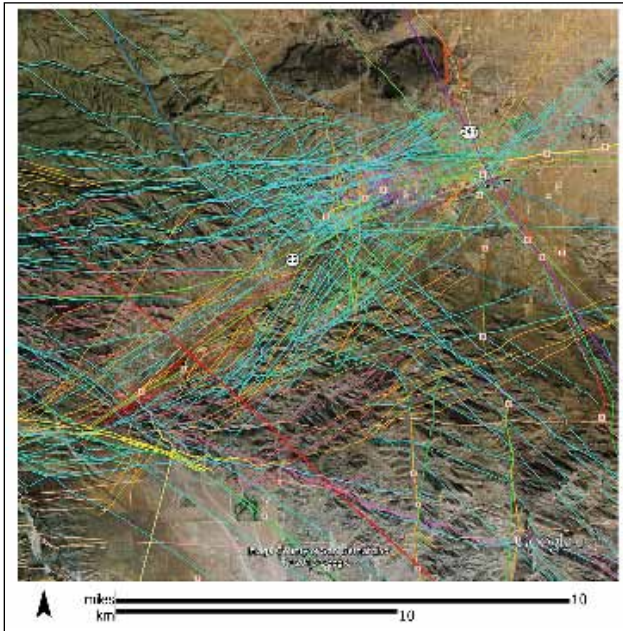


Figure 3: View of Morongo Valley with faults and lineaments (Google Earth Pro, 2012)

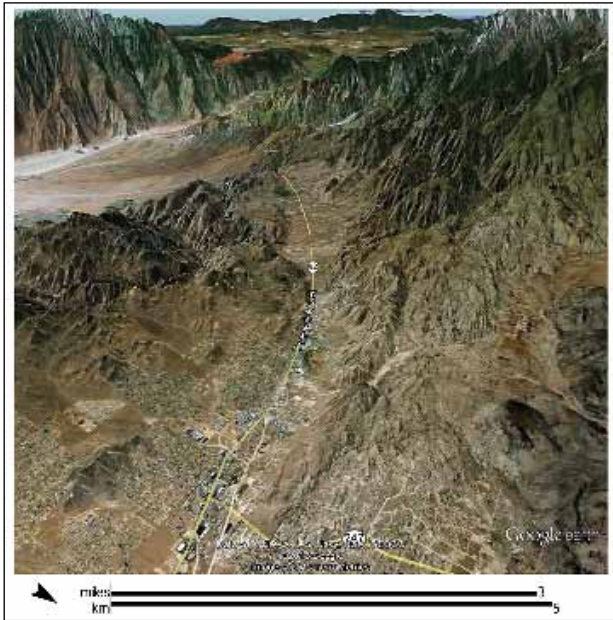


Figure 4: View of Morongo Valley, view to southwest (Google Earth Pro, 2012)

identifies a northwest-facing scarp extending from the southwest end of the mapped Morongo Valley fault out to at least the Mission Creek fault. This scarp is considered to represent the actual continuation of the main trace of the main Morongo Valley fault along the southeast side of the valley. An additional branch of the Morongo Valley fault is also identifiable running along the northwest side of Highway 62 on the aerial photography.

The generally symmetrical geomorphology of Morongo Valley suggests that, while the redefined northwest-dipping Morongo Valley fault accommodates most of the normal-sense of offset along the southeast side of the valley, the Pinto Mountain fault, as currently

mapped, would not appear to accommodate most of the normal movement along the north side of the valley. The Pinto Mountain fault, over most of its archetypal length, is mapped as a predominantly west-trending, left-lateral, strike-slip fault. Paleoseismic studies from fault trenches along the Pinto Mountain fault determined a slip rate of 2.5 millimeters/year (mm/yr) for the strike-slip portion of the fault (Anderson, 1979; Peterson and Wesnousky, 1994; Cao *et al.*, 2003). The Pinto Mountain fault, east of Yucca Valley, is recognized as forming the southern boundary of the Mojave Desert Province (Crowell, 1968; Dibblee, 1968b). The change in strike, mapped starting at the east end of Yucca Valley, is uncharacteristic of the

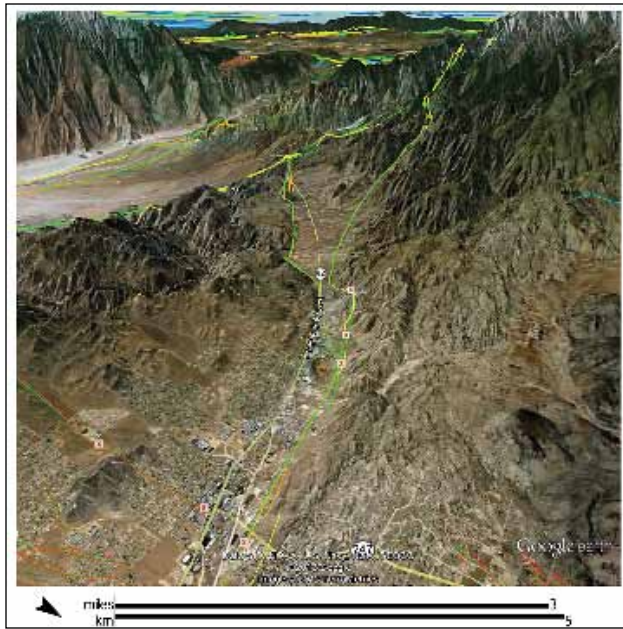


Figure 5: View of Morongo Valley, view to southwest with faults (Google Earth Pro, 2012)

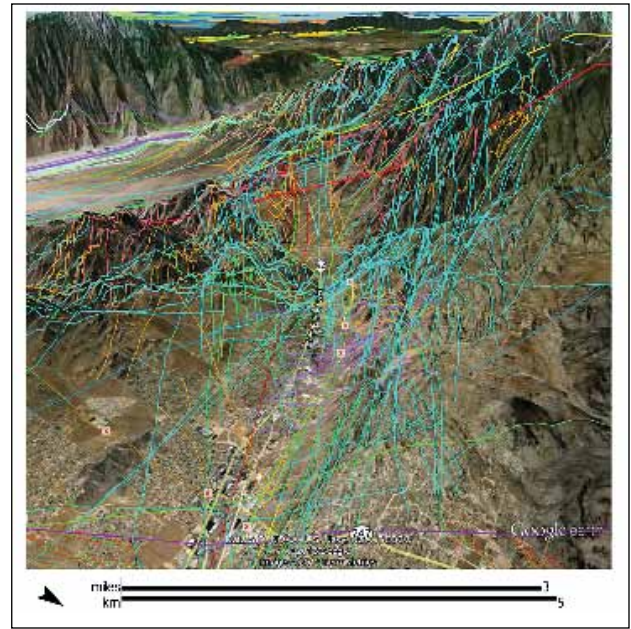


Figure 6: View of Morongo Valley, view to southwest with faults and lineaments. (Google Earth Pro, 2012)

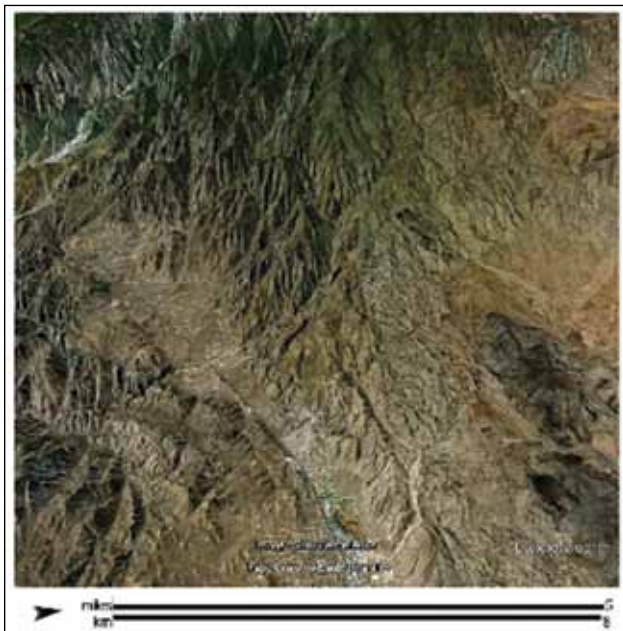


Figure 7: View of Morongo Valley, view to west (3 x vertical exaggeration). (Google Earth Pro, 2012)



Figure 8: View of Morongo Valley, view to west with SW-failing landslides. Google Earth Pro, 2012)

majority of the fault, as is the abrupt change in motion to a normal fault. These changes to the Pinto Mountain fault have been attributed to the presence of Morongo Valley, begging the question, “Does the valley control the geomorphology of the fault or does the fault control the shape of the valley?” The proper answer, geomorphologically, is that tectonophysics controls both. The southwestern portion of Morongo Valley proper has a relatively symmetrical shape, similar in width and form to the northeastern portion of the valley. Review of the aerial photography suggests that a previously unrecognized southeast-dipping branch of the Morongo Valley fault

zone accommodates normal movement along most of the northwest edge of the valley.

The western portion of the Pinto Mountain fault is mapped curving to the south through Yucca Valley, then curving to the north within Morongo Valley, eventually curving south again to intersect with the Mill Creek branch of the San Andreas fault (Allen, 1954, 1957; Dibblee, 1968a; Crowell, 1975; Matti *et al.*, 1982a, 1982b; Rasmussen and Reeder, 1986). The northward curve in the fault has been attributed to drag of the western portion of the fault by right-lateral offset along the Mill Creek-Mission Creek fault. Both southward bends in the

Pinto Mountain fault, however, argue against the physics of this drag, as does the unbent, straight-line projection of the Morongo Valley fault. Review of the digital aerial photography suggests that the western extension of the Pinto Mountain fault continues out of Yucca Valley and on to the west, producing linear, east-trending canyons north of Kitching Peak. The semi-circular fault consistently mapped as the westernmost portion of the Pinto Mountain fault appears to be a separate, normal fault more properly related to the Dillon shear zone (Rogers, 1969). Several curved canyons on the northwest side of Morongo Valley appear to correlate well with northwest-trending canyons southeast of the valley, separated only by the down-dropped graben. The currently mapped, curved, western portion of the Pinto Mountain fault probably developed in response to extensional (gravitational) stresses induced by the incipient, tensional pull-a-part of the Coachella Valley. Geomorphically, west-trending lineaments, saddles, aligned canyons, left-laterally offset drainages, and left-laterally offset terranes suggest that the western extension of the Pinto Mountain fault may traverse north of Kitching Peak and form the east-west trend of San Gorgonio Canyon, northwest of Burro flats. The presence of a similar west-trending alignment of canyons, saddles, and lineaments along the uplifted face of the north flank of the Big San Bernardino Mountains suggests that the original western extension of the Pinto Mountain fault, as well as the northern boundary of the mountains, may have been right-laterally offset approximately 9 miles (14 kilometers) to the northwest by the Landers-Johnson Valley fault zone Nur *et al.* (1993).

Several northwest-trending lineaments suggest that branches of northwest-striking faulting pass up the canyon just west of the water tank, as well as just east of Rockaway Avenue. These northwest-striking faults appear to be part of a larger, broader Helendale-Pipes Canyon fault zone. The southern end of the Pipes Canyon fault is coincident with the canyon about 2.7 miles (4.4 kilometers) down Morongo Grade from the water tank (Rogers, 1969; Bortugno, 1986; Bortugno and Spittler, 1986). Additional northwest-trending lineaments viewed on the aerial photography suggest that the eventual site of the valley was formerly traversed by numerous northwest-striking splays of the San Andreas fault zone. In this model, faulting originating from the Garnet Hill and Banning branches of the San Andreas fault zone splay off to form the Mission Creek, "Fawnskin," "Big Bear," Sky Hi Ranch, Helendale-Pipes Canyon, and Landers-Johnson Valley faults, as well as several other as yet unnamed splay faults (Byerly, 2010). The general symmetry of Morongo Valley suggests that the amount of movement along these northwest-striking faults may be low. However, southward propagation of offset along the 1992 Landers fault diminished from 10 feet (3 meters) north of Yucca Valley to zero across the trace of the Pinto Mountain fault in Yucca Valley, then increased to a maximum of 8 inches (20 centimeters) south of Yucca Valley (Treiman, 1992;

Rasmussen and Associates, 1992). The interplay of offset by northwest-striking faults across the east-striking Pinto Mountain fault is not well understood, geomorphically or tectonophysically.

Landsliding

In addition to the faulting, large, deep-seated landslides bracket both sides of the valley, forming the flanks of both the Little and Big San Bernardino Mountains. These landslides, as well as numerous failures within Morongo, Big Morongo, Little Morongo, and Dry Morongo Canyons provide the source materials for the countless debris flows that make up the alluvial fans emanating from the Big San Bernardino Mountains. Smaller, northwest- and southeast-facing triangular facets mark slide failures adjacent to the mapped and unmapped segments of the Morongo Valley fault zone. Larger blocks form the south-failing, rotational landslides that appear to originate from the previously unmapped scarps of the Pinto Mountain fault zone. The largest of these slides forms the eastern margin of Pipes Canyon and appears to have been offset by at least 15 splays of the Pinto Mountain fault zone and/or Dillon shear zone, based on review of the aerial photography. These slides have both buried, and been offset by, numerous fault scarps oriented in several directions. The curvilinear character of the westernmost portion of the Pinto Mountain fault, as well as the parallel to curving character of the faults that make up the Dillon shear zone, suggest that the western portion of the Little San Bernardino Mountains previously experienced gravitational failure to the southwest in response to pull-a-part extension of the upper Coachella Valley. This extension and gravitational failure would have predated the extension and down-dropping of the Morongo Valley.

Drainage morphology

The four major drainages within the valley uncharacteristically cross the valley floor perpendicular to its long axis, rather than flowing along the long axis to the topographical low point at the southern end of the valley. These four drainages are antecedent to formation of the valley. At one point, they all necessarily flowed across the old geomorphic surface etched on top of the ridges both northwest and southeast of the basin. The age of this old surface is not known, but may be related to initial uplift of the Big San Bernardino Mountains (Dibblee, 1971, 1975). Spotila *et al.* (1998) considered the ancient surface developed in the Big Bear region to be 21 to 64 Ma and the similar surface etched onto the San Gorgonio Mountain block to be 14 to 56 Ma. Renewed uplift of the Big San Bernardino Mountains is considered to have started about 1.5 million years ago, coinciding with development of the San Gorgonio structural knot in the San Andreas fault and the inception of movement along the San Jacinto fault (Morton and Matti, 1993).

Flow within the drainages across the valley floor has been sufficient to incise the surrounding mountains and maintain flow paths through the Little San Bernardino Mountains to their debouchments at Desert Hot Springs (Proctor, 1968). The reduction in flow rates of these drainages expected during the Holocene epoch suggests that the slip rate along the Morongo Valley fault is very small, otherwise, the stream flows would have been trapped within the valley and forced to flow southwestward to the topographical low point at the southwest corner of the valley. This corresponds to a low rate of seismicity for faults in the valley (Townley and Allen, 1939; Brune and Allen, 1967; Real *et al.*, 1978; USGS, 2008b, 2008c, 2009a, 2009b, 2009c; 1988, 1992; Goter *et al.*, 1994; EPI, 2009; Byerly, 2010). Renewed uplift of the Big San Bernardino Mountains is considered to have coincided with formation of the San Gorgonio structural knot in the San Andreas fault and movement associated with inception of the San Jacinto fault (Morton and Matti, 1993). Although slip rate data for the Morongo Valley fault, if determined, may be closely held from any previous paleoseismic studies conducted along the fault, the symmetrical shape of the valley suggests that the slip rates along the Morongo Valley fault zone (both the mapped southwestern and inferred northwestern branches) are similar, probably on the order of 0.5 millimeter per year or less.

Conclusions

Geomorphology allows for a more complete picture of the evolution of the Morongo Valley. The timing of opening of the valley postdates several tectonic occurrences in the area, including formation of the Mojave Desert, originations of the Pinto Mountain and San Andreas faults in the southern desert, combined uplift of the Little and Big San Bernardino Mountains, formation of the geomorphic surface across the combined uplift, extension of the Coachella Valley, subsequent formation of the Dillon shear zone and gravitational failure of the blocks in the Little San Bernardino Mountains towards the Coachella Valley, renewed uplift of the Big San Bernardino Mountains and the northwest portion of the Little San Bernardino Mountains and incision of the Morongo Valley stream courses across the west end of the Little San Bernardino Mountains. Extensional pull-a-part enables down-dropping along splays of the Morongo Valley fault, both on the southeast and northwest sides of the Valley. Subsequently, large landslides fail from the foothills into the valley, allowing the valley's stream courses to deposit large fans of alluvium transversely across the long axis of the valley. The southwestern end of the valley appears to have been offset by a branch of the Mission Creek (or Mill Creek) fault, causing a truncated, rhombohedral shape to the southwest end of the valley. The ability of the relatively small, perennial streams to maintain incision rates through the Little San Bernardino Mountains, in conjunction with the low rate of seismicity detected in the valley,

and the symmetrical shape of the valley suggest that the rate of offset along the Morongo Valley fault zone is low (less than 0.5 mm/yr.) and equally distributed across the northwest and southeast edges of the basin.

References

- Allen, C.R. (1954). "Geology of the north side of San Gorgonio Pass, Riverside County." *in* Jahns, R.H., ed., "Geology of southern California." California Division of Mines and Geology Bulletin 170, Map Sheet No. 20, 1" = 1 mile.
- Allen, C.R. (1957). "San Andreas fault zone in San Gorgonio Pass, southern California." *Geological Society of America Bulletin* 68 (3): 315-350.
- Anderson, J.G. (1979). "Estimating the seismicity from geologic structure for seismic-risk studies." *Bulletin of the Seismological Society of America* 69 (1): 135-158.
- Bader, J.S. and Moyle, W.R., Jr. (1960). "Data on water wells and springs in the Yucca Valley-Twenty-nine Palms Area, San Bernardino and Riverside Counties, California." California Resources Agency, Department of Water Resources Bulletin 91-2.
- Baird, A.K., Morton, D.M., Woodford, A.E. and Baird, K.M. (1974). "The Transverse Ranges: A unique petrochemical belt across the San Andreas fault system." *Geological Society of America Bulletin* 85: 163-174.
- Bortugno, E.J. (1986). "Map showing recency of faulting, San Bernardino quadrangle, California" *in* Bortugno, E.J., and Spittler, T.E., (compilers) (1986) "Geologic map of the San Bernardino Quadrangle." California Resources Agency, Department of Conservation, Division of Mines and Geology, Regional Geologic Map Series, Map No. 3A, Scale: 1" = 4 miles.
- Bortugno, E.J., and Spittler, T.E. (compilers) (1986). "Geologic map of the San Bernardino Quadrangle." California Resources Agency, Department of Conservation, Division of Mines and Geology, Regional Geologic Map Series, Map No. 3A, Scale: 1" = 4 miles.
- Brune, J.N., and Allen, C.R. (1967). "A micro-earthquake survey of the San Andreas fault system in Southern California." *Seismological of the Seismological Society of America Bulletin* 57: 277-296.
- Bryant, W.A. (compiler) (2005). "Digital database of Quaternary and Younger Faults form the Fault Activity Map of California, version 2.0." California Resources Agency, Department of Conservation, Geological Survey website: http://www.consrv.ca.gov/CGS/information/publications/Pages/QuaternaryFaults_ver2.aspx.
- Bryant, W.A. and Hart, E.W. (2007). "Fault-rupture hazard zones in California, Alquist-Priolo Earthquake Fault Zoning Act with index to Earthquake Fault Zones maps, interim revision." California Resources Agency, Department of Conservation, Geological Survey Special Publication, SP 42, 42 p.
- Byerly, John R., Inc. (2010). "Digital Fault and Earthquake Epicenter Map of California." John R. Byerly, Inc. software. California Division of Mines and Geology (July 1, 1974a). "Alquist-Priolo Earthquake Fault Zones Map (formerly Special Studies Zone Map), SE ¼ Morongo Valley Quadrangle, Official Map." California Resources Agency, Department of Conservation, Division of Mines and Geology, Scale: 1" = 2,000'.

- California Division of Mines and Geology (July 1, 1974b). "Alquist-Priolo Earthquake Fault Zones Map (formerly Special Studies Zone Map), SW ¼ Morongo Valley Quadrangle, Official Map." California Resources Agency, Department of Conservation, Division of Mines and Geology, Scale: 1" = 2,000'.
- California Division of Mines and Geology (July 1, 1993a). "Alquist-Priolo Earthquake Fault Zones Map (formerly Special Studies Zone Map), Yucca Valley North Quadrangle, Revised Official Map." California Resources Agency, Department of Conservation, Division of Mines and Geology, Scale: 1" = 2,000'.
- California Division of Mines and Geology (July 1, 1993b). "Alquist-Priolo Earthquake Fault Zones Map (formerly Special Studies Zone Map), Yucca Valley South Quadrangle, Revised Official Map." California Resources Agency, Department of Conservation, Division of Mines and Geology, Scale: 1" = 2,000'.
- Cao, T., Bryant, W.A., Rowshandel, B., Branum, D., and Wills, C.J. (2003). "The revised 2002 California probabilistic seismic hazards maps, June, 2003." California Resources Agency, Department of Conservation, Geological Survey Webpage: http://www.conservation.ca.gov/cgs/rghm/psha/fault_parameters/pdf/Documents/2002_CA_Hazard_Maps.pdf
- Clark, M. M., Harms, K.K., Lienkaemper, J.J., Harwood, D.S., Lajoie, K.R., Matti, J.C., Perkins, J.A., Rymer, M.J., Sarna-Wojcicki, A.M., Sharp, R.V., Sims, J.D., Tinsley III, J.C., and Ziony, J.I. (1984). "Preliminary slip-rate table and map of late-Quaternary faults of California." U.S. Department of the Interior, Geological Survey Open-File Report, OFR 84-106, Preliminary Report.
- Crowell, J.C. (1968). "Movement histories of faults in the Transverse Ranges and speculations on the tectonic history of California." in "Proceedings of Conference on Geologic problems of the San Andreas fault system," Stanford University, p. 323-341.
- Crowell, J.C. (1975). "The San Andreas fault in southern California," in Crowell, J.C. (editor) "San Andreas fault in southern California, a Guide to San Andreas fault from Mexico to Carrizo Plain." California Resources Agency, Department of Conservation, Division of Mines and Geology Special Report, SR 118, p. 7-27.
- Dibblee, T.W., Jr. (1967a). "Geologic map of the Morongo Valley Quadrangle, San Bernardino and Riverside Counties, California." U.S. Department of the Interior, Geological Survey Miscellaneous Geologic Investigations Map, I-517, Scale: 1" = 1 mile.
- Dibblee, T.W., Jr. (1967b). "Areal geology of the western Mojave Desert, California." U.S. Department of the Interior, Geological Survey Professional Paper, PP 522, Scale: 1" = 2 miles.
- Dibblee, T.W., Jr. (1968a). "Displacement of the San Andreas fault system in the San Gabriel, San Bernardino, and San Jacinto Mountains, southern California," in Dickinson, W.R., and Grantz, A., (editors) "Conference of geological problems of San Andreas fault system." Proceedings, Stanford University Publications, Department of Geological Sciences II: 260-276.
- Dibblee, T.W., Jr. (1968b). "Evidence of major lateral displacement on the Pinto Mountain fault, southeastern California." Geological Society of America Special Paper, SP 115, p. 322.
- Dibblee, T.W., Jr. (1971). "Geologic environment and tectonic development of the San Bernardino Mountains, California." Geological Society of America Abstracts with Programs 3 (2): 109-110.
- Dibblee, T.W., Jr. (1975). "Late Quaternary uplift of the San Bernardino Mountains on the San Andreas and related faults," in Crowell, J.C., (editor) (1975) "San Andreas fault in southern California, a guide to San Andreas fault from Mexico to Carrizo Plain." California Resources Agency, Department of Conservation, Division of Mines and Geology Special Report, SR 118, p. 127-135.
- Ehlig, P.L. (1977). "Structure of the San Andreas fault zone in San Geronio Pass, southern California." Geological Society of America Abstracts with Programs 9 (4): 516.
- EPI SoftWare (2009). "Unpublished earthquake epicenter compiler." EPI SoftWare.
- Farley, T. (1979). "Geology of a part of northern San Geronio Pass, California." California State University, Los Angeles, unpublished Master's Thesis.
- Frankel, A., Petersen, M., Mueller, C., Haller, K., Wheeler, R., Leyendecker, E., Wesson, R., Harmsen, S., Cramer, C., Perkins, D., and Rukstales, K. (2002). "Documentation for the 2002 Update of the National Seismic Hazard Maps." U.S. Department of the Interior, Geological Survey Open-File Report OFR-2002-0420.
- Gibson, R.G. (1964). "Geology of a portion of the Mill Creek area, San Bernardino County, California." University of California, Riverside, Unpublished M.S. Thesis.
- Google Earth (2012). "Google Earth Pro." Google. Digital aerial photography dated September 16, 2011.
- Goter, S.K. (1988). "Seismicity of California, 1808-1987." U.S. Department of the Interior, Geological Survey Open-File Report, OFR 88-286, Scale: 1" = 16 miles.
- Goter, S.K. (1992). "Southern California Earthquakes." U.S. Department of the Interior, Geological Survey Open-File Report, OFR 92-533, Scale: 1" = 6 miles.
- Goter, S.K., Oppenheimer, D.H., Mori, J.J., Savage, M.K., and Masse, R.P. (1994). "Earthquakes in California and Nevada." U.S. Department of the Interior, Geological Survey Open-File Report, OFR 94-647, Scale: 1" = 16 miles.
- Green, S.M. (1983). "Seismotectonic study of the San Andreas, Mission Creek, and Banning fault system." University of California, Los Angeles, unpublished M.S. thesis: 52 p.
- Grimes, G. (1986). "Sediments adjacent to a portion of the Pinto Mountain fault in the Yucca Valley area of San Bernardino County, California." in Kooser, M.A. and Reynolds, R.E., eds., "Geology around the Margins of the Eastern San Bernardino Mountains." Publications of the Inland Geological Society, V.1, p. 75-76.
- Grimes, G.J. (1987). "Geology at the convergence of the Pinto Mountain fault and Morongo Valley fault, southern California." California State University at Los Angeles Master of Science thesis, 102 pages, Scale: 1" = 1,000'.
- Hatheway, A.W. (1975). "Terminus of the Pinto Mountain fault, near Twentynine Palms, California," Geological Society of America Abstracts with Programs, Cordilleran Section, 71st Annual Meeting.
- Hope, R.A. (1969). "Maps showing recently active breaks along the San Andreas and related faults between Cajon Pass and Salton Sea, California." U.S. Department of the Interior, Geological Survey Open-File Report, OFR 39-130, Scale: 1" = 2,000'.
- Hopson, R.F. (1998). "Quaternary geology and neotectonics of the Pinto Mountain fault, Mojave Desert, southern California." California Geology 51 (6): 3-13.

- Jennings, C.W. (1975). "Fault map of California with locations of volcanoes, thermal springs, and thermal wells." California Resources Agency, Department of Conservation, Division of Mines and Geology Geologic Data Map Series, CDM No. 1, Scale: 1" = 12 miles.
- Jennings, C.W. (1977). "Geologic Map of California." California Resources Agency, Department of Conservation, Division of Mines and Geology Geologic Data Map Series, CDM No. 2, Scale: 1" = 12 miles.
- Jennings, C.W. (1992). "Preliminary fault activity map of California." California Resources Agency, Department of Conservation, Division of Mines and Geology Open-File Report, OFR 92-03, Scale: 1" = 12 miles.
- Jennings, C.W. (1994). "Fault activity map of California and adjacent areas with locations and ages of recent volcanic eruptions." California Resources Agency, Department of Conservation, Division of Mines and Geology California Geologic Data Map Series, CDM No. 6, Scale: 1" = 12 miles.
- Jennings, C.W., with modifications by Gutierrez, C., Bryant, W., Saucedo, G., and Wills, C. (2010). "Geologic map of California." California Resources Agency, Department of Conservation, Geological Survey Geologic Data Map No. 2, Scale: 1" = 12 miles. Accessed at: <http://www.quake.ca.gov/gmaps/GMC/stategeologicmap.html>.
- Jennings, C.W. and Bryant, W.A. (2010). "Fault activity map of California." California Resources Agency, Department of Conservation, Geological Survey Geologic Data Map series, CDM No. 6, Scale: 1" = 12 miles. Accessed at: <http://www.quake.ca.gov/gmaps/FAM/faultactivitymap.html>.
- Lewis, R.E. (1972). "Ground-water resources of the Yucca Valley-Joshua Tree area, San Bernardino County, California." U.S. Department of the Interior, Geological Survey Water Resources Division Open-File Report, OFR 72-234, 51p.
- Marcus, S.M. (1982). "Preliminary mineral resources evaluation of the Geology-Energy-Mineral Resource Area of the Morongo Valley, Eastern Transverse Ranges, California." in Fife, D.L. and Minch, J.A., eds., "Geology and Mineral Wealth of the California Transverse Ranges." South Coast Geological Society, Inc. 1982 Annual Symposium and Guidebook Number 10, Mason Hill Volume, p. 589-602.
- Matti, J.C., Cox, B.F., Obi, C.M., Powell, R.E., Hinkle, M.E., Griscom, A., and McHugh, E.L. (1982a). "Mineral resource potential map of the Whitewater Wilderness Study Area, Riverside and San Bernardino Counties, California." U.S. Department of the Interior, Geological Survey Miscellaneous Field Studies Map, MF-1478, Scale: 1" = 2,000'.
- Matti, J.C., Cox, B.F., Obi, C.M., Powell, R.E., Hinkle, M.E., and Griscom, A. (1982b). "Mineral resource potential of the Whitewater Wilderness Area, Riverside and San Bernardino Counties, California." in Fife, D.L. and Minch, J.A., eds., "Geology and Mineral Wealth of the California Transverse Ranges." South Coast Geological Society, Inc. 1982 Annual Symposium and Guidebook Number 10, Mason Hill Volume, p. 583-588.
- Matti, J.C., Morton, D.M., and Cox, B.F. (1985). "Distribution and geologic relations of fault systems in the vicinity of the Central Transverse Ranges, southern California." U.S. Department of the Interior, Geological Survey Open-File Report, OFR 85-365, 27 p., Scale: 1" = 4 miles.
- Matti, J.C., Morton, D.M., and Cox, B.F. (1992). "The San Andreas fault system in the vicinity of the Central Transverse Ranges Province, southern California." U.S. Department of the Interior, Geological Survey Open-File Report, OFR 92-354, Scale: 1" = 4 miles.
- Microsoft (2011). "Bing Maps 3D." Microsoft Corporation Website: <http://maps.live.com/default.aspx?v=2&cp=44.023938~-99.71&style=h&lvl=4&tilt=-89.875918865193&dir=0&alt=7689462.6842358>.
- Morton, D.M. and Matti, J.C. (1993). "Tectonic synopsis of the San Gorgonio Pass and San Timoteo Badlands areas, southern California." San Bernardino County Museum Association, Spring Quarterly 40 (2): 3-14.
- Morton, D.M. and Miller, F.K. (2003a). "Preliminary geologic map of the San Bernardino 30' X 60' quadrangle, California." U.S. Department of the Interior, Geological Survey Open-File Report, OFR 2003-0293, Scale: 1" = 1.5 miles.
- Morton, D.M. and Miller, F.K. (2003b). "Preliminary geologic map of the San Bernardino 30' X 60' quadrangle, California." in Morton, D.M., and Miller, F.K. (2006), "Geologic map of the San Bernardino and Santa Ana 30' X 60' quadrangles, California." U.S. Department of the Interior, Geological Survey Open-File Report, OFR 2006-1217, Version 1.0, Scale: 1" = 1.5 miles.
- Morton, D.M. and Miller, F.K. (2006). "Geologic map of the San Bernardino and Santa Ana 30' X 60' quadrangles, California." U.S. Department of the Interior, Geological Survey Open-File Report, OFR 2006-1217, Version 1.0, Scale: 1" = 1.5 miles.
- National Aeronautics and Space Administration [NASA] (April 27, 2011). "WorldWind, version 0.6.805.15357." National Aeronautics and Space Administration Website: [worldwind.arc.nasa.gov](http://arc.nasa.gov).
- Nur, A., Hagi, R., and Beroza, G.C. (1993). "The nature of the Landers-Mojave earthquake line." *Science*, 261, p. 201-203.
- Petersen, M.D., and Wesnousky, S.G. (1994). "Fault slip rates and earthquake histories for active faults in southern California." *Bulletin of the Seismological Society of America* 84 (5): 1608-1649.
- Plesch, A., and Shaw, J. H. (2002). "SCEC 3D Community fault model for southern California." *Eos Transactions of the American Geophysical Union* 83 (47), Fall Meeting Supplement, Abstract S21A-0966, and <http://structure.harvard.edu/cfma>.
- Plesch, A., Shaw, J.H., Benson, C., Bryant, W.A., Carena, S., Cooke, M., Dolan, J.F., Fuis, G., Gath, E., Grant, L., Hauksson, E., Jordan, T.H., Kamerling, M., Legg, M., Lindvall, S., Magistrale, H., Nicholson, C., Niemi, N., Oskin, M.E., Perry, S., Planansky, G. Rockwell, T., Shearer, P., Sorlien, C., Suess, M.P., Suppe, J., Treiman, J., and Yeats, R. (2007). "Community Fault Model (CFM) for Southern California." *Bulletin of the Seismological Society of America* 97 (6) 1793-1802.
- Proctor, R.J. (1968). "Geology of the Desert Hot Springs, Upper Coachella Valley area, California." California Resources Agency, Department of Conservation, Division of Mines and Geology Special Report, SR 94.
- Proctor, R.J. (1973). "Major earthquakes and recently active faults in the southern California region, in Moran, D.E., Slosson, J.E., Stone, R.O., and Yelverton, C.A., eds.) *Geology, seismicity and environmental impact.* Association of Engineering Geologists Special Publication, Scale: 1" = 2 miles.
- Rasmussen, G.S., and Reeder, W.A. (1986). "What happens to the real San Andreas fault at Cottonwood Canyon, San Gorgonio Pass, California? In Kooser, M.A., and Reynolds,

- R.E., editors, 1986, *Geology around margins of the eastern San Bernardino Mountains.* Inland Geological Society Publications 1: 57-62.
- Rasmussen & Associates (December 3, 1992). "Subsurface engineering geology investigation of Tract No. 10682-1 and -2, Lots 1-76, immediately south of Onaga Trail, west of Palomar Avenue, Yucca Valley, California." Gary S. Rasmussen & Associates, Inc. Project No. 3141.
- Real, C.R., Topozada, T.R. and Parke, D.L. (1978). "Earthquake epicenter map of California, 1900-1974." California Resources Agency, Department of Conservation, Division of Mines and Geology Map Sheet, MS 39, Scale: 1" = 16 miles.
- Riley, F.S., and Moyle, W.R., Jr. (1960). "Map of the Yucca Valley-Twenty-nine Palms area, California showing reconnaissance geology and locations of wells and springs (includes Warren, Copper Mountain, and Twenty-nine Palms Valleys and parts of means, Ames, Surprise, and Bessemer Valleys)." in Bader, J.S. and Moyle, W.R., Jr. (eds.), "Data on water wells and springs in the Yucca Valley-Twenty-nine Palms Area, San Bernardino and Riverside Counties, California." California Resources Agency, Department of Water Resources Bulletin 91-2, Scale: 1" = 1 mile.
- Riverside County (1976). "General Plan." Envicom.
- Riverside County (1989). "General Plan." Riverside County.
- Riverside County (2003). "RCIP – Riverside County Integrated Plan of the General Plan." Riverside County.
- Rogers, T.H. (1969). "Geologic map of California, Olaf P. Jenkins edition, San Bernardino Sheet." California Resources Agency, Department of Conservation, Division of Mines and Geology, Scale: 1" = 4 miles.
- Rymer, M.J. (2000). "Triggered surface slips in the Coachella Valley area associated with the 1992 Joshua Tree and Landers, California, earthquakes." *Bulletin of the Seismological Society of America* 90 (4): 832-848.
- Sadler, P.M. (1982). "Geology of the NE San Bernardino Mountains, San Bernardino County, California – Fawnskin 7.5 Minute Quadrangle." California Resources Agency, Department of Conservation, Division of Mines and Geology, Open-File Report OFR 82-18 L.A., Plate F, Scale: 1" = 2,000'.
- San Bernardino County (1974). "General Plan."
- San Bernardino County (1979). "General Plan."
- San Bernardino County (1989). "General Plan."
- San Bernardino County (2003). "General Plan."
- Smith, G.A. (2002). "Regional water table (2000) and groundwater-level changes in the Mojave River and the Morongo ground-water basins, San Bernardino County, California." United States Department of the Interior, Geological Survey, Water-Resources Investigations Report WRI 02-4277, website: <http://pubs.usgs.gov/wri/wri024277/>.
- Smith, G.A. and Predmore, S.K. (2000). "Regional water table (1998) and groundwater-level changes in the Mojave River and the Morongo ground-water basins, San Bernardino County, California." United States Department of the Interior, Geological Survey, Water-Resources Investigations Report WRI 00-4090.
- Smith, G.A., Stamos, C.L., and Predmore, S.K. (2004). "Regional water table (2002) and water-level changes in the Mojave River and Morongo ground-water basins, Southwestern Mojave Desert, California." United States Department of the Interior, Geological Survey, Scientific Investigations Report SIR 04-5081, website: <http://pubs.usgs.gov/sir/2004/5081/>.
- Spotila, J.A., Farley, K.A., and Sieh, K. (1998). "Uplift and erosion of the San Bernardino Mountains associated with transpression along the San Andreas fault, California, as constrained by radiogenic helium thermochronometry." *Tectonics*, 17 (3) 360-378.
- Stamos, C.L., Huff, J.A., Predmore, S.K., and Clark, D.A. (2004). "Regional water table (2004) and water-level changes in the Mojave River and Morongo ground-water basins, southwestern Mojave Desert, California." U.S. Department of the Interior, Geological Survey Scientific Investigations Report SIR 2004-5187.
- Townley, S.D. and Allen, M.W. (1939). "Descriptive catalog of earthquakes of the Pacific Coast of the United States 1769 to 1928." *Bulletin of the Seismological Society of America* 29 (1): 297 pgs.
- Treiman, J.A. (1992). "Eureka Peak and Burnt Mountain faults – two "new" faults in Yucca Valley, San Bernardino County, California." in "Landers earthquake of June 28, 1992, San Bernardino County, California, Field Trip Guidebook." Association of Engineering Geologists, Southern California Section, p.19-22.
- United States Geological Survey (2007). "2002 National Seismic Hazard Maps – California Fault Parameters." U.S. Department of the Interior, Geological Survey Webpage: http://gldims.cr.usgs.gov/webapps/cfusion/Sites/qfault/qf_web_search_res.cfm.
- United States Geological Survey (2008a). "Documentation for the 2008 Update of the United States National Seismic Hazard Maps: Appendix I. Parameters for Faults in California." U.S. Department of the Interior, Geological Survey Webpage: <http://pubs.usgs.gov/of/2008/1128/>
- United States Geological Survey (2008b). "Index Map of Recent Earthquakes in California-Nevada Fault Parameters." U.S. Department of the Interior, Geological Survey Earthquake Hazards Program – Northern California Latest Quake Info Webpage: <http://quake.usgs.gov/recenteqs/latest.htm>.
- United States Geological Survey (2008c). "Historic Worldwide Earthquakes." U.S. Department of the Interior, Geological Survey Earthquake Hazards Program – Northern California Latest Quake Info Webpage: <http://earthquake.usgs.gov/regional/world/historical.php>.
- United States Geological Survey (2009a). "California Earthquake History 1769-Present." U.S. Department of the Interior, Geological Survey Earthquake Hazards Program – Southern California Webpage: http://earthquake.usgs.gov/regional/sca/ca_eqs.php.
- United States Geological Survey (2009b). "California Earthquake History." U.S. Department of the Interior, Geological Survey Earthquake Hazards Program, Earthquake Center website: <http://earthquake.usgs.gov/earthquakes/states/california/history.php>
- United States Geological Survey (2009c). "Earthquake Search." U.S. Department of the Interior, Geological Survey Earthquake Hazards Program, Earthquake Center website: <http://neic.usgs.gov/neis/epic/epic.html>
- Yucca Valley (1995). "Safety Element of the General Plan." Town of Yucca Valley.
- Ziony, J.L., and Jones, L.M. (1989). "Map showing the Quaternary faults and 1978-1984 seismicity of the Los Angeles region, California." U.S. Department of the Interior, Geological Survey Miscellaneous Field Studies Map, MF-1964, Scale: 1" = 4 miles.

New records of fish from northern exposures of the Imperial Formation of Riverside County, California

Mark A. Roeder

San Diego Natural History Museum, San Diego, CA 92112, maroeder1731@aol.com

Introduction

In Riverside County, outcrops of the Imperial Formation consist of Late Miocene and Pliocene marine siltstones and sandstones which are evidence of an extension of the ancient Gulf of California (Figure 1) into the northern portion of the Salton Trough, the Coachella Valley, and San Gorgonio Pass.

According to Carreno and Smith (2007), there were at least three Neogene marine incursions into this area of late Middle Miocene, Late Miocene and Pliocene age. Evidence of the earliest incursion, of which no marine sedimentary deposits exist, is based on rare and poorly preserved reworked nannofossils (microfossils) found within the Late Miocene age sediments named Imperial Formation in the Whitewater section near Cabazon, and date to the late Middle Miocene (McDougall et al. 1999). In the San Gorgonio Pass, late Miocene Imperial Formation sections are present near Whitewater, in Lion Canyon near Cabazon and on Garnet Hill near Palm Springs (Figure 2). On the eastern side of the Coachella Valley, Pliocene age Imperial Formation sections (Figure 2) are present at Willis Palms, at the mouth of Pushawalla Canyon and in the northwestern Indio Hills (Powell, et al 2011)2

Recent investigations of two localities in the Imperial Formation at Super Creek near Whitewater and Willis Palm near Thousand Palms, Riverside County, have yielded the first fossil records of fish. The fish remains consist of isolated fish otoliths (earstones) and fish and shark teeth. Fish otoliths, or earstones, are not skeletal elements, but calcium carbonate bodies with distinct



Figure 1. Late Miocene–Pliocene seas of North and Central America.

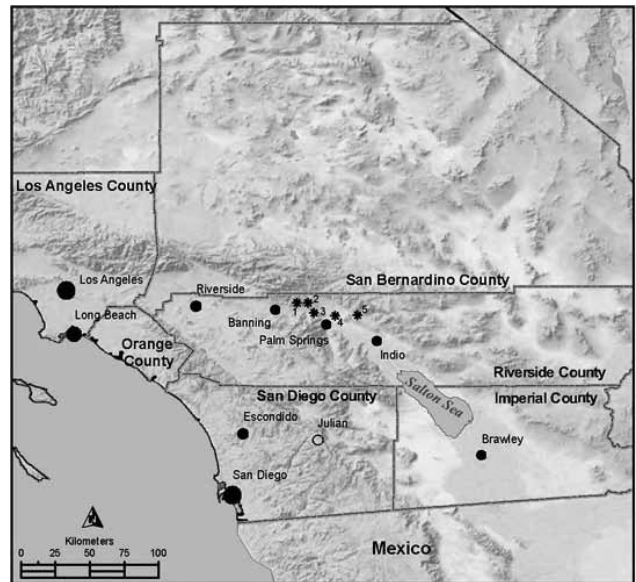


Figure 2. Northern exposures of the Imperial Formation, Riverside County, California. (1) Lion Canyon; (2) Whitewater; (3) Garnet Hill; (4) other sites.

shapes that form in the auditory capsules in the skulls of all Osteichthyes or bony fishes (Nolf 1985). Most actinopterygians, or ray-finned fishes, have three pairs of otoliths, three on each side of the base of the skull. These pairs are called the sacculith (=sagitta), utriculith (=lapillus), and lagenar (=astericus). In most fishes, the sacculith is the largest of the three otolith types. The geometric shape and other structures on the surface of the sacculith are most useful for family, genus, and species identifications.

The modern environmental information, ranges, and other data used in systematic accounts were taken from Castro 1983; Compagno et al. 2005; Eschmeyer and Herald 1983; Fitch and Lavenberg 1968; Goodson 1976,1988; Miller and Lea 1976; Nelson 1976; Randall 1968; Robins and Ray 1986; Thomson and McKibben 1986; Thomson et al, 1987.

Super Creek locality

This locality (University of California, Riverside Geology Department Locality No. 7477) is north of the Banning Fault approximately one-half mile on the east bank of Super Creek where the creek cuts across the generally

NE–SW trending strike of the east dipping Imperial Formation at a slight angle. The abandoned Super Creek Mine is nearby.

The stratigraphy in this area consists of a lower member of the Imperial Formation which is a coarse to medium grained sandstone and conglomerate. This section is about 20 meters thick. Overlying the lower member is a one meter thick “worm tube bed” consisting of fossil marine mollusk (clam and snails) bearing siltstone and sandstone, separating the upper and lower members of the Imperial Formation (Carreno and Smith 2007).

The upper member consists of medium to fine-grained sandstones and siltstones about 75 meters thick.

It is from the “worm tube layer” that the matrix samples were collected and processed for fish remains. The lithology consists of a gray fossiliferous clayey siltstone with a diverse assemblage of marine invertebrates (bryozoans, corals, clams, snails) and fishes. This interval is within the part of the formation known as the “*Callianassa*” (shrimp) (Murphy 1986) or “worm tube” (McDougall 1999) bed because of abundant white calcareous tubes that are actually a gastropod (snail) (Vermetidae, *Thylacodes*) (LaFollette, this volume).

On the basis of foraminifers (microfossils), McDougall et al. (1999) and McDougall (2008) considered the age of this locality to be late Miocene, below but near the Miocene–Pliocene boundary (5.3 million years) and may date from 6.2 to 6.5 million years (McDougall et al. 1999). McDougall (2008) noted that the benthic (bottom-dwelling) foraminifers indicate a rapid increase in water depth from approximately 37 m to 150 m in this stratigraphic interval. However, the tubes of this gastropod, *Thylacodes*, are the most abundant elements of the fauna and this gastropod is known to live only in the intertidal zone (LaFollette, this volume).

The fossil fishes described in this report were collected by the disaggregation of fossiliferous shell-bearing sediments in water, and the water screening of this material through 30-mesh (30 openings per inch) screen boxes. This removed most of the clay, silt and fine sands. The residue or concentrate remaining in the screens was carefully “dumped” on several layers of newspaper to dry in the sun. Once the concentrate was dry, it was gently sifted through three different size sieves (U. S. Standard Sieve Series 12 mesh, 16 mesh, and 20 mesh sieves). Then the concentrate in each sieve was searched for invertebrate and fish remains with the aid of a binocular microscope. In all, over 700 kilograms of matrix from this site were water screened. After the concentrate was picked of fish remains, the fish otoliths and teeth were compared to modern comparative material for identification. The author’s private comparative collection and literature were utilized. Also, Mr. Richard W. Huddleston assisted the author in identification of some of the fish otoliths. At

Table 1. Fish Remains from the Super Creek (UCR 7477) Whitewater, Riverside County, California. Imperial Formation (late Miocene)

| Taxon | Otolith | Tooth |
|---|-----------|----------|
| Atherinidae—silversides | 1 | |
| <i>Bregmoceras</i> —codlet | 1 | |
| <i>Diaphus</i> —headlightfish | 17 | |
| Myctophidae—lanternfish | 1 | |
| <i>Lepophidium</i> —cusk—eel | 12 | |
| Congridae—conger eels | 13 | |
| <i>Apogon</i> —cardinalfish | 1 | |
| <i>Gerres</i> —mojarra | 1 | |
| Gerreidae—mojarras | 1 | |
| <i>Lutjanus</i> —snapper | | 1 |
| Haemulidae—grunts | 1 | |
| <i>Orthopristis</i> —grunt | 1 | |
| <i>Umbrina</i> cf. <i>U. roncadorensis</i> —yellowfin croaker | 1 | |
| Sciaenidae—croakers | 2 | |
| Gobiidae—gobies | 35 | |
| <i>Citharichthys</i> —sanddab | 2 | |
| Balistinae—triggerfishes | | 1 |
| Perciform fishes | 2 | |
| Unknown | 1 | |
| Totals: | 93 | 2 |

least 16 kinds of bony fishes (Table 1) were identified from the Super Creek locality.

Super Creek locality Systematic Accounts

Atherinidae-silversides

These elongate silvery fishes are found in estuarine or marine waters in temperate and tropical seas worldwide (Figure 3). A few species are found in freshwater. Worldwide, there are about 29 genera with 156 species. Today in the northwestern Atlantic there are seven species of silversides, in the Gulf of California eight species, and off California three species (Figure 3)



Figure 3. Silverside.

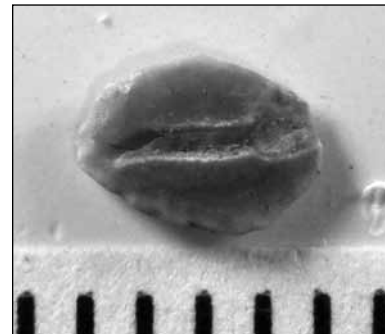


Figure 4. Silverside otolith.

Atherinid— silverside

I compared the Super Creek fossil

otolith (Figure 4) with otoliths from three modern species off California, *Atherinops affinis* (topsmelt), *Atherinopsis californiensis* (jacksmelt), and *Leuresthes tenuis* (California grunion), and one species from the northern Gulf of California, *Colpichthyes regis* (false grunion). None of the species compare well with the fossil atherinid.

Material: left otolith

Bregmacerotidae—codlets

This small relative of cods (usually less than four inches in length) is found in tropical and subtropical seas (Figure 5). Worldwide there is one genus, *Bregmaceros*, with eight species. In the northwest Atlantic, there are at least two species and in the eastern Pacific, one species. Codlets are found from the water surface to 1800 feet. At least one species makes diurnal migrations, living in deep water during the day and migrating to the water surface at night.

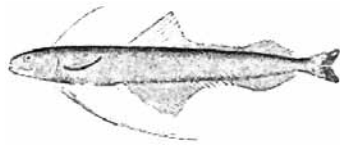


Figure 5. Codlet.

Bregmaceros—codlet

There is only one genus, *Bregmaceros*, in the family Bregmacerotidae. Because of lack of comparative material, the single otolith (Figure 6) was only identified to the genus *Bregmaceros*.

Material: right otolith

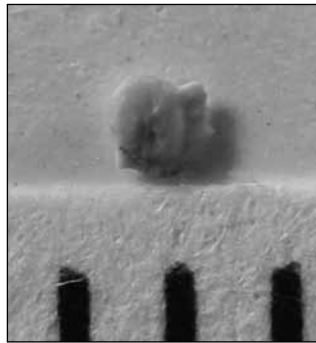


Figure 6. Codlet otolith.

Myctophidae—lanternfishes

Lanternfishes is a large family of small deep sea fishes with light producing photophores. There are about 32 genera and 220 species. Most are oceanic, living at moderate to deep depths during the day and migrating near and to the water surface at night. More than 30 species of lanternfishes belonging to 20 genera inhabit the waters off California.

Diaphus—headlightfish

Today, four species of *Diaphus* inhabit deep waters off California (Figure 7). One species, *Diaphus theta* (California headlightfish) is found from the Gulf of Alaska to Cedros Island, central Baja California,

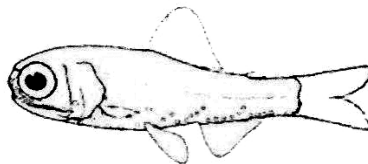


Figure 7. Headlightfish.

Mexico (Fitch 1969). *D. theta* during daylight is found at depths of 1000 feet or more and at night migrates upward within 30 feet of the water surface (Fitch 1968). Fossil otoliths have been reported from localities in the middle Eocene of San Diego and the middle Miocene of Bakerfield (as *Diaphus*) and the Pliocene and Pleistocene of southern California (as *Diaphus theta*) (Fitch 1966).

Until more comparative material becomes available, the fossil otoliths of *Diaphus* (Figure 8) from Super Creek will be assigned to generic level.

Material: 17 otoliths

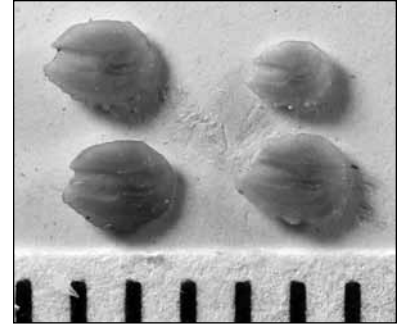


Figure 8. Headlightfish otoliths.

Myctophid—lanternfish

A single fossil lanternfish otolith was recovered. With more comparative material available, identification to genus and/or species level may be possible.

Material: otolith

Ophidiidae—brotulas and cusk-eels

These long tapering fishes (Figure 9) are found in temperate and tropical seas with a few species in fresh-water. Worldwide, there are about ten genera and 35 species of brotulas and cusk-eels. Cusk eels are found in shallow as well as deep marine waters. There are 14 species of cusk-eels in the northwestern Atlantic Ocean, at least two species in the Gulf of California, and five species off California.

Lepophidium—cusk eel

Today, one species, *Lepophidium negropinna* (giant cusk-eel) has not been captured north of Cedros

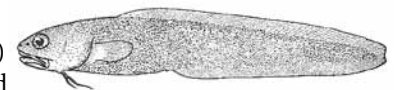


Figure 9. Cusk-eel.

Island, central Baja

California, Mexico (Fitch 1964) and ranges throughout

the Gulf of California to Talara, Peru. The giant cusk-eel is found in shallow water on firm smooth bottoms. Fitch (1970) reported fossil otoliths of *Lepophidium negropinna* from



Figure 10. Cusk-eel otoliths.

localities in the Late Pleistocene (120,000 years ago) Palos Verdes Sand of southern California. There is a second species of *Lepophidium*, *L. stigmatistium*, in the Gulf of California (Aceves-Medina et al. 2003). Until comparative material of this species and other species of *Lepophidium*, becomes available, the Super Creek cusk-eel otoliths (Figure 10) can be only assigned to genus. There may be two species present.

Material: 12 otoliths

Congridae—conger eel

This large family of eels (Figure 11) is found worldwide in tropical waters of all oceans. Congrid eels are found both in shallow and deep water, and usually inhabit burrows on soft bottoms. Worldwide, there are about 38 genera and 100 species.



Figure 11. Conger eel.

Fossil congrid otoliths are extremely abundant in North American Eocene deposits, and are present in later Oligocene and Miocene. However, it is very difficult to distinguish species from otoliths alone (Fitch and Lavenberg 1983). Comparative otolith material from recent conger species is not available, for the most part, because most congrid eels are secretive in their living habits and are rarely collected. Because of this, it is hard to place isolated fossil otoliths in a genus, and fossil conger eel material is usually only identified to family level. Until more comparative conger eel otolith material becomes available, either through papers that illustrate conger otoliths or actual identified conger otoliths, clarification of the fossil record of this family will remain uncertain (Fitch and Lavenberg 1983)

Congrid—conger eel

As part of their study of the Pliocene Yorktown Formation fish otoliths recovered at the Lee Creek Mine, Aurora, North Carolina, Fitch and Lavenberg (1983) noted a number of congrid otoliths. They identified five types of congrid otoliths only to family level and labeled them

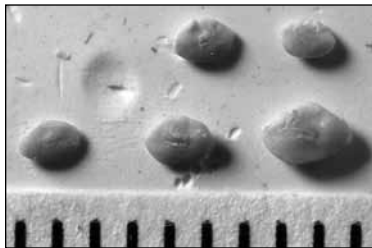


Figure 12. Conger eel otoliths.

Congrid species A through Congrid species E. None of the Super Creek congrids (Figure 12) have any resemblance to Lee Creek Mine Congrid otoliths. There may be at least two kinds of conger otoliths (Figure 12).

Material: 13 otoliths

Apogonidae—cardinalfishes

Cardinalfishes are small (usually less than 4 inches). During the day, these brightly colored fishes (Figure 13) are found hiding in the cracks and crevices of coral reefs, burrows, or empty shells. At night they are active, but rarely seen by underwater divers.

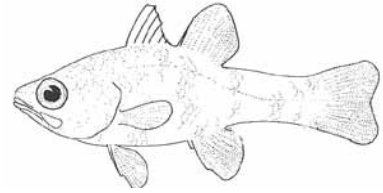


Figure 13. Cardinalfish.

Worldwide, there are 20 genera with about 170 species of cardinalfishes. In the northwestern Atlantic Ocean twenty shallow-water species are known, most of which occur in the Caribbean. Today in the Gulf of California there are four species of cardinalfishes, with only the barspot cardinal fish (*Apogon retrosella*) being common.

Apogon—cardinalfish
The Super Creek fossil otolith (Figure 14) needs to be compared with modern species in order to place it in an existing species or to determine if it is a new species.

Material: left otolith



Figure 14. Cardinalfish otolith.

Gerreidae—mojarras

These small silvery fishes occur in shallow tropical and warm temperate coastal waters off North and South America, and in the western Pacific and Indian Oceans (Figure 15). Although most mojarras are marine, a few enter brackish or freshwater. Usually they are abundant in inshore areas over sand and sand-mud bottoms, but also are found over rocky bottoms with numerous sandy patches. Worldwide, there are seven genera and about 40 species. In the northwestern Atlantic Ocean, there is one species of *Gerres*. There are eight species of

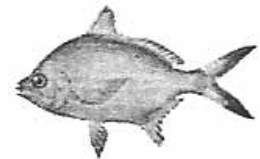


Figure 15. Mojarra.

mojarras in the Gulf of California. There are a few records of two mojarras off southern California



Figure 16. Mojarra otolith.

(*Eucinostomis argenteus*—spotfin mojarra, *E. gracilis*—flagfin mojarra).

Gerres—mojarras

The Super Creek *Gerres* otolith (Figure 16) needs to be compared to otoliths of other modern species of this genus.

Material: right otolith

Lutjanidae—snappers

Snappers are found in marine waters of the Atlantic, Pacific and Indian Oceans, and rarely in estuaries (Figure 17). Lutjanids are usually found in tropical shore waters. Several species are wide-ranging and oceanic, while others inhabit deeper waters or reefs. There are genera and about 230 species. In the northwestern Atlantic Ocean, there are four species, and in the Caribbean at least 18 species. In the Gulf of California, there are nine species of snappers.

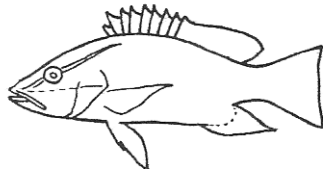


Figure 17. Snapper.

32

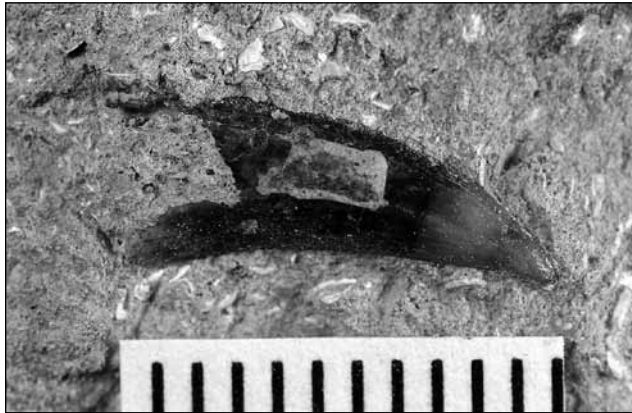


Figure 18. Snapper tooth.

Lutjanus—snapper

A single canine-like jaw tooth was recovered. *Lutjanus novemfasciatus* (dogtooth snapper) has the largest canine of any of the Pacific snapper. And with more comparative material, the isolated fossil snapper tooth (Figure 18) may be identified to this species.

Material: A single “canine” jaw tooth

Haemulidae—grunts

Grunts are found in subtropical and tropical coastal waters of the Atlantic, Indian and Pacific Oceans. A few occur in temperate seas. A small number of species is present in brackish water and few in freshwater. During the day, grunts are found on reefs and other sheltered

areas, while at night they feed over open sandy, muddy and grassy areas. Worldwide, there are twenty-one genera with about 175 species.

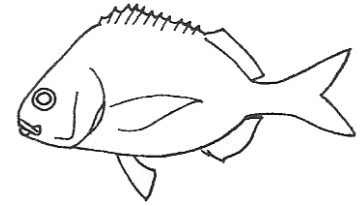


Figure 19. Grunt.

In the northwestern Atlantic, there are 20 species of grunts, while in the Caribbean 17 species are present. In the Gulf of California, there are 25 species (Figure 19).

Orthopristis—grunt

In the Atlantic Ocean, there are two species of the genus *Orthopristis*, *O. chrysoptera* (pigfish) and *O. ruber* (Corocoro), while in the Gulf of California there is one species, *O. reddingi* (bronzestriped grunt), which is present from

Bahia Sebastian Viscaïno, Baja California, Mexico and throughout the Gulf of California. This species is abundant over muddy and sandy bottoms.

With more comparative material, assignment of this otolith (Figure 20) to a modern species or even a fossil species may be possible

Material: left otolith



Figure 20. Grunt otolith.

Sciaenidae—croakers

These elongate, usually silvery fishes are found in Atlantic, Pacific and Indian Oceans in marine and brackish waters. But a few species are found in freshwater, particularly in South America. Croakers are abundant shore fishes in tropical and temperate seas, with fewer species in cold waters. There are 28 genera of sciaenids with about 160 species. In the northwestern Atlantic, there are twenty-two species of croakers, while in the Gulf of California there are 28 species.

Umbrina cf. U. roncadorensis—yellowfin croaker

Today, there are at least two species of *Umbrina* in the Gulf of California (*U. xanti* and *U. roncadorensis*)—yellowfin croaker (Figure 21). The partial fossil otolith compares favorably with

Umbrina roncadorensis



Figure 21. Yellowfin croaker.



Figure 22. Yellowfin croaker otolith.

(Figure 22). In southern California, the yellowfin croaker prefers the very shallow waters in the surfzone, near rocks, in bays and tidal sloughs over sandy bottoms, from the shore to 25 feet. Fossil otoliths of *Umbrina roncadorens* have been recovered from the late Pleistocene of

southern California (Fitch 1970).

Material: partial left otolith

Sciaenid—croaker

Two juvenile croaker otoliths were also recovered, but they are too small to identify to genus or species level.

Material: two otoliths

Gobiidae—gobies

One of the most speciose of fish families, gobies number more than 2000 species worldwide. These very small bottom-dwelling fish are found in marine, brackish, and occasionally freshwater environments (Figure 23). Gobies are found over a wide range of habitats from deep water to high tide pools, and from ocean reefs to hypersaline lagoons. Although most gobies are found on the bottom, some are mid-water swimmers and substrate-burrowing species.



Figure 23. Goby.

In the northwestern Atlantic Ocean, there are at least 79 species of gobies, while the Gulf of California has at least 60 species.

Gobiid—goby

Because of lack of comparative material, the goby otoliths (Figure 24) are only assigned to family level. There may be at least two species.

Material: 35 otoliths

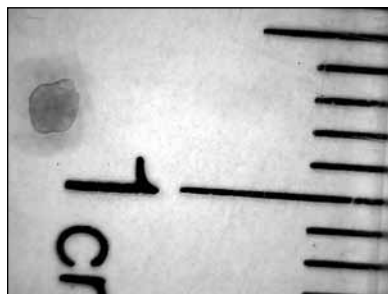


Figure 24. Goby otolith.

Bothidae—lefteye flounders

Lefteye flounders are abundant in temperate and tropical waters with a few species in cold waters. Most

are found in bays, lagoons, and shallow coastal waters with a few species in brackish and freshwater. Worldwide, bothids are found in the Arctic, Pacific and Atlantic Oceans with 41 genera with about 99 species.

Citharichthys—sanddab

In the northwestern Atlantic Ocean, there are five species of *Citharichthys* (sanddabs) and at least three species in the Gulf of California (Figure 25).

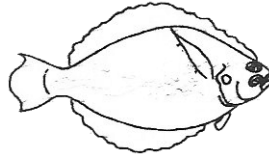


Figure 25. Sanddab.

A comparison with the two species of *Citharichthys* (*C. sordidus*, *C. stigmaeus*) found off California to southern Baja California, Mexico, and with *C. xanthostigma* found off

southern California into the Gulf of California, indicates that Super Creek specimens are not among these species. Today, there are three species of *Citharichthys* (*C. fragilis*, *gordae*, *platophrys*) in the Gulf of California. Schwarzhans (1999) only illustrates otoliths of *C. fragilis*. But the Super Creek specimen (Figure 26) is more like the otoliths of the northwestern Atlantic species, *C. spilopetrus* (bay swift) (Schwarzhans 1999). Until otoliths of *C. gordae* and *C. platophrys*, and other species of *Citharichthys* become available, identification can only be taken to the genus level.

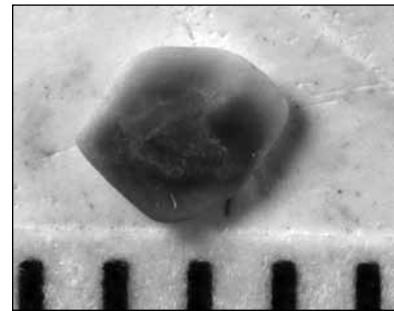


Figure 26. Sanddab otolith

Material: two otoliths

Balistidae—filefishes and triggerfishes

The family Balistidae is sometimes split into two families, filefishes (one or more families) and triggerfishes (one family). Triggerfishes are deep-bodied and compressed fishes with three dorsal spines (Figure 27). The first dorsal spine can be locked in the upright position, deterring predators from attempting to swallow this fish.

Triggerfishes are found in the Atlantic, Pacific, and Indian Oceans with seven genera with 35 species. They occur in

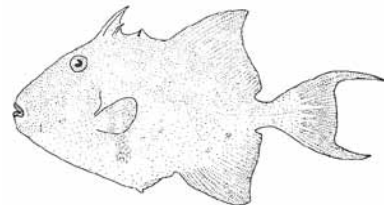


Figure 27. Triggerfish.

warm seas over rocky areas and reefs, but a few are found over soft bottoms. In the northwestern Atlantic Ocean, there are six species of



Figure 28. Triggerfish tooth.

triggerfishes, while in the Gulf of California, two species.

Balistinae—triggerfish

Until more comparative material becomes available, the Super Creek triggerfish tooth (Figure 28) will be assigned to the subfamily, Balistinae

(triggerfishes)

Material: “canine” tooth fragment

Willis Palm locality

This locality (Charles Powell Field Locality CP01172011) is located near Willis Palms Oasis in the Indio Hills, Riverside County, California. The Imperial Formation in this area has been correlated to the Pliocene part of the Imperial Formation to the south in Imperial and San Diego counties (Powell, et al 2011). These deposits may date to 3.1 to 3.2 million years (Powell 1987). Environmental data on extant marine mollusks collected at this site indicate water depth of between 5 and 30 meters in a low-energy, protected, marine environment (Powell, et al 2011). Benthic foraminifers (microfossils) from this site indicate inner neritic (shallow inshore) water depths (0–50m) (Powell, et al 2011).

A section measured consisted of 53 meters of very pale medium to fine-grained sandstone, with three fossil shell-bearing horizons near the base of the unit. A 200-kilogram sample was collected and processed from the third highest bed, which was 15 meters above the base of the

Table 2. List of fish remains from the Willis Palm site (Field Locality CP01172011), Riverside County, California Imperial Formation (Pliocene)

| Taxon | Otolith | Tooth |
|------------------------------------|-----------|-----------|
| <i>Mustelus</i> —smoothhound | | 1 |
| <i>Carcharhinus</i> —requiem shark | | 1 |
| Rhinobatidae—guitarfish | | 1 |
| Dasyatidae—round stingrays | | 1 |
| Myliobatoidea—large stingrays | | 3 |
| <i>Cynoscion</i> —corvina | 5 | |
| Sciaenidae—croakers | 8 | |
| Kyphosidae—sea chubs | | 1 |
| Gobiidae—gobies | 3 | |
| Osteichthys—bony fish | | 2 |
| Totals: | 16 | 10 |

section and consisted primarily of a white shell-bearing oyster bed.

At least three kinds of bony fishes and four kinds of sharks and rays were identified from the Willis Palm locality (Table 2).

Triakididae—smoothhounds

Smoothhounds are small to moderately large sharks that occur in all oceans, usually in temperate and tropical waters. They are mainly continental in range, inhabiting inshore and near shore environments.

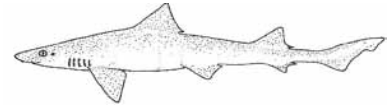


Figure 29. Smoothhound.

Smoothhounds are also common in shallow bays. Worldwide, there are 11 genera with about 35 species. Within the genus *Mustelus* (Figure 29) in the northwestern Atlantic there are at least four species, in the Eastern Pacific eight species, and in the Gulf of California three species.

Mustelus—smoothhound

Fossil teeth of *Mustelus* have been reported from the middle Miocene of Orange County (Lander 2003).

Fossil smoothhound teeth (*Mustelus californicus*—gray smoothhound, *Mustelus henlei*—brown smoothhound) have been reported from the Late Pleistocene Palos Verdes Sand of Orange County, California (Long 1993). The Super Creek tooth (Figure 30) compares favorably to the teeth of the gray smoothhound, but until comparative material of other species of *Mustelus*

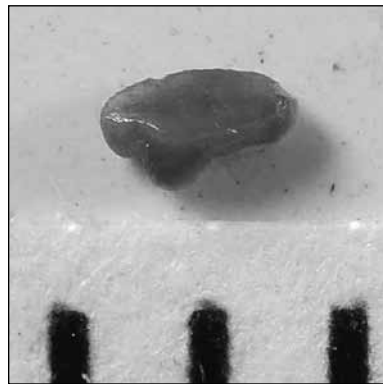


Figure 30. Smoothhound tooth.

from the eastern Pacific and western Atlantic Oceans is available, identification will be to the generic level.

Material: tooth

Carcharhinidae—requiem sharks

Requiem sharks are a large and diverse family of small to large sharks. These sharks are the dominant shark of the tropics and are found in all oceans. A few species are found in cold waters.

Requiem sharks occur on continental shelves, around islands, and on the high seas. Within this family, there are nine genera with about 45 species

Carcharhinus sp.—requiem shark

Within Carcharhinidae, the genus *Carcharhinus* makes up over half of the species of this family (Figure 31). In the northwestern Atlantic Ocean, there are at least 14 species; in the eastern Pacific, there are at least 16 species of *Carcharhinus*; and in the Gulf of California,

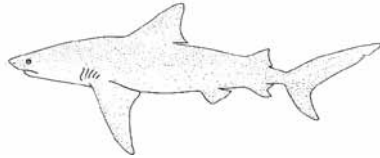


Figure 31. Requiem shark.



Figure 32. Requiem shark tooth.

six species (Kato et al. 1967). Fossil teeth of *Carcharhinus* has been reported the middle Miocene of California and Baja California (Mitchell, 1965; Demere et al. 1984). The single *Carcharhinus* tooth (Figure 32) recovered may be assigned to a modern species or a fossil species as more comparative material becomes available.

Material: one tooth

Rhinobatidae—guitarfishes

Guitarfishes have a body shape midway between a shark and a skate and are found in the Atlantic, Pacific and Indians Oceans (Figure 33). These medium sized fishes are found in tropical and temperate shore waters, sometimes entering tropical rivers. Worldwide, there are three genera of guitarfishes. In the northwestern Atlantic Ocean, there is one species of *Rhinobatos*, and three species in two genera in the Gulf of California, *Rhinobatos* and *Zapteryx*.

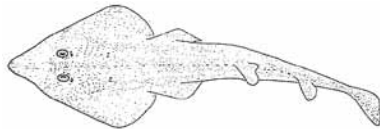


Figure 33. Guitarfish.

Rhinobatid—guitarfish

Until comparative material becomes available, the single very small fossil guitarfish tooth is identified to the family level (Figure 34).

Material: one tooth



Figure 34. Guitarfish tooth.

Myliobatoidea—eagle and cownose rays

Worldwide, there are five genera of myliobatoid rays: *Aetobatis*, *Aetomylaeus*, *Pteromylaeus*, *Rhinoptera*, and *Myliobatis* (Figure 35) and 25 species.

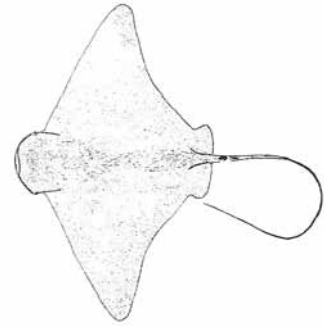
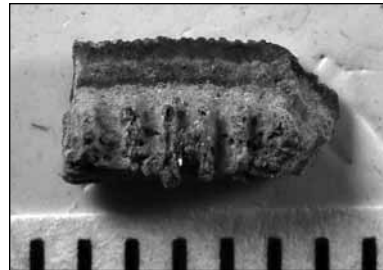
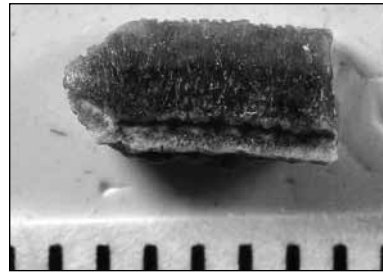


Figure 35. Eagle ray.

Myliobatoidea—eagle and cownose rays

A preliminary analysis of over 300 individual jaws of modern California bat stingray *Myliobatis californicus* revealed that morphology of teeth is



Figures 36 and 37. Eagle ray tooth, top and bottom.

highly variable and “transcends virtually all supposed generically distinct dental patterns of other myliobatid rays” (Welton and Zinsmeister 1980). In the northwestern Atlantic Ocean, three genera, *Aetobatus*, *Myliobatis*, *Rhinoptera*, are present, while in the eastern Pacific, *Pteromylaeus*, *Myliobatis*, and *Rhinoptera* are known. The Willis Palm ray teeth (Figures 36, 37) can

be identified only to the superfamily level.

Material: two broken medial teeth

Dasyatididae—stingrays

These rays have a thin whiplike tail with one or more venomous barbed spines near the base (Figure 38). Worldwide, there are seven genera and 45 species. In the western Atlantic and eastern Pacific Oceans, there are three genera, *Dasyatis*—stingray, *Gymnura*—butterfly ray, and *Urolophus*—round sting ray.

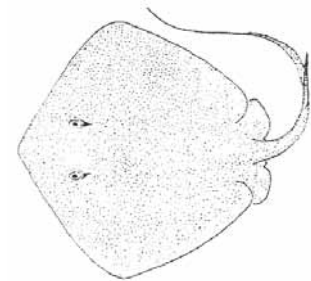


Figure 38. Stingray.

cf. Dasyatid?

A single very small ray tooth was assigned to this family (Figure 39).

Material: tooth

Sciaenidae—croakers

Cynoscion—corvinas
 “The genus *Cynoscion* (Figure 40) is one of the many speciose in the family Sciaenidae” (Schwarzans 1993). In the northwestern Atlantic, there are 13 species of *Cynoscion* while in the Pacific Ocean, 9 species. Most bonyfish have a juvenile otolith form that is morphologically distinct from the adult shape. Unfortunately,



Figure 39. Ray tooth.

Material: “incisor-like” jaw tooth

Gobiidae—gobies
 (Figure 44)

Gobiid—goby
 Because of lack of comparative material, the Willis Palm goby otoliths (Figure 45) are only assigned to family level.

Material: two otoliths



Figure 43. Sea chub tooth.

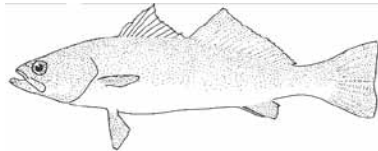


Figure 40. Corvina.

all of the Willis Palm *Cynoscion* otoliths (Figure 41) are from juveniles, precluding identification to the species level.

Because the modern *Cynoscion* otoliths are well documented (Schwarzans 1993), if larger fossil (adult form) otoliths are recovered with additional sampling of this site, it would allow identification to a modern species or possibly an extinct species.

Material: five juvenile otoliths



Figure 41. Corvina otolith.

Sciaenid—croaker

Eight juvenile croaker otoliths were also recovered, but they are too small to identify to genus or species level.

Material: eight juvenile otoliths

Kyphosidae—sea chubs

Sea chubs are deep-bodied, oval-shaped, and omnivorous fishes found in the Atlantic, Pacific, and Indian Oceans (Figure 42). They feed on benthic algae, plankton, and small invertebrates with their small mouth and fine jaw teeth. Sea chubs are found in temperate and warm seas inshore over rocky bottoms and coral reefs.

There are two species of sea chubs in the northwestern Atlantic Ocean, seven species in the Gulf of California, and three species off southern California.

Kyphosid—sea chub

Because of lack of comparative material, the jaw tooth (Figure 43) could be identified only to family level.



Figure 42. Sea chub.

Discussion

Super Creek

Early work on the northern exposures of the Imperial Formation, including Super Creek, by Bramkamp (1935) identified many species of marine corals and mollusks (clams and snails).



Figure 45. Goby tooth.

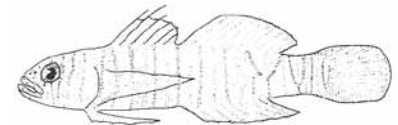


Figure 44. Goby.

Recently there has been renewed interest in the paleontology of Whitewater area. Research has been conducted on microfossils (McDougal et al 1999; McDougal), bryozoans (Wilson and Cuffey 1998) mollusks (Schremp 1981; Carreno and Smith 2007; Powell 1985, 1986, 1987, 1988: LaFollette, this volume), crabs (Tucker et al 1994), and whales (Thomas and Barnes 1993). Roeder and Huddleston (2011) reported the first fossil records of marine fish from the Imperial Formation of the Super Creek area.

The fish remains, primarily otoliths, chronicle the fish fauna of the ancestral Gulf of California some 6 million years ago.

Except for the *Diaphus* (headlightfish) and *Bregmaceros* (codlet), the fossil fish species recovered from this site indicate a very shallow marine paleoenvironment.

Today, the cardinalfish (*Apogon*), mojarra (*Gerres*), grunt (*Orthopristis*), and snapper (*Lutjanus*) are considered warm water species. Records off southern California are either rare or nonexistent.

Today some species of *Diaphus* and *Bregmaceros* make diurnal migrations from fairly deep water to shallow waters at night. The presence of these fish in the Super Creek fauna may indicate the presence of a nearby offshore deep water basin.

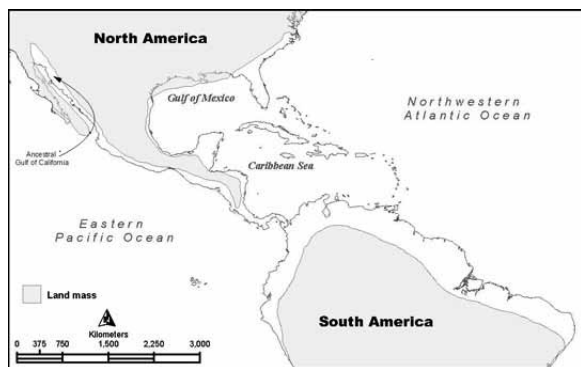


Figure 46. Late Miocene-Pliocene seas of North and Central America..

During the Late Miocene, a seaway existed across what is today Panama, until closure in the middle Pliocene (Figure 46). Prior to its closure, there was free exchange of marine waters of the eastern Pacific and Caribbean Sea. Early work on the northern exposures the Imperial Formation by Bramkamp (1935) identified a number of marine corals and mollusks (clams and snails) that today are not present in the eastern Pacific, but are living in the Caribbean Sea. Herein lies the challenge in the identification of the fish species from the Super Creek locality. For example, in comparing the fossil otoliths of *Citharichthys* (sanddab) with illustrations of sanddab otoliths from the eastern Pacific and western Atlantic Oceans (Schwarzhan 1999), the Super Creek otoliths are more like the western Atlantic species of sanddabs. There is a possibility that many of the fish otoliths and teeth belong to Caribbean species, like earlier identified species of fossil bryozoans, corals and mollusks. Collections of comparative otoliths and osteological material from the Caribbean Sea are incomplete. Even if some of the fossil fish material is eastern Pacific Ocean species, comparative material is lacking. Because of this many of the otoliths and teeth from the Super Creek can only be identified to family and/or genus level.

But at least one species of fish, *Umbrina* cf. *U. roncadorensis* (yellowfin croaker) was identified to a modern species. It is possible that with more comparative material, many of the fish otoliths and teeth can be identified to modern species. Because of the age of the Super Creek locality, which is over 6 million years, there may be several species that are extinct.

Water screening and sorting of 700 kilograms of fossil-bearing sediment from the Super Creek locality yielded at least 16 taxa of bony fish. Surprisingly, no shark or ray remains were recovered.

Additional processing of fossiliferous sediments from the Super Creek locality should yield additional material of known taxa as well as records of new species. Although for the most part fish remains are scarce, I have averaged

one new taxa for every 100 kg of sediment processed (water screened and sorted).

Willis Palm

The Willis Palm locality, which is Pliocene (Powell, et al 2011) in age, gives us an opportunity to look at fish faunas from a younger exposure of the Imperial Formation. Even though sediments were deposited in shallow marine environments like the older Super Creek locality, the fish fauna is very different. For one thing, there are sharks and rays, which are absent at Super Creek. With more investigation, the Willis Palm locality fish may be more like the fish faunas of the present-day northern Gulf of California. Today, there are several species of croaker of the genus *Cynoscion* (corvina) in the northern Gulf and up until recently they were very abundant. Even though the fossil *Cynoscion* otoliths recovered from Willis Palm were from juveniles, with additional sampling and processing of fossiliferous sediments from this site there is an excellent chance to recover adult *Cynoscion* and other croaker otoliths which could be speciated.

ACKNOWLEDGEMENTS—I would like to thank Edward Wilson, curator emeritus of the Invertebrate Paleontology Section of Natural History Museum of Los Angeles County, for his encouragement and advice on this project. Ed, Pat LaFollette, and Diane Jovee accompanied me in the field, helping with the collection of the samples. Special thanks to Diane Jovee, who picked the concentrate from Super Creek and found many of the fish species described in this report. Also, all materials were collected under Charles L. Powell, II, of the U. S. Geological Survey, Menlo Park permits. Special thanks to Bob Reynolds for making the guidebook possible. Pat LaFollette took the photographs of the fish remains. And finally, Mr. Richard W. Huddleston of Scientific Research Systems assisted the author in identification of some of the fish otoliths.

References

- Aceves-Medina, G., Jimenez-Rosenburg, S. P. A., Hinojosa-Medina, A., Funes-Rodriguez, R., Saldierna, R. J., Lluch-Belda, D., Smith, P. E., and W. Watson, 2003, Fish larvae from the Gulf of California. *Scientia Marina*. Volume 67. Number 1. p. 1-11.
- Carreno, A. L. and J. T. Smith, 2007, Stratigraphy and Correlation of the Ancient Gulf of California and Baja California Peninsula, Mexico. *Bulletin of American Paleontology*. Number 372. p. 1-146.
- Castro, J. I., 1983, The Sharks of North America. The W. L. Moody, Jr., Natural History Series, No. 5. Texas A&M University Press, College Station, Texas. 180p.
- Compagno, L., Dando, M. and S. Fowler, 2005, Sharks of the World. Princeton Field Guides. Princeton University Press. Princeton and Oxford. 368p.

- Demere, T. A., Roeder, M. A., Chandler, R. M., and J. A. Minch, 1984, Paleontology of the Middle Miocene Los Indios Member of the Rosarito Beach Formation, Northwestern Baja California in Minch, J. A. and J. R. Ashby, editors, *Miocene and Cretaceous Depositional Environments, Northwestern Baja California, Mexico*. Published by the Pacific Section, American Association of Petroleum Geologists, Los Angeles. Volume 54, p. 47-56.
- Eschmeyer, W. N. and E. S. Herald, 1983, A Field Guide to Pacific Coast Fishes of North America. The Peterson Field Guide Series Houghton Mifflin Company, Boston. 336p.
- Ebert, D. A., 2003, Sharks, Rays and Chimaeras of California. California Natural History Guide No. 7. University of California Press. Berkeley and Los Angeles, London. 285p.
- Fitch, J. E., 1964, The Fish Fauna of the Playa Del Ray Locality, a Southern California Marine Pleistocene Deposit. Natural History Museum of Los Angeles County Contributions in Science. Number 82. p.1-35p.
- _____, 1968, Otoliths and other Fish Remains from the Timms Point Silt (Early Pleistocene) at San Pedro, California. Natural History Museum of Los Angeles County Contributions in Science. Number 146. p.1-29.
- _____, 1969, Fossil Lanternfish Otoliths of California, with notes on Fossil Myctophidae of North America. Natural History Museum of Los Angeles County. Number 173. p. 1-20.
- _____, 1970, Fish Remains, mostly otoliths and teeth from the Palos Verdes Sand (Late Pleistocene) of California. Natural History Museum of Los Angeles Contributions in Science. Number 199. p. 1-41.
- Fitch, J. E. and R. J. Lavenberg, 1968, Deep-water Fishes of California. California Natural History Guide No. 25. University of California Press. Berkeley and Los Angeles. 155p.
- _____, 1983, Teleost Fish Otoliths from the Lee Creek Mine, Aurora, North Carolina (Yorktown Formation: Pliocene) in Ray, C. E., editor, *Geology and Paleontology of the Lee Creek Mine, North Carolina*, I. Smithsonian Contributions to Paleobiology. Smithsonian Institution Press, Washington. Number 53. p.509-529.
- Goodson, G., 1985, Fishes of the Atlantic Coast. University of Stanford Press. Stanford. 202p.
- _____, 1988, Fishes of the Pacific Coast. University of Stanford Press. Stanford. 267p.
- Kato, S., Springer, S., and M. H. Wagner, 1967, Field Guide to Eastern Pacific and Hawaiian Sharks. U. S. Fish and Wildlife Service, Bureau of Commercial Fisheries. Washington, D.C. Circular No. 271. 47p.
- Lander, E. B., 2003, Eastern Transportation Corridor, Paleontologic Resource Impact Mitigation Program, Final Technical Report of Results and Findings: Part 1 of 2 (text and Appendices A to D). Submitted to the Foothill/Eastern Transportation Corridor Agency, Irvine, California, prepared by E. Bruce Lander, Paleo Environmental Associates, Inc, Altadena, California.
- Long, D. J., 1993, Preliminary List of Marine Fishes and Other Vertebrate Remains from the Late Pleistocene Palos Verdes Sand Formation at Costa Mesa, Orange County, California. PaleoBios. Volume 15. Number 1. p. 9-13.
- McDougall, K, Poore, R. Z., and J. Matti, 1999, Age and Paleoenvironment of the Imperial Formation near San Geronio Pass, Southern California. Journal of Foraminiferal Research. Volume 29. Number 1. p. 4-25
- Miller, D. J. and R. N. Lea, 1976, Guide to the Coastal Fishes of California. Fish Bulletin 157. California Department of Fish and Game. 249p.
- Mitchell, E., 1965, History of Research at Sharktooth Hill, Kern County, California. Special Publication of the Kern County Historical Society and the County of Kern through its Museum. 45p.
- Murphy, M. A., The Imperial Formation at Painted Hill, near Whitewater, California. In Geology Around the Margins of the Eastern San Bernardino Mountains, M. A. Kooser and R. E. Reynolds, editors. Publication of the Inland Geological Society, Redlands, California. 1: p. 63-69
- Nelson, J. S., 1976, Fishes of the World. A Wiley-Interscience Publication. John Wiley and Sons. New York, London, Sydney, and Toronto. 416p.
- Nolf, D., 1985, Otolithi piscium. In H. Schultze, editor, Handbook of Palaeoichthyology, Volume 10. New York:Gustav Fisher Verlag. 145p.
- Powell, C. L., II, 1985, Bivalve molluscan paleoecology of northern exposures of the marine Neogene Imperial Formation in Riverside County, California. Western Society of Malacologists Annual Report, August 1985. Volume 17 for 1984.
- _____, 1986, Stratigraphy and bivalve molluscan paleontology of the Neogene Imperial Formation in Riverside County, California. San Jose, California. M. S. Thesis, San Jose State University, 325p.
- _____, 1987, Correlation between sea level events and deposition of marine sediments in the proto-Gulf of California during the Neogene. Geological Society of America, Abstracts with program, 19(7): p.809
- _____, 1988, The Miocene and Pliocene Imperial Formation of Southern California and its molluscan fauna. Western Society of Malacologists. San Diego, California. Annual Report, Volume 20, p. 11-18.
- Powell, C. L., II, Roeder, M. A., and K. McDougall, 2011, A Preliminary Report on the Paleontology of the Imperial Formation (Ancestral Gulf of California:Pliocene) in the Indio Hills, Riverside County, Southern California. CalPaleo 2011 abstracts with program, p. 22.
- Randall, J. E., 1968, Caribbean Reef Fishes. T. F. H. Publications. Jersey City. 318p.
- Robins, C. R. and G. C. Ray, 1986, A Field Guide to Atlantic Coast Fishes of North America. The Peterson Field Guide Series. Houghton Mifflin Company, Boston. 354p.
- Roeder, M., 2005, Fossil Fishes of the Anza-Borrego Region in Program and Abstracts for Fossil Treasures of the Anza-Borrego Desert. Anza-Borrego Institute, California State Parks, and Sunbelt Publications, San Diego. P. 16-17.
- Roeder, M. A. and R. W. Huddleston, 2011, First records of fossil fish remains from northern exposures of the marine Imperial Formation, Riverside County, California. Annual Meeting, Abstract No. 133, Bulletin of the Southern California Academy of Sciences, Volume 110, p. 115-116.
- Schremp, L. A., 1981, Archaeogastropoda from the Pliocene Imperial Formation of California. Journal of Paleontology. Volume 55, Number 5, p. 1123-1136.
- Schwarzans, W., 1993, A Comparative Morphological Treatise of Recent and Fossil Otoliths of the Family Sciaenidae (Perciformes). Part Otolithi Piscium. Volume 1. Piscium Catalogus. Editor Dr. Friedrich Pfeil. Munchen, Germany. 245p.

- _____, 1999, A Comparative Morphological Treatise of Recent and Fossil Otoliths of the Order Pleuronectiformes, Part Otolithi Piscium, Volume 2, Piscium Catalogus. Editor Dr. Friedrich Pfeil., Munchen, Germany. 391p.
- Thomas, H. W., 1993, Discoveries of fossil whales in the Imperial Formation, Riverside County, California: possible further evidence of the northern extent of the proto-Gulf of California. In Ashes, Faults, and Basins, edited by R. E. Reynolds and J. Reynolds, San Bernardino County Museum Association Special Publication 93(1): 34-36.
- Tucker, A. B., Feldmann, R. M., and C. L. Powell, II, 1994, *Speo-carcinus berglundi* n. sp. (Decapods:Brachyura), a new crab from the Imperial Formation (late Miocene-late Pliocene) of southern California. Journal of Paleontology, volume 68, number 4, p. 800-807.
- Thomson, D. A., Findley, L. T. and A. N. Kerstitch, 1987, Reef fishes of the Sea of Cortez. University of Arizona Press. Tucson.
- Thomson, D. A. and N. McKibben, 1986, Gulf of California Fishwatcher Guide. Golden Puffer Press. 75p.
- Wilson, Edward Carl and Roger J. Cuffey (1998). "The Early Pliocene Caribbean bryozoan *Acanthodesia savarti monilifera* in the Imperial Formation near Whitewater, Riverside County, California." San Bernardino County (California) Museum Association Quarterly 45(1-2): 108.

Shell rubble beds of the mollusk *Thylacodes* (Gastropoda: Vermetidae) in the upper Miocene Imperial Formation near Whitewater, Riverside County, California, previously called the “worm tube bed.”

Patrick I. LaFollette

Research Associate in Malacology, Natural History Museum of Los Angeles County

ABSTRACT—In the upper Miocene Imperial Formation northeast of Whitewater, Riverside County, California, a distinctive thin marker bed has been known as the “worm tube bed,” based on the presence of numerous cylindrical internal molds and a few tube shaped shell fragments. Extensive collecting now allows these tubes to be identified as fragments of the tube forming colonial gastropod *Thylacodes*. The bed is renamed the *Thylacodes* tube bed.

The upper Miocene Imperial Formation (~6Ma, McDougall, 2008) is represented in the hills on the north side of the San Geronio Pass, just east of the Whitewater River, western Riverside County, California, by exposed sections totaling about 50 meters. Thin beds of jumbled “worm tube” fragments and rubble in deposits otherwise composed predominantly of silt are recognized marker beds (Murphy, 1986; Powell, 1986, McDougall, 2008, McDougall, et al., 2009) and are discussed by Carreño and Smith, 2007. Significant conglomerate beds occur below the “worm tube” bed in some exposures in this area. The “worm tube” beds range from five centimeters to a meter thick, but are sufficiently distinctive to be correlated from exposure to exposure over kilometer distances. The tubes in these rubble beds have been called “worm tubes” in sections drawn by Powell, 1986, Carreño and Smith, 2007, and McDougall, 2008 and “reworked *Callianassa* burrows” by Murphy, 1986. Powell, 1996, recognized these tubes to be vermetid gastropods. (personal communication published by McDougall, et al., 1999: 15)

Due to differences in the mineral composition (aragonite vs. calcite) and structure of the shells, certain molluscan taxonomic groups, particularly oysters, scallops, and *Atrina* “pen shells” are often found well preserved in the Imperial Formation, while shells of most other mollusks are either completely dissolved away, leaving only impressions or molds and casts (steinkerns) or just traces of white powdery residue that crumbles away when touched.

The white shell (aragonite) of mollusks is somewhat better preserved at one locality, though these remains have been crushed and shattered by tectonic deformation



Figure 1. Imperial Formation exposure. Collecting locality on east side of Super Creek Canyon, near Whitewater, Riverside County, California. The beds are near vertical, up-section is to right. 1. Basal conglomerate. 2, 3. *Thylacodes* tube beds are visible nearly to top of cliff. Scale: the author.



Figure 2. Internal molds of *Thylacodes* tubes, *Thylacodes* tube bed in unnamed canyon west of Super Creek, near Whitewater, Riverside County, California. Image approximately 30 cm wide.

of the sediments into fragments on a millimeter scale. This locality is located at, and stratigraphically just above, the “worm tube” bed level in Super Creek Canyon. The beds here are tilted almost 90 degrees from horizontal, and strike NNE.

In the course of extensive collecting of this locality by the author and Mark A. Roeder over a three-year period, we have recovered an extensive fauna, including sufficiently well-preserved specimens of these “worm-tubes” to allow identification to genus, and to suggest events that may have formed these “worm tube” beds. At this locality, there are two “worm tube” beds, each 20-30cm thick, separated by approximately 1m of silt. Bulk samples, totaling about 700 kilograms, have been collected, some from the “worm tube” beds, but mostly from the shell-rich silt between and just above these beds. These bulk samples are returned to the lab, broken up with a press to look for macro-specimens, then washed through graduated screens and the size fractions, down to 30 mesh (~0.5 mm). The washed material is picked under magnification for microscopic specimens.

The “worm tubes” are here identified as fragments of the sessile colonial tube forming vermetid gastropod *Thylacodes*, Guettard, 1770, previously known as *Serpulorbis* Sasso, 1827 (Bieler and Petit 2010, 2011). *Thylacodes* lives attached to rocks and shells in the lowest intertidal zone. Typically, colonies of *Thylacodes* grow in robust tightly coiled clumps, sculptured with longitudinal ribs. *Thylacodes* colonies can be extensive. In periods of rapid sedimentation, however, *Thylacodes* can form long, more or less straight, thin, fragile, unsculptured tubes in an attempt to keep their apertures above the sediment. At intervals, *Thylacodes* seals off earlier tube growth with a characteristic hemispherical septum. In the Imperial “worm tube” beds, broken sections of straight unornamented *Thylacodes* tube predominate, but some bits of coiled tube with characteristic longitudinal sculpture, and a few examples of the hemispherical septa have been found. In exposures where only internal molds are preserved, they sometimes exhibit hemispherical ends formed by the septa. Though undoubtedly representing



Figure 3. *Thylacodes* shell tubes in matrix. *Thylacodes* tube bed, Imperial Formation, east side of Super Creek Canyon, near Whitewater, Riverside County, California. Scale bar: 1 cm.



Figure 4. *Thylacodes squamigerus* (Carpenter, 1857). Uncoiled form. Recent, Coast Guard Station, Newport Bay, Orange County, California. Scale bar: 1 cm.



Figure 5. *Thylacodes* shell tube fragments, *Thylacodes* tube bed, Imperial Formation, east side of Super Creek Canyon, near Whitewater, Riverside County, California. Scale bar: 1 cm.

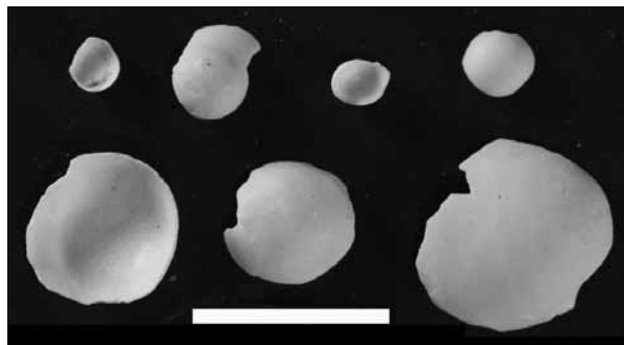


Figure 6. *Thylacodes* detached septa. Imperial Formation, Beteen and above *Thylacodes* tube beds, east side of Super Creek Canyon, near Whitewater, Riverside County, California. Scale bar: 5 mm.

an undescribed species, it is unlikely that specimens of this snail that are sufficiently complete and well preserved to allow formal description will be found in exposures in this area. This identification leaves the former “worm tube bed” without an appropriate name. I propose that it be designated the “*Thylacodes* tube bed.”

In addition to numerous fragments of *Thylacodes* tubes that have given the beds their name, the bed is composed of a jumble of pebbles, coarse-to-fine grained sand, silt, and broken fragments of mollusks, barnacles, bryozoans, and small corals. Because of the broken and

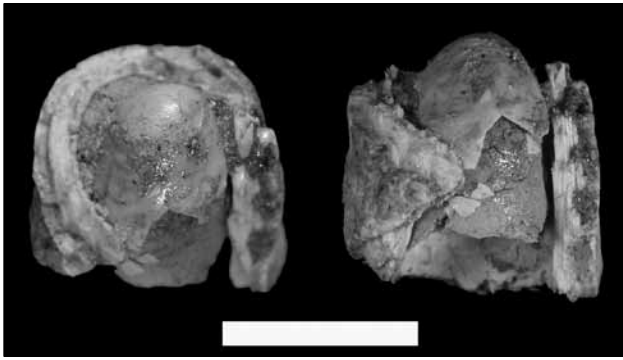


Figure 7. *Thylacodes* septum in place in tube fragment. Exterior on left, side view on right. Imperial Formation, Beteen and above *Thylacodes* tube beds, east side of Super Creek Canyon, near Whitewater, Riverside County, California. Scale bar: 5 mm.



Figure 9. *Thylacodes* internal mold showing round end formed by septum. *Thylacodes* tube bed, Imperial Formation, east side of Super Creek Canyon, near Whitewater, Riverside County, California. Scale bar: 1 cm.

random orientation of the shell fragments in the bed, I speculate that it represents storm debris, broken up in the intertidal zone and washed offshore to form a layer on the shallow offshore silty bottom. The molluscan fauna of the silt immediately above and below the *Thylacodes* tube layers suggest a sheltered seabed at a depth of 10 to 30 meters. Taxonomic work on the molluscan fauna of Super Creek is still at a preliminary stage. A new species *Liamorpha* (Gastropoda: Pyramidellidae) is in manuscript. Ongoing field-work continues to add to the known fauna. The mollusks will be reported on at a future date.

Paleontological writings on the late Miocene and early Pliocene molluscan faunas of the Caribbean and tropical eastern Pacific, before the closure of the Panama seaway, have generally not treated the micro-mollusks, so there is little comparative literature to work from. For example, no members of the family Caecidae are mentioned in the major references, though six species in three genera have been found at this locality. Most of these tiny mollusks are likely undescribed. There is a general resemblance of this fauna on the generic or familial level to the shallow offshore molluscan fauna of the modern northern Gulf of California. Some molluscan groups, however, such as the bivalves *Ctenoides* (Limioidea) and *Timothyus*

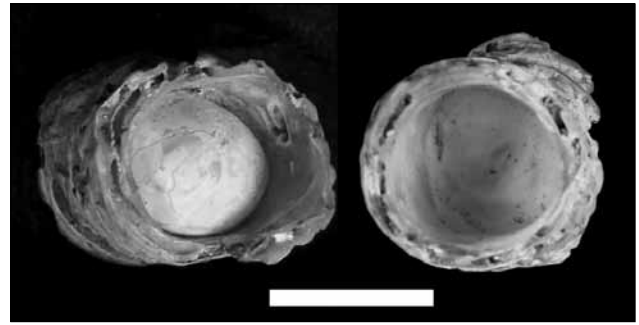


Figure 8. *Thylacodes squamigerus* (Carpenter, 1857). Septum in tube fragment. Exterior on left, interior on right. Recent, Coast Guard Station, Newport Bay, Orange County, California. Scale bar: 1 cm.



Figure 10. *Thylacodes* coiled form showing traces of longitudinal sculpture. Beteen and above *Thylacodes* tube beds, east side of Super Creek Canyon, near Whitewater, Riverside County, California. Scale bar: 1 cm.

(Ungulinidae) and the gastropod *Meioceras* (Caecidae) are not known to live in the eastern Pacific Ocean, though they are found living today in the Caribbean Sea. **ACKNOWLEDGMENTS**—Sincere thanks to Charles L. Powell, II, Mark A. Roeder, and Edward C. Wilson for their encouragement, guidance, advice, and editorial assistance.

Literature cited

- Bieler, R. and R. E. Petit (2010). "*Thylacodes* - *Thylacodus* - *Tulaxodus*: Worm-snail name confusion and the status of *Serpulorbis* (Gastropoda: Vermetidae)." *Malacologia* 51(1): 183-187.
- Bieler, R. and R. E. Petit (2011). "Catalogue of recent and fossil "worm-snail" taxa of the families Vermetidae, Siliquariidae, and Turritellidae (Mollusca: Caenogastropoda)." *Zootaxa*, New Zealand, 2948: 1-103.
- Carreño, A. L. and J. T. Smith (2007). "Stratigraphy and correlation for the ancient Gulf of California and Baja California Peninsula, Mexico." *Bulletins of American Paleontology* 371: 1-146.
- McDougall, K. (2008). "Late Neogene marine incursions and the ancestral Gulf of California. in Reheis, Marith C., Hershler, R., Miller, D., eds. 2008. Late Cenozoic Drainage History of the southwestern Great Basin and lower Colorado

- River region: Geologic and biotic perspectives.” Geological Society of America. Special Papers **439**: 353-371.
- McDougall, K. A., R. Z. Poore, and Matti, J. C. (1999). “Age and paleoenvironment of the Imperial Formation near San Geronio Pass, Southern California.” *Journal of Foraminiferal Research* **29**(1): 4-25.
- Murphy, M. A. (1986). The Imperial Formation at Painted Hill, near Whitewater, California. *in* Kooser and R. E. Reynolds, eds., *Geology around the margins of the Eastern San Bernardino Mountains*. M. A. Publications of the Inland Geological Society. **1**: 63-69.
- Powell, C. L., II. (1986). Stratigraphy and bivalve molluscan paleontology of the Neogene Imperial Formation in Riverside County, California. San Jose, CA. San Jose State University, 323 pp.

The desert fan palm: a recent invader in the American Southwest

James W. Cornett

JWC Ecological Consultants, P.O. Box 846, Palm Springs, CA 92263, jcornett@jwccornett@aol.com

Palms are one of the oldest plant families in existence. Pollen grains resembling those of modern palms have been recovered from Lower Cretaceous rocks nearly 120 million years of age (Dransfield et al., 2008). The oldest unequivocal palm fossils date back to the Upper Cretaceous, approximately 84 million years before present (Daghlian, 1981). Upper Cretaceous palm fossils have also been taken from rocks in the western U.S. (Tidwell, 1998).

Though palms, in general, have been in existence for tens of millions of years, the only native palm living today in the western U.S. is the desert fan palm, *Washingtonia filifera* (Linden ex André) H. Wendl. ex de Bary (Cornett, 1985). Axelrod (1950) asserted that the scattered and isolated populations of this species were relict populations and his conclusion has been cited repeatedly for more than half a century without evidence to support it (Vogl and McHargue, 1966; Olin, 1977; Nabhan, 1985; Pavlik, 2008).

Relict species are those that “formerly had a much wider distribution” (Allaby, 1994), which “survive now only in a few islands of favourable climate” (Cox et al., 1973) and “are descendents of once widespread taxa (or populations) that now have a narrow geographic distribution” (Habel et al., 2010). In 1966, Richard Vogl and Lawrence McHargue speculated that *W. filifera* was endangered, its populations were threatened and its numbers were declining. Although they had scant field data to support such a conclusion, Axelrod’s 1950 paper provided the foundation for their assertion.

Following extensive field work involving an analysis of every known desert fan palm oasis known to occur in North America, it was concluded that no evidence existed supporting the hypothesis that *W. filifera* is a relict species (Cornett, 2010). In fact, the available data strongly suggests the desert fan palm is a recently evolved, invasive species. Four bodies of evidence support this conclusion. (1) The range of the desert fan palm is expanding, not contracting. (2) A formal census indicates that *W. filifera* numbers are increasing. (3) The genetic composition of isolated *W. filifera* populations lacks divergence. (4) No fossil evidence exists indicating a once broader distribution, greater numbers than present or existence in past geological times.

Range expansion

The geographical area occupied by the desert fan palm is presently expanding. New populations are appearing at a rate approaching one per year at such locations as Clapp

Spring near Blythe, California (Cornett, 1986), in Death Valley National Park (Cornett, 1987), southern Nevada (Cornett, 1988), Sacramento Springs, San Bernardino County (Cornett, 1989) and the Desert Studies Center near Baker, California (Rob Fulton, personal communication, 2011). Interestingly, most of the new locations lie to the north of the historical range of the species suggesting a relationship with global warming.

According to evolutionary theory a relict species would be expected to have a contracting, not an expanding distribution (Cox et al., 1973). That the current range of the desert fan palm is clearly expanding is evidence supporting the perspective that *W. filifera* is not a relict species.

Increasing numbers

In addition to a range expansion, palm numbers are increasing. For example, Willis Palms situated along the San Andreas Fault in the Coachella Valley, contained 370 palms over 4 meters in height in 1965 (Henderson, 1965). By 1983 that number had grown to 612, a 65% increase in just 18 years. By 1990, increases were recorded in most palm oases (Cornett, 2010). By the end of the twentieth century, wild palm numbers had more than doubled from when Henderson began his counts in the 1950s (Cornett, 2010). These results are contrary to the idea that *W. filifera* is a relict species. A relict species would, in general, be expected to have declining numbers, not an increasing number of individuals.

Lack of genetic divergence

Because of genetic drift, a relict species would be expected to show significant genetic diversity between populations, particularly if those populations were remote and isolated (Habel et al., 2010). A study by McClenaghan and Beauchamp (1986), however, indicated the reverse was true for *W. filifera*. In their study, leaf tissue samples from palms growing in isolated oases in Anza-Borrego Desert State Park were collected. They found genetic divergence was greater between palms in the same oasis than between palms in different oases. This was the precise opposite of what evolutionary theory would predict. Oasis palms should be most closely related to the palms in their own oases, the ones from which they are most likely sired through pollination. They should be less related to palms established far away in distant oases since cross pollination between distant palm groves would be rare if not impossible.



Willis Palms, 1983 fire. Richard Misrach photograph.



Willis Palms, one year after the 1983 fire. J. W. Cornett photograph.

McClenaghan and Beauchamp's research suggested *Washingtonia filifera* was a relatively new species in the American Southwest. The lack of genetic diversity was best explained as the result of the desert fan palm having recently dispersed out of the Baja Peninsula, the likely origin of the genus *Washingtonia*. The palms had not had time to diverge and so, genetically speaking, were all close relatives—as if they had been separated for only a relatively short time (probably less than a few thousand years).

Absence of fossils

If the desert fan palm is a relict species, one would expect a fossil record indicating *W. filifera* had a broader range or that its numbers were greater in the past than they are today. The fossil record, however, supports neither premise. Thus far, no fossils attributable to *Washingtonia* have been discovered and described. Axelrod's reference (1950) to a *Washingtonia* fossil cannot be confirmed because there is no specimen (Cornett, 2010). Remeika (2006) found anatomical pore structure of fossil palm wood from Anza-Borrego Desert State Park to be identical with wood from the trunk of a modern *Washingtonia*. However, he informed me (personal communication, 2008) that his fossil was never compared with blue fan palm wood (*Erythea*), the closest relative of *Washingtonia* and a genus well known from California fossil deposits (Raven and Axelrod, 1978). It may be that *Erythea* wood is identical to Remeika's fossil. Therefore, the fossil may be either *Washingtonia*, *Erythea* or a member of some other genus entirely. Without abundant or widespread unequivocal fossil evidence, there is no justification for the assumption that *W. filifera* was more widespread in the past than it is today.

Summary

In summary, increasing numbers, expanding range, lack of genetic diversity and absence of fossil evidence indicate the desert fan palm, *W. filifera*, is not a relict but most likely a recently evolved invasive species in the American Southwest.

ACKNOWLEDGMENTS—The research presented in this paper was made possible through grants from the Garden Club of The Desert, Joshua Tree National Park Association and Richard King Mellon Foundation. I thank Thomas Schweich for the critical review of the manuscript.

Literature Cited

- Allaby, M. 1994. *The Concise Oxford Dictionary of Ecology*. Oxford University Press, Oxford, England.
- Axelrod, D. I. 1950. Evolution of desert vegetation in western North America. Carnegie Institution of Washington Publication 590:215-306.
- Cornett, J. W. 1985. Reading the Fan Palms. *Natural History* 94(10):64-73.
- Cornett, J. W. 1986. A New Locality for Desert Fan Palms in California. *Desert Plants* 7:164
- Cornett, J. W. 1987. Naturalized Populations of The Desert Fan Palm, *Washingtonia filifera*, in Death Valley National Monument. In: *Plant Biology of Eastern California*, C. A. Hall, Jr., and V. Doyle Jones, editors. White Mountain Research Station, University of California at Los Angeles, pp.167-174.
- Cornett, J. W. 1988. The Occurrence of the Desert Fan Palm, *Washingtonia filifera*, in Southern Nevada. *Desert Plants* 8(4):169-171.
- Cornett, J. W. 1989. Another new locality for the desert fan palm in California. *Crossosoma* 15(2):1-4.
- Cornett, J. W. 2010. *Desert Palm Oasis: A Comprehensive Guide*. Nature Trails Press, Palm Springs, California.
- Cox, C. B., I. N. Healey and P. D. Moore. 1976. *Biogeography: An Ecological and Evolutionary Approach*. Blackwell Scientific Publications, Oxford, England.
- Daghlian, C. P. 1981. A review of the fossil record of monocotyledons. *The Botanical Review* 47:517-555.
- Dransfield, J, N. W. Uhl, C. B. Asmussen, W. J. Baker, M. M. Harley and C. E. Lewis. 2008. *Genera Palmarum, the Evolution and Classification of Palms*. Kew Publishing, Royal Botanic Gardens, Kew, England.
- Habel, J. C., T. Assmann, T. Schmitt and J. C. Avise. 2010. Relict Species: From Past to Future. In *Relict Species: Phylogeography and Conservation Biology*. Springer-Verlag, Berlin, Germany.
- Henderson, R. 1965. Unpublished notes on file at the Western Heritage Center, University of Wyoming, Laramie, Wyoming.
- McClenaghan, L. R. Jr. and A. C. Beauchamp. 1986. Low genic differentiation among isolated populations of the California fan Palm (*Washingtonia filifera*). *Evolution* 40:315-322.
- Nabhan, G. P. 1985. *Gathering the Desert*. University of Arizona Press, Tucson, Arizona.
- Olin, G. 1977. *House in the Sun*. Southwestern Parks and Monuments Association, Tucson, Arizona.
- Pavlik, B. M. 2008. *The California Deserts*. University of California Press, Berkeley, California.
- Tidwell, W. D. 1998. *Common Fossil Plants of Western North America*. Smithsonian Institution Press, Washington D.C.
- Vogl, R. J. and L. T. McHargue. 1966. Vegetation of California fan palm oases on the San Andreas Fault. *Ecology* 47(4):532-540.

San Andreas fault geomorphology and slip rate in the Indio Hills, Riverside County, California

David K. Lynch
USGS and Thule Scientific

ABSTRACT—The Indio Hills range consists of Miocene-Pleistocene sediments that have been upwarped at the Pacific-North American plate boundary. Here the San Andreas fault splits into the Banning fault and the Mission Creek Fault. Motion along the faults has produced many tectonic landforms in the Indio Hills and we present examples here: dramatic vegetation lineaments, offset stream channels, shutter ridges, soil color & texture boundaries, pressure ridges, beheaded channels and slope breaks. Slip rates, total slip distances and a model of the fault are also presented.

I. Introduction

The San Andreas Fault (SAF) is an active, continental, right lateral transform (strike-slip) fault separating the North American and Pacific plates in California. In most places the fault is locked, though in central California, it is creeping, as it may do to a small extent everywhere. Owing to a major left hand (restraining) bend, the southern SAF system is thought to be a likely place for a major (7.0 – 7.9) or great (> 8.0) earthquake (Field et al. 2008). The recent ShakeOut exercise (Jones et al. 2008) examined one such scenario for a major quake nucleating in the Imperial Valley and propagating northwest through the Indio Hills to the Leona Valley.

Southeast of the Indio Hills (Keller et al. 1982; Norris 1994), the SAF cleanly marks the present plate boundary. Following the fault north from Bombay Beach, it starts to turn westerly (left) near North Shore resulting in a restraining bend. It continues to swing left until near Biskra or Curtis Palms, the plate boundary splits into two strands: the Mission Creek strand to the north and the Banning Fault (BF) to the south, each continuing to bend more westerly as they approach the San Bernardino Mts to the west (Figure 1). The main topographic consequence of these converging/intersecting right lateral faults is the Indio Hills, a

pressure ridge-like structure raised by transpressional components of movement of the two faults. Thus the Indio Hills are composed primarily of upwarped nonmarine fan sediments.

The Indio Hills are about 20 miles long and up to 4 miles wide, trending WNW. They consist of loosely consolidated Miocene to Pleistocene deposits: sandstone, conglomerate, shale, siltstone with minor limestone, evaporites and sedimentary breccia, primarily from the Pleistocene Ocotillo Conglomerate (Proctor 1968). Small

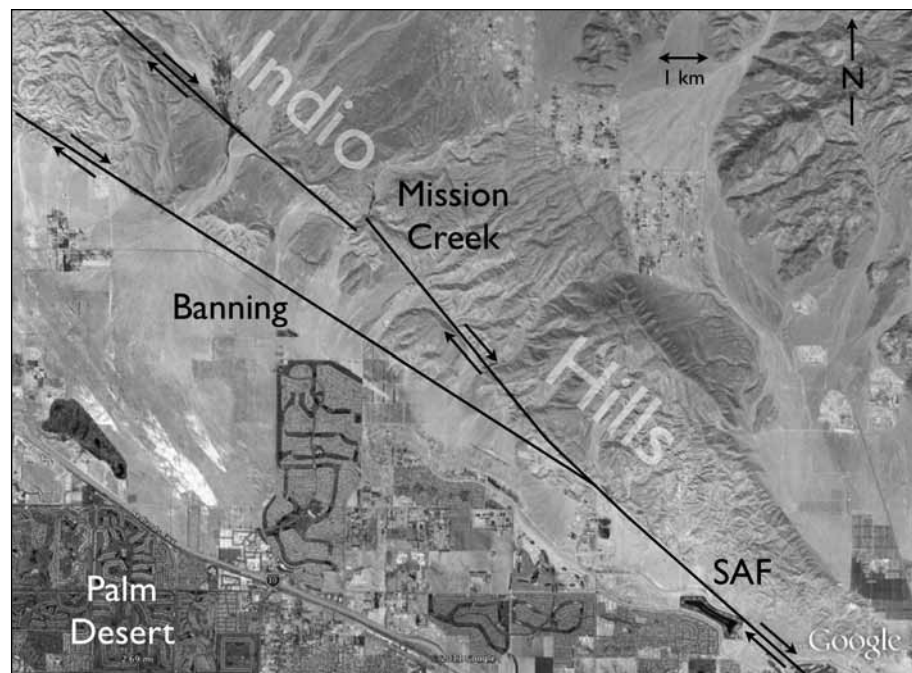


Figure 1. The Indio Hills are a wedge-shaped range running from lower right (SE) to upper left (NW). Shown here are the central Indio Hills and the main trace of the SAF (lower right) that splits into the Mission Creek strand and the Banning strand. Right lateral slip on the two strands leads to convergence that has uplifted the Indio Hills. The faults strike on average N52W, representing a restraining bend in the SAF system, the plate boundary motion being ~ N45W. (Imagery from Google Earth)

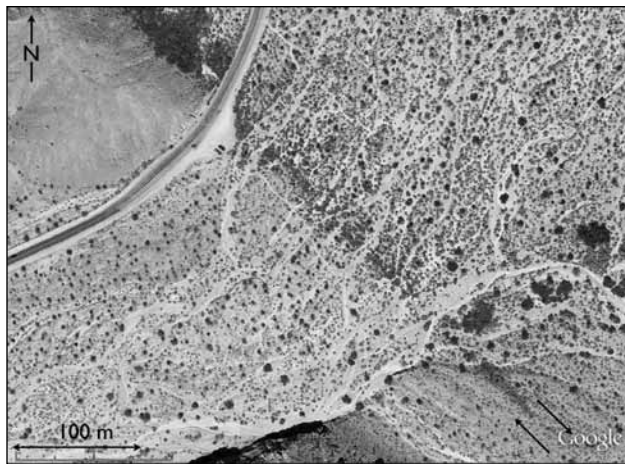


Figure 2 Vegetation lineament in the Thousand Palms Oasis, marking the trace of the Mission Creek strand of the SAF. Underground water flows from upper right to lower left, nearly perpendicular to the fault trace. Note that the vegetation is denser uphill of the fault than below it. (Imagery from Google Earth)

exposures exposures of the underlying marine Pliocene Imperial Formation are found several places, notably at Willis Palms. The hills are surrounded by fans of Pliocene-Holocene alluvium, much of it sourced from gneiss and diorite from the Little San Bernardino Mts to the north and east.

The last surface rupture on the SAF in the Indio Hills involved triggered slip from the 28 June 1992 Landers earthquake (Mw 7.3). Perhaps relevant, the Landers quake was only five days after the much closer (to Indio Hills) Mw 6.1 Joshua Tree earthquake of 23 June 1992. Dextral slip of up to 5 mm was reported in the Indio Hills by Rymer (2000) and others. Previously, coseismic triggered slip and minor surface rupture were observed following the 8 July 1986 (Mw 6.1) North Palm Springs earthquake on the Mission Creek strand (Williams et al. 1988).

Perhaps nowhere else in California is the geomorphic expression of the fault more evident and readily accessible



Figure 4. Macomber Palms. The vegetation lineament on the Mission Creek strand is only about 100 meters wide and sits in stark contrast to the surrounding hardscrabble desert where there is little vegetation. (Photo by David K. Lynch)

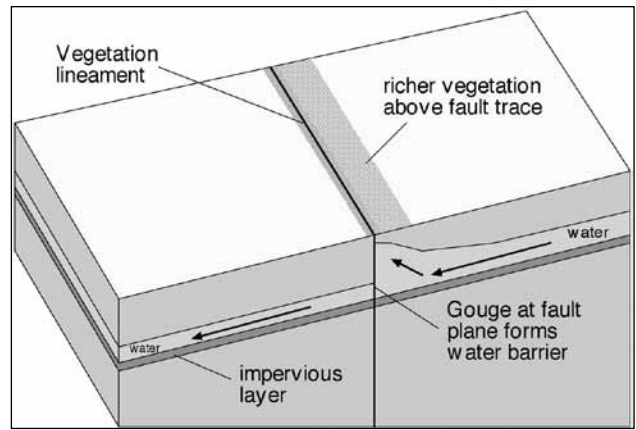


Figure 3. Vegetation lineaments form where subsurface water runs into fault gouge. At the fault plane, gouge hampers the flow, and the water table uphill of the fault plane rises. Vegetation thrives at fault trace due to the presence of shallow moisture.

than in the Indio Hills. In addition to dramatic vegetation lineaments in the form of linear palm oases on both strands, there are abundant offset stream channels, shutter ridges, soil color & texture boundaries, pressure ridges, beheaded channels and slope breaks. Some of the most revealing parts of the fault are at the Thousand Palms Preserve, Curtis Palms and Willis Palms, all readily accessible by car or a short walk.

In this paper we show examples of many fault land forms and review the current knowledge of the slip rates of the SAF in and around the Indio Hills.

2. Geomorph expression

2.1 Vegetation lineaments

Vegetation lineaments or “veg lines” are narrow, linear strips of enhanced vegetation along a fault (Figure 2). In the Indio Hills they form where subsurface water flowing southwesterly toward the Salton Sea runs into fault gouge (Figure 3). At the fault plane, clayey gouge acts as an aquatard and hinders the flow, forcing water upward. In

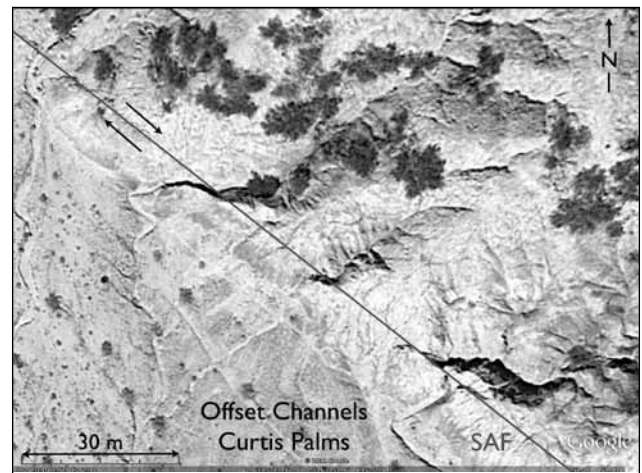


Figure 5. Line of closely-spaced, right-laterally offset channels. Also note the abrupt change in topography along the fault line, rugged badlands to the north, flat fan to the south. (Imagery from Google Earth)

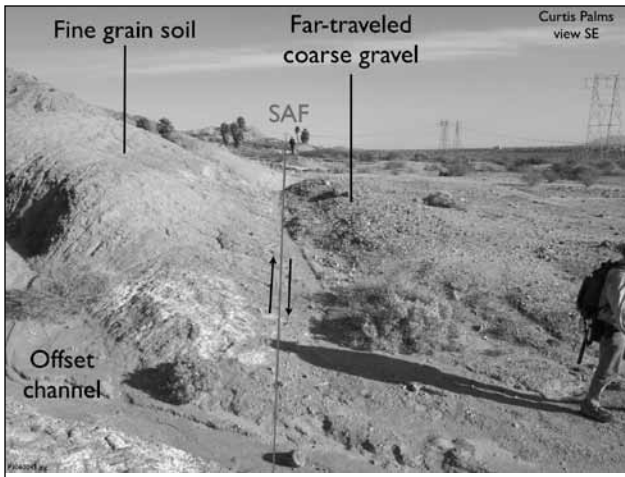


Figure 6 Offset channel, soil boundary and slope boundary along the SAF in Curtis Palms. (Photo by David K. Lynch)

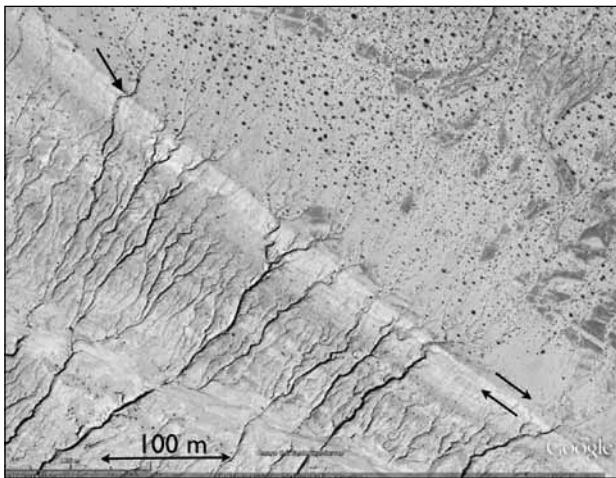


Figure 7. The SAF trace is evident at a distinct soil color change running from lower right to upper left in this aerial image in Imperial County. Water flow is from upper right to lower left. Note the relatively abundant vegetation above the SAF and its almost complete absence below the fault. Many prominent beheaded channels are obvious. At the upper left (arrow), a stream channel crossing the fault is offset right laterally. (Imagery from Google Earth)

some places standing pools are found (Thousand Palms, Pushwalla Palms), or marshy wetlands (Biskra Palms). The presence of localized water at or near the surface allows vegetation to flourish, creating prominent veg lines (Figure 4).

2.2 Offset channels, shutter ridges, beheaded channels

Earthquakes and creep on transform faults that cut across streams produce offset channels, especially when a convergent component of motion raises a shutter ridge. Such offsets are common in the Indio Hills (Figure 5 & 6).

2.3 Soil color and texture boundaries

By juxtaposing one lithologic unit against another, dramatic differences in rock across a transform fault are sometimes found. Owing to erosion and local geologic

effects, however, such differences in the Indio Hills are subtle (Figure 6). Further south, however, they can be easily seen (Figure 7)

2.4 Slope breaks

Slope breaks can often signal the location of a strike-slip fault trace. These occur when two different geologic units are juxtaposed against one another. An initial surface discontinuity is to be expected, and later as the junction is blended into the landscape by erosion, the two units wear down at different rates, often resulting in a slope break (Figure 8). In many cases, the different units can be visually distinguished by color or texture.

2.5 Topographic lineaments

Motion along a transform fault juxtaposes terrain from one location against that of another. In many places in the Indio Hills, this has the effect of shearing off the foot of the hills and replacing it with landscape with much less topographic development (Figure 9). Minor dip-slip

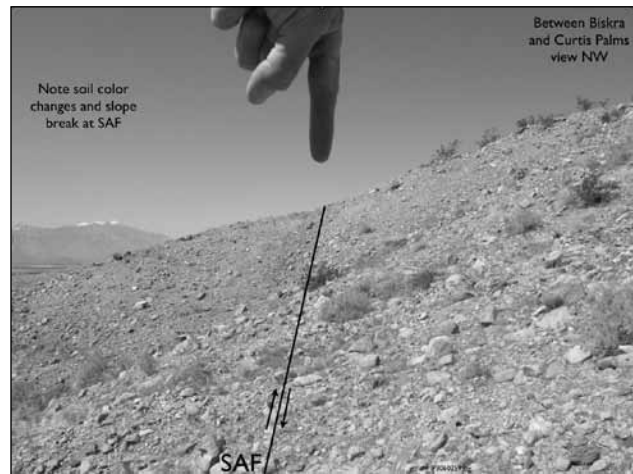


Figure 8. Slope break and soil color boundary along the Mission Creek Strand of the SAF. (Photo by David K. Lynch)

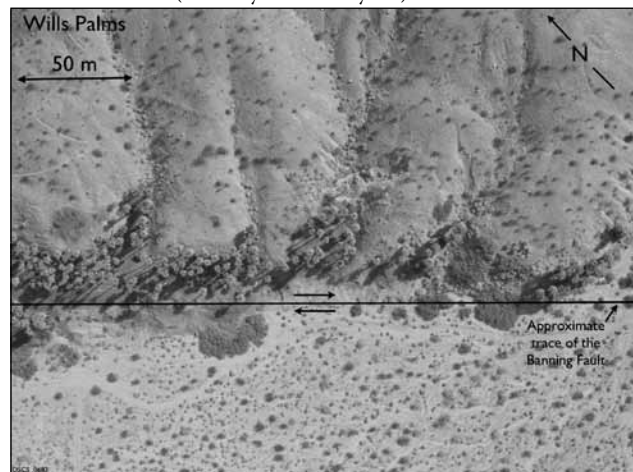


Figure 9. Willis Palms topography lineament. Note the high relief and deeply incised channels north of the Banning fault (top), and the broad, topographically ~featureless fan to the south of the vegetation lineament (bottom). (Photo by David K. Lynch)

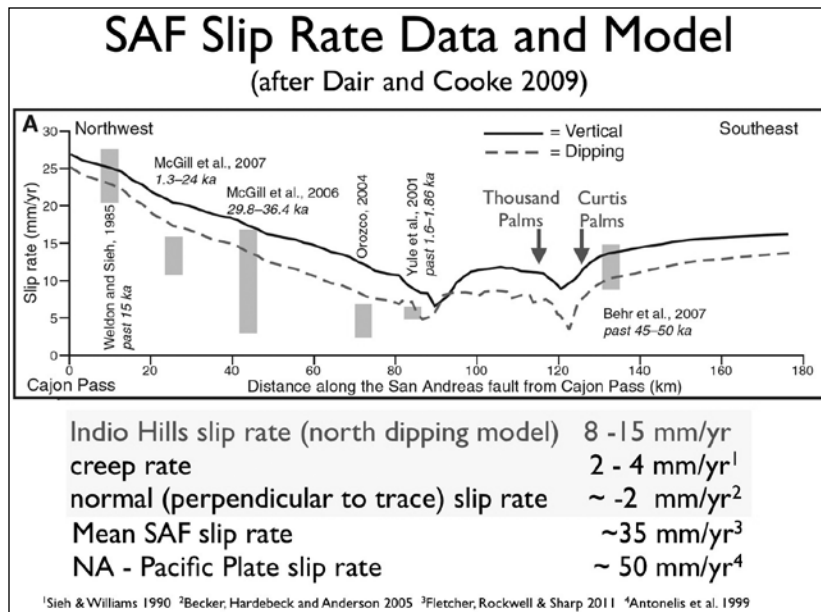


Figure 10. Though there is considerable scatter in the measurements, it is clear that the fault in the Indio Hills is slipping much slower than the rest of the SAF. This is due to its geometry relative to the plate boundary motion that represents restraining geometry.

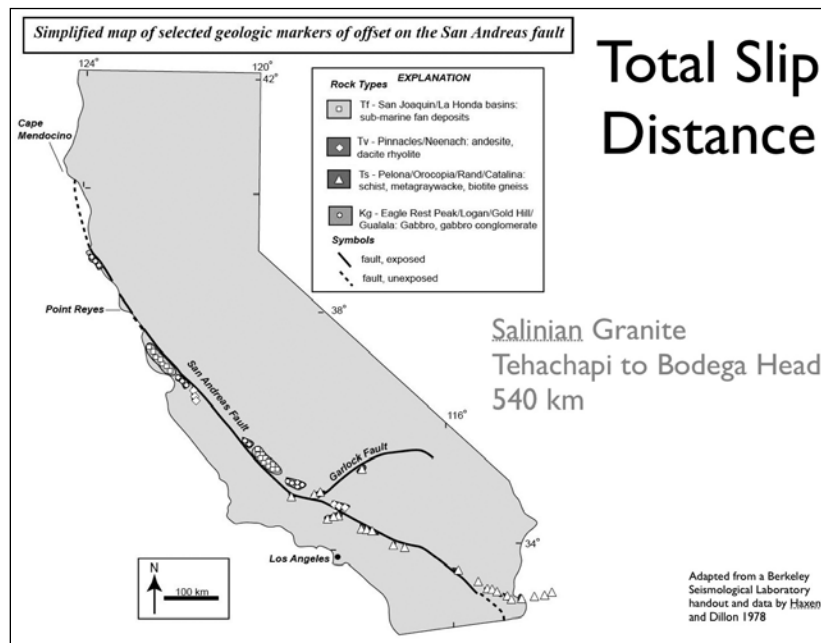


Figure 11. Geologic markers indicating large offsets along the SAF.

components of the motion can produce similar topographic structures.

3. Slip rates and total slip

Owing to its accessibility and its importance to southern California communities, the SAF in the Indio Hills has been well studied. Slip rates can be measured in several ways. Recent GPS and INSAR measurements that have a duration of a few years are consistent with those averaging over thousands of years based on trenching and dating offset beds by methods such as ¹⁴C, ¹⁰Be-²⁶Al surface exposure, OSL, desert varnish, etc. These have been

summarized along with tectonic models of the southern SAF system (Figure 10) by Dair and Cooke (2009). Total slip along the fault as judged by common lithographic species is at least 540 km (Figure 11). Owing to jumps in the plate boundary, uncertainties in identifying common lithologies and unequal slip rates along the current and previous plate boundaries, it is difficult to assign time intervals to large offsets (Irwin 1990).

4. Conclusions

The Indio Hills owe their existence to an unusual tectonic structure: a restraining bend in the plate boundary that causes bifurcation of the SAF into the Mission Creek strand and the Banning fault, both being right lateral transform faults. Resistance by this bend retards the SAF slippage to approximately half that of the SAF as a whole. Many tectonic landforms are well-exposed along the strands including vegetation lineaments, offset and beheaded channels, shutter ridges, soil and rock differences across the fault, slope breaks and topographic lineaments.

ACKNOWLEDGEMENTS—

The author is grateful to Patrick Williams and Kenneth Hudnut for assistance in the field, and David Miller for helpful comments on the paper. This work was supported in part by a grant from the Southern California Earthquake Center (SCEC).

References

Antonelis, Kyle, Daniel J. Johnson, M. Meghan Miller and Randy Palmer 1999 GPS determination of current Pacific-North American plate motion, *Geology* 27 No 4, 299-302

Becker, T. W., Hardebeck, J. L., and Anderson, G.: Constraints on fault slip rates of the southern California plate boundary from GPS velocity and stress inversions. *Geophys J. Int.*, 160, 634-650, 2005.

Dair, L., and Cooke, M.L., 2009, San Andreas Fault geometry through the San Geronio Pass, California: *Geology*, v. 37, p. 119-122.

Field, Edward H., Kevin R. Milner and the 2007 Working Group on California Earthquake Probabilities 2008 Forecasting California's Earthquakes—What Can We Expect in the Next 30 Years? <http://pubs.usgs.gov/fs/2008/3027/>

Fletcher, K.E.K., Rockwell, T.K., and Sharp, W.D., 2011, Late Quaternary slip rate of the southern Elsinore fault, southern California: Dating offset landforms via ²³⁰Th/U on pedogenic carbonate. *J. Geophysical Research*, 116, F02006,

- Haxel, G.B., and Dillon, J., 1978, The Pelona-Orocopia schist and Vincent-Chocolate Mountain thrust system, southern California, in, *Mesozoic Paleogeography of the Western United States*, Howell, D.G., and McDougall, eds., Pacific Section Society of Economic Paleontologists and Mineralogists: Los Angeles, p. 453-470.
- Irwin, W.P., 1990, Geology and plate-tectonic development, in Wallace, R.E., ed., *The San Andreas fault system in California*: United States Geological Survey, Professional Paper 1515, Chapter 3.
- Jones, Lucile M., Richard Bernknopf, Dale Cox, James Goltz, Kenneth Hudnut, Dennis Mileti, Suzanne Perry, Daniel Ponti, Keith Porter, Michael Reichle, Hope Seligson, Kimberley Shoaf, Jerry Treiman, and Anne Wein 2008 *The ShakeOut Scenario*, U.S. Geological Survey Open File Report 2008-1150 California Geological Survey Preliminary Report 25 version 1. <http://pubs.usgs.gov/of/2008/1150/>
- Keller, E. A., M. S. Bonkowski, R. J. Korsch & R. J. Shlemon 1982 Tectonic geomorphology of the San Andreas fault zone in the southern Indio Hills, Coachella Valley, California, *GSA Bulletin* 93 No 1(Jan). 46-56
- Norris, Robert M 1994 The Indio Hills "Desert Badlands", *California Geology*, 47 (Sept/Oct), 127-133
- Proctor, R. J., 1968. *Geology of the Desert Hot Springs-Upper Coachella Valley Area, California*. California Division of Mines and Geology Special Report 94, 50 pp.
- Rymer, Michael J. 2000 Triggered Surface Slips in the Coachella Valley Area Associated with the 1992 Joshua Tree and Landers, California, Earthquakes, *Bulletin of the Seismological Society of America*, 90, 4, pp. 832-848, August
- Sieh, K., and P. Williams, 1990, Behavior of the southernmost San Andreas Fault during the past 300 years, *J. Geophys. Res.* 95, 6629-6645.
- Williams, Patrick L., Sally Fagerson McGill, Kerry E. Sieh, Clarence R. Allen and John N Louie 1988 Triggered Slip along the San Andreas Fault after the 8 July 1986 North Palm Springs Earthquake, *Bulletin of the Seismological Society of America*, 78, No. 3, 1112-1122.

The Pliocene fossil record of Anza-Borrego Desert State Park, western Salton Trough, California

G.T. Jefferson, L.K. Murray, and S.D. Keeley

California Department of Parks and Recreation, Colorado Desert District Stout Research Center, Anza-Borrego Desert State Park*, Borrego Springs, CA 92004

Introduction

Anza-Borrego Desert State Park (ABDSP) lies in a unique geologic setting along the western margin of the Salton Trough, California (Dorsey et al., 2006, Dorsey et al., 2011). This major topographic depression forms the northernmost end of an active rift valley and continental plate boundary. The Trough extends from the Gulf of California north to San Geronio Pass and from the eastern rim of the Peninsular Range east to the San Andreas Fault Zone. Over the past approximately 7 million years (myr), a relatively complete sequence of fossiliferous sediments has been deposited within ABDSP, along this rift valley's western margin. Exposures of these sediments cover over 400 km² (154 square miles) of ABDSP.

Although the paleontologic record of ABDSP ranges in age from mid-Paleozoic to Holocene the most significant and abundant remains are from late Mio-Pliocene marine deposits, and Plio-Pleistocene terrestrial deposits. The early part of the Pliocene record in the western Salton Trough is primarily marine, yielding diverse and abundant invertebrate assemblages, but includes both marine and terrestrial vertebrates. These deposits occur in an upward shallowing sequence from deeper water to deltaic and near-shore sediments. The latter part of the Pliocene is represented by terrestrial deltaic sediments, which produce abundant fossil woods but few vertebrate remains.

The Pliocene sediments in the western Salton Trough encompass about 3.3 km of the continuous 5.5 km-thick stratigraphic section. Stratigraphic nomenclature for these deposits is presently under revision (G. Jefferson and C. Powell, pers. comm.). The nomenclature used herein follows Jefferson and Lindsay (2006) where the lower and upper parts of the Imperial Formation have been designated the Latrania and Deguynos Formations respectively and placed within the Imperial, elevated to group rank by Winker and Kidwell (1996). For an historical summary and correlation of stratigraphic nomina see Remeika (1998) and Lindsay and Jefferson (2006).

Within this stratigraphic sequence in ABDSP, the Mio-Pliocene boundary occurs near the base of the Mud Hills member of the Deguynos Formation of the upper Imperial Group. The Deguynos Formation includes three superposed members, from oldest to youngest; Mud

Hills, Yuha, and Camels Head. The latter two members are laterally equivalent to the basin margin Jackson Fork member of the Deguynos Formation. The Deguynos Formation is overlain by the basal units of the Palm Spring Group (Cassiliano, 2002), which include three laterally equivalent formations at its base. These facies, from basin margin to basin center, are the lower Canebrake Conglomerate, Olla Formation, and Arroyo Diablo Formation. The Pliocene-Pleistocene boundary at 2.58 myr (Gibbard et al., 2010) falls immediately above the base of the Hueso Formation and Tapiado Claystone in the upper part of the Palm Spring Group, above the tops of the Olla and Arroyo Diablo Formations. The Hueso Formation and Tapiado Claystone are laterally equivalent to the uppermost Canebrake Conglomerate, in the upper part of the Palm Spring Group. The following discussion will cover the Deguynos Formation, upper Imperial Group, and the Arroyo Diablo and Olla Formations, lower Palm Spring Group, but not the bases of the Hueso Formation or Tapiado Claystone.

Pliocene formations and fossils

Marine claystones and sandy and silty rhythmities of the Mud Hills member of the Deguynos Formation, largely transported to the Salton Trough by the ancestral Colorado River, overlie the late Miocene Latrania Formation. The Latrania Formation comprises the base of the Imperial Group, and is composed of near shore sands and deeper water sandy turbidites (Dorsey et al., 2011). Within the boundaries of ABDSP, the lower part of the approximately 5.1 to 4.49 myr old Mud Hills member (Dorsey et al., 2007, Dorsey et al. 2006; Dorsey et al., 2011) records the deepest Pliocene marine conditions (Remeika, 1998; McDougall, 2008) of the stratigraphic section exposed in Fish Creek Wash. Although fossils recovered from the approximately 400 m-thick member have not been completely examined, identifications from the lower part of the member include foraminifera (McDougall, 2008) (Appendix I, Table 1), a variety of Mollusca, *Dentalium* (tusk shells), *Tellina* (tellins), Buccinidae (whelks), Echinodermata (sand dollars and star fish), Decapoda (includes crabs), Osteichthyes (bony fish) (P. Gerdson, pers. comm.), and the deep water gulper shark (Centrophoridae) (M. Roeder, 2007). Rhythmities

(Lynch and Adams, 2009) in the upper part of the Mud Hills member are devoid of macrofossils.

Up section, the Mud Hills member claystones and rhythmites are replaced by sandstones and silty sandstones of the 600 m-thick Yuha member. These approximately 4.49 to 4.35 myr old sediments (Dorsey et al. 2006; Dorsey et al., 2011) record basin filling by the ancestral Colorado River and shallowing marine water (Remeika, 1998; Deméré, 2006). The Yuha member is typified by sandstone coquina lenses interpreted as tempestites (storm deposits) that were deposited on the growing river delta front. The coquinas are composed primarily of *Dendostrea vespertina* (oyster), *Anomia costata* (jingle shell), and *Argopecten deserti* (scallop); all are brackish water or estuarine forms. However, invertebrates in the uppermost part of the Yuha member, in near shore deposits, are abundant and include a broad diversity of taxa as documented in Appendix I, Table 2 (also see Deméré and Rugh, 2006). The faunal assemblage has Caribbean affinities, is indicative of warm, shallow waters, and predates closure of the eastern Pacific-Caribbean marine connection by formation of the Isthmus of Panama.

The fossil marine vertebrates from the Yuha and Camels Head members, of the upper Deguynos Formation (Appendix I, Table 3) include a variety of Chondrichthyes (sharks and rays) (M. Roeder, pers. comm.), Osteichthyes (bony fish) (H. Fierstine, pers. comm.; M. Roeder, pers. comm.), super family Chelonioidae (sea turtle), Odontoceti (dolphins and porpoises), Mysticeti (baleen whales), and Pinnipedia (seals, sea lions and walruses) (Deméré pers. comm.; Atterholt and Jefferson; 2008; Atterholt et al., 2008). Of particular interest are the remains of the walrus *Valenictus imperialensis*. Based on a nearly complete and unusually small humerus, femur and tibia (probably female), this species appears to represent a dwarfed form related to *V. chulavistensis*, the latter taxon is found in Pliocene deposits on the San Diego coast (Atterholt and Jefferson, 2007; Atterholt et al., 2008).

Terrestrial vertebrates from the Yuha member are represented by isolated, often incomplete, abraded bones and teeth that have been transported to the delta. Taxa include a Crocodylia (alligators, caimans and crocodiles), *Megalonyx* (ground sloth), Procyonidae (raccoons), *Dinohippus* (primitive horse) (E. Scott pers. comm.), large, medium, and small-sized Camelidae (camels and llamas), and Cervidae or Antilocapridae (deer or pronghorn). Magnetostratigraphic data (Dorsey et al. 2006; Dorsey et al., 2011) indicate sediments of the Yuha Member are of reversed polarity, lie entirely within subchron C3n.1r and are between about 4.49 and about 4.35 myr. The age of the sediments and presence of the terrestrial genera *Dinohippus* and *Megalonyx* are consistent with assignment of the faunal assemblage to the early part of the Blancan North American Land Mammal Age (NALMA, Bell et al., 2004).

Overlying the Yuha member, the approximately 4.35 to 4.24 myr old, 600 m-thick Camels Head member (Dorsey et al. 2006; Dorsey et al., 2011) of the Deguynos Formation records a transition to terrestrial deltaic conditions. The unit interfingers at its base with the Yuha member and at its top with terrestrial deltaic sandstones of the overlying Arroyo Diablo Formation. Camels Head member sandstones, silty sandstones and siltstones were deposited largely within the tidal zone and record beach and mudflat conditions. The member yields a rich near-shore marine molluscan assemblage similar to that from the Yuha member (see Deméré and Rugh, 2006) as well as fossil woods typically found in the Arroyo Diablo Formation (see below). T. Downs and J. White used the informal name *Loop Wash local fauna* for the mammalian fossil assemblage from the Yuha and Camels Head members on faunal lists and collections records at the Natural History Museum of Los Angeles County (Murray, 2008). Fossil mammals from the Camels Head member conform with assemblages elsewhere associated with the early Blancan NALMA.

Upper members of the Deguynos Formation, the Yuha and Camels Head, interfinger laterally with basin margin deposits of the Jackson Fork member. This sandstone is composed of local clastic debris shed from the western terrestrial edge of the Salton Trough (Winker, 1999). The member yields scattered *Dendrostrea vespertina* (oyster), *Argopecten* (scallop), *Turritella imperialis* (tower snail), *Cerithium* (cerith snail), *Oliva* (olive snail), *Encope* (sand dollar), Decapoda (includes crabs), but few vertebrate remains. Of note is a complete mandible of the llama *Hemiauchenia vera* (ABDSP 2340/V6616, Figure 1) from Travertine Palms Wash (see Summary and Discussion below). This latest Miocene, Hemphillian NALMA taxon also occurs in the Olla Formation from the Truckhaven

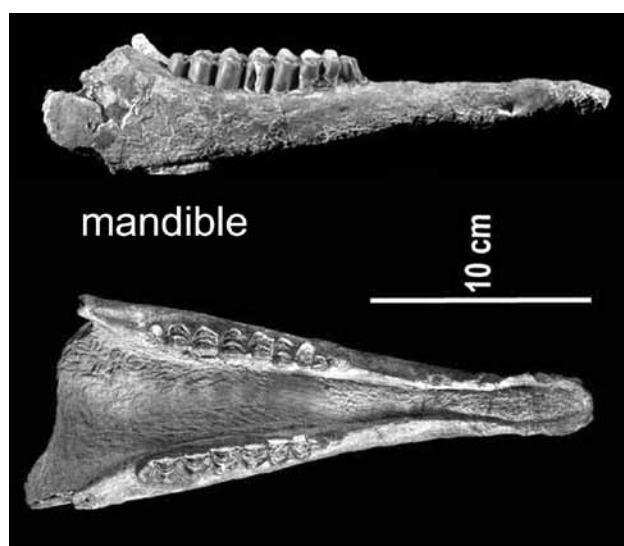


Figure 1. *Hemiauchenia vera* mandible. The specimen, ABDSP 2340/V6616, was recovered from the Jackson Fork Member of the Deguynos Formation, southwest of Garnet Wash. Although not visible in this image, *Dendostrea vespertina* was found adhering to the lingual surface of the right dentary.

Rocks (discussed below) where it is associated with Mio-Pleistocene Blancan NALMA forms.

The Arroyo Diablo Formation (Cassiliano, 2002), about 4.25 to 2.8 myr old (Dorsey et al. 2006; Dorsey et al., 2011), is an approximately 2.5 km-thick sequence of terrestrial deltaic sands and silts transported by the ancestral Colorado River. It yields a rich paleoflora, named the *Carrizo local flora* by Remeika (2006a, 2006b) (Appendix I, Table 4) and is comprised largely of fossil logs and driftwood. Modern representatives of taxa identified in the assemblage have coastal California and central Mexico affinities. This suggests that the ancestral Peninsular Range did not block maritime air flow at that time, and rainfall as far inland as southeastern California and southern Arizona may have been as high as 63 cm/year (25 in/year) (Remeika, 2006a). This sequence also produces Cretaceous fossil pollen that has been reworked from deposits on the Colorado Plateau (Remeika and Fleming, 1995).

Vertebrate remains identified from the Arroyo Diablo Formation include *Gomphotherium* (welded beast) (McDaniel and Jefferson, 2002). However, this assignment may be in error and requires re-evaluation. Also present are cf. *Dinohippus* sp. (primitive horse) (Scott, 2006), and Camelidae (camels). Based on magnetostratigraphic data, the sediments of the Arroyo Diablo Formation in the Fish Creek Wash section were deposited between about 4.24–2.8 myr. The earliest sediments of the unit retain normal polarity, interpreted as the last part of the Cochiti subchron (C3n.1n). The remainder of the formation produces reversed polarity signal of subchron C2Ar (Dorsey et al. 2006; Dorsey et al., 2011). The age of the sediments derived from the polarity sequence suggests an associated faunal assemblage of early mid-Blancan NALMA affinities. However, occurrences of *Gomphotherium* and *Dinohippus* are known elsewhere exclusively from sediments no younger than the Hemphillian-Blancan transition (5.2-4.6 myr; Bell et al., 2004). The ABDSP specimens upon which these two local taxa are based require more detailed evaluation.

The Fish Creek/Vallecito Creek badlands exposures of the Olla Formation in the southern part of ABDSP date from approximately 4.25 to 2.8 myr (Dorsey et al. 2006; Dorsey et al., 2011). Here, the Olla Formation interfingers basinward with the Arroyo Diablo Formation. Toward the basin margin it interfingers at its base with the Jackson Fork member of the Deguynos Formation and up-section with the Canebrake Conglomerate. Winker (1987; Winker and Kidwell, 1996) described the Olla Formation as composed of locally derived fluvial sandstones and siltstones interbedded with Arroyo Diablo Formation-like Colorado River sediments.

Mammal fossils from the Olla Formation in the Fish Creek/Vallecito Creek badlands conform with assemblages elsewhere associated with the Blancan NALMA. Based on magnetostratigraphy (late subchron C2Ar through mid-C2An.1n) are approximately 3.75-2.75

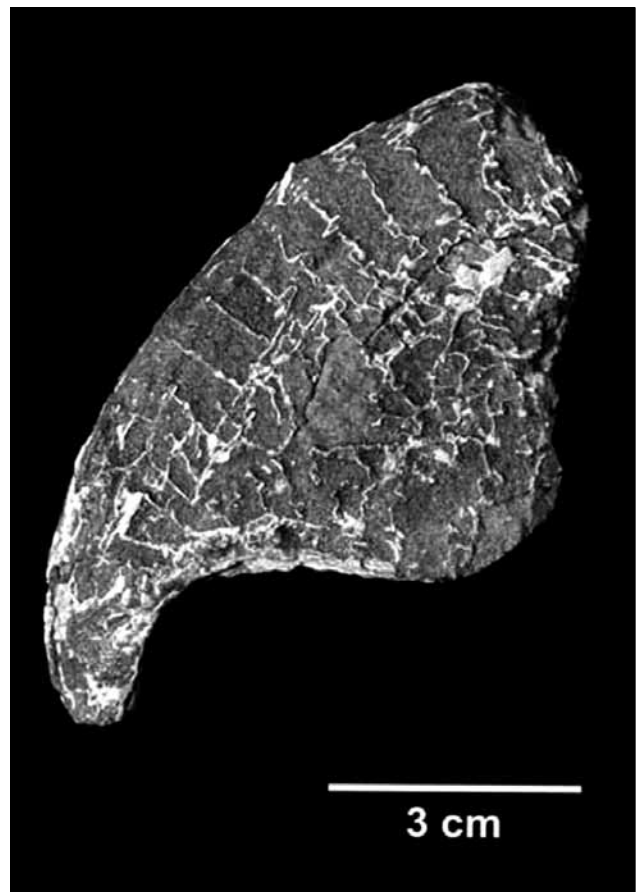


Figure 2. ?*Titanis* premaxilla. The specimen, ABDSP(LACM) 6747/V26697, was recovered from the Olla Formation in Fish Creek Wash.

myr in age (Dorsey et al., 2006; Dorsey et al., 2011). Downs and White (1968; Murray, 2008) referred to fossil assemblages from these exposures as the *Layer Cake local fauna* (Appendix I, Table 5) (Cassiliano, 1999). A rich assemblage of mammalian ichnofossils (tracks and trackways), named the *Fish Creek Canyon Ichnofauna* by Remeika (2006c), is also known from the Olla Formation (Appendix I, Table 6). The deposit produced three identified avian fossils, a set of tracks assigned to *Gruipeidia diabloensis* (Diablo least sandpiper) (Remeika, 2006c), a specimen identified as *Pelicanus* (pelican) (Howard, 1963; Jefferson, 2006), and a specimen tentatively referred to *Titanis* (terror bird) (R. Chandler, pers. comm.) (ABDSP[LACM] 6747/V26697, Figure 2). The latter specimen was previously assigned to *Teratornis incredibilis* (Howard, 1963) and was subsequently placed in the new genus *Aiolornis* by Campbell et al. (1999) (see Jefferson 2006). *Titanis* is typically found in Blancan NALMA deposits along the Gulf of Mexico coast and in Florida. Its presence in the Salton Trough represents a major westward range extension.

At Truckhaven Rocks in the northern part of ABDSP, exposures of the approximately 620 m-thick Olla Formation are largely fluvial channel sandstones (often cross-bedded) and overbank sandy and silty claystones (Mroz et al., 2011). Tongues of Arroyo Diablo Formation-like

sediments, as described by Winker (1987) for deposits exposed in Fish Creek Wash, appear mainly in the upper part of the unit where they also interfinger with lacustrine claystones of the Borrego Formation.

Recently recovered vertebrate fossils from the Olla Formation at Truckhaven Rocks (Appendix I, Table 7) (Mroz et al. 2011), are assigned to the late Hemphillian and/or early Blancan NALMAs based on the occurrence of *Hypolagus*, *Hemiauchenia vera*, and *Blancocamelus*. The base of the Blancan NALMA dates to between 5.2 to 4.6. Ma (Bell et al., 2004). The genus *Hypolagus* appears in the fossil record elsewhere in North America from mid-Miocene through Pliocene age localities. The latest records of *Hypolagus* in the Fish Creek/Vallecito Creek basin occur at about 3.2 myr. *Blancocamelus* is reported from only a limited number of Plio-Pleistocene localities, including the type site of the Blancan NALMA, Mt. Blanco, Texas. Whereas, *Hemiauchenia vera* is reported exclusively from Hemphillian NALMA localities (Honey, 1998) which are latest Miocene in age. Lacking absolute dates, precise correlation of these rocks with the type Olla Formation in the Fish Creek/Vallecito Creek basin is uncertain, but the Olla Formation at Truckhaven Rocks is latest Miocene or early Pliocene in age..

The Borrego Formation is not exposed in the southern part of ABDSP in the Fish Creek/Vallecito Creek badlands. To the north it interfingers with and overlies the Arroyo Diablo Formation, producing the fresh water snails *Physa humerosa* and *Gyraulus* sp., and the bivalve *Anodonta californiensis*. The lower part of the Borrego Formation interfingers with the Arroyo Diablo Formation where tongues of the Arroyo Diablo Formation yield reworked fossil wood and shells of *Dendostrea vespertina*, *Argopecten* and *Anomia*, possibly derived from the Yuha member of the Deguynos Formation. Lacustrine and playa deposits of the Borrego Formation were deposited in the Salton Trough on the north side of the ancestral Colorado River delta which was located east and southeast of ABDSP.

Summary and discussion

Some Pliocene deposits that crop out along the western Salton Trough in ABDSP may be correlative to those outside of ABDSP in the northern and eastern Trough, others may not be. Lithology and the fossils contained in these deposits allow an assessment of depositional environments and may provide the basis for tentative correlations where absolute dates are lacking. Such observations could aid in interpreting the sequence of depositional events in the Trough, and could help answer questions about facies changes and time transgressions.

Marine claystones and rhythmites of the Mud Hills member are the oldest Pliocene deposits on the west side of the Salton Trough, where the unit conformably overlies relatively deep water turbidites of the late Miocene-age Latrania Formation (Dorsey et al., 2007). Sediments in

the Mud Hills member were deposited basinward of the advancing ancestral Colorado River delta (Remeika, 1998; Deméré, 2006). At that time, the ancestral Colorado River delta was located on the northeastern-most margin of the Trough. To our knowledge, Mud Hills member-like deposits have not been identified in exposures in the northern Trough on either side of the San Andreas Fault. This is not unexpected given the location of the Ancestral Colorado River delta relative to ABDSP.

Above the Mud Hills member, depositional environments in the Yuha and Camels Head members are interpreted as a marine delta front shallowing up section into near-shore delta conditions (Remeika, 1998; Deméré, 2006). The Yuha and Camels Head member deposits grade laterally into locally derived Jackson Fork member sandstones. Fossil invertebrates from upper members of the Deguynos Formation (Table 2), generally correlate in age and taxonomic content to assemblages recovered from exposures further north on the west side of the Salton Trough. These sites in Wonderstone Wash (Mroz et al., 2011), Travertine Point (Powell, 2008), and along Travertine Palms Wash and Garnet Wash (= Garner Wash) (King et al., 2002) are not contiguous. All locations apparently represent near shore depositional settings but may be slightly different in age. Powell (2008) assigned a Pliocene age to the Travertine Point assemblage, and the presence of *Hemiauchenia vera* suggests a latest Miocene age (see Jackson Fork Formation above) for the most western site.

Only *Dendostrea vespertina* is known from the Wonderstone Wash locality south of Travertine Point. Although *Dendostrea vespertina* is the most abundant taxon in the Yuha member tempestites, the lack of other molluscan taxa at Wonderstone Wash precludes a firm temporal or facies correlation of this locality with the upper members of the Deguynos Formation or with the Garnet Wash and/or Travertine Palms Wash deposits.

The Garnet Wash deposits including Travertine Point (Powell, 2008) are described by King et al. (2002) as:

Those deposits . . . consist of yellow- to olive-gray marine sandstone and conglomerate that overlie and interfinger with nonmarine sandstone, conglomerate, and rock-avalanche breccia derived from the west. They contain a diverse suite of bivalves, gastropods, echinoids, barnacles, and corals. The main body of marine strata consists of gypsiferous olive-gray mudstone and very fine sandstone containing shark and ray teeth, Neogene benthic forams, and recycled Cretaceous coccoliths. Intercalated beds of coquina and coarse sandstone contain disarticulated oysters and clams, barnacles, sand dollars, and sparse gastropods. A variegated sequence of gray, brown, pink, and orange paralic sandstone and mudstone with sparse clams and oysters caps the marine section.

Although the authors have not provided specific taxa, the listed fossils can not be distinguished from assemblages from the upper Deguynos Formation. Furthermore the presence of coquina, and the described lithologies compare with those in exposures of the Jackson Fork, Camels Head and Yuha members in the Fish Creek Wash stratigraphic section. Only seven taxa are shared between the Travertine Point assemblage (invertebrate taxa N=22) (Powell, 2008) and fossils from the Yuha and Camels Head members (invertebrate taxa N=33) (see Table 2). Although of similar age, the shared taxa of the Yuha and Camels Head members are largely estuarine forms, whereas the Travertine Point fossils, for the most part, suggest deeper water conditions (Powell, 2008). From east to west, localities along Travertine Palms Wash appear to represent increasingly shallower water depths. The mouth of the ancestral Colorado River was located northeast of Fish Creek Wash, and Travertine Palms Wash at that time.

Deposits in the northeastern Salton Trough that are potentially correlative with the upper Deguynos Formation lie between two branches of the San Andreas Fault at the Indio Hills Palms Covered Wagon localities (Jefferson and Musick, 2008) and Willis Palms (Ballard, 1971; Bauerfield, 1971; Morgan, 1971; Powell, 1986; Mc Dougal pers. comm., 1995, 2008; Powell et. al. 2011) (Appendix I, Table 8). The Indio Hills marine deposits (Willis Palms and Covered Wagon localities, invertebrate taxa N=45) and the upper members of the Deguynos Formation (invertebrate taxa N=33) have 13 invertebrate taxa and one vertebrate taxon (*Myliobatis* or eagle ray) in common (see Table 2). Recovered foraminifera from Willis Palms (Table 8) indicate a Pliocene or younger age and very shallow marine water depths (McDougall, 2008). Although coquinas are not present at either the Willis Palms or Covered Wagon localities, lithologies are otherwise similar to the upper Yuha and in part Camels Head members of the Deguynos Formation. Because marine deposits along the eastern side of the Trough may have been moved northwestward along the fault, proximity to the mouth of the ancestral Colorado River at that time is uncertain.

No fossil wood bearing Arroyo Diablo Formation-like deposits have been reported in the northern or eastern part of the Salton Trough. However, Arroyo Diablo Formation-like sandstones are associated with Borrego Formation-like deposits that crop out in the Mecca Hills on the east side of the Trough between branches of the San Andreas Fault (Dorsey pers. comm.). Fluvial sandstones and finer-grained overbank deposits that resemble exposures of the Olla Formation at the Truckhaven Rocks also crop out in the southern Mecca Hills, east of and between branches of the San Andreas Fault. However, these deposits apparently do not contain interbedded Arroyo Diablo Formation-like sandstones (Winker, 1987). During deposition of the Arroyo Diablo and Olla Formations, the mouth of the ancestral Colorado River was east-northeast to east of ABDSP. However because deposits on the east

side of the Salton Trough may have been moved northwestward along the San Andreas Fault, proximity of these deposits to the mouth of the ancestral Colorado River at that time is uncertain.

No Pliocene age invertebrate fossils have been reported from the Mecca Hills. Although sediments that are the same age as the upper Palm Spring Group and Ocotillo Conglomerate of ABDSP (Indio Formation of Buwalda and Stanton, 1930; and Palm Spring Formation of Dibblee, 1954, 1997, and Rhymer, 1991) have been mapped in the Indio Hills and Mecca Hills, no vertebrate remains have been reported from the Indio or Mecca Hills from lithological equivalents of formations in the Pliocene lower Palm Spring Group. It is anticipated that the present geological investigations in the Mecca Hills by Dorsey et al. (pers. comm.) will shed light on possible lithological correlations with Pliocene formations and depositional events recorded by deposits on the western side of the Salton Trough.

References

- Atterholt, J., and G.T. Jefferson 2007. New vertebrates from the Yuha member of the Deguynos Formation of Anza-Borrego Desert State Park. *Journal of Vertebrate Paleontology* 27(3):42A.
- Atterholt, J., G.T. Jefferson, E. Schachner, and J. Hughes 2008. Marine vertebrates from the Yuha Member of the Deguynos Formation, Anza-Borrego Desert State Park. In *Trough to Trough the Colorado River and Salton Sea*, edited by R.E. Reynolds, The 2008 Desert Symposium Field Guide and Proceedings, California State University, Desert Studies Consortium and L.S.A. Associates Inc. p. 110-111.
- Ballard, A. 1971. The paleoecology of a marine deposit in the northwest Indio Hills. *Geology* 111B, Department of Geological Sciences, University of California, Riverside 12 p.
- Bauerfield, A.G. 1971. Paleoecology of the Tertiary fauna Willis Palms Formation, Thousand Palms quadrangle, California. *Geology* 111B, Department of Geological Sciences, University of California, Riverside 19p.
- Bell, C. J., E. L. Lundelius Jr., A. D. Barnosky, R. W. Graham, E. H. Lindsay, D. R. Ruez Jr., H. A. Semken Jr., S. D. Webb, and J. R. Zakrzewski 2004. The Blancan, Irvingtonian, and Rancholabrean mammal ages; pp. 232-314 in M. O. Woodburne (ed.), *Late Cretaceous and Cenozoic Mammals of North America, Biostratigraphy and Geochronology*. Columbia University Press, New York, New York, 391 pp.
- Buwalda, J.P., and Stanton, W.L., 1930, Geologic events in the history of the Indio Hills and the Salton Basin, California: *Science (new series)*, v. 71, p. 104-106.
- Buwalda, J.P. 1997. Geology of the southeastern San Andreas Fault Zone in the Coachella Valley area, southern California. In *Southern San Andreas Fault Whitewater to Bombay Beach, Salton Trough, California*, edited by J. Baldwin, L. Lewis, M. Payne, and G. Roquemore, South Coast Geological Society Field Trip Guide Book 25:35-56.
- Campbell, K.E., Jr., E. Scott, and K.B. Springer 1999. A new genus for the incredible teratorn (Aves: Teratornithidae). In *Avian Paleontology at the Close of the 20th Century: Proceedings of the 4th International Meeting of the Society*

- of Avian Paleontology and Evolution, edited by S.L. Olson, Smithsonian Contributions to Paleobiology 89:169-175.
- Cassiliano, M.L. 1999. Biostratigraphy of Blancan and Irvingtonian mammals in the Fish Creek-Vallecito Creek section, southern California, and a review of the Blancan-Irvingtonian boundary. *Journal of Vertebrate Paleontology* 19(1):169-186.
- Cassiliano, M.L. 2002. Revision of the stratigraphic nomenclature of the Plio-Pleistocene Palm Spring Group (new rank), Anza-Borrego Desert, southern California. *Proceedings of the San Diego Society of Natural History* 38:1-30.
- Deméré, T.A. 2006. The Imperial Sea: marine geology and paleontology. *In* The Fossil Treasures of the Anza-Borrego Desert, edited by G.T. Jefferson and L. Lindsay, Sunbelt Publications, San Diego, California p. 29-42.
- Deméré, T.A., and N.S. Rugh 2006. Invertebrates of the Imperial Sea. *In* The Fossil Treasures of the Anza-Borrego Desert, edited by G.T. Jefferson and L. Lindsay, Sunbelt Publications, San Diego, California p. 43-69.
- Dibblee, T.W., Jr., 1954. Geology of the Imperial Valley region, California, in Jahns, R.H., ed., *Geology of southern California: California Division of Mines and Geology Bulletin*, no. 170, p. 21-81.
- Dorsey, R.J., A.L. Fluette, B.A. Housen, K.A. McDougall, S.U. Janecke, G.J. Axen, C. Shirvell. 2006. Chronology of Late Miocene to Early Pliocene Sedimentation at Split Mt. Gorge, Western Salton Trough: Implications for Development of the Pacific-North America Plate Boundary. Poster presented at RCL-Cortez Workshop: "Lithospheric Rupture in the Gulf of California -Salton Trough Region," Ensenada (Mexico), January 9-13, 2006.
- Dorsey, R.J., A. Fluette, K. McDougall, B.A. Housen, S. Janecke, G.J. Axen, and C.R. Shirvell 2007. Chronology of Miocene-Pliocene deposits at Split Mountain Gorge, southern California: a record of regional tectonics and Colorado River evolution. *Geology* 35(1):57-60.
- Dorsey, R.J., B.A. Housen, S.U. Janecke, C.M. Fanning, and A.L.F. Spears 2011. Stratigraphic record of basin development within the San Andreas fault system: Late Cenozoic Fish Creek-Vallecito basin, southern California. *Geological Society of America Bulletin* 123(5,6):771-793.
- Downs, T., and J.A. White 1968. A vertebrate faunal succession in superposed sediments from late Pliocene to middle Pleistocene in California. *In* Tertiary/Quaternary Boundary, International Geological Congress 23, Prague 10:41-47.
- Gastil, R.G., D.L. Krummenacher, and P.L. Abbott 1996. Arrival of the Colorado River in the Salton Trough defined by magnetic susceptibility. *In* Sturzstorms and Detachment Faults Anza-Borrego Desert State Park California, edited by P.L. Abbott and D.C. Seymour, South Coast Geological Society Annual Field Trip Guide Book Number 24:203-208.
- Gibbard, P.L., M.J. Head, and M.J.C. Walker 2010. Formal ratification of the Quaternary System/Period and the Pleistocene Series/Epoch with a base at 2.58 Ma. *Journal of Quaternary Science*, 25: 96-102.
- Honey, J.G., J.A. Harrison, D.R. Prothero, and M.S. Stevens 1988. Camelidae; pp. 439-462 in C. M. Janis, K. M. Scott, and L. L. Jacobs (eds.), *Evolution of Tertiary Mammals of North America*. Cambridge University Press, Cambridge, United Kingdom, 691 pp.
- Howard, H.H. 1963. Fossil birds from the Anza-Borrego Desert. *Los Angeles County Museum Contributions in Science* 73:1-33.
- Jefferson, G.T. 2006. The fossil birds of Anza-Borrego. *In* The Fossil Treasures of the Anza-Borrego Desert, edited by G.T. Jefferson and L. Lindsay, Sunbelt Publications, San Diego, California p. 151-158.
- Jefferson, G.T., and L. Lindsay (editors) 2006. *The Fossil Treasures of the Anza-Borrego Desert*, Sunbelt Publications, San Diego, California 394 p.
- Jefferson, G.T., and S.T. Musick 2008. Indio Hills Palms 646, paleontologic resources inventory and management recommendations. Document on File, Department of Parks and Recreation Natural Resources Division, Sacramento, and Colorado Desert District Stout Research Center Library, Borrego Springs 15 p.
- King, T., B.F. Cox, J.C. Matti, C.L. Powell, II, L.E. Osterman, and L.M. Bybell 2002. Previously unreported outcrops of Neogene Imperial Formation in southern Santa Rosa Mountains, California, and implications for tectonic uplift. *Geological Society of America Abstracts with Program* 34:124.
- Lindsay, L., and G.T. Jefferson 2006. Appendix Table 4: Stratigraphic names correlation table. *In* The Fossil Treasures of the Anza-Borrego Desert, edited by G.T. Jefferson and L. Lindsay, Sunbelt Publications, San Diego, California 365 p.
- Lynch, D.K., and P.M. Adams 2009. Fish Creek rhythmites and aperiodic temporal sedimentation. *In* Landscape Evolution at an Active Plate Margin, The 2009 Desert Symposium Field Guide and Proceedings, edited by R.E. Reynolds and D.R. Jessey, California State University Desert Studies Consortium and LSA Associates, Inc., p. 159-164.
- McDaniel, G., and G.T. Jefferson 2002. A new gomphothere from the Mid-Pliocene ancestral Colorado River deltaic deposits in Anza-Borrego Desert State Park, California. *In* Between the Basins: Exploring the Western Mojave and Southern Basin and Range Province, edited by R.E. Reynolds, California State University, Desert Studies Consortium p. 77.
- McDougall, K. 2008. Late Neogene marine incursions and the ancestral Gulf of California. *Geological Society of America Special Paper* 439:353-371.
- Morgan, T.G. 1971. Paleoecology of the Willis Palms oyster beds. *Geology* 11B, Department of Geological Sciences, University of California, Riverside 11p.
- Mroz, A., G.T. Jefferson, and L.K. Murray 2011. Deferred Maintenance Program project report July 2011: Truckhaven Rocks #158280. Document on File, Department of Parks and Recreation Natural Resources Division, Sacramento, and Colorado Desert District Stout Research Center Library, Borrego Springs 26 p.
- Murray, L.K. 2008. Effects of taxonomic and locality inaccuracies on biostratigraphy and biochronology of the Hueso and Tapiado formations in the Vallecito Creek-Fish Creek section, Anza-Borrego Desert, California. *Doctoral Dissertation*, Department of Geology, University of Texas, Austin 531 p.
- Powell, C.L. 1986. Stratigraphy and bivalve molluscan paleontology of the Neogene Imperial Formation in Riverside County, California. *Master of Science Thesis*, Department of Geology, California State University, San Jose 275 p.
- Powell, C.L. 2008. Pliocene invertebrates from the Travertine Point outcrop of the Imperial Formation, Imperial County, California. *U.S. Geological Survey Scientific Investigations Report* 2008-5155 25 p.
- Powell, C.L. II, M.A. Roeder, and K. McDougall 2011. A preliminary report on the paleontology of the Imperial Formation (ancestral Gulf of California; Pliocene) in the Indio Hills, Riverside County, southern California. *CalPaleo 2011 Abstracts with Program*, Sierra College, Rocklin, California p. 22.
- Remeika, P. 1998. Marine invertebrate paleontology and stratigraphy of the Vallecito-Fish Creek Basin: a historic review, synthesis, and revision. *In* *Geology and Hydrothermal Resources of the Imperial and Mexicali Valleys*, edited by L. Lindsay and W.G. Hample, San Diego Association of Geologists Annual Field Trip Guidebook 1998 p. 59-92.
- Remeika, P. 2006a. Ancestral woodlands of the Colorado River delta plain. *In* The Fossil Treasures of the Anza-Borrego Desert, edited by G.T. Jefferson and L. Lindsay, Sunbelt Publications, San Diego, California p. 75-87.
- Remeika, P. 2006b. Ancestral woodlands of the Colorado River delta plain. *In* The Fossil Treasures of the Anza-Borrego

- Desert, edited by G.T. Jefferson and L. Lindsay, Sunbelt Publications, San Diego, California p. 75-87.
- Remeika, P. 2006c. Fossil footprints of Anza-Borrego. *In* The Fossil Treasures of the Anza-Borrego Desert, edited by G.T. Jefferson and L. Lindsay, Sunbelt Publications, San Diego, California p. 293-327.
- Remeika, P., and R.F. Fleming 1995. Cretaceous plynoflora and Neogene angiosperm woods from Anza-Borrego Desert State Park, California: implications for Pliocene climate of the Colorado Plateau and age of the Grand Canyon. *In* Paleontology and Geology of the Western Salton Trough Detachment, Anza-Borrego Desert State Park, California, edited by P. Remeika and A. Sturz, Field Trip Guidebook and Volume for the 1995 San Diego Association of Geologists Field Trip to Anza-Borrego Desert State Park, Volume 1:64-81.
- Roeder, M.A., and R.W. Huddleston 2012, and needs to be added to the references. First records of fossil fish remains from northern exposures of the marine Imperial Formation, Riverside County, California. *Southern California Academy of Science* 110(2):115-116.
- Rymer, M.J., 1991, The Bishop Ash bed in the Mecca Hills, in Walawender, M.J., and Hanan, B.B., eds., Geological excursions in southern California and Mexico: Geological Society of America annual meeting guidebook, San Diego, p. 388-396.
- Roeder, M.A. 2007. A late Miocene record of a fossil gulper shark (Family Centrophoridae) from the Mud Hills Member of the Deguynos Formation of the Imperial Group, Lycium Wash, Fish Creek Basin, Anza Borrego Desert State Park, San Diego County, California. *In* Wilde, Scenic and Rapid, a Trip Down the Colorado River Trough, edited by R.E. Reynolds, the Desert Symposium Field Guide and Abstracts from Proceedings California State University, Desert studies Consortium and LSA Associates, Inc. p. 83.
- Scott, E. 2006. Extinct horses and their relatives. *In* The Fossil Treasures of the Anza-Borrego Desert, edited by G.T. Jefferson and L. Lindsay, Sunbelt Publications, San Diego, California p. 253-271.
- Winker, C.D. 1987. Neogene stratigraphy of the Fish Creek-Vallecito section, southern California: implications for early history of the northern Gulf of California and Colorado delta. Doctoral Dissertation, Department of Geosciences, University of Arizona, Tucson 494 p.
- Winker, C.D., and S.M. Kidwell 1996. Stratigraphy of a marine rift basin: Neogene of the western Salton Trough, California. *In* Field Conference Guide, edited by P.L. Abbott and J.D. Cooper, Pacific Section of American Association of Petroleum Geologists, GB 73, Pacific Section Society of Economic Paleontologists and Mineralogists, Book 80:295-336.

Appendix I: Tables

Table 1. Foraminifera from the Mud Hills member of the Deguynos Formation, (list extracted from McDougall, 2008).

Bolivina subexcavata
Cibicides mckennai
Hanzawaia nitidula
Nonionella basispinata
Tarifarina angulosa
Elphidium poeyanum
Nonionella stella
Valvulineria inflata
Ammonia beccaree
 planktic foraminifers

Table 2. Marine invertebrate fossils from upper members of the Deguynos Formation in Fish Creek. (* = taxa in common with the Travertine Point and Garnet Wash assemblages; ** = taxa in common with Willis Palms and Covered Wagon localities)

| | |
|---|--|
| Phylum Cnidaria | |
| Class Anthozoa | |
| Subclass Zoantharia (corals) | |
| Order Scleractinia | |
| Family Rhizangiidae (= Astrangiidae) (cup corals) | |
| <i>Astrangia haimeii</i> | |
| Family Faviidae (star corals) | |
| <i>Solenastrea</i> * | |
| Family Poritidae (finger corals) | |
| <i>Porites</i> | |
| Phylum Annelidae | |
| Class Polychaeta (worms) | |
| Order Canilapalpa | |
| Family Serpulidae | |
| <i>Serpula</i> | |
| Phylum Mollusca | |
| Class Gastropoda (marine snails) | |
| Order Patellogastropoda | |
| Family Lottiidae (limpets) | |
| " <i>Patella</i> " | |
| Order Neotaenioglossa | |
| Family Calyptraeidae (cup and saucer snails) | |
| <i>Crucibulum scutellatum</i> | |
| Order Neogastropoda | |
| Family Buccinidae (whelks) | |
| <i>Cantharus</i> | |
| <i>Solenosteira anomala</i> | |
| Family Nassariidae | |
| <i>Nassarius</i> ** | |
| Family Cancellariidae (nutmeg snails) | |
| <i>Cancellaria</i> | |
| Family Terebridae (auger snails) | |
| <i>Terebra</i> | |
| Class Bivalvia (marine clams) | |
| Order Arcoida | |
| Family Arcidae (ark clams) * | |
| <i>Anadara carrizoensis</i> ** | |
| Order Pterioidea | |
| Family Pinnidae (penshells) | |
| <i>Pinna latrania</i> | |
| <i>Atrina</i> | |

- Order Ostreoida
 Family Ostreidae (true oysters)
Myrakeena angelica *
Dendostrea vespertina * **
 Family Gryphaeidae (oysters)
Pycnodonte heermanni *
 Family Pectinidae (scallops)
Argopecten **
A. deserti *
Flabelliger
 Family Anomiidae (jingles)
Anomia subcostata **
- Order Veneroida
 Family Lucinidae (lucine clams) **
Miltha *
 Family Crassatellidae (crasstellas)
Eucrassatella **
 Family Cardiidae (cockles or heart clams)
 Family Veneridae (Venus clams)
Chione **
- Order Myoida
 Family Pholadidae (rock piddocks)
Cyrtopleura costata **
- Phylum Echinodermata**
 Class Asteroidea (sea stars)
- Order Paxillosida
 Family Astropectinidae (sand stars)
Astropecten armatus
 Subclass Ophiuroidea
 Family, genus and species indeterminate (brittle stars)
 Class Echinoidea (sea urchins and sand dollars)
- Order Echinoida
 Family Strongylocentrotidae (sea urchins)
Strongylocentrotus purpuratus
- Order Clypeasteroida **
 Family Mellitidae (key-hole sand dollar)
E. tenuis
- Phylum Bryozoa**
 Class Gymnolaemata (bryozoans)
- Order Cheilostomata
 Family Membraniporidae
Conopeum **
- Phylum Arthropoda**
 Subphylum Crustacea
 Class Maxillopoda
- Order Sessilia
 Family Balanidae
Balanus **
- Class Malacostraca
- Order Decapoda
 Family Callinassidae
Callinassa (shrimp)
 Family indet.
 Genus and species indet. (crab) **

Table 3. Marine Vertebrate Fossils from Upper Members of the Deguynos Formation (H. Fierstine pers. comm.; M. Roeder pers. comm.; and Atterholt and Jefferson 2007).

- Class Chondrichthyes
- Order Galeomorpha
 Family Cetorhinidae
Cetorhinus sp. (basking sharks)
 Family Carcharinidae
Carcharhinus sp. (requiem sharks)
Hemipristus serra (east Indian Ocean shark)
 Family Lamnidae
Carcharocles megalodon (giant white shark)
Carcharodon sp. (white sharks)
 Family Odontaspidae
Odontaspis ferox (sand shark)
- Order Myliobatiformes
 Family Myliobatidae
Myliobatis sp. (eagle rays)
- Class Actinopterygii
- Order Clupeiformes
 Family Clupeidae
 Genus and species indeterminate (herrings)
- Order Tetraodontiformes
 Family Tetraodontidae
Arothron sp. (puffer fish)
 Family Balistidae
 Genus and species indeterminate (triggerfish)
- Order Perciformes
 Family Labridae
Semicossyphus sp. (sheepshead)
 Family Sphyraenidae
Sphyraena sp. (barracudas)
- Class Reptilia
- Order Testudines
 Family Cheloniidae
 Genus and species indeterminate (sea turtles)
- Class Mammalia
- Order Carnivora
 Superfamily Pinnipedia
 Family Odobenidae
Valenictus imperialensis (Imperial walrus)
 Family indeterminate
 Genus and species indeterminate (seals and sea lions)
- Order Cetacea
 Suborder Odontoceti (toothed whales)
 Family indeterminate
 Genus and species indeterminate (dolphins and porpoises)
 Suborder Mysticeti
 Family indeterminate
 Genus and species indeterminate (baleen whales)

Table 4. The Carrizo Local Flora (modified from Remeika 2006a, 2006b).

| |
|--|
| Class Gymnospermae |
| Order Coniferales |
| Family Cupressaceae |
| <i>Pinoxylon</i> sp. (cedar or juniper) |
| Class Angiospermae |
| Subclass Dicotyledones |
| Order Laurales |
| Family Lauraceae |
| <i>Persea coalingensis</i> (avocado) |
| <i>Umbellularia salicifolia</i> (bay-laurel) |
| Order Malpighiales |
| Family Salicaceae |
| <i>Populus</i> sp. (cottonwood) |
| <i>Populus</i> sp. cf. <i>P. alexanderi</i> (Alexander's cottonwood) |
| <i>Salix</i> sp. (willow) |
| <i>Salix goodingii</i> (Gooding's willow) |
| Order Lamiales |
| Family Oleaceae |
| <i>Fraxinus caudata</i> (ash) |
| Order Fagales |
| Family Juglandaceae |
| <i>Juglans pseudomorpha</i> (walnut) |
| Order Sapindales |
| Family Hippocastanaceae |
| <i>Aesculus</i> sp. (buckeye) |
| Subclass Monocotyledones |
| Order Arecales |
| Family Arecaceae |
| <i>Washingtonia</i> sp (fan-palm) |
| Genus and species indeterminate (palm) |

Table 5. Layer Cake Local Fauna from the Olla Formation, Fish Creek Badlands (modified from Cassiliano, 1999). Avian and mammalian ichno-taxa from the Olla Formation are listed in Table 6

Pelicanus (pelican)
 ?*Titanis* (terror bird)
Hypolagus vetus (ancient rabbit)
Pewelagus dawsonae (Dawson's rabbit)
Geomys anzensis (Anza gopher)
Dipodomys compactus (extinct kangaroo rat)
D. hibbaridi (Hibbard's kangaroo rat)
Dipodomys n. sp. A (extinct kangaroo rat)
Perognathus sp. (pocket mice)
Neotoma (Hodomys) sp. (woodrats)
Sigmodon minor (cotton rat)
Felis (Lynx) rufus (bob cat)
 ?*Dinohippus* sp. (extinct horse)
Hemiauchenia sp. (llama)

Table 6. The Fish Creek Canyon Ichnofauna (modified from Remeika 2006c).

| |
|---|
| Division Vertebratichnia |
| Class Avipedia |
| Order Gruiformipeda |
| Morphofamily Gruipedidae |
| <i>Gruipeda diabloensis</i> (Diablo least sandpiper track) |
| Class Mammalipedia |
| Order Carnivoripedia |
| Morphofamily Mustelipedidae |
| <i>Mustelidichnum vallecitoensis</i> (Vallecito river otter track) |
| Morphofamily Canipedidae |
| <i>Chelipus therates</i> (claw-footed dog track) |
| Morphofamily Felipedidae |
| <i>Pumaeichnum milleri</i> (Miller's lynx-sized cat track) |
| <i>P. stouti</i> (Stout's cheetah track) |
| <i>Pumaeichnum</i> sp. (bobcat-sized felid track) |
| Order Proboscipedida |
| Morphofamily Gomphotheriipedidae |
| <i>Stegomastodonichnum garbanii</i> (Garbani's gomphotherere track) |
| Order Perissodactipedida |
| Morphofamily Hippipedidae |
| <i>Hippipeda downsi</i> (Downs' horse track) |
| Order Artiodactipedida |
| Morphofamily Tayassuipedidae |
| <i>Tayassuichnum</i> sp. (peccary track) |
| Morphofamily Pecoripedidae |
| <i>Lamaichnum borregoensis</i> (Borrego small llama track) |
| <i>Megalamaichnum albus</i> (White's large llama track) |
| Morphofamily Cervipedidae |
| <i>Odocoichnum</i> sp. (deer track) |

Table 7. Fossil Assemblage from the Olla and Borrego Formations, Truckhaven Rocks (modified from Mroz et al. 2011).

Plantae (wood)
Chara (pond weed)
Anodonta (fresh water clams)
 ?*Physa humerosa* (fresh water snail)
Gyraulus (fresh water snails)
 Arthropoda (shrimps and/or insects)
 ?Osteichthyes (boney fish)
 Emydidae (?*Clemmys* sp.) (pond turtle)
Hesperotestudo (giant tortoises)
 ?Iguanidae (iguanaid lizard)
 Aves (birds)
Megalonyx (ground sloth)
Hypolagus (extinct rabbits)
 ?*Sylvilagus* (cottontails)
Geomys (gopher)
 Cricetidae (mice)
Sigmodon (cotton rats)
 Carnivora (? Canidae) (dogs)
 Ursidae (bears)
Equus (extinct large horse)
Equus (extinct small horse)
Platygonus (peccaries)
 Cervidae (deer)
 Antilocapridae (pronghorns)
Hemiauchenia vera (small llama)
Hemiauchenia or *Paleolama* (llamas)
Blancocamelus (stilt-legged camels)
 cf. *Camelops* (camels)

Table 8. Fossils from the Willis Palms and Covered Wagon Localities, Indio Hills. This list is compiled and modified from Ballard (1971), Bauerfield (1971), Morgan (1971), Mc Dougal (pers. comm., 1995), Powell (pers. comm., 1995), Jefferson and Musick (2008), Roeder and Huddleston (2012), and institutional collections records.

| Willis Palms Localities Assemblage | | |
|--|--|--|
| Phylum Protozoa | | |
| Class Sarcodina | | |
| Order Foraminifera (marine foraminifera) | | Family Turritellidae |
| Suborder Miliolacea | | <i>Turritella</i> sp. cf. <i>T. imperialis</i> |
| Family Miliolidae | | <i>Vermicularia eburnea</i> |
| <i>Quinqueloculina lamarckiana</i> | | Family Muricacea |
| Suborder Rotaliina | | <i>Eupleura muriciformis</i> |
| Family Nonionidae | | Family Nassariidae |
| Elphidium gunteri | | <i>Nassarius</i> n. sp.? aff. <i>N. collaris</i> |
| <i>Elphidium</i> sp. cf. <i>E. subarcticum</i> | | Family Turridae |
| Nonionella stella | | ? <i>Crassispira</i> sp. |
| Family Buliminidae | | Order Tectibranchiata |
| <i>Buliminella elegantissima</i> | | Family Bullidae |
| <i>Bolivina compacta</i> | | <i>Bulla striatus</i> |
| Family Glabratellidae | | Family Pyramidellidae |
| <i>Glabratella californica</i> | | <i>Odostoma</i> n. sp.? |
| Family Caucasinidae | | Order Basommatophora |
| <i>Fursenkoina seminuda</i> | | Family Melampidae |
| Family Anomalinidae | | <i>Melampus?</i> sp. |
| <i>Hanzawaia nitidula</i> | | |
| Phylum Mollusca | | Phylum Arthropoda |
| Class Bivalvia (marine clams) | | Class Crustacea |
| Order Arcoida | | Order Cirripeda |
| Family Arcidae | | Family Balanidae |
| <i>Anadara carrizoensis</i> | | gen. et sp. indet. (barnacles) |
| Family Glycymerididae | | Order Decopoda |
| <i>Glycymeris maculata</i> | | Family indet. |
| Order Osteroida | | gen. et sp. indet. (crabs) |
| Family Ostreidae | | |
| <i>Dendostrea? vespertina</i> | | Phylum Bryozoa |
| Family Pectinidae | | Class Ctenostomata |
| <i>Argopecten?</i> sp. | | Order Cheilostomata |
| <i>Cyclopecten</i> sp. cf. <i>C. pernomus</i> | | Family indet. |
| <i>Leptopecten palmeri</i> | | gen. et sp. indet. (bryozoans) |
| Family Anomiidae | | |
| <i>Anomia</i> sp. cf. <i>A. peruviana</i> | | Phylum Vertebrata |
| Order Eulamellibranchia | | Class Chondrichthyes |
| Family Chamidae | | Order Myliobatiformes |
| <i>Chama</i> sp. cf. <i>C. buddiana</i> | | Family Myliobatidae |
| <i>Chama</i> sp. cf. <i>C. frondosa</i> | | <i>Myliobatus</i> sp. (eagle rays) |
| Order Veneroida | | Order Rajiformes or Order Torpediniformes |
| Family Lucinidae | | Family indet. |
| <i>Lucina</i> sp. | | gen. et sp. indet. (rays) |
| Family Corbulidae | | Class Osteichthyes |
| <i>Corbula aequivalis fossilis</i> | | Family indet. |
| Family Crassatellidae | | gen. et sp. indet. (bony fish) |
| <i>Crassatella?</i> sp. | | |
| Family Veneridae | | Covered Wagon Locality Assemblage |
| <i>Chione</i> sp. | | Phylum Mollusca |
| Order Myoida | | Class Bivalvia (marine clams) |
| Family Pholadidae | | Order Pteronchida |
| <i>Cryptopleura costata</i> | | Family Ostreidae |
| | | <i>Dendostea? vespertina</i> |
| Class Gastropoda (marine snails) | | <i>Undulostrea megedon</i> |
| Order Diotocardia | | Family Pectinidae |
| Family Patellacea | | <i>Argopecten?</i> sp. |
| gen. et sp. indet. | | |
| Order Neogastropoda | | Class Gastropoda (marine snails) |
| Family Fasciolaridae | | Family Turbinidae |
| ? <i>Fusinus</i> sp. | | <i>Turbo</i> sp. |
| ? Family Vermetidae | | Order Monocardia |
| ? <i>Serpulorbis</i> sp. | | Family Turritellidae |
| | | <i>Turritella</i> sp. cf. <i>T. imperialis</i> |
| | | |
| | | Phylum Arthropoda |
| | | Class Crustacea |
| | | Order Cirripeda |
| | | Family Balanidae |
| | | gen. et sp. indet. (barnacles) |

Phylum Echinodermata

Class Echinoidea

Order Clypeasteroida

?Family Scutellidae

gen. et sp. indet. (sand dollars)

Phylum Chordata

Subphylum Vertebrata

Superclass Osteichthyes

Family Sciaenidae

Cynoscion (croaker)

Family Gobiidae (gobies)

Family Kyphosidae (marine chubs)

Class Chondrichthyes

Family Triakididae

Myliobatis (leopard shark)

Family Dasyatididae

Dasyatis (stingrays)

Family Myliobatididae

Myliobatis (bat rays)

Family Rhynobatididae

Rhinobatos or *Zapteryx* (guitarfishes)

Earliest delivery of sediment from the Colorado River to the Salton Trough at 5.3 Ma: evidence from Split Mountain Gorge

Rebecca Dorsey

Department of Geological Sciences, University of Oregon, Eugene, OR 97403-1272, rdorsey@uoregon.edu

Introduction

Recent debate has focused on the timing of events that initiated the Colorado River and first delivered sediments to fault-bounded basins in the Salton Trough. Any successful model for integration of this system must include regional linkages from the Colorado River source to the basinal depocenter in the Salton Trough. The Bouse Formation is a regionally extensive, latest Miocene or earliest Pliocene sedimentary sequence along the lower Colorado River trough that represents this link. It includes a thin basal limestone that was deposited in either a marine estuary (Metzger, 1968; Metzger et al., 1973; Smith, 1970; Buising, 1988, 1990) or nonmarine lakes (Spencer and Patchett, 1997; Poulson and John, 2003; House et al., 2005, 2008), or both (McDougall, 2008), overlain by deltaic and fluvial claystone and sandstone. Recent studies document deposition of the basal Bouse limestone in lake waters that were delivered suddenly to the lower Colorado River corridor by large floods, thus heralding the earliest flows of the Colorado River (House et al., 2005, 2008; Spencer et al., 2008, 2011).

Despite recent advances, age constraints from two locations challenge our current understanding of how the Colorado River system first formed and became regionally integrated. According to any model for the Bouse Formation (lake, marine-estuary, or mixed), the earliest through-going Colorado River should post-date deposition of the basal Bouse limestone. A tuff near Buzzards Peak, which was recently correlated to the 4.83-Ma Lawlor Tuff based on major-element geochemistry (Sarna-Wojcicki et al., 2011), is interbedded with and overlain by basal limestone of the Bouse Formation. This predicts that the Colorado River should have first delivered sediment to the Salton Trough after 4.83 Ma. However, a well-dated section in the Fish Creek – Vallecito basin (FCVB), western Salton Trough, records first arrival of Colorado River sands there ~0.5 million years earlier, at 5.3 Ma (Fig. 1; Dorsey et al., 2007, 2011). An alternate route for the early Colorado River has not been fully tested, but seems unlikely.

The oldest Colorado River sands in the FCVB section are found at Split Mountain Gorge (Fig.

1), in the lower part of a 5.5-km thick section that has extremely tight age control based on multiple datasets (Dorsey et al., 2007, 2011). Below I review the data that provide a definitive age of 5.3 Ma for the first arrival of Colorado River sand at Split Mt. Gorge, and discuss some aspects of the problem raised by contradictory ages at Buzzards Peak and the FCVB.

Stratigraphy and age controls

Figure 2 shows the 5.5-km thick stratigraphic column for the FCVB in the western Salton Trough (Dorsey et al., 2007, 2011), with the Wind Caves member of the Latrania Formation highlighted in the lower part of the section. The age of this section has been determined from extensive study of paleomagnetism, microfossil biostratigraphy, and high-precision U-Pb dating of zircons in two ash beds (Dorsey et al., 2007, 2011). The dated ash beds high in the section unambiguously establish correlation of our magnetic-reversal chronology to the geomagnetic polarity time scale (GPTS). Dense sample

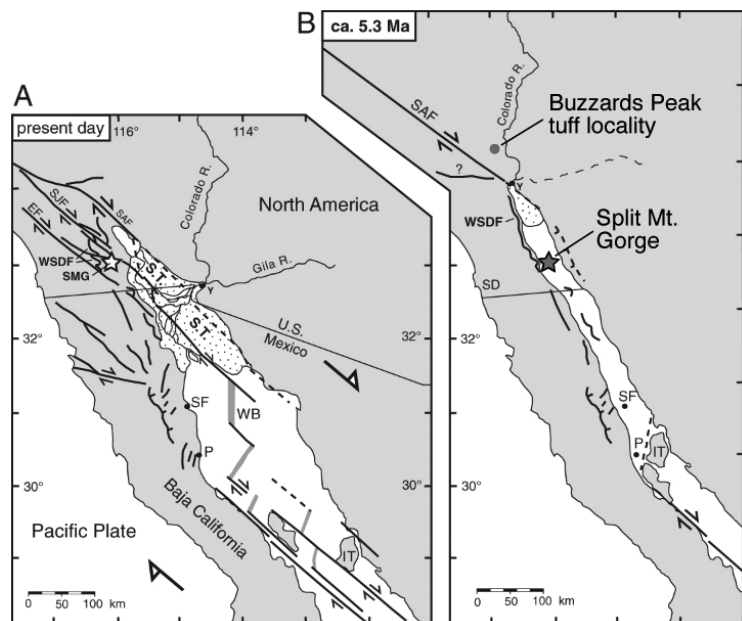


Figure 1. A. Regional tectonic map showing major faults in SE California and northwestern Mexico, and location of Split Mountain Gorge (SMG, star) in the western Salton Trough. B. Reconstruction for 5.3 Ma, restores ~250 km of dextral offset on the San Andreas fault. Note location of Buzzards Peak tuff locality. Stipple pattern shows area of subaerial Colorado Delta deposition, observed in the present-day and inferred for 5.3 Ma. Modified from Dorsey et al. (2007).

spacing below that level ensures that we captured all of the magnetic reversals in the section. Tests of other possible correlations to the GPTS show that this is the only age model that does not impose unrealistic extreme anomalies in sediment-accumulation rates (Dorsey et al., 2011). Our preferred correlation to the GPTS is further confirmed by the 5.33-Ma Miocene-Pliocene boundary, which was identified using microfossil biostratigraphy by K. McDougall (in Dorsey et al., 2007).

The Wind Caves member is cut by several strike-slip and normal faults that add some uncertainty to the stratigraphic thicknesses and sedimentation rates in this part of the section. These faults deform a well-known stratigraphy. The Wind Caves member fines up-section into the lower claystone of the Mud Hills member of the Deguynos Formation, and the Mud Hills member coarsens gradually up into marine rhythmites that are capped by the base of the Yuha member (Winker, 1987; Winker and Kidwell, 1996; Dorsey et al., 2007, 2011). If the offset on these faults was large enough to juxtapose a younger magnetochron into the lower part of the measured section, it would be clearly revealed in the geology because the offset would produce an abrupt change to a different part of a well-known stratigraphy. Thus, although the section is cut by some faults, my mapping shows them to have rather small offset. Moreover, based on stratigraphic arguments it is highly unlikely that unidentified large faults could have

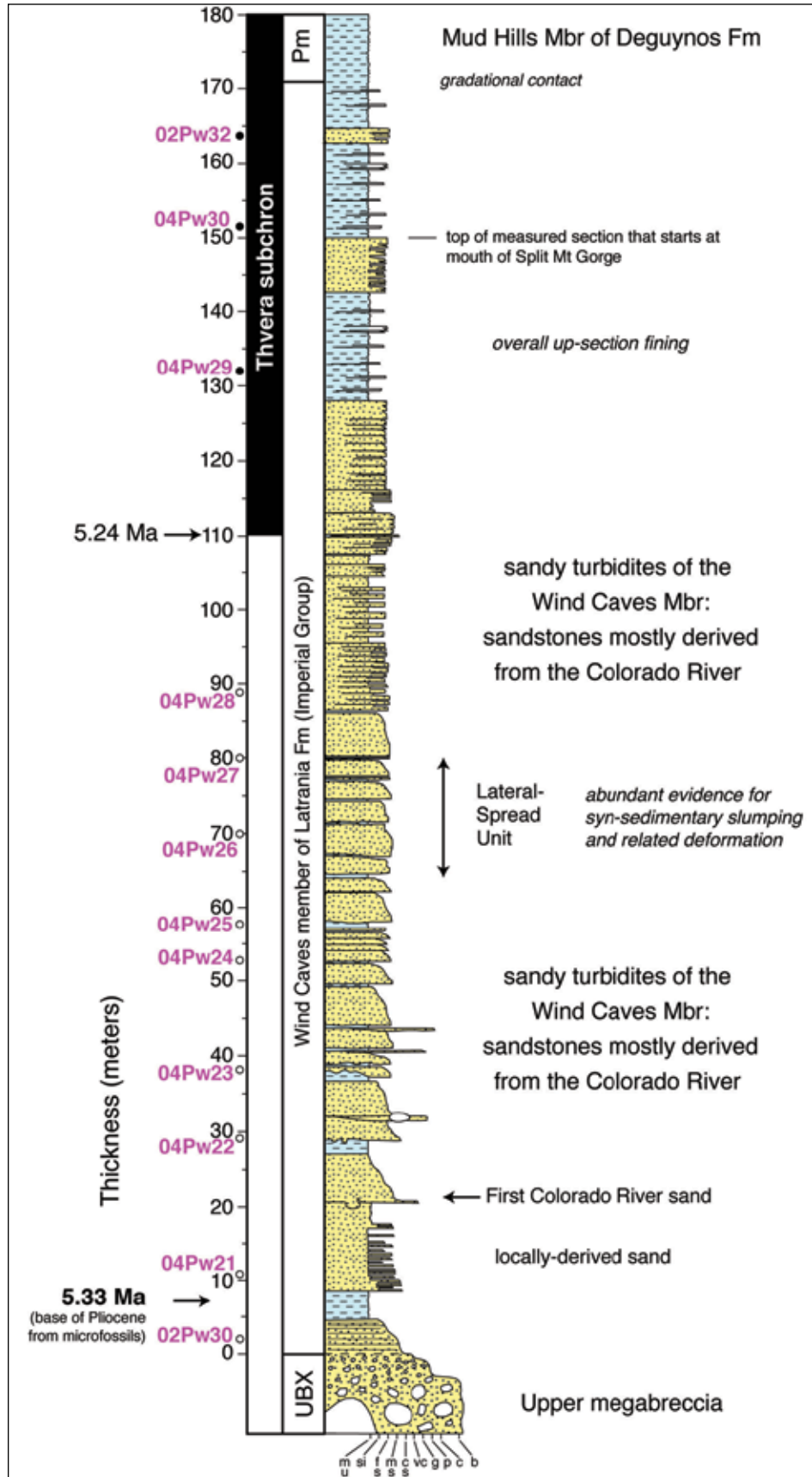


Figure 3. Measured section for the Wind Caves member of the Latrania Formation. Paleomagnetic sample sites (colored numbers) are from Dorsey et al. (2011).

caused us to misidentify the reversals and magnetochrons shown in Figures 2 and 3.

Figure 3 is a detailed measured section of the Wind Caves member (Pw) that shows the main variations in grain size and sedimentary structures. The continuous section starts at the southern mouth of Split Mountain Gorge (UTM 582,449 E; 3,651,021 N; WGS84, zone 11S) and ends on a ridge above the wash (582,151 E; 3,650,875 N). The upper 30 m of the section in Figure 3 was constructed by visual correlation of a sandstone bed south across an intervening ridge and into the main FCVB section (see map in Dorsey et al., 2007 Data Repository). The base of Pw is marked by a gradational contact with the underlying upper megabreccia, or "sturzstrom", which formed from a large rock avalanche (Kerr and Abbott, 1996; Winker and Kidwell, 1996; Abbott et al., 2002) (Figs. 2, 3). The lowest sandstone in Pw likely was deposited from a dilute turbidity current that trailed behind or was somehow related to subaqueous emplacement of the sturzstrom. Above that is ~5 m of mudstone overlain by well bedded turbidites composed of locally-derived sand (described below).

Starting ~21 m above the base of Pw, a normally graded thick sandstone bed (single-event turbidite) contains a 5-10 cm thick concentration of locally derived pebbly granule conglomerate that grades into sandstone composed of distinctive Colorado River sand (described below) mixed with locally-derived sand (Fig. 3). Sand in the upper part of this bed is mainly of Colorado River origin. Above that, thick-bedded turbidites are composed of Colorado-River sands with some basal concentrations of local pebbly sand with angular clasts of metamorphic rock similar to that of the megabreccia. Geologic mapping shows that the lower part of Pw onlaps irregular paleotopography on top of the megabreccia, suggesting that the concentrations of metamorphic pebbles and coarse locally derived sand may have been reworked from the breccia deposit before it was buried by the large influx of Colorado River sand and mud.

Sand compositions

As documented by Winker (1987), Colorado River-derived sands are easily distinguished from locally-derived sands through visual inspection with a hand lens and binocular microscope, and by observation of thin sections with a petrographic microscope. Locally-derived sands are lithic arkose composed of angular to subrounded feldspar, quartz, and detrital biotite, all eroded from nearby plutonic and metamorphic rocks. In contrast, Colorado River-derived sands are sublitharenites dominated by fine- to medium-grained, moderately to well rounded pink quartz, with lesser amounts of lithic fragments and feldspar. This difference is easy to see with a hand lens. In thin section, quartz grains display characteristic hematite coatings and syntaxial quartz overgrowths. The thin hematite

coatings often are encased between the core grains (which are very well rounded) and attached quartz overgrowths that are in optical continuity with the core grains (and are less well rounded). These features are attributed to derivation from the Colorado Plateau (Busing, 1988, 1990), but this inference has not been rigorously tested.

Detrital zircon evidence

A recent study by Kimbrough et al. (2011) shows that Colorado River sands have a remarkably similar detrital zircon age signature through time, remaining statistically constant from the oldest sandstones dated at 5.3 Ma (Wind Caves member), through the Late Cenozoic stratigraphic section, into modern sands of the present-day Colorado river and delta system. Because of the geological dilemma posed by the published 4.83-Ma age of Bouse Formation at Buzzards Peak (as summarized above), Kimbrough suggested that perhaps the older sands of the Wind Caves member were derived from the Gila River instead of the main stem of the Colorado River. While this explanation has rapidly gained popularity among people who worry about these things, I believe that the idea is not supported by the existing data. This hypothesis is also contradicted by my recent visual inspection of a modern sand from the Gila River.

Several points are worth elaborating. (1) Figure 2 of Kimbrough et al. (2011) shows that detrital zircon ages of the Wind Caves sample fall well within the statistical variation of detrital zircon ages seen in all modern Colorado River and Delta sand samples, as defined by the 2 sigma envelope on a cumulative probability plot. An excursion produced by a relatively small age peak at ~1.1 Ga (Grenville age) deviates from the Colorado Delta reference curve less than another sample higher in the section that is ca. 3.0 Ma and nobody questions is from the Colorado River. (2) When compared to the Colorado River reference curve (Fig. 3 of Kimbrough et al., 2011), Gila River sand strays well outside of the 2 sigma error envelope, due primarily to a paucity of grains between ~500 and 1,300 Ma. This shows that Gila River sand has detrital-zircon ages that are statistically unlike those of Colorado River sand. (3) Sands in the Wind Caves member and all other Colorado River sands contain a small but distinctive population of grains dated between ~500 and 700 Ma. In contrast, modern sand from the Gila River lacks analyzed zircon grains of this age (Kimbrough et al., 2011). (4) I recently collected a modern sand from the Gila River main channel, well upstream of any detectable influence of Colorado River sediments. This is a well sorted medium-grained sand with abundant lithic fragments, some feldspar, and much less quartz than Colorado River sands (including sands from the Wind Caves member). None of the quartz grains contain the distinctive pink color produced by hematite coatings, and they do not display the well developed

rounding and frosted appearance typical of Colorado River sands.

Thus, although it would be convenient if sandstones in the Wind Caves member were derived from the Gila River, I believe this hypothesis is unlikely for the reasons explained above.

Summary

Sand compositions and detrital zircon data for the Wind Caves member indicate that it was derived from the main stem of Colorado River, not the Gila River, starting at 5.3 Ma. While further tests of the sandstone provenance are needed, the age is firm and it seems unlikely that the Colorado-River source will be overturned. Geochemical data from the Buzzards Peak tuff support correlation to the 4.83-Ma Lawlor tuff (Sarna-Wojcicki et al., 2011), but the Buzzards Peak tuff has not been successfully dated using modern geochronological methods. Damon et al (1978) obtained an age of 5.47 ± 0.2 Ma from K-Ar dating of glass in the tuff, and Spencer et al. (2001) got perturbed age spectra using the $^{40}\text{Ar}/^{39}\text{Ar}$ method that yielded a best estimate of 5.01 ± 0.09 Ma, also from glass. This leaves us with an interesting and as-yet unresolved problem.

ACKNOWLEDGMENTS—I thank Keith Howard for a thorough and constructive review of this paper, and for many thoughtful discussions about this intriguing scientific problem. Bob Reynolds is thanked for organizing this volume, and for his good-natured patience in the face of extended delays.

References cited

- Abbott, P.L., Kerr, D.R., Borron, S.E., Washburn, J.L., and Rightmer, D.A., 2002, Neogene sturzstrom deposits, Split Mountain area, Anza-Borrego Desert State Park, California, in Evans, S.G., and DeGraff, J.V., eds., *Catastrophic Landslides: Effects, Occurrence, and Mechanisms: Geological Society of America, Reviews in Engineering Geology*, v. 15, p. 379–400.
- Buising, A.V., 1988, Depositional and tectonic evolution of the northern proto-Gulf of California and Lower Colorado River, as documented in the Mio-Pliocene Bouse Formation and bracketing units, southeastern California and western Arizona [Ph.D. thesis]: Santa Barbara, University of California, 196 pp.
- Buising, A.V., 1990, The Bouse Formation and bracketing units, southeastern California and western Arizona: Implications for the evolution of the proto-Gulf of California and the lower Colorado River: *Journal of Geophysical Research*, v. 95, p. 20,111–20,132.
- Damon, P.E., Shafiqullah, M., and Scarborough, R.B., 1978, Revised chronology for critical stages in the evolution of the lower Colorado River: *Geological Society of America Abstracts with Programs*, v. 10, p. 101–102.
- Dorsey, R.J., Fluette, A., McDougall, K., Housen, B.A., Janecke, S.U., Axen, G.J., and Shirvell, C.R., 2007, Chronology of Miocene-Pliocene deposits at Split Mountain Gorge, southern California: A record of regional tectonics and Colorado River evolution: *Geology*, v. 35, p. 57–60.
- Dorsey, R.J., Housen, B.A., Janecke, S.U., Fanning, C.M., and Spears, A.L.F., 2011, Stratigraphic record of basin development within the San Andreas fault system: Late Cenozoic Fish Creek-Vallecito basin, southern California. *Geol. Soc. America Bulletin*, v. 123, p. 771–793.
- House, P.K., Pearthree, P.A., Howard, K.A., Bell, J.W., Perkins, M.E., Faulds, J.E., and Brock, A.L., 2005, Birth of the lower Colorado River—Stratigraphic and geomorphic evidence for its inception near the conjunction of Nevada, Arizona, and California, in Pederson, J.L., and Dehler, C.M., eds., *Interior Western United States: Boulder, Colorado, Geological Society of America Field Guide 6*, p. 357–387.
- House, P.K., Pearthree, P.A., and Perkins, M.E., 2008, Stratigraphic evidence for the role of lake spillover in the inception of the lower Colorado River in southern Nevada and western Arizona, in Reheis, M.C., Hershler, R., and Miller, D.M., eds., *Late Cenozoic Drainage History of the Southwestern Great Basin and Lower Colorado River Region: Geologic and Biotic Perspectives: Geological Society of America Special Paper 439*, p. 335–353.
- Kerr, D.R., and Abbott, P.L., 1996, Miocene subaerial sturzstrom deposits, Split Mountain, Anza-Borrego Desert State Park, in Abbott, P.L., and Seymour, D.C., eds., *Sturzstroms and Detachment Faults, Anza-Borrego Desert State Park, California: Santa Ana, California, South Coast Geological Society*, p. 149–163.
- Kimbrough, D.L., Grove, M., Gehrels, G.E., Mahoney, J.B., Dorsey, R.J., Howard, K.A., House, P.K., Pearthree, P.A., and Flessa, K., 2011, Detrital Zircon Record of Colorado River Integration into the Salton Trough. In: Beard, L.S., Karlstrom, K.E., Young, R.A., and Billingsley, G.H., eds., 2011, *CREvolution 2 – Origin and evolution of the Colorado River system, workshop abstracts: U.S. Geological Survey Open-File Report 2011-1210*, p. 168–174.
- McDougall, K., 2008, Late Neogene marine incursions and the ancestral Gulf of California, in Reheis, M.C., Hershler, R., and Miller, D.M., eds., *Late Cenozoic Drainage History of the Southwestern Great Basin and Lower Colorado River Region: Geologic and Biotic Perspectives: Geological Society of America Special Paper 439*, p. 355–373.
- Metzger, D.G., 1968, The Bouse Formation (Pliocene) of the Parker-Blythe-Cibola Area, Arizona and California: U.S. Geological Survey Professional Paper 600-D, p. D126–D136.
- Metzger, D.G., Loeltz, O.J., and Irelan, B., 1973, Geohydrology of the Parker-Blythe-Cibola Area, Arizona and California: U.S. Geological Survey Professional Paper 486-G, 130 p.
- Poulson, S.R., and John, B.E., 2003, Stable isotope and trace element geochemistry of the basal Bouse Formation carbonate, southwestern United States: Implications for the Pliocene uplift history of the Colorado Plateau: *Geological Society America Bulletin*, v. 115, no. 4, p. 434–44.
- Sarna-Wojcicki, A.M., Deino, A.L., Fleck, R.J., McLaughlin, R.J., Wagner, D., Wan, E., Wahl, D., Hillhouse, J.W., and Perkins, M., 2011, Age, composition, and areal distribution of the Pliocene Lawlor Tuff, and three younger Pliocene tuffs, California and Nevada: *Geosphere*, v. 7; n. 3, p. 599–628.
- Smith, P.B., 1970, New evidence for a Pliocene marine embayment along the lower Colorado River area, California and Arizona: *Geological Society of America Bulletin*, v. 81, p. 1411–1420.

- Spencer, J.E., and Patchett, P.J., 1997, Sr isotope evidence for a lacustrine origin for the upper Miocene to Pliocene Bouse Formation, lower Colorado River trough, and implications for timing of Colorado Plateau uplift: *Geological Society of America Bulletin*, v. 109, p. 767–778.
- Spencer, J.E., Peters, L., McIntosh, W.C., and Patchett, P.J., 2001, $^{40}\text{Ar}/^{39}\text{Ar}$ geochronology of the Hualapai Limestone and Bouse Formation and implications for the age of the lower Colorado River, in Young, R.A., and Spamer, E.E., eds., *The Colorado River: Origin and evolution: Grand Canyon, Arizona*, Grand Canyon Association Monograph 12, p. 89–91.
- Spencer, J.E., Pearthree, P.A., and House, P.K., 2008, An evaluation of the evolution of the latest Miocene to earliest Pliocene Bouse lake system in the lower Colorado River valley, southwestern USA, in Reheis, M.C., Hershler, R., and Miller, D.M., eds., *Late Cenozoic drainage history of the southwestern Great Basin and lower Colorado River region: geologic and biotic perspectives: Geological Society of America Special Paper 439*, p. 375–390.
- Spencer, J.E., Sarna-Wojcicki, A.M., Patchett, P.J., Roskowski, J.A., Pearthree, P.A., House, P.K., and Faulds, J.E., 2011, Circa 4.8 Ma age for inception of the modern Colorado River: *Geological Society of America Abstracts with Programs, GSA National Meeting*, Abstract No. 189-42.
- Winker, C. D., 1987, Neogene stratigraphy of the Fish Creek-Vallecito section, southern California: implications for early history of the northern Gulf of California and the Colorado Delta, Ph.D. Thesis, 494 pp., Univ. of Arizona, Tucson.
- Winker, C.D., and Kidwell, S.M., 1996, Stratigraphy of a marine rift basin: Neogene of the western Salton Trough, California, in Abbott, P.L., and Cooper, J.D., eds., *Field Conference Guidebook and Volume for the American Association of Petroleum Geologists Annual Convention: AAPG, Bakersfield, California*, p. 295–336.

Before the big chill—a quick look at global climate in the Pliocene, Earth’s last sustained warm period

Richard (Tony) VanCuren

Air Quality Research Center, UC Davis. ravancuren@ucdavis.edu

ABSTRACT—The Pliocene (5.3–2.6 Ma) was the last period of sustained high temperature in Earth’s history, with global temperature about 3° C higher than today. Temperate climates extended into subarctic Alaska, Canada, and Siberia. Greenland’s ice sheet was 60 percent smaller than today, and its southern third was forested. The West Antarctic Ice Sheet was small and unstable, and sea levels are variously estimated to have been 10–25m higher than today, with consequent shifts in atmospheric and ocean circulation. This paper provides a quick overview of the earth, and California in particular, during the Pliocene, highlighting both similarities and differences between then and now.

Introduction

When the idea that Earth’s climate has varied over time was first argued scientifically (Agassiz, 1840), and for most of the century to follow, geology was a science of description and comparative and qualitative analysis. Although pioneering geologists achieved great insights into past climates by interpreting fossils, sediments, and landforms, the tools to calibrate the past in time, and to quantitatively estimate temperature, precipitation, and other paleoclimate variables, had to wait for the revolutions in understanding the Earth’s radiation balance that came in the late 19th and early 20th centuries, in basic and applied physics and chemistry in the first half of the 20th century, and the computational revolution of the last few decades for the tools to be at hand.

Over the past 50 years, the study of both present and past climates has evolved from a descriptive and statistical enterprise into a process-oriented science. Tools such as radio-isotope dating, stable isotope paleothermometry, deep ice cores and systematic deep-ocean drilling have revolutionized the types of information available to describe the physical and chemical processes that control climate. The last 25 years have seen the rise of computational climatology, and the advent of super-computers has made it possible to construct mechanistic models of the circulation of the atmosphere and oceans and to establish a dialog between theory and observation that is moving earth science toward a new, quantitative, and predictive synthesis of geology, geochemistry, biology, oceanography, and atmospheric science.

In this context, understanding the future states of Earth’s climate can be illuminated by examining the past. As anthropogenic increases in atmospheric CO₂ approach

400 ppm and understanding climate change becomes a pressing topic across a wide range of human activities far from the earth sciences, the Pliocene—the last geologic period that experienced such high CO₂—becomes more than just a distinctive period in the rock record, but a laboratory to examine Earth under those conditions, and to test our models to see if they really can predict what the coming high-CO₂ world will be like.

In order to put the Pliocene into perspective, this paper presents a brief overview of the Pliocene climate and how we have come to know it. This is far from a thorough treatment of what is known about Pliocene climatic conditions; rather it is intended to provide an introduction to the large body of material available. Much of this discussion is drawn from a compilation of Pliocene data prepared by the US Geological Survey for use in the Pliocene Model Intercomparison Project (PlioMIP) (Haywood *et al.*, 2010; Haywood *et al.*, 2011), which has greatly simplified preparation of this overview.

Large-scale cenozoic climate dynamics

Earth’s climate is largely governed by the concentration of CO₂ in the atmosphere, but that gaseous pool of carbon is only a tiny fraction of the planetary carbon cycle (Figure 1), so that small perturbations in fluxes among

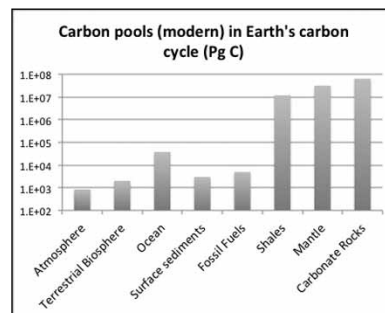


Figure 1. Distribution of carbon across Earth’s major carbon pools (Honisch *et al.*, 2012).

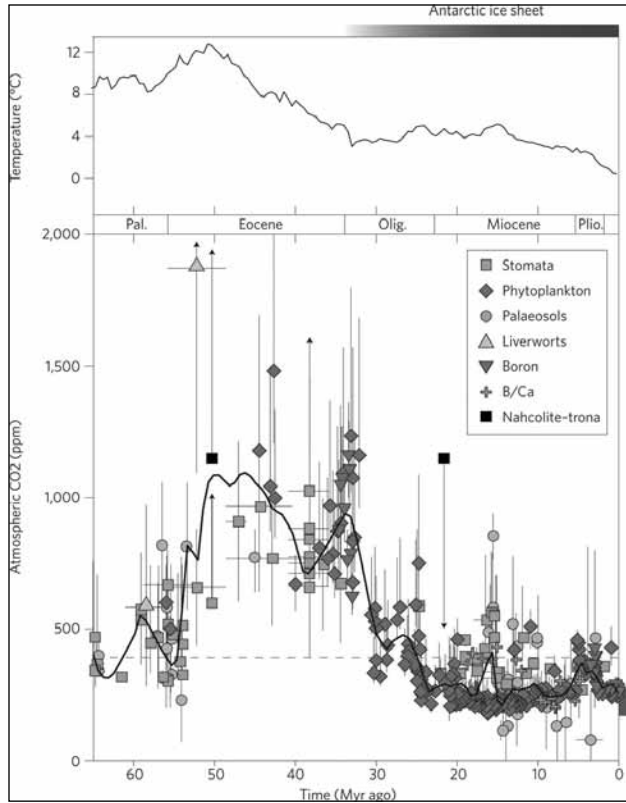


Figure 2. Atmospheric CO₂ Cenozoic to present (Beerling and Royer, 2011).

the large pools of CO₂ may initiate climate change. CO₂ concentrations for the Holocene and late Pleistocene have been directly measured from air trapped in ice, but for deeper time, they must be estimated by proxies ranging from plant leaf stomatal density to various geochemical signatures (Figure 2).

The early Cenozoic was characterized by very high atmospheric CO₂, reaching a peak around 1000 ppm (about 4 times the 18th century preindustrial value), identified as the Paleocene–Eocene Thermal Maximum (PETM), about 50 Ma. Through the rest of the Cenozoic, Pleistocene, and early Holocene, long-term (millions of years) mean CO₂ was progressively drawn down by high rates of weathering of silicate rocks and deposition to marine carbonate sediments, driven by the intense tectonic uplift and consequent rapid erosion associated with the growth of the Himalayan Plateau and other major mountain chains (Raymo et al., 1988). On shorter time scales (10³–10⁵ years), CO₂ has been cycled among ocean, soil, and biologic reservoirs primarily in response to variations in the distribution of heat between the tropics and polar regions, as governed by orbital dynamics and varying obliquity of Earth’s axis (Milankovitch, 1941; Hays et al., 1976).

Tectonics are also believed to have played a role near the end of the Pliocene with the closing of the Panama

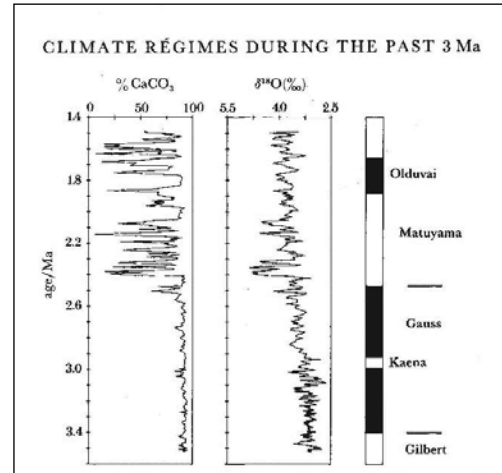


Figure 3. Global marine ¹⁸O variation from the Pliocene to the present in an ocean sediment core from the North Atlantic (57° N). The inception of Pleistocene glaciation is marked by the appearance of ice-raftered material in the previously predominantly carbonate sediment column (Ruddiman and Raymo 1988).

seaway, which redirected warm tropical Atlantic water into the Gulf Stream, warming the Atlantic in the vicinity of Labrador and providing an enhanced moisture source for the growth of northern ice sheets in the Pleistocene (Haug and Tiedemann, 1998).

Pliocene marine climate records

Sea water evaporation is energetically biased in favor of water molecules containing the common oxygen isotope ¹⁶O compared to water containing the rarer (about 3 in 1000), heavier isotope ¹⁸O, thus cool periods which remove water from the oceans to ice accumulated on land impart a small enrichment of ¹⁸O to ocean waters. In addition to this partitioning, lower temperatures are biased in favor of ¹⁸O in the aqueous mineralization of dissolved carbonic acid to carbonate (calcite) in foraminifera. These phenomena together have been used to estimate both the temperature of the sea where fossil foraminifera lived and to estimate the global partitioning of water between ocean and ice over time.

Global temperature estimates are based on calibration with modern forams across multiple sampling sites, and ice mass is computed from a simple mixing model adjusted for the mineralization bias.

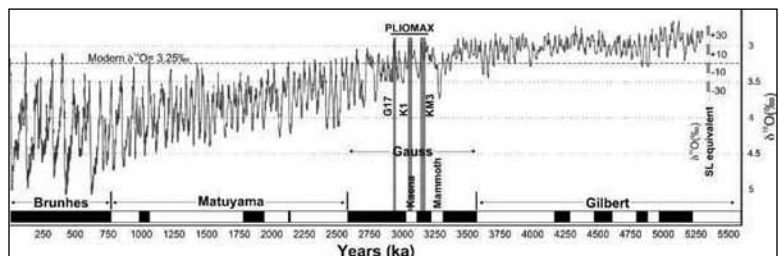


Figure 4. The global composite ¹⁸O record for the Pliocene to today, with the Pliocene warm periods marked in red (Raymo et al., 2009).

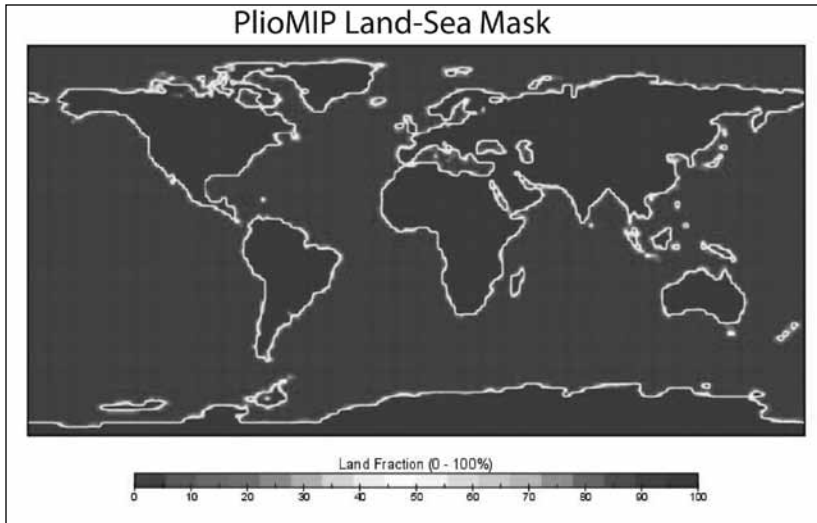


Figure 5. The global pattern of land and ocean during the late Pliocene warm (Haywood et al., 2010).

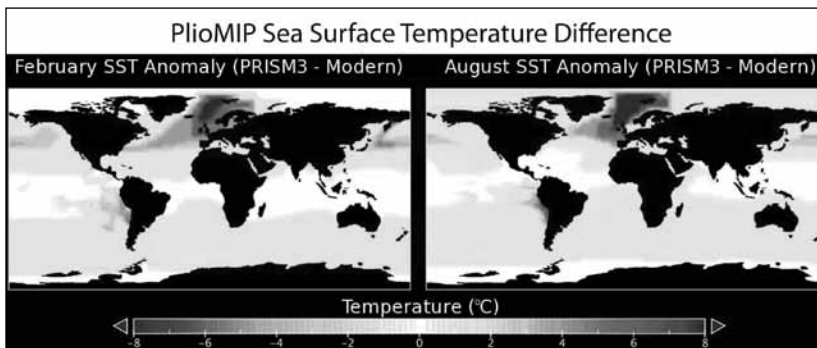


Figure 6. Sea ice in the Pliocene warm periods was much reduced compared to today, with little perennial ice around Antarctica, and no evident summer ice in the Arctic (Haywood et al., 2010).

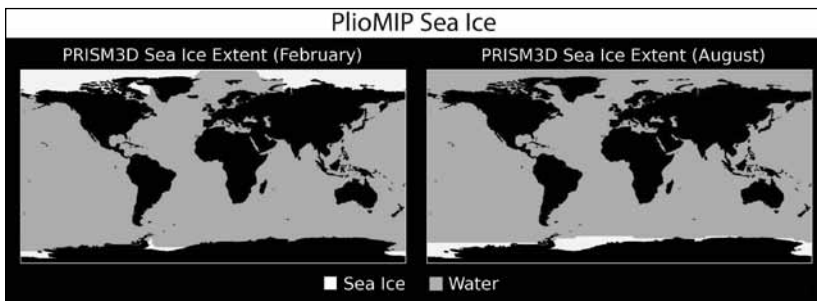


Figure 7. Sea surface temperature in the Pliocene warm period was much warmer in the Greenland Sea and the cold upwelling currents in eastern South Pacific were much reduced, however tropical oceans were not much different from today (Haywood et al., 2010).

The record from one drilling site in the North Atlantic (Figure 3) shows the transition from the Pliocene to Pleistocene as marked by both the ^{18}O record and sedimentary evidence of glacial rafting of continental debris to this mid-ocean location (Ruddiman and Raymo, 1988).

The global ocean ^{18}O trend from the Pliocene to today, reconstructed by combining large numbers of ocean sediment cores (Lisiecki and Raymo, 2005) (Figure 4, from Raymo et al., 2009). The Pliocene is marked by shallow cycles of warming and cooling, timed with Earth's

obliquity cycles (Milankovitch, 1941; Hays et al., 1976) on the right-hand side, and it ends with the Pleistocene overprinting of progressively colder cycles, clearly seen in the left-hand (younger) end of the plot.

Pliocene geography

The Pliocene represents a time when many of the features of the modern Earth were falling into place. The continents had arrived at more or less their current arrangement, and the flora and fauna were organized into ecosystems that broadly parallel those seen on Earth today. However, the planet was generally warmer, and thus the polar regions, particularly in the Arctic, were substantially different. In addition, the lower level of the Panama sill and higher sea levels of the Pliocene significantly reduced the barriers to tropical ocean circulation (Haug and Tiedemann, 1998). Utilizing the compilation of the PlioMIP project (Haywood et al., 2010), the major features of Pliocene geography are summarized here.

The global pattern of land and ocean during the late Pliocene warm period is shown in Figure 5 (Haywood et al., 2010). The higher sea levels and tectonic differences with modern oceans are most notable in the open Panama seaway, and the much more open seas around the Malaysian peninsula and neighboring islands.

Sea ice in the Pliocene warm periods was much reduced compared to today (Figure 6), with little perennial ice around Antarctica, and no evident summer ice in the Arctic (Haywood et al., 2010). Similarly, the pattern of sea surface temperature (Figure 7) also shows warmer polar regions in the Pliocene warm period, with much warmer water in the Greenland Sea, and the cold upwelling currents in eastern South Pacific were much reduced. Tropical oceans were not much different from today (Haywood et al., 2010).

The uplift of the modern mountain chains and highland regions was well along in the Pliocene, so that the global topography (Figure 8) was similar to today, but with modestly lower peak altitudes for the emerging areas (Haywood et al., 2010).

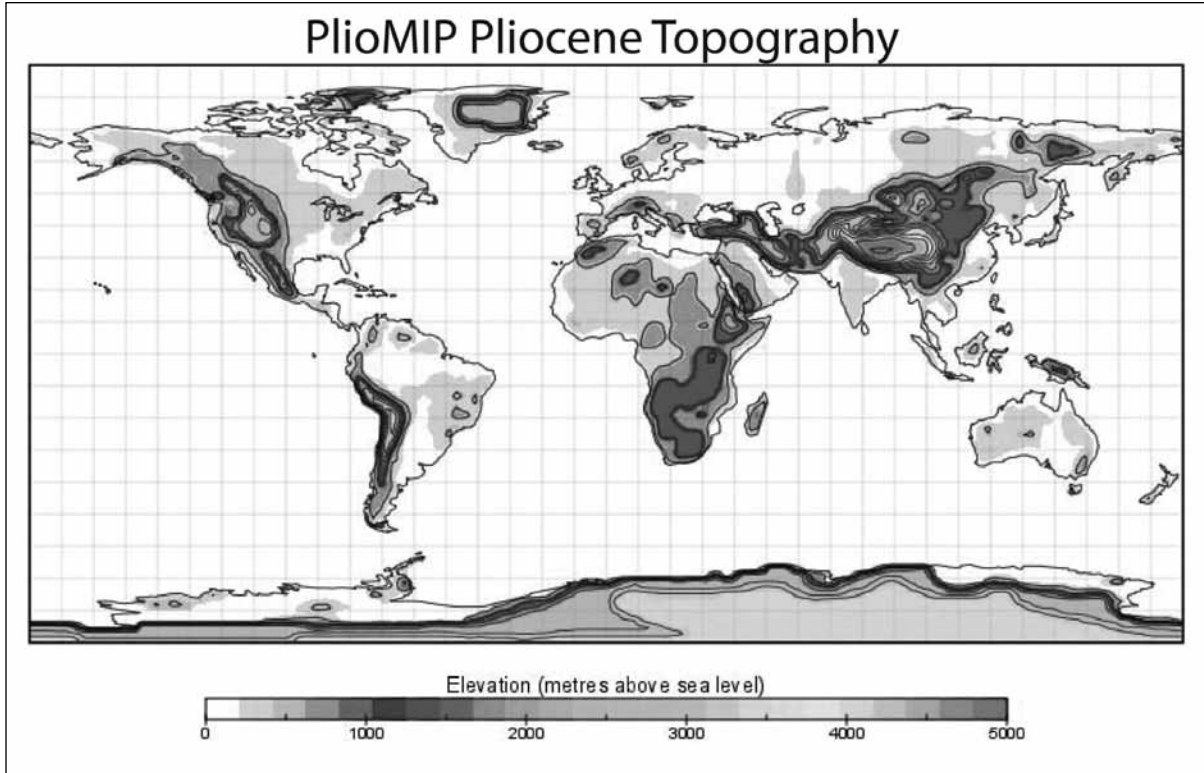


Figure 8. The global distribution of mountains and highlands in the Pliocene was similar to today, but with modestly lower peak altitudes for the emerging areas (Haywood et al., 2010).

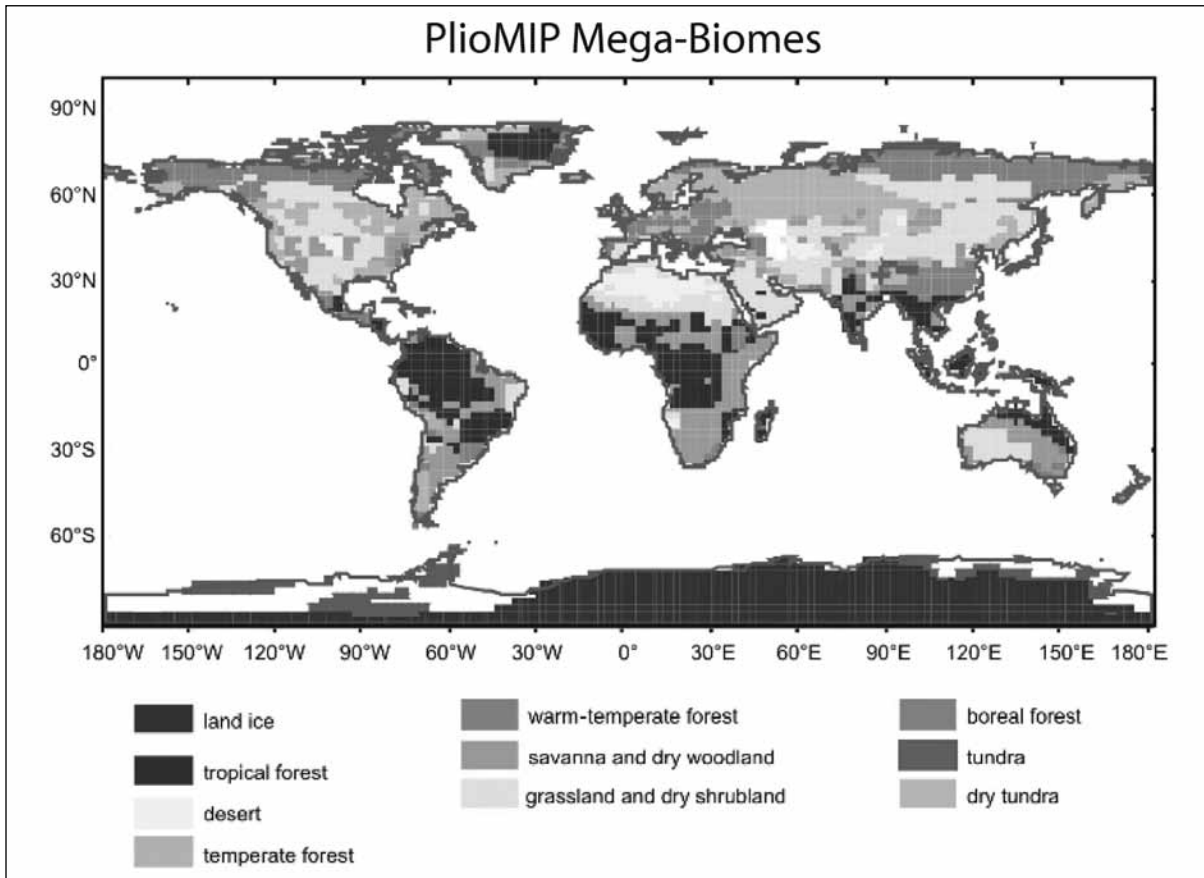


Figure 9. The global pattern of vegetation during the late Pliocene warm period mapped as major biome regions shows a significantly greater extent of forest, especially in Alaska, Canada, Siberia, and Greenland. (Haywood et al., 2010).

The global pattern of vegetation during the late Pliocene warm period (Figure 9) reflects the much less intense cold in the polar regions, with major forest biome regions reaching much farther north and supporting significantly greater extents of forest in Alaska, Canada, Siberia, and Greenland. In lower latitudes, dry regions were much smaller, with a significantly reduced Sahara and extensive grasslands in southwest Asia, western North America, and western Australia (Haywood et al., 2010).

Conclusions

The Pliocene warm period is thought to represent what an equilibrium 400 ppm CO₂ climate might look like. It is important to realize, however, that the present-day changes are occurring at a much greater rate than the evolution of Pliocene CO₂ variations, which leaves large uncertainties about how both marine and terrestrial biological systems will change in response to the new atmosphere. If the Pliocene is a guide to the end product of the induced warming, then it indicates a wetter, more equable planet, but how these adjustments will occur is still unknown. Finally, the intensive use of fossil fuels has the potential to drive CO₂ concentrations much higher than 400ppm, reaching closer to levels seen in the PETM, and there is no geological analog for those conditions that so clearly resembles the present as does the Pliocene. Getting climate modeling right for the past will only be the first step to understanding future climates.

References cited

- Aggasiz, L., 1840, Études sur les glaciers; ouvrage accompagné d'un atlas de 32 planches. Jent et Gassmann, Neuchatel, *in French*.
- Beerling, D. J., and D. L. Royer, 2011, Convergent Cenozoic CO₂ history, *Nature Geoscience* 4, 418–420 (2011) doi:10.1038/ngeo1186.
- Haug, G. H., and R. Tiedemann, 1998, Effect of the formation of the Isthmus of Panama on Atlantic Ocean thermohaline circulation, *Nature* 393, 673–676.
- Hays, J. D., J. Imbrie, N.J. Shackleton, 1976, Variations in the Earth's Orbit: Pacemaker of the Ice Ages, *Science* 194, 1121–1132.
- Haywood, A. M., H. J. Dowsett, B. Otto-Bliesner, M. A. Chandler, A. M. Dolan, D. J. Hill, D. J. Lunt, M. M. Robinson, N. Rosenbloom, U. Salzmann, and L. E. Sohl, 2010, Pliocene Model Intercomparison Project (PlioMIP): experimental design and boundary conditions (Experiment 1), *Geosci. Model Dev.*, 3, 227–242, www.geosci-model-dev.net/3/227/2010/.
- Haywood, A. M., Dowsett, M. M. Robinson, D. K. Stoll, A. M. Dolan, D. J. Lunt, B. Otto-Bliesner, and M. A. Chandler, 2011, Pliocene Model Intercomparison Project (PlioMIP): experimental design and boundary conditions (Experiment 2), *Geosci. Model Dev.*, 4, 571–577, www.geosci-model-dev.net/4/571/2011/, doi:10.5194/gmd-4-571-2011.
- Hönisch, Bärbel, Andy Ridgwell, Daniela N. Schmidt, Ellen Thomas, Samantha J. Gibbs, Appy Sluijs, Richard Zeebe, Lee Kump, Rowan C. Martindale, Sarah E. Greene, Wolfgang Kiessling, Justin Ries, James C. Zachos, Dana L. Royer, Stephen Barker, Thomas M. Marchitto Jr., Ryan Moyer, Carles Pelejero, Patrizia Ziveri, Gavin L. Foster, Branwen Williams, 2012, The Geological Record of Ocean Acidification, *Science* 335, 1058–1063.
- Lisiecki, L. E., and M. E. Raymo, 2005, A Pliocene–Pleistocene stack of 57 globally distributed benthic δ¹⁸O records, *Paleoceanography*, 20, PA1003, doi:10.1029/2004PA001071.
- Milankovitch, M. K., 1941, Canon of Insolation and the Ice Age Problem, *Roy. Serb. Acad., Beogr., Spec. Publ.* 132 (translated by the Israel Pro-gram for Scientific Translations, Jerusalem, 1969).
- Raymo, M. E., J. X. Mitrovica, M. J. O'Leary, R. M. DeConto and P. J. Hearty, 2011, Departures from eustasy in Pliocene sea-level records, *Nature Geosci.* 4(5), 328–332, DOI: 10.1038/NNGEO1118.
- Raymo, M. E., P. Hearty, R. De Conto, M. O'Leary, H.J. Dowsett, M.M. Robinson, and J.X. Mitrovica, 2009, PLIOMAX: Pliocene maximum sea level project, http://pages-142.unibe.ch/products/newsletters/NL2009-2_lowres.pdf
- Raymo, M. E., W. F. Ruddiman, P. N. Frolich, 1988, Influence of late Cenozoic mountain building on ocean geochemical cycles, *Geology* 16, 649–653.

Searching for a pupfish migration route—back to the Pliocene?

Jeffrey Knott

Department of Geological Sciences, California State University-Fullerton

Blackwelder (1933; 1954) hypothesized that, during the Last Glacial Maximum ~20 ka, the basins of eastern California contained lakes connected by the Owens, Amargosa and Mojave Rivers. This hypothesis was supported by the biological studies of Hubbs and Miller (1948) who hypothesized that the pupfish (*Cyprinodontidae*) species within the Owens, Amargosa and Colorado drainage systems diverged from a mutual ancestry. Further support for these hypotheses was provided by studies of the Owens River pluvial lakes (Mono, Owens, Searles, Gale [Panamint Valley] and Manly [Death Valley]) (see Jannik et al., 1991 for a review).

Smith et al. (2002) and Echelle et al (2005) showed with mitochondrial deoxyribonucleic acid (mtDNA) that pupfish are genetically linked and hypothesized that the divergence through isolation began ~3-2 Ma. Knott et al. (2008) showed that the elevation of ~3 Ma Lake Manly in Death Valley was insufficient to have integrated with the Colorado River drainage. They also showed that the 180 ka high stand of Lake Manly did not encompass pluvial Lake Mojave (Silver and Soda playas)—the “gateway” to the Colorado River. The study by Knott et al. (2008) cast doubt on integration of Death Valley with the Colorado River in the last 3 Ma.

This left the physical pathway for pupfish migration unresolved. Knott et al. (2008) hypothesized that studies suggesting that Miocene-Pliocene age fluvial deposits in eastern California may provide physical divergence route. The key to these studies is the presence of clasts of leucomonzogabbro from the Hunter Mountain batholiths (Figure 1). The Hunter Mountain batholith is located in the Cottonwood Mountains, which bound the west side of Death Valley. The igneous rocks of Hunter Mountain are distinct with mafic phenocrysts of clinopyroxene, biotite, hornblende and olivine (Niemi et al., 2001). Wright and Troxel (1993) mapped deposits containing Hunter

Mountain clasts in central Death Valley. Wright et al. (1999) found Hunter Mountain clasts in fluvial deposits of the ~5 Ma upper Artists Drive Formation at Gower Gulch. Niemi et al. (2001) described Hunter Mountain clasts in the 11.6–15.0 Ma Eagle Mountain Formation in the Amargosa Valley and Chicago Valley east of Death Valley. The east side of Chicago Valley marks the present drainage divide between the Amargosa and Colorado River systems. Renik and Christie-Blick (2004) reinterpreted the sedimentary deposits of the Eagle Mountain Formation as fluvial deposits.

These data support a possible fluvial connection between the west side of Death Valley (Hunter Mountain)

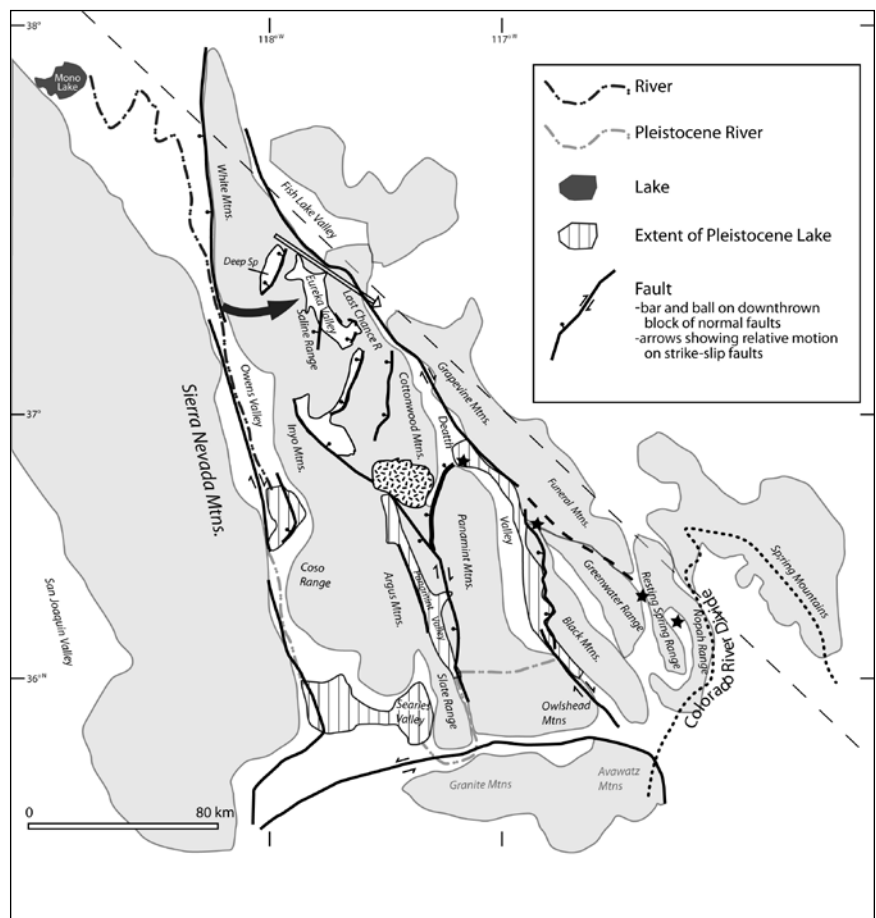


Figure 1 – Map of Death Valley region showing present-day mountain ranges (gray), valleys and major faults. The Pleistocene drainage system is Mono-Owens-Searles-Panamint-Death Valley. The stippled area near the center is the leucomonzogabbro of Hunter Mountain. The stars indicate Miocene-Pliocene deposits that contain leucomonzogabbro clasts. The black arrow from Owens Valley toward Eureka Valley is the proto-Owens River route proposed by Phillips (2008). The unfilled arrow shows the proposed basalt flows from the White Mountains to Death Valley. The present-day Colorado River drainage divide is shown in the southeast.

to the edge of the Colorado River (Chicago Valley) in the Miocene to early Pliocene. Although the time frame is beyond the divergence time frame supported by mtDNA, it does provide a starting point.

So, if a river flowed from Hunter Mountain—what evidence is there for flow from Owens Valley to Hunter Mountain? There is nothing definite; however, Deep Springs and Eureka Valleys, which separate Owens Valley from Death Valley in the north, have garnered some attention. Miller (1928) described wind gaps through the Deep Springs Range between Deep Springs Valley and Eureka Valley. Lee et al. (2001) found the 0.77 Ma Bishop Ash Bed in wind gap sediments indicating that wind gaps formation is < 1 Ma. Reheis and Sawyer (1997) dated basalts in the Deep Springs and Last Chance Ranges between 11-5 Ma. Many of these basalt flows are associated with sedimentary deposits (McKee and Nelson, 1967) indicating that the basalts possibly flowed in river channels and today's topography is inverted. Based on the elevation of the Waucoba Beds, Phillips (2008) proposed that the proto-Owens River flowed over the White/Inyo Mountains and into Eureka Valley.

These studies raise some interesting initial questions regarding Miocene-Pliocene river systems.

- Wright et al. (1999) estimated the 5 Ma age of the Artists Drive Formation, Knott et al. (2008) found that the overlying Furnace Creek Formation is 4–3 Ma—are there Hunter Mountain clasts in these deposits?
- McKee and Nelson (1967) mapped sedimentary deposits in the Last Chance Range—do these deposits include clasts from the Deep Springs or Inyo Ranges to the west?
- There are no volcanic centers in the Deep Springs or Last Chance Ranges—where did the basalts come from?

References

- Blackwelder, E., 1933, Lake Manly, an extinct lake of Death Valley: *Geographical Review*, v. 23, p. 464-471.
- _____, 1954, Pleistocene lakes and drainage in the Mojave region, southern California, in Jahns, R. H., ed., *Geology of Southern California*: Sacramento, CA, California Division of Mines and Geology, p. 35-40.
- Echelle, A., Carson, E., Echelle, A., and Bussche, R. A. V. D., 2005, Historical Biogeography of the New-World Pupfish Genus *Cyprinodon* (Teleostei: Cyprinodontidae): *American Society of Ichthyologists* p. 320-339.
- Hubbs, C. L., and Miller, R. R., 1948, The Zoological Evidence: Correlation between fish distribution and hydrographic history in the desert basins of western United States: *Bulletin of the University of Utah*, v. 38, no. 29, p. 17-166.
- Jannik, N. O., Phillips, F. M., Smith, G. I., and Elmore, D., 1991, A ³⁶Cl chronology of lacustrine sedimentation in the Pleistocene Owens River System: *Geological Society of America Bulletin*, v. 103, p. 1146-1159.
- Lee, J., Rubin, C. M., and Calvert, A., 2001, Quaternary faulting history along the Deep Springs fault, California: *Geological Society of America Bulletin*, v. 113, no. 7, p. 855-869.
- McKee, E. H., and Nelson, C. A., 1967, Geologic map of the Soldier Pass Quadrangle, California and Nevada, scale 1:62500.
- Miller, W. J., 1928, Geology of Deep Springs Valley, California: *Journal of Geology*, v. 36, p. 510-525.
- Niemi, N. A., Wernicke, B. P., Brady, R. J., Saleeby, J. B., and Dunne, G. C., 2001, Distribution and provenance of the middle Miocene Eagle Mountain Formation, and implications for regional kinematic analysis of the Basin and Range province: *Geological Society of America Bulletin*, v. 113, no. 4, p. 419-442.
- Phillips, F., 2008, Geological and hydrological history of the paleo-Owens River drainage since the Miocene, in Reheis, M. C., Hershler, R., and Miller, D. M., eds., *Late Cenozoic drainage history of the southwestern Great Basin and lower Colorado river region: Geologic and biotic perspectives*: Boulder, Colorado, Geological Society of America Special Paper 439, p. 115-150.
- Reheis, M. C., and Sawyer, T. L., 1997, Late Cenozoic history and slip rates of the Fish Lake Valley, Emigrant Peak, and Deep Springs fault zones, Nevada and California: *Geological Society of America Bulletin*, v. 109, no. 3, p. 280-299.
- Renik, B., and Christie-Blick, N., 2004, Reevaluation of Eagle Mountain Formation and implications for extreme extension across Death Valley, CA: *Geological Society of America Abstracts with Programs*, v. 35, no. 5, p. 23.
- Smith, G. R., Dowling, T. E., Gobalet, K. W., Lugaski, T., Shiozawa, D. K., and Evans, R. P., 2002, Biogeography and timing of evolutionary events among Great Basin fishes, in Hershler, R., Madsen, D. B., and Currey, D. R., eds., *Great Basin Aquatic Systems History*: Washington, D.C., Smithsonian Institution Press, p. 175-234.
- Wright, L. A., Greene, R. C., Cemen, I., Johnson, F. C., and Prave, A. R., 1999, Tectonostratigraphic development of the Miocene-Pliocene Furnace Creek Basin and related features, Death Valley region, California, in Wright, L. A., and Troxel, B., eds., *Cenozoic Basins of the Death Valley Region*: Boulder, CO, Geological Society of America, p. 87-114.
- Wright, L. A., and Troxel, B. W., 1993, Geologic Map of the central and northern Funeral Mountains and adjacent areas, Death Valley region, southern California: US Geological Survey.

Thermal tolerances for the desert pupfish (*Cyprinodon macularius*): a case for rapid evolution

Allan A. Schoenherr

Professor of Ecology, Emeritus, Fullerton College

Tolerances among pupfishes (*Cyprinodon* spp.) for environmental extremes are legendary (Deacon and Minckley 1974, Feldmeth 1981, Schoenherr 1988). Based on experiments with various species of pupfish the following generalizations may be made:

1. Thermal tolerances vary with acclimation temperature and season (Feldmeth, Stone, and Brown 1974).

2. Species from constant temperature habitats have narrow ranges of tolerance, and those tolerances are inherited (Hirschfield and Feldmeth 1980).

Cyprinodon macularius fits these criteria. Preliminary experiments were published by Schoenherr and Feldmeth (1993). Published data for critical thermal maxima (Ctmax) and minima (Ctmin) of fish acclimated to field conditions showed a range of extremes from 7°C to 44.6°C. Bob Feldmeth (now deceased) and I asked the question, "How long do pupfish populations have to be isolated in order to change their inherited thermal tolerances?" We tested fish from four populations by acclimating them to 29°C in the laboratory. By raising and lowering their temperatures 1°C per 2 minutes we determined Ctmax and Ctmin for these populations (Table 1). Fish from constant-temperature Oasis Spring (28°C) were tested twice in order to confirm consistency. Results showed a Ctmax of 42.7°C and 42.6°C and a Ctmin of 5.3°C and 6.3°C. We also tested fish from native habitat at variable-temperature Salt Creek and San Felipe Creek and found Ctmax temperatures comparable to those of Oasis Spring. The Ctmin temperatures were similar to each other, but lower than those of the constant temperature Oasis Spring. For comparison, a population of fish transferred from Salt Creek to variable-temperature habitat at Thousand Palms also were tested and showed values similar to the parental populations. (The minimum temperature of 4.4° C at Thousand Palms is the lowest ever recorded for the species.) The Oasis Spring population originally transferred from variable temperature native habitat was isolated for 13 years, approximately 13 generations. During that time their Ctmax remained the same, but it appears that they lost a significant bit of their cold tolerance, clearly a rapid case of change.

Other cases of changes in thermal tolerances for pupfishes have been recorded for populations that have

been separated for thousands to millions of years. Data for pupfish populations from Chihuahua, Mexico showed the most significant differences in Ctmax for populations that were separated about a million years (Soltz and Feldmeth personal communication). Comparing *Cyprinodon nevadensis* from Ash Meadows to those from the Amargosa River, Hirschfield, Feldmeth, and Soltz (1980) showed significant differences for populations that were separated for several thousand years. The population of *Cyprinodon macularius eremus* from Quitobaquito Spring in Organ Pipe Cactus National Monument has been separated from the Colorado River and Salton

Table 1.
A SUMMARY OF THERMAL TOLERANCES FOR PUPFISH FROM CONSTANT VS. VARIABLE TEMPERATURE HABITATS, RIVERSIDE COUNTY, CALIFORNIA

| | Oasis Spring | Oasis Spring | Thsnd Palms | Salt Creek | San Felipe Cr. |
|---------------|--------------|--------------|-------------|------------|----------------|
| CTMax (°C) | 42.7 | 42.6 | 42.4 | 41.9 | 42.2 |
| CTMin (°C) | 5.3 | 6.3 | 4.4 | 4.6 | 4.5 |
| Thermal Scope | 37.4 | 36.3 | 38.0 | 37.3 | 37.7 |

Sea populations of *C. m. macularius* for a minimum of 100,000 years (Miller and Fuiman 1987). The Ctmax of 44.6° C reported by Lowe and Heath (1969) is significantly higher than our experiments showed for fish from Oasis Spring. These data show that inherited thermal tolerances change with time, and in our experiments they changed in about 13 years, clearly a case of rapid evolution. Rapid evolution of behaviors in Death Valley pupfish also has been confirmed (Lema 2006, 2008).

Literature cited

- Deacon, J.E. and W. L. Minckley. 1974. Desert Fishes. Pp. 385-488 in Brown, G.W. Jr. (ed), Desert Biology, Vol. II, Academic Press, New York.
- Feldmeth, C.R. 1981. The evolution of thermal tolerance in Desert Pupfish (Genus *Cyprinodon*). Pp. 357-384 in Naiman, R.J. and D.L. Soltz (eds.), Fishes in North American Deserts. Wiley-Interscience Publication, John Wiley & Sons, New York.
- Feldmeth, C.R., E.A. Stone and J.H. Brown. 1974. An increased scope for thermal tolerance upon acclimating pupfish (*Cyprinodon*) to cycling temperatures Journal of Comparative Physiology, 89:39-44.

- Hirshfield, M.F., C.R. Feldmeth and D.L. Soltz. 1980. Genetic differences in physiological tolerances of Amargosa Pupfish (*Cyprinodon nevadensis*) populations. *Science*, 207:999-1001.
- Lema, S.C. 2006. Population divergence in plasticity of the AVT system and its association with aggressive behaviors in a Death Valley Pupfish. *Hormones and Behavior* 50:183-193.
- Lema, S.C. 2008. The phenotypic plasticity of Death Valley's pupfish. *American Scientist* 96:28-36.
- Lowe, C.H. and W.G. Heath. 1969. Behavioral and physiological responses to temperature in the desert pupfish, *Cyprinodon macularius*. *Physiological Zoology*, 42:53-59.
- Miller, R.R. and L.A. Fuiman. 1987. Description and conservation status of *Cyprinodon macularius eremus*, a new subspecies of pupfish from Organ Pipe Cactus National Monument, Arizona. *Copeia*, 593-609.
- Schoenherr, A.A. 1988. A review of the life history and status of the desert pupfish, *Cyprinodon macularius*. *Bulletin of the Southern California Academy of Science*, 87:104-134.
- Schoenherr, A.A. and C.R. Feldmeth. 1993. Thermal tolerances for relict populations of desert pupfish, *Cyprinodon macularius*. *Desert Research Symposium: San Bernardino County Museum Association Quarterly*, 40:32-33.

The dazed and confused identity of Agassiz's land tortoise, *Gopherus agassizii* (Testudines, Testudinidae), the new desert tortoise, *Gopherus morafkai*, and consequences for conservation

R. W. Murphy,^{1,2} K. H. Berry,³ T. Edwards,⁴ A. E. Leviton,⁵ A. Lathrop,¹ and J.D. Riedle⁶

¹Royal Ontario Museum, Ontario, Canada

²Kunming Institute of Zoology, Chinese Academy of Sciences, Kunming, China

³U.S. Geological Survey, Western Ecological Research Center, Riverside, California

⁴Arizona Research Laboratories, University of Arizona Genetics Core, Tucson, Arizona

⁵California Academy of Sciences, San Francisco, California

⁶Lincoln University, Jefferson City, Missouri

During the last decade we have investigated a myriad of problems associated with the taxonomic history of the desert tortoise, *Gopherus agassizii*, and the species complex it represents (Berry et al. 2002, Murphy et al. 2007, 2011). As few as two and as many as four species may be present in the complex (Berry et al. 2002). As early as 1989, the Colorado River was recognized as being an important geographic barrier between populations occurring in the Mojave and western Sonoran deserts of California, Nevada, Utah and northwestern Arizona and those in the Sonoran Desert of Arizona and Mexico (Lamb et al. 1989). Gradually evidence mounted that the populations differ in several morphological, physiological, and ecological attributes (Berry et al. 2002, Murphy et al. 2011). Nevertheless, some major obstacles and minor conundrums remained for recognizing and naming a new species. These topics included the date of publication of the original description by Western explorer and naturalist James G. Cooper, the location of the type locality, the location and current existence of the specimens collected by Cooper, changes in common names over the years, the likely number of species in the *G. agassizii* complex, and the taxonomic validity of the taxon named from Baja California (*G. lepidocephalus*).

We believed that the topics of type locality of *G. agassizii* and potential origins of the Baja California specimen could be addressed if genetic evidence in the form of mitochondrial DNA and microsatellite DNA alleles could be obtained from the single remaining specimen collected by Dr. Cooper almost 150 years ago and currently at the National Museum of Natural History and from the single non-skeletal specimen of *G. lepidocephalus*. Fortunately sufficient DNA evidence was available to indicate that the locality of Dr. Cooper's specimen was from the Mojave Desert of California and

has an evolutionary origin consistent with the Mojave and western Sonoran deserts. Thus *G. agassizii* represents the population of tortoises occurring primarily north and west of the Colorado River. The genetic fragments obtained from the *G. lepidocephalus* specimen were from the most common haplotype in the Mojave Desert. That being the case, *G. lepidocephalus* is not a tortoise from the Sonoran Desert of Arizona or Mexico. Rather, we have shown it to be a junior synonym of *G. agassizii*, and thus the name is not available for the new species we now recognize from the Sonoran Desert of Arizona and Mexico.

The new species of desert tortoise was named *G. morafkai*, in honor of our colleague Dr. David J. Morafka. The specimen selected as the holotype is a juvenile from Tucson, Pima County, Arizona, collected in July of 1912 by H. Brown. We recommend Morafka's desert tortoise as the common name for this tortoise from the Sonoran Desert and, following Cooper's original description, that the name Agassiz's desert tortoise be used as the common name for *G. agassizii*.

With the naming of the new species, Agassiz's desert tortoise has experienced a reduction of 70% of its geographic range (Murphy et al. 2011). It is currently listed as a federally threatened species. Although Morafka's desert tortoise has a geographic range in both the United States and Mexico, this species has limited federal protections: in the U.S., its listing is "warranted but precluded" by other, higher priorities; whereas in Mexico, the federal listing is equivalent to threatened status in the U.S. With the major reductions in geographic ranges for the two species, a re-evaluation of the threats and management strategies are appropriate to ensure that adequate conservation measures are in place.

References

- Berry, K.H., D.J. Morafka, and R.W. Murphy. 2002. Defining the desert tortoise(s): our first priority for a coherent conservation strategy. *Chelonian Conservation and Biology* 4:249–262.
- Lamb, T., J.C. Avise, and J.W. Gibbons. 1989. Phylogeographic patterns in mitochondrial DNA of the desert tortoise (*Xerobates agassizii*), and evolutionary relationships among the North American gopher tortoises. *Evolution* 43:76–87.
- Murphy, R.W., K.H. Berry, T. Edwards, and A.M. McLuckie. 2007. A genetic assessment of the recovery units for the Mojave population of the desert tortoise, *Gopherus agassizii*. *Chelonian Conservation and Biology* 6:229–251.
- Murphy, R. W., K.H. Berry, T. Edwards, A. E. Leviton, A. Lathrop, and J.D. Riedle. 2011. The dazed and confused identity of Agassiz's land tortoise, *Gopherus agassizii* (Testudines, Testudinidae) with the description of a new species, and its consequences for conservation. *ZooKeys* 113:39–71.

What do we know about the effects of climate change, especially global warming, on desert tortoises?

Jeff Lovich

U.S. Geological Survey, Southwest Biological Science Center, 2255 N. Gemini Drive, MS-9394 Flagstaff, AZ 86001-1600. jeffrey_lovich@usgs.gov

Climate, especially rainfall and temperature, exert a strong influence on the behavior and ecology of desert tortoises, including *Gopherus agassizii* and *G. morafkai*. In the former species, climate influences surface activity, and hence detectability by surveyors; feeding activity; clutch phenology; and ultimately reproductive output (Duda et al., 1999; Freilich et al., 2000; Lovich et al., 1999, 2012). The biology of the latter species is strongly affected by the timing and strength of the North American (Arizona) Monsoon (Van Devender, 2002). Recent modeling results for Joshua Tree National Park suggest that *G. agassizii* may be sensitive to climate change (Barrows, 2010). Global warming is one possible outcome of projected climate change yet little is known of the effect of warming climates on the distribution and biology of desert tortoises. In this mini-review I provide a synopsis of work in progress (Lovich, unpublished data).

It is important to place projected future global warming in the context of deep ecology. Turtles are an ancient lineage remaining virtually unchanged in their morphology for over 200 million years (Ernst and Lovich, 2009). During that time there have been numerous global temperature changes and mass extinctions that turtles survived as an evolutionary line. For example, dramatic temperature changes of 15-20° C occurred from the Paleocene to the Neogene with another 10° C change in the Pleistocene (Bluemle et al., 1999). At the start of the Holocene, temperatures in southwestern North America increased about 4° C over less than 100 years (Cole, 2009). The massive extinctions that occurred at the K-T Boundary appear to have been caused by an asteroid impact (Schulte et al., 2010) in the vicinity of what is now the Yucatan Peninsula, and it caused the extinction of the dinosaurs, in part due to attendant post-impact climate change. Fires, “global winter”, lethal ground-level ozone levels, and environmental sex determination are all possible factors contributing to those extinctions. However, many other taxonomic groups, including turtles (Hutchison and Archibald, 1986), survived the cataclysm. Impacts to amphibious species, like turtles, may have been buffered by coastal and aquatic systems. Alternatively, ground-level ozone lethality (0.1 ppm toxicity) may have been selective (Kikuchi and Vanneste, 2010), thus sparing turtles. Because of their antiquity, turtles experienced, and survived, numerous other

climatic changes including repeated glacial and interglacial periods.

Against this backdrop it seems logical to ask why there is concern about the effects of global warming on tortoises today. Given the listed status of *G. agassizii* as threatened and the continued decline of many populations, it is important to understand threats to their continued survival and impediments to recovery. Tortoises have the capacity to survive natural global warming, as shown by their evolutionary history, but when added to the complex interaction of anthropogenic factors contributing to their overall decline, the ability to persist may be compromised.

One factor that contributes to the sensitivity of tortoises to global warming relates to their recent exposure to modern North American desert conditions. Ancestors of *G. agassizii* appeared only 17-19 million years ago, or about 12 million years before the formation of North American Deserts. Modern *G. agassizii* may have appeared only 3-5 million years ago. Current desert climates and plant communities formed during the last 1% of that time period, mostly in the last 7,000 years. As such, desert tortoises are newcomers to the desert (Morafka and Berry, 2002). How do they manage to survive under such relatively novel conditions? Some scientists believe that many of the survival strategies tortoises utilize are exaptations (Morafka and Berry, 2002), not necessarily adaptations to current conditions. An exaptation is a trait that evolved for one situation but proves to be useful in another context. For example, the ancestors of *Gopherus* may have evolved burrowing to escape exposure in grasslands and that adaptation was exapted for avoiding predators later in their evolutionary history when their habitat was converted to desert. As such, desert tortoises may not be well-adapted for desert conditions at all, and increases in global temperature may make the desert less hospitable for them. Other traits, such as the ability to survive wide fluctuations in osmotic state and field metabolic rates could be ancient exaptations as well (Morafka and Berry, 2002).

Another sensitivity of the desert tortoise to warming is related to environmental sex determination. Unlike mammals and birds that possess genetic sex determination, many turtles, including the genus *Gopherus*, have embryo sex determined by incubation temperature (Ernst

and Lovich, 2009). Desert tortoises exhibit a pattern where male hatchlings are produced in cool incubation temperatures (below about 30.5° C) while females are produced at warm incubation temperatures (above about 32.5° C). The pivotal temperature that produces both sexes is fairly high when compared to other turtles ranging from 31.3-31.8° C, a range of only 0.5° C (see review in Ernst and Lovich, 2009). Several scientific papers have discussed the potential vulnerability of organisms with environmental sex determination to climate warming scenarios (e.g., Hulin et al, 2009).

There are at least four potential responses of desert tortoises to global warming scenarios: 1) no effect, 2) deleterious effects (extirpation/extinction), 3) evolution of a higher/wider threshold temperature for sex determination, or 4) adaptation via shifts in elevational range, shifts in geographic range, shifts in clutch phenology and nesting season, or changes in nest depth or location. I focus on scenario 3 for the remainder of this mini-review.

Recent research modeling the effect of climate change (+2° C, - 50 mm precipitation) on tortoise habitat and distribution in Joshua Tree National Park demonstrated substantial losses of habitat in both the Sonoran and Mojave Desert portions of the region, especially in the former (Barrows, 2010). Reductions in habitat were accompanied by shifting to higher elevations as well. This supports the idea that tortoises may shift their ranges in three-dimensional space, but it is important to note that this strategy will only work if food plants and other habitat needs arrive in the new space before or at the same time as tortoises move in. It is also possible that tortoises will collapse their overall range toward the monsoon-influenced portion of the Sonoran Desert where rainfall is more abundant and predictable. However, the precipitation scenario in the Sonoran Desert is far from certain under climate change (Weiss and Overpeck, 2005).

My research on clutch and nesting phenology in tortoises demonstrates that these aspects of their biology respond to climatic variation with wide year-to-year variation, but in a predictable fashion (Lovich et al., unpublished data). In Palm Springs, most clutches are first visible in X-radiographs sometime in April, but in cool years, clutches may not be shelled and ready for oviposition until May. Differences appear to be due to minimum heat unit accumulation necessary to support the physiological process of egg production. Given that tortoises appear to have flexibility in when they produce and lay eggs, it is possible that they can accommodate gradual warming. There is some flexibility in hatchling emergence time as shown by the fact that many turtles, possibly even desert tortoises, emerge from the nest in either the fall and in the spring of the year following nesting (Ernst and Lovich, 2009). However, resources need to be properly timed to meet the nutritional and habitat needs of hatchlings that emerge from nests. Research on the possible

role of global warming on the physiology and survivorship of hatchling tortoises is not yet available.

Another strategy tortoises may use to respond to climate change relates to nest depth and location. Many *G. agassizii* nests are located in burrows constructed by the female. At Palm Springs in 2000 we observed 17 nests inside burrows, 3 directly beneath the mouth of the burrow, 3 nests located on the burrow apron, and 1 nest under a shrub (Ennen et al., in press). Plotting the depth from the soil surface to the top of the uppermost egg against the distance from the burrow opening demonstrated a statistically significant relationship between the two variables. Nests deeper inside the burrow where the microclimate is cooler were shallower than nests closer to the entrance where the microclimate is warmer. If females have the ability to dig deeper nests, or to nest deeper inside their burrows, it is possible that they can adaptively respond to warming that will affect the sex ratio or survivorship of their clutches.

The question remains: can desert tortoises adapt to a warming climate scenario? Three factors suggest that they can. First, turtles have experienced warming climates many times before in their evolutionary history. Second, their exaptations may allow them to survive additional warming. Third, and finally, is possession of a potentially adaptive capacity to shift ranges and adjust nest season, nest depth, and nest location enough to compensate for increased temperatures. However, existing and emerging factors, such as habitat fragmentation caused by development of utility-scale renewable energy development (Lovich and Ennen, 2011), may limit the ability to shift and adjust ranges, and ironically, may contribute to warming microclimates.

Literature cited

- Barrows, C.W. 2011. Sensitivity to climate change for two reptiles at the Mojave-Sonoran Desert interface. *Journal of Arid Environments* 75:629-635.
- Bluemle, J.P., J.M. Sabel and W. Karlén. 1999. Rate and magnitude of past global climate change. *Environmental Geosciences* 6:63-75.
- Cole, K.L. 2009. Vegetation response to early Holocene warming as an analog for current and future change. *Conservation Biology* 24:29-37.
- Duda, J.J., A.J. Kryzysik, and J.E. Freilich. 1999. Effects of drought on desert tortoise movement and activity. *Journal of Wildlife Management* 63:1181-1192.
- Ennen, J.R., K.P. Meyer, and J.E. Lovich. 2012. Female Agassiz's desert tortoise activity at a wind energy facility in southern California: the influence of an El Niño event. *Natural Science* 4:30-37.
- Ennen, J.R., J.E. Lovich, K. Meyer, C. Bjurlin, and T.R. Arundel. *In press*. Nesting ecology of a Desert Tortoise (*Gopherus agassizii*) population at a utility-scale renewable energy facility in southern California. *Copeia*.
- Ernst, C.H. and J.E. Lovich. 2009. *Turtles of the United States and Canada*. Second edition. Ernst, Johns Hopkins University Press. Baltimore.

- Freilich, J., K.P. Burnham, C.M. Collins, and C.A. Garry. 2000. Factors affecting population assessments of desert tortoises. *Conservation Biology* 14:1479-1489.
- Hulin, V., V. Delmas, et al. (2009). Temperature-dependent sex determination and global change: are some species at greater risk? *Oecologia* 160:493-506.
- Hutchison, J.H. and J.D. Archibald. 1986. Diversity of turtles across the Cretaceous/Tertiary boundary in northeastern Montana. *Palaeogeography, Palaeoclimatology, Palaeoecology* 55:1-22.
- Kikuchi, R. and M. Vanneste. 2010. A theoretical exercise in the modeling of ground-level ozone resulting from the K-T asteroid impact: its possible link with the extinction selectivity of terrestrial vertebrates. *Palaeogeography, Palaeoclimatology, Palaeoecology* 288:14-23.
- Lovich, J.E. and J.R. Ennen. 2011. Wildlife conservation and solar energy development in the Desert Southwest, United States. *BioScience* 61:982-992.
- Lovich, J. E., P. Medica, H. Avery, K. Meyer, G. Bowser, and A. Brown. 1999. Studies of reproductive output of the desert tortoise at Joshua Tree National Park, the Mojave National Preserve, and comparative sites. *Park Science* 19:22-24.
- Morafka, D. J. and K. H. Berry 2002. Is *Gopherus agassizii* a desert-adapted tortoise, or an exaptive opportunist? Implications for tortoise conservation. *Chelonian Conservation and Biology* 4:263-287.
- Schulte, P. *et al.* 2010. The Chicxulub asteroid impact and mass extinction at the Cretaceous-Paleogene Boundary. *Science* 327:1214-1218.
- Van Devender, T. R. (ed.). 2002. *The Sonoran desert tortoise: Natural history, biology and conservation*. Univ. Arizona Press, Tucson.
- Weiss, J.L. and J.T. Overpeck. 2005. Is the Sonoran Desert losing its cool? *Global Change Biology* 11:2065-2077.

Desert reptiles and climate change: winners and losers in a warming world

Cameron W. Barrows

Center for Conservation Biology, University of California Riverside, Riverside, CA 92521-0334, USA,
cbarrows@ucr.edu

ABSTRACT—Desert reptiles live in an environment of extremes, but will adaptations to a world where high temperatures and drought are the norm allow them to survive the current climate change or will that change push them beyond their physiological limits? To address this question I constructed climate shifted niche models coupled with mechanistic explanations and empirical observations to assess the sensitivity of a set of desert reptiles to predicted levels of climate change. I selected five lizard species in the region within and surrounding Joshua Tree National Park; three that were broadly distributed desert species, desert horned lizards, *Phrynosoma platyrhinos*, desert spiny lizards, *Sceloporus magister*, and common chuckwallas, *Sater obesus*, and two species whose range only marginally reaches into desert habitats, coast horned lizards, *P. blainvillii*, and western fence lizards, *S. occidentalis*. Simulated shifts in climate, starting with current conditions and extending to what may be a “worst case scenario” of a +3° C mean July maximum temperature shift resulted in predictable shifts in the extent of suitable habitat for the five lizards. Species with broad distributions extending into the lower Sonoran Desert over diverse habitats had the least reduction in their current range. Those higher elevation species, whose more coastal distributions only marginally occur within the park, will likely be extirpated. While each lizard species’ modeled habitats decreased with simulated climate warming, those habitat areas for desert restricted species were likely large enough to sustain populations, indicating resilience to the expected levels of climate change over the next century. One caveat to this prediction of survival will be the unpredictable severity and length of future droughts.

Through the Pleistocene climates oscillated with shifting influences between cool-wet glacial and hot-dry interglacial periods; the present Holocene being just the most recent of the warmer-drier cycles. Although reptiles occupying North American deserts today have demonstrated their adaptability by surviving those previous temperature and precipitation fluxes, current climate change predictions of increased temperatures and increases in the variability and frequency for both temperature and precipitation may reach levels unprecedented in the recent evolutionary history of these species. The arid southwestern United States and northwestern Mexico are predicted to have departures from current climate conditions larger than any other region of sub-polar North America, with the greatest departures centered on California’s Mojave and Colorado Deserts (Kerr, 2008). Limited data from tropical and temperate lizards, where their climate can be hot but not as variable as in deserts, has indicated that even the relatively small increases in temperature that have occurred to date have resulted in reduced reproductive success, distributional shifts or even local extinctions (Huey et al. 2008, Sinervo et al. 2010). Desert reptiles already live in an environment of extremes, but will the current climate change push

them beyond their physiological limits, or has living in a world where high temperatures and drought are the norm resulted in adaptations that will allow them to survive? Here I couple climate shifted niche models with mechanistic explanations and empirical observations to predict how a set of desert reptiles may respond to predicted levels of climate change.

In extremely arid environments variation in annual precipitation is high; long periods of drought are often broken with rare pulses of wet conditions (Noy-Meir 1973, Bell 1979, MacMahon 1979). For desert species rainfall patterns often dictate reproductive success and so ultimately persistence within a given geographic area; however, unlike predictions of increasing temperatures in this current climate shift, modeled changes for precipitation have much less agreement (IPCC 2007). The one climate change-related precipitation prediction with broad model support is that rainfall will become more variable and droughts as well as wet periods will become more extreme (Lioubimtseva 2004, IPCC 2007). It is the intensity and duration of those projected droughts that are likely to drive much of the climate change-related shifts in suitable habitat within this region (Parmesan et al. 2000, Barrows et al. 2010, and Barrows 2011). In lieu of



local-scale predictions of how precipitation or temperature will shift, modeling the sensitivity of species to a gradient of climate change scenarios can provide insights as to potential effects of local-scale changes in temperature and precipitation. A useful tool in assessing species sensitivity to changing conditions is niche modeling (Rotenberry et al. 2002, 2006,) which includes habitat variables, such as climate, soils and terrain, in an attempt to assess the complex interaction of factors that constrain a species' distribution. Once accurate niche models are created that describe a species current distribution, shifting model variables for temperature and precipitation may provide land managers important insights as to the sensitivity of species to climate change and how they might respond to such changes. Even with those insights such models don't capture the stochastic nature of drought intensity and duration, events that can dictate species' survivorship; however understanding species' responses to drought coupled with their reproductive longevity can provide inferences as to drought severity levels that would result in range shifts (Barrows et al. 2010, Barrows 2011). Another challenge is that modeling species distributions using novel, projected climates is intrinsically uncertain; nevertheless many such models

Figure 1. The four lizard species analyzed here. A coast horned lizard *Phrynosoma blainvillii*; B desert horned lizard *P. platyrhinos*; C western fence lizard, *Sceloporus occidentalis*; D desert spiny lizard, *S. magister*; and E common chuckwalla *Satur obesus*. All photos by Cameron Barrows.

Table 1. Area of suitable habitat, rounded to the nearest ten ha, available to each lizard species under three climate change scenarios. Percentages represent the proportion of suitable habitat remaining at each temperature increase.

| Species | Temperature Scenario | | | |
|----------------------|----------------------|------------------|------------------|------------------|
| | Current | +1°C | +2°C | +3°C |
| Desert Horned Lizard | 332,560 ha | 308,370 ha – 93% | 254,120 ha – 76% | 187,450 ha – 56% |
| Coast Horned Lizard | 7,860 ha | 5,300 ha – 67% | 840 ha – 11% | 0 |
| Desert Spiny Lizard | 61,700 ha | 37,320 ha – 60% | 31,460 ha – 51% | 24,860 ha – 40% |
| Western Fence Lizard | 21,180 ha | 15,250 ha – 72% | 6,544 ha – 31% | 756 ha – 4% |
| Common Chuckwalla | 119,810 ha | 86,040 ha – 72% | 6 6,092 ha – 55% | 56,696 ha – 47% |

have provided surprisingly accurate projections of climate impacts to date (Ackerly et al. 2010).

I chose the region within and surrounding Joshua Tree National Park as it straddles the Mojave and Sonoran (Colorado) Deserts and abuts the cismontane coastal ecoregion, capturing much of the range of conditions species might select as suitable habitat. Within that region I selected five lizard species; three that were broadly distributed desert species, (desert horned lizards, *Phrynosoma platyrhinos*, and desert spiny lizards, *Sceloporus magister*, and common chuckwallas, *Sater obesus*) and two species whose range only marginally reach into desert habitats, (coast horned lizards, *P. blainvillii*, and western fence lizards, *S. occidentalis*) (Figure 1). See Jones and Lovich (2009) for more detailed habitat descriptions and range maps.

Developing niche models begins with compiling accurate location data for each species that are analyzed. Observations included in the following analyses result from my own fieldwork, my students, collaborators, National Park reports and museum records. I used the Mahalanobis distance statistic (D^2) (Rotenberry et al. 2002, 2006) to model the distribution of suitable habitat for each species. The Mahalanobis statistic yields for any location or map cell an index of its habitat similarity to locations where the species being analyzed is known to occur. This analysis tool has several advantages over other geographic information system (GIS) modeling approaches, the foremost being that only species-presence data are required for the dependent variable. Because only positive occurrence data are required, location records from a variety of sources can be used, regardless of survey methodology, as long as the species records are correctly assigned to precise ground locations so that the correct environmental variables can be used in the model.

For the niche-modeling process, a GIS map was divided into 200 m × 200 m cells; only one species observation was included in any one cell. Each cell was scored for underlying environmental variables. I used ArcGIS 9.3 (ESRI 2008) to provide a spatial model (niche map) of the similarity (multivariate mean) of occupied cells to each cell within the mapped area and to calculate the area

mapped as suitable habitat under each climate scenario. I selected habitat variables based on my expectation of their likely influence on the distribution of the selected species. I constructed partitioned Mahalanobis D^2 models with different suites of abiotic variables derived from GIS layers readily available from internet sources in 2008 (Table 1); soils (Natural Resources Conservation Service 2008); ruggedness (United States Geological Survey 2009, Sappington et al. 2007); and climate (PRISM Climate Group 2004). Due to the lack of agreement among climate models as to what direction and to what degree precipitation will shift in this region under climate change scenarios (Hayhoe et al. 2004, Seager et al. 2007), I created niche models in which precipitation was not included as an independent variable; mean July maximum temperatures are negatively correlated with precipitation ($r = -0.839$) so, given rainfall uncertainties, the inclusion of that temperature variable served as a proportional proxy for precipitation conditions, consistent with current-recent temperature-precipitation relationships. I used three levels of increasing mean July maximum temperatures as climate change scenarios, +1°, +2° and +3° C, under the assumption that these temperatures would represent periods of maximum stress on the lizards. Since climate warming is predicted to be asymmetric (more warming in cold seasons than in the hot seasons) (Easterling et al. 1997) these temperature scenarios likely meet or exceed the maximum levels of climate change expected within the next century; a +3° C mean July maximum temperature would represent a “worst case scenario” (IPCC 2007).

Results

Modeled shifts in the area of suitable habitat indicated desert-restricted lizard species were relatively resistant to expected levels of climate change within the next century; lizards with ranges that only reach the desert edge will likely be extirpated from desert habitats (Table 1). Reductions in the areal extent of suitable habitat followed predictable patterns with ground dwelling desert horned lizards having the largest current distribution of suitable habitat and the greatest resistance to increasing summer

Table 2. Spatial distribution of modeled suitable habitat of each lizard species, rounded to the nearest 10 ha, between the Sonoran (Colorado) and Mojave Deserts. Percentage values indicate the proportion of the suitable habitat located in each desert ecoregion under each modeling scenario.

| Species | Ecoregion | |
|-----------------------------|---------------------------|-----------------|
| | Sonoran (Colorado) Desert | Mojave Desert |
| Desert Horned Lizard | | |
| Current | 248,880 ha – 75% | 83,680 ha – 25% |
| +3° C | 101,770 ha – 54% | 85,680 ha – 46% |
| Coast Horned Lizard | | |
| Current | 312 ha – 4% | 7,552 ha – 96% |
| +3° C | 0 | 0 |
| Desert Spiny Lizard | | |
| Current | 11,270 ha – 18% | 50,430 ha – 82% |
| +3° C | 1,280 ha – 5% | 23,580 ha – 95% |
| Western Fence Lizard | | |
| Current | 2,270 ha – 12% | 18,550 ha – 88% |
| +3° C | 8 ha – 1% | 750 ha – 99% |
| Common Chuckwalla | | |
| Current | 64,740 ha – 54% | 55,080 ha – 46% |
| +3° C | 8,140 ha – 14% | 48,550 ha – 86% |

temperatures. In each modeled shift, reductions in suitable habitat were correlated with increases in the mean elevation where the lizards' habitat was distributed. Desert horned lizards' modeled habitat occurred at the lowest mean elevation (494 m, s.d. 259 m), and increased 189 m with a simulated +3°C in mean maximum July temperatures. Chuckwalla current mean suitable habitat was also low (682 m, s. d. 247 m), but it habitat increased in mean elevation by 460 m with a simulated +3°C, a greater increase in elevation than any of the species analyzed here. The current mean elevation for both coast horned lizards and western fence lizards was much higher (1320 m, s. d. 86 m; 1266 m, s. d. 163 m, respectively) putting them approaching the highest elevations within the park. These species had less room to move to higher elevations with simulated increases in mean maximum July temperature, increasing 118 m (coast horned lizard) and 88 m (western fence lizard). Desert spiny lizards were intermediate, with a current mean elevation for suitable habitat of 1060 m (s. d. 253 m), extending up to 1284 m with a simulated +3° C mean July maximum temperature shift. Each species' suitable habitat retreated up from lower elevations and from more easterly Sonoran Desert regions of the park and expanded into the higher elevation western Mojave Desert areas (Table 2).

Discussion

Simulated shifts in climate, starting with current conditions and extending to what may be a “worst case scenario” of a +3° C mean July maximum temperature shift resulted in predictable shifts in the extent of suitable habitat for the five lizards I analyzed here. Species with broad distributions extending into the lower Sonoran Desert over diverse habitats had the least reduction in the distribution within the greater Joshua Tree National Park region. Those higher elevation species, whose more coastal distributions only marginally occur within the park, will likely be extirpated. While each lizard species' modeled habitats decreased with climate warming, those habitat areas for desert restricted species were likely large enough to sustain populations through the climate changes I simulated here. There are, however, multiple assumptions attached to these predicted outcomes: 1) the current species distributions within Joshua Tree National Park fully capture the range of habitats and climates these species can occur, and so their modeled niches accurately depict their adaptive capabilities; 2) these lizard species are sufficiently mobile to disperse sufficient distances to track and then occupy shifting niche envelopes; 3) precipitation will become overall more arid with increasing temperatures but not in excess of current

temperature-rainfall correlations, and 4) drought intensity and duration will continue within historic levels.

Assumptions regarding precipitation and drought lack strong empirical or theoretical footing; assuming current relationships will continue is a conservative approach but only with future analyses will those assumptions be tested. While warming temperatures at stations surrounding Joshua Tree National Park are following patterns predicted by climate change models, precipitation patterns have yet to show marked departures from historic patterns (Western Regional Climate Center, Indio and Twentynine Palms Reporting Stations; <http://www.wrcc.dri.edu/>). Still, the one climate change-related precipitation prediction with broad model support is that rainfall will become more variable and droughts as well as wet periods will become more extreme (Lioubimtseva 2004, IPCC 2007). If drying exceeds current patterns my predictions here likely underestimate habitat losses, whereas if it becomes wetter losses may not be as severe. If the intensity and duration of those projected droughts increases the result would be pulsed population declines with the potential of reestablishment when wetter conditions return. Previously I conducted a simulation increases in drought intensity and duration for Coachella Valley fringe-toed lizards, *Uma inornata*; pulsed droughts dramatically increased local extirpations as compared to mean rainfall declines, a pattern exacerbated by habitat fragmentation and barriers to between-fragment movements (Barrows et al. 2010).

The first assumption, that modeled niches accurately depict the lizards' adaptive capabilities, is an important question involving ecological scale. If the analysis is conducted at too fine of scale the breadth of a species' suitable habitat can be missed. Alternatively if the scale is too large multiple populations across diverse gradients of temperature and precipitation conditions could be included. The problem is that statistical analyses imbedded in the modeling approach would homogenize those different local conditions and local adaptations, and in doing so fail to accurately characterize the unique niche of the individual populations, especially those at the periphery of a species' distribution which could be considered statistical outliers. Resolving this "Goldilocks dilemma" of scales being too big or too small, and determining the scale that is "just right" depends on the question being asked and the topographic diversity of the region being modeled. Here I have limited my observation data and analyses of shifts in the lizards' distributions to the greater Joshua Tree National Park region, an area with diverse topography and spanning two desert ecoregions. The desert horned lizards, desert spiny lizards and common chuckwallas are also common in the adjacent Coachella Valley where elevations are typically lower and the climate is both warmer and dryer than most of the park. However my modeled area does incorporate

portions of the Coachella Valley, and so captures much of those lower elevation habitats and species relationships.

For an accurate assessment of the second assumption, that dispersal is sufficient to track and then occupy a shifting niche envelope, a measure of both dispersal distances and the rate of change in the suitable habitat niche would be required. In lieu of such lizard data, data describing shifts in woody vegetation tracking climate does occur. Near Joshua Tree National Park, Kelly and Goulden (2008) measured shifts in vegetation related to changing climate on an elevation gradient extending above the Coachella Valley floor. While individual plant species moved at different rates, the mean shift was roughly 60 m in elevation over a +/- 30 year time span. Assuming a 2 m/year shift, it's reasonable to assume any of the lizard species could traverse distances and elevations at that scale.

Despite shifting niches from lower desert habitats to incrementally higher elevations, desert lizards will likely persist through much of their current range in the face of climate change over the next century. Although they were not modeled here because of too few observations available to provide robust models, hot-loving lizards such as desert iguanas, *Dipsosaurus dorsalis*, will likely expand their range as temperatures increase. In addition to relatively high mobility and behavioral avoidance of otherwise lethal weather patterns (droughts, heat waves), many desert lizards are able to maintain osmotic balances during droughts by expelling salts through nasal glands. This ability provides a physiological advantage not shared by all desert reptiles such as desert tortoises, *Gopherus agassizii*, giving an otherwise similar sized vegetarian lizard, the common chuckwalla, an edge in their sensitivity to climate change (Barrows 2011). The caveat to this prediction of survival will be the severity and length of future droughts (i.e. Barrows et al. 2010).

High elevation and otherwise more coastally distributed species such as coast horned lizards and western fence lizards will likely not persist within the park if climate change predictions reach expected levels. These species' ranges within the park may be relicts of past cooler-wetter periods within the southern California deserts. Taking a longer view, maintaining connectivity to the cismontane habitats abutting the western end of the park may facilitate re-establishment of these species when our current climate heating abates.

ACKNOWLEDGEMENTS—Mark Fisher, Don Scriven, Rob Black, and Bayard Brattstrom contributed lizard locations that enabled me to construct the niche models used in this analysis.

Literature cited

- Ackerly, D.D., S.R. Loarie, W.K. Cornwell, S.B. Weiss, H. Hamilton, R. Branciforte, and N.J.B. Kraft. 2010. The geography of climate change: implications for conservation biology. *Diversity and Distributions* 16:476-487.
- Barrows, C.W. 2011. Sensitivity to climate change for two reptiles at the Mojave-Sonoran desert interface. *Journal of Arid Environments* 75:629-635.
- Barrows, C.W., J.T. Rotenberry, and M.F. Allen. 2010. Assessing sensitivity to climate change and drought variability of a sand dune endemic lizard. *Biological Conservation* 143:731-743.
- Bell, F. C. 1979. Precipitation. Pages 373-392 in D. W. Goodall, R. A. Perry, and K. M. W. Howes, editors. *Arid-land ecosystems: structure, functioning and management*. Cambridge University Press, Cambridge, United Kingdom.
- Easterling, D.R., B. Horton, P.D. Jones, T. C. Peterson, T.R. Karl, D. E. Parker, M. Salinger, V. Razuvayev, N. Plummer, P. Jamason, and C. K. Folland. 1997. Maximum and Minimum Temperature Trends for the Globe. *Science* 5324: 364-367.
- ESRI (Environmental Systems Research Institute, Inc.). 2008. ArcGIS Desktop 9.3 ESRI, Redlands, California, USA.
- Hayhoe, K., D. Cayan, C.B. Field, et al. 2004. Emission pathway, climate change, and impacts on California. *PNAS* 101:12422-12427.
- Huey, R.B., Deutsch, C.A., Tewksbury, J.J., Vitt, L.J., Hertz, P.E., Alvarez Pérez, H.J., and Garland T., Jr., 2009. Why tropical forest lizards are vulnerable to climate warming. *Proc. of the Royal Society B* doi:10.1098/rspb.2008.1957, 1-10.
- IPCC (2007) Climate change 2007—the physical science basis. 2007 Contribution of the working group I to the fourth assessment of the IPCC. Cambridge University Press, Cambridge, United Kingdom.
- Jones, L.L.C. and R.E. Lovich. 2009. *Lizards of the American Southwest: A Photographic Field Guide*. Rio Nuevo Publishers, Tucson, Arizona. 567 Pages.
- Kelly, A.E., and M.L. Goulden. 2008. Rapid shifts in plant distribution with recent climate change. *PNAS* 105:11823-11826
- Kerr, R. A. 2008. Climate change hot spots mapped across the United States. *Science* 321: 909.
- Lioubimtseva, E. 2004. Climate change in arid environments: revisiting the past to understand the future. *Progress in Physical Geography* 28: 502-530.
- MacMahon, J. A. 1979. North American deserts: their floral and faunal components. Pages 21-82 in D. W. Goodall, R. A. Perry, and K. M. W. Howes, editors. *Arid-land ecosystems: structure, functioning and management*. Cambridge University Press, Cambridge, United Kingdom.
- Natural Resources Conservation Service, United States Department of Agriculture, Soil Survey Staff. 2008. Soil Survey of Western Riverside Area, Riverside County, Coachella Valley Area, and San Bernardino National Forest Area, California and U.S. General Soil Map Coverage. <<http://soildatamart.nrcs.usda.gov/Survey.aspx%3fState%3dMT>>.
- Noy-Meir, I. 1973. Desert ecosystems: environment and producers. *Annual Review of Ecology and Systematics* 4:25-51.
- Parmesan, C., T.L. Root, and M.R. Willig. 2000. Impacts of extreme weather and climate on terrestrial biota. *Bulletin of the American Meteorology Society* 81:443-450.
- PRISM Climate Group. 2004. Oregon State University. <<http://www.prismclimate.org>>.
- Rotenberry, J. T., S. T. Knick, and J. E. Dunn. 2002. A minimalist's approach to mapping species' habitat: Pearson's planes of closest fit. Pages 281-290 in J. M. Scott, P. J. Heglund, M. L. Morrison, J. B. Haufler, M. G. Raphael, W. A. Wall, and F. B. Samson, editors. *Predicting species occurrences; issues of accuracy and scale*. Island Press, Covelo, California, USA.
- Rotenberry, J. T., K. L. Preston, and S. T. Knick. 2006. GIS-based niche modeling for mapping species habitat. *Ecology* 87:1458-1464.
- Sappington, J.M., K.M. Longshore, and D.B. Thomson. 2007. Quantifying landscape ruggedness for animal habitat analysis: a case study using bighorn sheep in the Mojave Desert. *Journal of Wildlife Management* 71:1419-1426.
- Seager, R., M. Ting, I. Held, Y. Kushnir, J. Lu, G. Vecchi, H. Huang, N. Harnik, A. Leetmaa, N. Lau, C. Li, J. Velez, and N. Naik. 2007. Model predictions of an imminent transition to a more arid climate in southwestern North America. *Science* 316: 1181-1184.
- Sinervo, B., Méndez-de-la-Cruz, F., Miles, D.B., Heulin, B., Bastiaans, E., Villagrán Santa Cruz, M, Lara-Resendiz, R., Martínez-Méndez, N., Calderón-Espinosa, M.L., Meza-Lázaro, R.N., Gadsden, H., Avila, L.J., Morando, M., De la Riva, I.J., Sepúlveda, P.V., Duarte Rocha, C.F., Ibargüengoytia, N., Aguilar Puntriano, C., Massot, M., Lepetz, V., Oksanen, T.A., Chapple, D.G, Bauer, A.M., Branch, W.R., Clobert, J. Site,s J.W., Jr., 2010. Erosion of lizard diversity by climate change and altered thermal niches. *Science* 328:894–899.
- United States Geological Survey. 2009. National Elevation Dataset 1/3 Arc-Second (NED 1/3) Courtesy of the U.S. Geological Survey. Earth Resources Observation and Science (EROS) Center, Sioux Falls, SD. <<http://seamless.usgs.gov/ned1.php>>.

Age, stratigraphy, depositional environment and vertebrate ichnology of the Pliocene Copper Canyon Formation, Death Valley, California

Torrey Nyborg,* Paul Buccheim and Kevin E. Nick

Department of Earth and Biological Sciences, Loma Linda University, Loma Linda, CA, 92350, *tnyborg06g@llu.edu

ABSTRACT—The Copper Canyon Formation, a fluvial-lacustrine deposit exposed within the Black Mountains of Death Valley National Park, has only previously been broadly included in regional tectonic and depositional analyses. The formation is significant because it preserves numerous shoreline-playa features including highly abundant and diverse mammal and bird tracks. To date, twenty-six ichnospecies of cat, camel, horse, mastodon, and bird tracks have been identified from 60+ localities spanning over 1200 m of lacustrine deposits. The formation is composed of approximately 1800 m of conglomerates, basalt flows, and fluvial-lacustrine sediments exposed within Copper and Coffin Canyons on the west side of the Black Mountains in southern Death Valley National Park, California. The Formation is divided into three new members; the Greenwater Conglomerate, Coffin Canyon, and Barnyard and three new basalt flows; Coffin Peak, Gyp Hill, and Carnivore Ridge based upon stratigraphic and lithologic characteristics. Basalt flows, paleomagnetic analysis, and a tuff bed stratigraphically above the formation, give dates of 5.20 Ma for the base of the formation and 3.15 Ma for the top of the formation. Across that time interval 6 normal and 5 reversed magnetozones are identified (chron 3n.4n to 2An.2n). Further stratigraphic works limits the upper Copper Canyon Formation lacustrine deposition in Copper Canyon to between 4.73 and about 3.2 Ma, which is significant because it constrains the timing of the most prevalent animal activity. In addition, temporal placement of the Copper Canyon Formation within the other Cenozoic basin fill deposits of Death Valley is also now possible. The abundance and diversity of fossil mammal and bird tracks was previously only superficially recognized. Detailed measured sections within the Copper Canyon and Coffin Canyon reveal that the distribution of the tracks is much more widespread and is coincident with spring deposits and freshwater limestone, suggesting a fresh water source in an otherwise brackish to saline lake environment. The limestone contains invertebrates, plant material, tufa mounds, and stromatolites. The tufa mounds provide evidence of a significant spring water source to the lake. Animals were attracted to the freshwater and associated food, leaving their tracks in the playa mud flat. Rapid burial of tracks by local flash floods and associated sheet wash across the mud flat probably were responsible for the preservation of the trackways.

Introduction

The Copper Canyon Formation crops out in an area approximately 13 km², in Copper and Coffin canyons on the west side of the Black Mountains in southern Death Valley National Park, California (Figure 1). The formation represents approximately 1800 m of conglomerates, basalt flows, and lacustrine deposits. Radiometric age determination on the basalt flows, paleomagnetic analysis, and a radiometric age on a tuff bed stratigraphically above the Copper Canyon Formation, give dates of 5.20 Ma for the base of the formation and 3.15 Ma for the top of the formation (Figure 1). The Copper Canyon Formation is subdivided into three members and three basalt flows. The members are the Greenwater Conglomerate,

Coffin Canyon, and Barnyard, and three basalt flows are the Coffin Peak, Gyp Hill, and Carnivore Ridge (Figure 1; Table 1) based on stratigraphic and lithologic characteristics. Table 1 shows the divisions of the Copper Canyon Formation into members and beds as mapped in Figure 1.

The Copper Canyon Formation is significant because: 1) the formation preserves one of the world's most abundant and diverse fossil mammal and bird track records; and 2) the Copper Canyon Formation was deposited during an important tectonic episode that formed the present Death Valley and Black Mountains. Thus an understanding of the accumulation of these rock units is important to explain the tectonic development at this time, how the formation relates to the other Cenozoic basin-fill deposits of Death Valley, and the depositional

conditions that led to the preservation of the tracks. This paper represents a shortened version of the dissertation work of the lead author and ideas and figures presented herein are further discussed in Nyborg (2011).

Geologic setting

Outcrops of the Copper Canyon Formation are exposed within an approximately 13 km² drainage basin within Copper and Coffin canyons on the west side of the Black Mountains in southern Death Valley National Park, California between longitude 116° 46' 30" and 116° 42' 30" and along latitude 36° 7' 00" and 36° 10' 30" (Figure 1). A 1:24,000 geologic map of the Copper Canyon Formation was prepared noting members and basalt flows of the formation and their contacts with the surrounding geology (Figure 1).

The formation is underlain by Precambrian metasedimentary rocks of the Mormon Point Turtleback to the south and lower Tertiary older volcanics (as reported by Drewes, 1963) to the north (Figure 1). It is overlain by conglomerates of the Pliocene Funeral Formation to the east (Figure 1). The Copper Canyon Formation is divided into three members and three basalt flows based on their vertical, sequential changes and lithologic characteristics (Figure 1, 2; Table 1). Figure 2 shows an aerial view of the Copper Canyon Formation and a general vertical and lateral relationship model for the distribution of the members and flows.

Surrounding Black Mountain deposits consist of limestones of the Ordovician Pogonip Group (Nolan et al., 1956), carbonates of the Neoproterozoic Noonday Dolomite (Wright et al., 1978), quartzite of the Neoproterozoic Stirling Quartzite (Stewart, 1970), and Tertiary volcanics (Ottens, 1977). The Copper Canyon lake developed about 5 Ma and was infilled from sediments from the uplifting Black Mountains and Mormon Point Turtleback. The position of the Black Mountain Fault Zone is inferred to have stepped

Table 1. Division of Copper Canyon Formation into members and basalt flows. Acronyms in parenthesis refer to map unit (Figure 1).

| COPPER CANYON FORMATION | |
|-------------------------------|-----------------------|
| MEMBERS | BASALT FLOWS |
| Greenwater Conglomerate (Tcg) | Coffin Peak (Tbc) |
| Coffin Canyon (Tcc) | Gyp Hill (Tbg) |
| Barnyard (Tcb) | Carnivore Ridge (Tbr) |

basinward sometime after deposition ceased in Copper Canyon Lake, at about 3 Ma (Knott et al., 2005). During that time the Copper Canyon Formation was uplifted and folded into a syncline.

Type section

An approximately 1800 m thick section was measured in detail from the base to the uppermost exposures of the

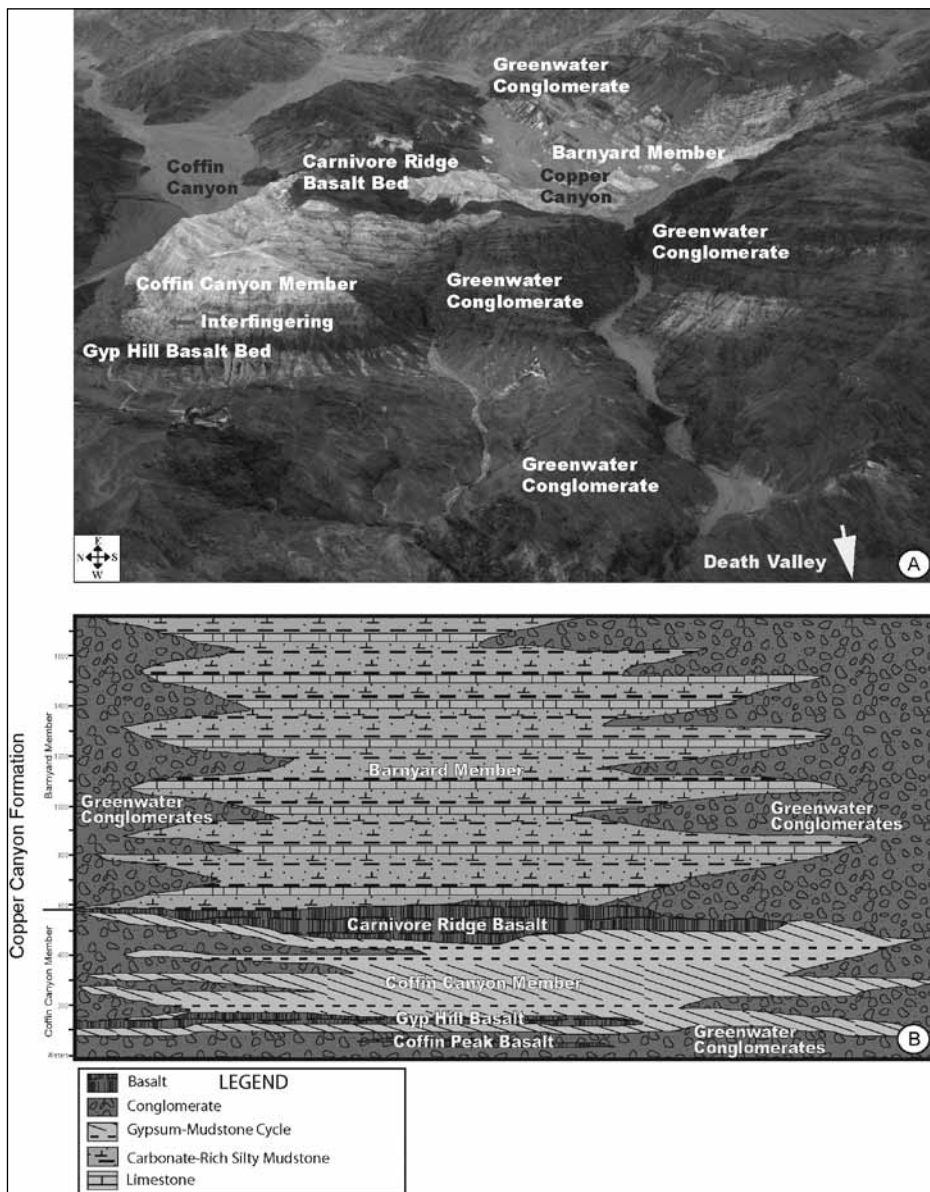


Figure 2. (A), Aerial photograph of the Copper Canyon Formation with labels showing division of the formation into members and basalt flows; aerial photo taken by author. (B), Vertical and lateral relationships (idealized cross section) of the Copper Canyon Formation members and basalt flows.

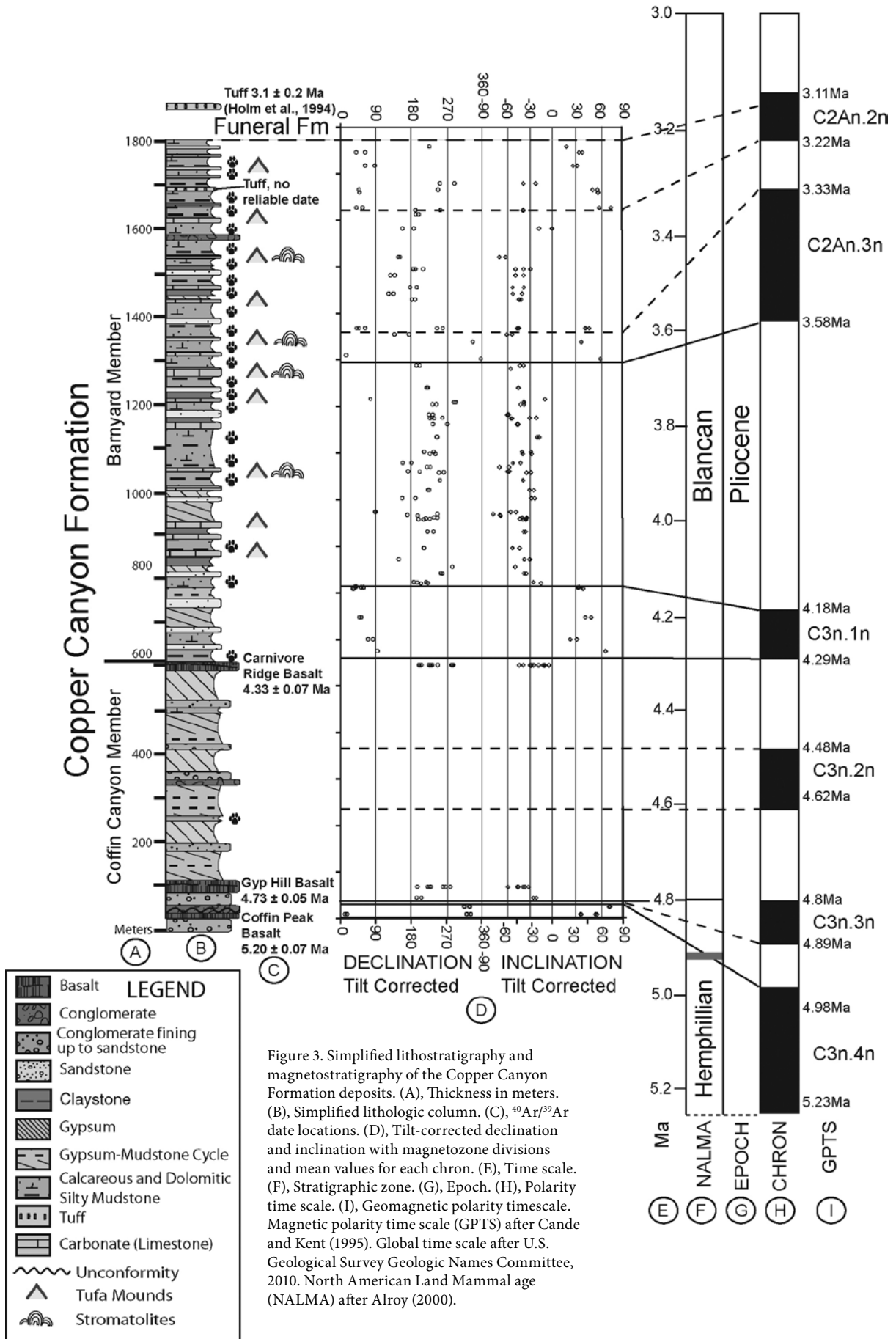


Figure 3. Simplified lithostratigraphy and magnetostratigraphy of the Copper Canyon Formation deposits. (A), Thickness in meters. (B), Simplified lithologic column. (C), $^{40}\text{Ar}/^{39}\text{Ar}$ date locations. (D), Tilt-corrected declination and inclination with magnetozones and mean values for each chron. (E), Time scale. (F), Stratigraphic zone. (G), Epoch. (H), Polarity time scale. (I), Geomagnetic polarity timescale. Magnetic polarity time scale (GPTS) after Cande and Kent (1995). Global time scale after U.S. Geological Survey Geologic Names Committee, 2010. North American Land Mammal age (NALMA) after Alroy (2000).

formation noting lithologies, sedimentary features, tufa mounds, stromatolites, and animal tracks. A generalized stratigraphic column showing these features is presented in Figure 3. The blue lines on Figure 1 represent the detailed measured section (type section) taken from the best exposed and accessible outcrops (refer to Nyborg, 2011 for detailed drafted sections and localities). The stratigraphic column for the Copper Canyon Formation, as displayed in Figure 3 shows the thickness and division of the formation into members and basalt flows, their vertical sequence, and their stratigraphic location.

A combination of $^{40}\text{Ar}/^{39}\text{Ar}$ dates and magnetostratigraphy has produced a well-constrained correlation to chronostratigraphy for the Copper Canyon Formation

(Figure 3). The age of the top of the formation is bracketed, but not precisely dated, by magnetostratigraphic and radiometric data. A maximum age of 3.22 Ma is implied by the date of the base of the normal polarity of the upper formation and its correlation to the C2An.2n chron. The minimum age limit is from a tuff near the base and within the overlying Funeral Formation conglomerates with a reported date of 3.1 ± 0.2 Ma (Holm et al., 1994). The age of the Copper Canyon Formation spans the lower Blancan North American Land Mammal Ages (NALMA) (Alray, 2000; Lindsay et al., 2002; Woodburne, 2004).

The Coffin Canyon Member consists of a basal 70 m of conglomerate, sandstone, and the Coffin Peak and Gyp Hill basalt flows (Figures 1, 3), followed by 500 m of

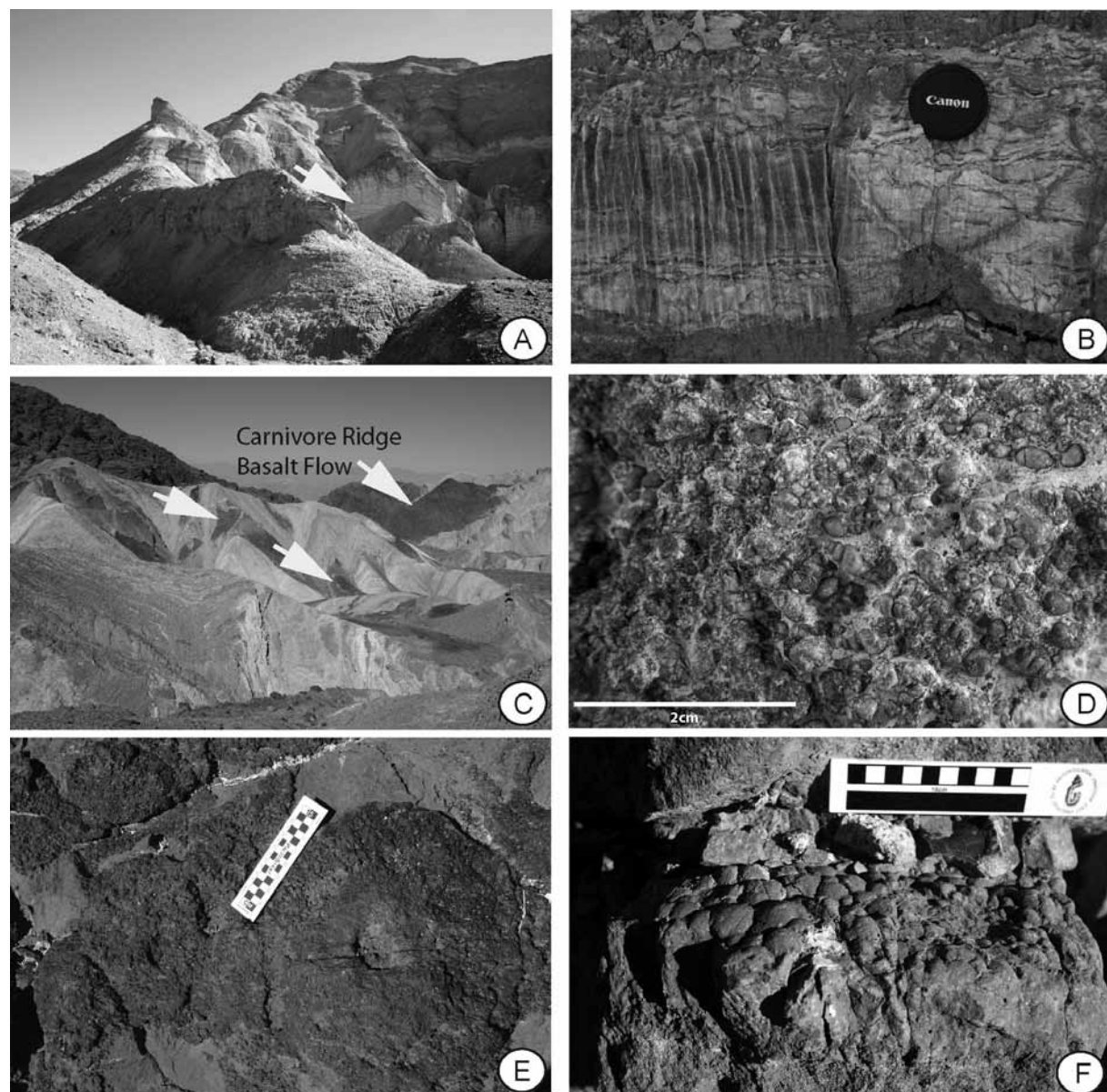


Figure 4. Several outcrop images representing lithologies in the Copper Canyon Formation. (A), Interbedded gypsum and mudstone within the Coffin Canyon Member (arrow). (B), Thick gypsum bed exposed within the Coffin Canyon Member. (C), Limestone beds (dark brown) within the upper two-thirds Barnyard Member. Limestone beds are interbedded with lighter calcareous-dolomitic silty mudstone beds; upper arrow points to Carnivore Ridge Basalt Flow and lower two arrows point to several limestone beds. (D), Skeletal packstone with gastropods and ostracods. (E), Tufa mound showing central micritic pipe and surrounding porous tufa. (F), Bedding plane surface showing small, domical, 1-3 cm diameter stromatolites associated with skeletal packstone beds.

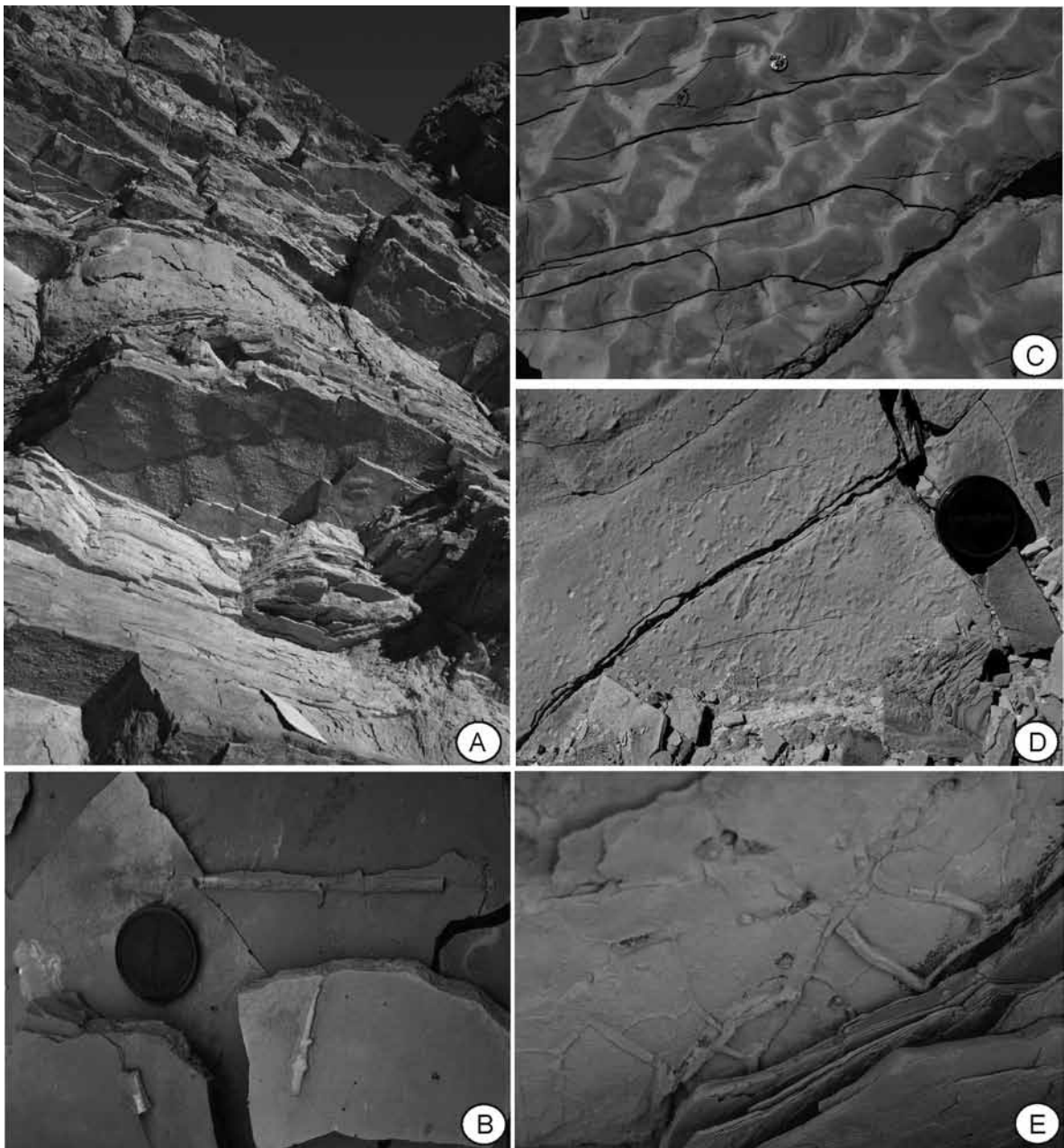


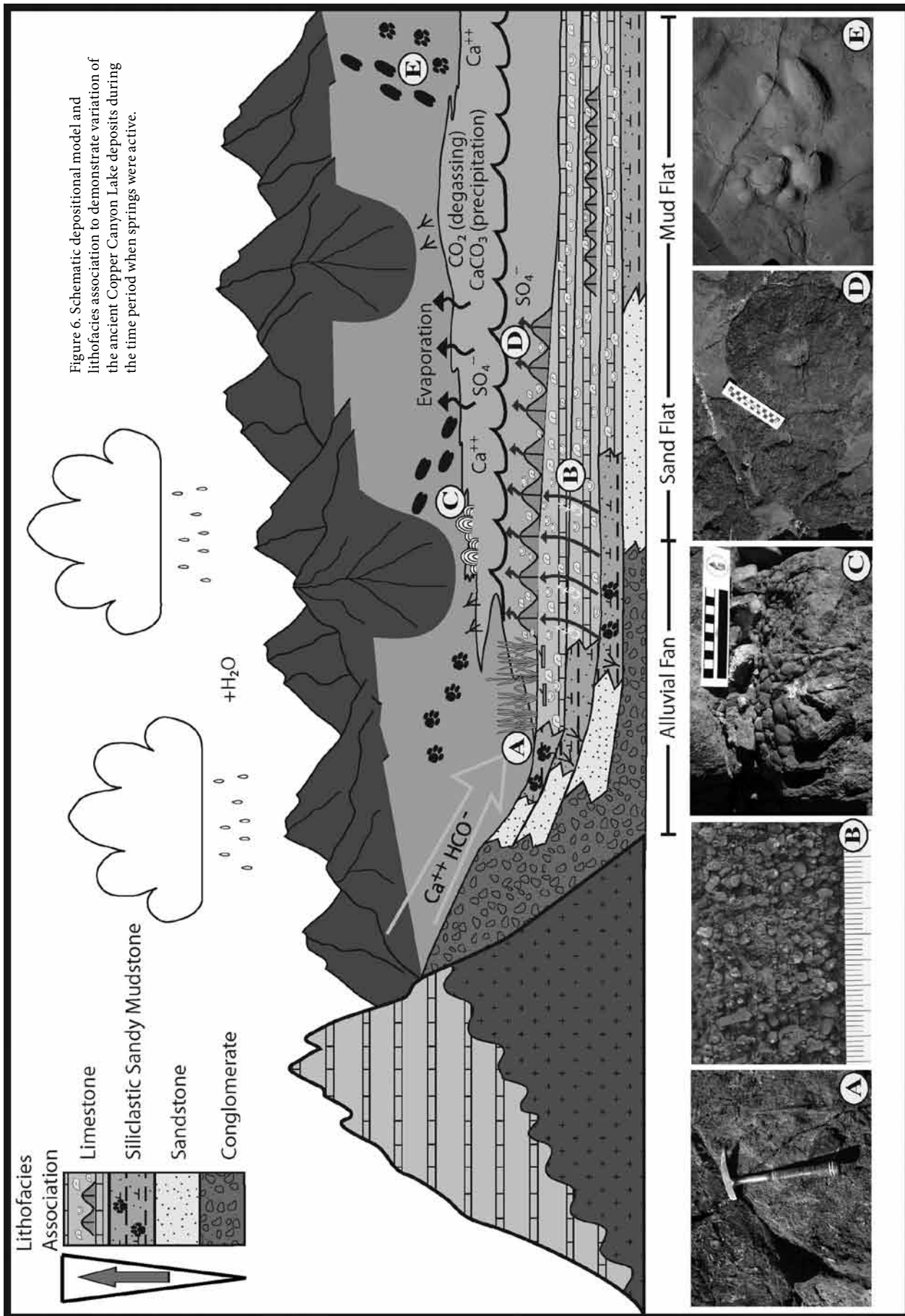
Figure 5. Sedimentary structures typical of the calcareous-dolomitic silty mudstone facies. (A), Typical outcrop within the Barnyard Member; camelid track in the center of the image and directly above on another thin bed there are wave ripples; above the ripples, and after a few more calcareous-dolomitic silty mudstone beds, there is a thick gray sandstone bed; no scale, overhanging outcrop. (B), Reed casts on bedding surface. (C), Sinuous current ripples in the process of becoming linguoid ripples; note the finer mudstone infilling many of the ripple troughs; penny for scale. (D), Raindrop impressions on bedding surface. (E), Polygonal mudcracks on bedding surface.

mainly gypsum interbedded with mudstone (Figure 3). During this stage of the ancient Copper Canyon lake, tracks are limited to thin calcareous-dolomitic silty mudstone beds. The Barnyard Member consists of 1200 m of calcareous-dolomitic silty mudstone and limestone cycles (Figure 3). The calcareous-dolomitic silty mudstone beds contain shoreline features, animal tracks, and soft sediment deformation structures. Limestone beds are composed of invertebrate and charophyte packstone with about ten of the limestone beds containing tufa mounds and stromatolites (Figure 3).

Copper Canyon Formation—description and justification

The Copper Canyon Formation has been mapped and is distinguished from underlying volcanic and metamorphic units and overlying basalt-rich conglomerate of the Funeral Formation (Figure 1). The formation is named for Copper Canyon basin where it crops out within Copper and Coffin canyons (Figure 1). The name is derived from an old copper mine in the upper part of the canyon.

The Copper Canyon Formation is underlain by metasedimentary rocks of the Mormon Point



Turtleback to the south and older volcanics (as reported by Drewes, 1963) to the north. It is overlain by conglomerates of the Funeral Formation to the east (Figure 1). Surrounding the Copper Canyon Formation are deposits in the Black Mountains including limestones of the Pogonip Group (Nolan et al., 1956), carbonates of the Noonday Dolomite (Wright et al., 1978), quartzite of the Stirling Quartzite (Stewart, 1970), and volcanics (Otten, 1977). (Figure 1). Based on an examination of the detailed measured section, sequential vertical and lateral changes of rock units, and on mapping of the basin filling rocks, the formation was divided into three new sedimentary members and three new basalt flows (Figure 1; Table 1).

The Greenwater Conglomerate Member underlies and interfingers with the Coffin Canyon and Barnyard members (Figure 1, 2). Defining boundaries is therefore difficult; however, the member possesses distinct lithologic properties distinguishing it from adjacent members; therefore making it possible to map the rock units as part of this member (Figure 1, 2). The Greenwater Conglomerate Member at the base of the Copper Canyon Formation is about 70 m thick (Figures 1, 2). At about 70 m the conglomerates grade into the Coffin Canyon Member. From about 70-1780 m the Greenwater Conglomerates are present at the basin margins and interfinger with the Coffin Canyon and Barnyard members (Figure 2). At the top of the Copper Canyon Formation, the Greenwater Conglomerates partially overlie the Barnyard Member (Figure 2). The member is named for the Greewater Range to the northeast of Copper Canyon.

The Coffin Canyon Member crops out between the Gyp Hill and Carnivore Ridge basalt flows from about 70 to 600 m (Figure 1-3). The member consists mainly of gypsum interbedded with mudstone and a few isolated beds of calcareous-dolomitic silty mudstone (Figure 4A-C). The member is named for Coffin Canyon where it crops out (Figures 1, 2). The name is derived from the fact that there is no easy outlet from the canyon to Death Valley. Bird tracks and one ichnospecies of camel track have been located within this member. Gypsum is often interbedded with mudstone forming meter scale cycles in outcrop (Figure 4A-C). In several places, beds of pure gypsum several meters thick occur. The name Coffin Canyon has been published on numerous maps of the area.

The Barnyard Member crops out between Carnivore Ridge Basalt Flow up to the top of the formation from about 600 to 1780 m (Figure 1, 3). The member consists of interbedded calcareous-dolomitic silty mudstone and limestone deposits (Figure 1-3, 4D). The member is named for calcareous-dolomitic silty mudstone outcrops that contain a number of fossil tracks resembling a barnyard floor. Bedding is variable from planar to cross bedded with many beds having sharp, erosional surfaces. Load casts and soft sediment deformation are common, with flame structures and flute casts prominent. Bioturbation cross cuts many of the beds. These beds often preserve

animal tracks and playa mudflat shoreline features such as ripples, raindrop impressions, and mud cracks (Figure 5). In several places fossil reeds occur as casts (Figure 5B). Limestone beds are numerous within the Barnyard Member (Figure 4D). Tufa mounds, ranging from 5 cm to several meters in diameter and height, and stromatolites occur in about 10 of the limestone beds (Figure 4E, F). Tufa mound original internal structure consists of porous and crystalline (thinolitic) fabric often associated with aquatic vegetation remains (laminated casts). Petrographically, tufa is much more porous than the other limestone beds. Pores are partially filled with mudstone, invertebrate skeletal fragments, and charophyte material that are often coated. In addition, fossil reeds and one fossil palm occur on the same bedding plane as the tufa mounds. Interbedded 1-3 cm diameter domal stromatolites are often associated (on the same bedding plane) with the tufa mound bearing limestone (Figure 4F).

Calcareous-dolomitic silty mudstone and limestone beds are mainly deposited within the upper two-thirds of the formation within the Barnyard Member with a few scattered beds occurring in the lower Coffin Canyon Member (Figure 3). The Barnyard Member deposits crop out between the Carnivore Ridge Basalt to the top of the formation from about 600 to 1780 m (Figure 1-3). The name derives from references, including unpublished maps, by Donald Curry who first reported animal tracks in the Copper Canyon basin.

The Barnyard Member represents a lithologic shift from interbedded gypsum and mudstone of the Coffin Canyon Member to interbedded calcareous-dolomitic silty mudstone and limestone deposits of the Barnyard Member (Figures 1-3). The transition between these two members is the Carnivore Ridge Basalt Flow (Figures 1-3).

Three basalt flows (Coffin Peak, Gyp Hill, and Carnivore Ridge) occur within the Copper Canyon Formation at 3, 65, and 570 m from the base of the type section (Figures 1-3). Each basalt flow possesses distinct lithologic properties distinguishing it from the other basalt flows and members. In addition, each basalt flow gave distinct $^{40}\text{Ar}/^{39}\text{Ar}$ dates. The Coffin Peak Basalt Flow is named for a prominent bluff to the north of the formation. The Gyp Hill Basalt Flow is named for gypsum deposits that outcrop in Coffin Canyon. The name has been used in unpublished maps by Donald Curry that are housed at Death Valley National Park. The Carnivore Ridge Basalt Flow is named for calcareous-dolomitic silty mudstone outcrops that contain a number of fossil carnivore tracks.

Tufa mounds and track distribution

In the Copper Canyon Formation about 100 limestone packstone beds with gastropods, bivalves, ostracods, and charophytes have been measured. In addition, about 10 of the limestone beds contain tufa mounds and stromatolites, suggesting active spring deposition. Many of the tufa mounds have a central micritic vent surrounded by

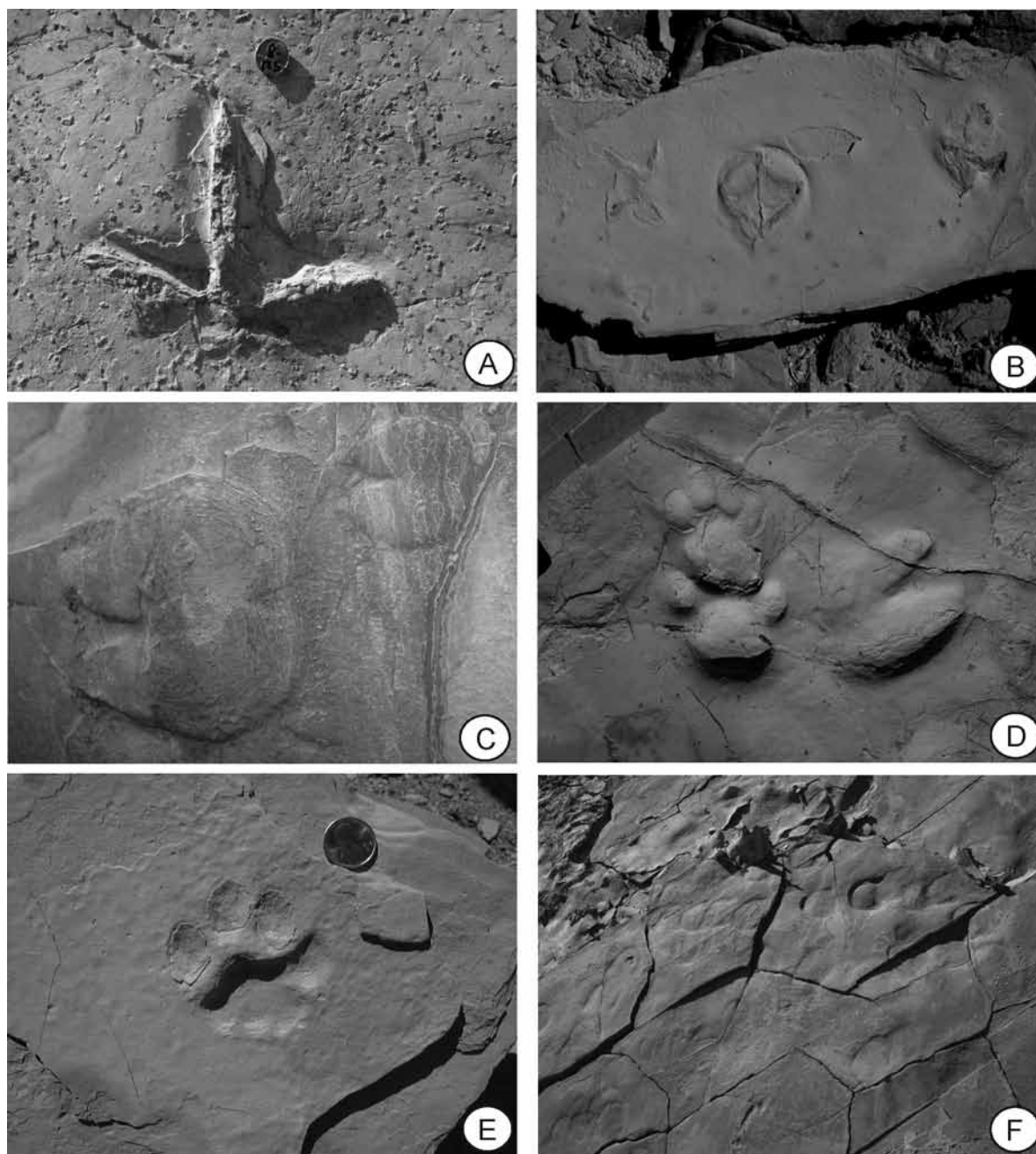


Figure 7. Typical vertebrate tracks from the Copper Canyon Formation. (A), Large bird track; note the bioturbation; penny for scale. (B), Several ichnospecies of bird tracks on bedform of talus material; no scale but similar to size as A. (C), two camel tracks representing an adult and juvenile animals; tracks are approximately 5 and 10 cm wide. (D), large single camel track and two cat tracks on bedform; tracks are approximately 20cm wide. (E), Cat track; penny for scale. (F), Trackway of horse tracks representing several individuals; tracks are approximately 10 cm wide.

porous limestone suggesting active, lake-groundwater (in the form of springs and seeps) flow. The tufa mounds formed when fresh, calcium and bicarbonate rich spring/seep waters mixed with calcium-sulfate rich, lake waters. Tufa mound internal structure consists of porous and crystalline (thinolitic) fabrics often associated with aquatic vegetation. Times when the lake was recharged by spring water allowed a more abundant and diverse fauna/flora population to thrive. Analysis of units and stratigraphic sections from lake margin to center indicate the tufa mounds formed around the margin of the ancient Copper

Canyon lake. Animal activity coincides with the appearance and distribution of the limestone spring deposits, suggesting a cause and effect.

Figure 6 shows a schematic depositional model of the ancient Copper Canyon lake both laterally and as a vertical lithofacies association. The model shows the lithofacies association, both laterally and vertically, during the time springs were active. Alluvial-fan conglomerates were deposited as sheetwash from the surrounding mountains into the lake basin. As gradient and velocity decreased, the larger clasts were deposited such that the lateral lithofacies

from basin margin to center reflects deposits from alluvial fan to mudflat depositional environments. As the lake went through highstand and lowstand cycles, the lake margin migrated and the type of sediments changed. Calcium and bicarbonate-rich waters entered the lake and precipitated calcite. The source of the calcium and bicarbonate rich surface and groundwater inflow into the ancient Copper Canyon lake most likely was derived from the Paleozoic Pogonip Group, which underlies and forms part of the bedrock and surrounding mountains of the Black Mountains (Nolan et al., 1956) (Figure 3). The Pogonip Group consists of three carbonate formations with the Antelope Valley Limestone Formation the probable source of carbonate ions and clasts deposited into the Copper Canyon lake (Nolan et al., 1956; Otton, 1977).

Animal tracks are in the form of individual tracks and trackways (Figure 7). The assortment of tracks has been interpreted to represent migratory animals (Scrivener and Bottjer, 1986). However, many of the calcareous-dolomitic silty mudstone beds contain a very high abundance and diversity of tracks usually in the form of individual animals. There is no evidence of animal migration; for example, trample tracks/trackways are very rare. Another possibility is animals were walking across the mudflat of the ancient Copper Canyon lake to the freshwater springs for water and food. That would explain the individual tracks and trackways and lack of trample tracks. The animals going to and from the lake springs is the best explanation for the distribution of the animal tracks as shown in Figure 6.

Conclusions

The Copper Canyon Formation depositional history can be roughly divided into three parts: 1) in the early tectonic basin, alluvial fans deposited conglomerate and sandstone (Greenwater Conglomerates) into the basin as a low relief, ephemeral, saline lake developed; 2) the first lacustrine stage consisted of a hypersaline-evaporative lake with a sulfate dominated chemistry that favored gypsum deposition (Coffin Canyon Member); and 3) a later lacustrine stage dominated by a perennial fresh to saline lake fed by springs, with mudflat deposits (Barnyard Member). Interbedded in the lower third of the formation are three basalt flows (Figure 1, 2, 4). Near the top of the formation, calcareous-dolomitic silty mudstone and limestone beds are replaced with sequences of limestone-mudstone beds (Figure 3). Animal tracks are mainly confined to the upper two-thirds of the Copper Canyon Formation (Barnyard Member) reflecting animal activity being coincidental with the appearance and distribution of the limestone spring deposits and a switch to an open hydrographic basin (See Nyborg, 2011 for further discussion). The Copper Canyon Formation is a distinct formation with diverse local deposits preserving a record of a tectonic basin-fill deposit.

Previously, mammal and bird track abundance and diversity were only broadly known from the Copper Canyon Formation (Curry, 1939, 1941; Scrivener and Bottjer, 1986). Detailed measured sections within Copper Canyon and observations in Coffin Canyon reveal that the distribution of the tracks is much more widespread. That said, animal tracks are mainly confined to the upper two-thirds of the Copper Canyon Formation (Barnyard Member) reflecting animal activity being coincidental with the appearance and distribution of the limestone spring deposits, suggesting a cause and effect.

The invertebrates, charophytes, reeds, palm fossils, and tufa mounds indicate a vegetated freshwater spring environment. Times when the lake was fed by spring water allowed a more abundant and diverse fauna/flora population to thrive. Distribution and abundance of animal activity increased in the perennial fresh to saline lake depositional environment due to the freshwater springs and associated vegetation. Track distribution and abundance are tied to freshwater springs and associated limestone beds. Animal activity was preserved in the tracks they left in the fringing mudflat of the lake. The subaerial exposure and cycles of low-and-highstand lake levels helped preserve the tracks, and thusly the evidence and history of animal activity in the Copper Canyon Formation.

References

- Alroy, J. 2000. New methods for quantifying macroevolutionary patterns and processes: *Paleobiology*, V. 26, p. 707-733.
- Cande, S.C. and Kent, D.V., 1995, Revised calibration of the geomagnetic polarity timescale for the late Cretaceous and Cenozoic: *Journal of Geophysical Research-Solid Earth*, v. 100, issue B4, p. 6093-6095.
- Curry, D.H., 1939, Tertiary and Pleistocene mammal and bird tracks in Death Valley: *Geological Society of America Bulletin*, v. 50, p. 1971-1972.
- Curry, D.H., 1941, Mammalian and avian ichnites in Death Valley: *Geological Society of America Bulletin*, v. 52, p. 1979.
- Drewes, H., 1963, Geology of the Funeral Peak Quadrangle, on the east flank of Death Valley: *U.S. Geological Survey Professional Paper* 413, 78 p.
- Holm, D.K., Fleck, R.J., and Lux, D.R., 1994, The Death Valley turtlebacks as Miocene-Pliocene folds of a major detachment surface: *The Journal of Geology*, v. 102, p. 718-727.
- Knott, J.R., Sarna-Wojcicki, A.M., Machette M.N., and Klinger, R.E., 2005, Upper Neogene stratigraphy and tectonics of Death Valley - a review: *Earth-Science Reviews*, v. 73, p. 245-270.
- Lindsay, E., Mou, Y., Downs, W., Pederson, J., Thomas, K.S., Henry, C., and Trexler, J., 2002. Recognition of the Hemphillian/Blancan boundary in Nevada. *Journal of Vertebrate Paleontology* 22, p. 429-442.
- Nolan, T.B., Merriam, C.W., Williams, J.S., 1956, The stratigraphic section in the vicinity of Eureka, Nevada: *U. S. Geological Survey Professional Paper* 276, 77p.
- Nyborg, T., 2011. Age, Stratigraphy and Depositional Environment of the Pliocene Copper Canyon Formation, Death Valley, California: PhD Dissertation, Loma Linda University, Loma Linda, California, 300p.

- Otton, J.K., 1977. Geology of the central Black Mountains, Death Valley, California - the turtlebacks terrain: [Ph.D. thesis]: College Park, Pennsylvania State University, 406 p.
- Scriver, P.J. and Bottjer, D.J., 1986, Neogene avian and mammalian tracks from Death Valley National Monument, California: their context, classification and preservation: *Palaeogeography, Palaeoclimatology, Palaeoecology*, v. 56, p. 285-331.
- Stewart, J.H., 1970, Upper Precambrian and Lower Cambrian strata in the southern Great Basin, California and Nevada: U.S. Geological Survey, Professional Paper 620, 206p.
- Woodburne, M. O., 2004. Late Cretaceous and Cenozoic Mammals of North America: Biostratigraphy and Geochronology. Columbia University Press, New York, 288 p.
- Wright, L.A., Williams, E.G., and Cloud, P., 1978, Algal and cryptalgal structures and platform environments of late pre-Phanerozoic Noonday Dolomite, eastern California: *Geological Society of America Bulletin*, v. 89, p. 321-333.

Review of proboscideans from the Middle Miocene Barstow Formation of California

Don L. Lofgren,¹ Abby Hess,² Drew Silver,² and Peter Liskanich²

¹Raymond M. Alf Museum of Paleontology, Claremont, California 91711

²The Webb Schools, Claremont, California 91711

Introduction

Tracks and skeletal remains of proboscideans are rare in Miocene aged strata in North America. The earliest immigrants were the Mammutidae (represented by *Zygodon*) which arrived in the late Hemingfordian (Webb 1992; Tedford et al. 2004; Prothero et al. 2008), while the Gomphotheriidae (represented by *Gomphotherium*) migrated in the early Barstovian (Tedford et al. 1987; Tedford et al. 2004). *Zygodon* and *Gomphotherium* are both present in the unnamed upper member of the Barstow Formation (Tedford et al. 1987; Woodburne et al. 1990; Tedford et al. 2004; Pagnac 2005, 2009; Lofgren et al. 2011; Lofgren and Anand 2011), located in the Mud Hills north of Barstow California (Figure 1).

The first proboscidean remains reported from the Barstow Formation were tooth fragments (Merriam 1919). Later, large scale quarrying by Frick Laboratory crews from the 1920's to the 1950's (specimens now housed at the American Museum of Natural History) yielded about a dozen proboscidean specimens including two isolated teeth designated as co-types of "*Trilophodon bartonis*" (Frick 1933).

Barstow Formation field work by the Raymond M. Alf Museum of Paleontology (RAM) was initiated in 1936 by Raymond Alf. It wasn't until the late 1950's that Alf located proboscidean remains. Early finds by the Alf Museum included a dentary with tusk/m3 of *Zygodon*, a partial skull of *Zygodon*, and a track way consisting of four tracks (Lofgren and Anand 2010; Lofgren and Anand 2011). Concerted prospecting efforts in the Barstow Formation by RAM crews (which includes students and faculty of The Webb Schools on whose campus the RAM is located) since the early 1990's, has resulted in the recovery of additional proboscidean specimens. The size of the RAM proboscidean collection from the Barstow Formation now exceeds that of any other institution.

In spite of their rarity, few proboscidean specimens from the Barstow Formation have been described. Here we review the proboscidean collections housed at the RAM, as well as those at the American Museum of Natural History, the Natural

History Museum of Los Angeles County, and the San Bernardino County Museum.

Abbreviations

Institutional abbreviations—AMNH, American Museum of Natural History, New York, New York; F:AM, Frick American Museum, New York, New York; LACM, Los Angeles County Museum, Los Angeles, California; RAM, Raymond M. Alf Museum of Paleontology, Claremont, California; SBCM, San Bernardino County Museum, San Bernardino, California

Other abbreviations—Ba1, Barstovian Biochron 1; Ba2, Barstovian Biochron 2; BAR, field collection crate number for F:AM specimens; NALMA, North American Land Mammal Age; RAM vertebrate locality records employ a V followed by numbers (e.g., V94276).

Survey of Barstow proboscidean specimens

Molars of *Zygodon* and *Gomphotherium*, the only proboscidean genera known from the Barstow Formation, are morphologically distinct. The valleys between the lophs of molars in *Zygodon* lack accessory cusps and *Gomphotherium* molars have accessory cusps in the

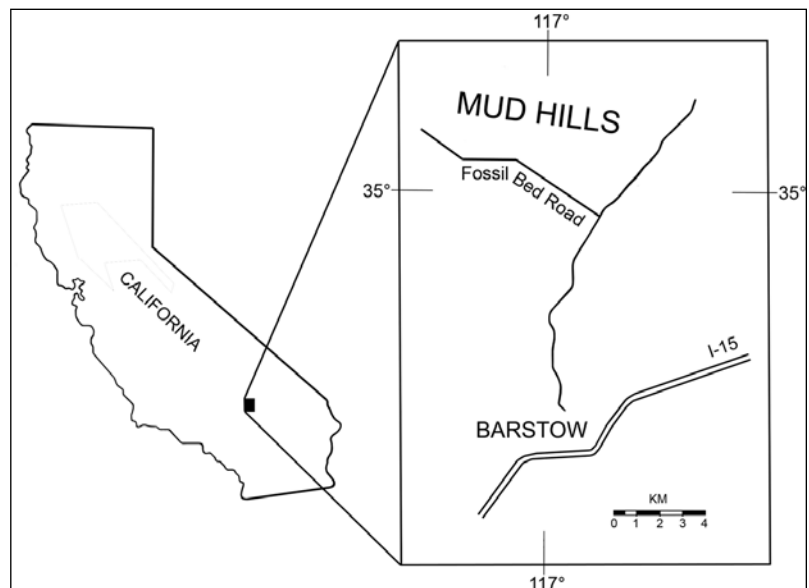


Figure 1: Location of the Mud Hills in the Mojave Desert, California (adapted from Steinen 1966).

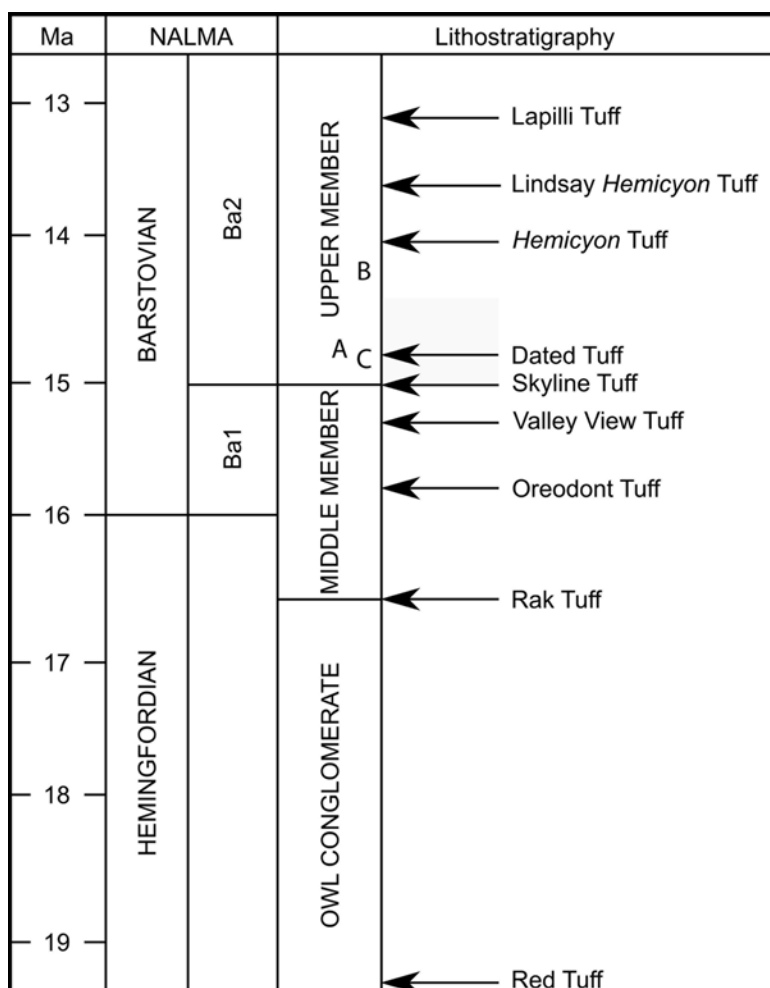


Figure 2: Geochronology and biostratigraphic subdivision of the Barstow Formation (adapted from Pagnac 2009). Letters refer to the approximate stratigraphic positions of the *Proboscipeda* sp. track way (A) (RAM 187), oldest record of *Gomphotherium* (B) (RAM 10362), and oldest record of *Zygodolophodon* (C) (F:AM 126896).

valleys between lophs. Thus, isolated molars from the Barstow Formation can easily be identified to genus.

Identification of the premolars and deciduous teeth is more difficult because comparative material for this part of the dentition of *Zygodolophodon* is very rare. To identify non-molar cheek teeth, we used absence or presence of accessory cusps in the valleys between lophs. Those with accessory cusps in valleys between lophs were referred to *Gomphotherium*, and those that lacked these accessory cusps were assigned to *Zygodolophodon*. The accessory cusp distinction for molars of *Zygodolophodon* and *Gomphotherium* also appears to apply to premolars and deciduous teeth because SBCM A489-200 (likely a dp4) has cusps in the valleys between its three lophs, and therefore represents *Gomphotherium*.

Compounding the difficulty of generic identification is the uncertainty of the tooth site of isolated premolars and deciduous teeth from the Barstow Formation. Identifications were provided by Frick (1926, 1933) for Paleogene and Neogene North American proboscideans, but good examples for Middle Miocene proboscideans are few.

Tooth site identifications that are questionable are noted for those specimens. Much work needs to be done to confirm the tooth site and generic assignment of isolated deciduous teeth and premolars of these early records of North American proboscideans.

RAM specimens were collected from 1959 to 2011 and we provide a collection date for all specimens where it was recorded. Two RAM specimens (RAM 187 and RAM 908) are from sites about 1.5 km east of Owl Canyon. All other proboscidean fossils in the RAM collections are from sites within sections 9, 14, 15, and 16 (Township 11 north, Range 2 west), an area informally known in old Alf Museum locality records as “West Barstow.” This general area is over 5 km west of Owl Canyon.

AMNH specimens from the Barstow Formation were collected over a long span of time, from at least 1927 to 1950, by crews employed by Childs Frick. These fossils were packed into crates and each was assigned a unique number preceded by BAR. We refer to these uncataloged AMNH specimens by their BAR numbers. All locality data recorded on AMNH specimen labels is repeated here. The majority of AMNH proboscidean fossils were collected from areas described as “near Chert Ridge Quarry” or “north end of formation,” which would be the same general area as “West Barstow.”

As presently known, all proboscidean specimens from the Barstow Formation are from the unnamed upper member whose base is equal to the stratigraphic position of the Skyline Tuff (Figure 2). The one exception is impressions from a site in the Calico Mountains to the east of the Mud Hills identified as proboscidean tracks from strata interpreted to be equivalent to the Middle Member (Reynolds and Woodburne 2001).

Digital calipers were used to measure all specimens except RAM 187 which required a standard measuring tape.

***Proboscipeda* sp.**

Specimen and locality: RAM 187 is a track way consisting of four well-preserved tracks that average 42.6 cm in diameter and record a stride length of 267.0 cm, from RAM locality V94176. This site is located about 40 meters above the Skyline Tuff, which would place it at the approximate stratigraphic position of the Dated Tuff (Figure 2) of Woodburne et al. (1990); the Dated Tuff is not present in the local stratigraphic section that yielded RAM 187.

Description—discussion: In the late 1960’s, a set of four well preserved tracks were discovered on steeply



Figure 3: RAM 187, proboscidean track way under excavation in 1969.

inclined strata of the unnamed upper member (Figure 3). Because proboscidean tracks are very rare, the track way (RAM 187) was collected in 1969 to preserve it from vandals and erosion. By 1971, this track way was on exhibit and it is still displayed at the RAM more than 40 years later (Figure 4).

RAM 187 was described by Reynolds (1999) who did not assign the tracks to a known ichnogenus. We refer them to *Proboscipeda* sp. based on comparison to tracks of similar size and shape from Copper Canyon in Death

Valley National Park described by Scrivner and Bottjer (1986). RAM 187 has four sets of oval prints with their large size indicating they were made by an adult proboscidean (Figure 4). With proboscidean tracks, an overstepping pattern can be assumed, as a modern elephant always places its left or right hind foot in the track of its respective front foot as it walks. Thus, each preserved track of RAM 187 is representative of the pes, as manus impressions have been overprinted.

Miocene proboscidean track ways are rare. Some other described examples include specimens from Romania (Panin and Avram 1962), the United Arab Emirates (Higgs et al. 2005), and other sites in California (Scrivner and Bottjer 1986; Reynolds 1999; Reynolds and Woodburne 2001). RAM 187 remains the best preserved track way of a proboscidean from Miocene strata in North America.

Zygalophodon cf. *Z. proavus*

Specimen and locality: RAM 908, a crushed partial skull of *Zygalophodon* cf. *Z. proavus* preserving the ventral portion of the palette, zygomatic arches, and basicranium, with complete RM3 and LM3 and partial RM2 and LM2 (Figure 5), from RAM locality V201006.

Description: RAM 908 is a partial skull preserving most of the ventral surface of the cranium posterior to the

M2's. The thin zygomatic arches, broad glenoid fossi, robust occipital condyles, and well preserved M3's are the most distinct features of RAM 908. The maximum cranial width of RAM 908 at the zygomatic arches is 54.3 cm, length of the skull from the occipital condyles to the anterior edge of the M2's is 56.0 cm, and the length and maximum width of the M3's are about 127.5 mm and 75.0 mm respectively. Additional measurements and a complete description of RAM 908 are provided by Lofgren and Anand (2011).

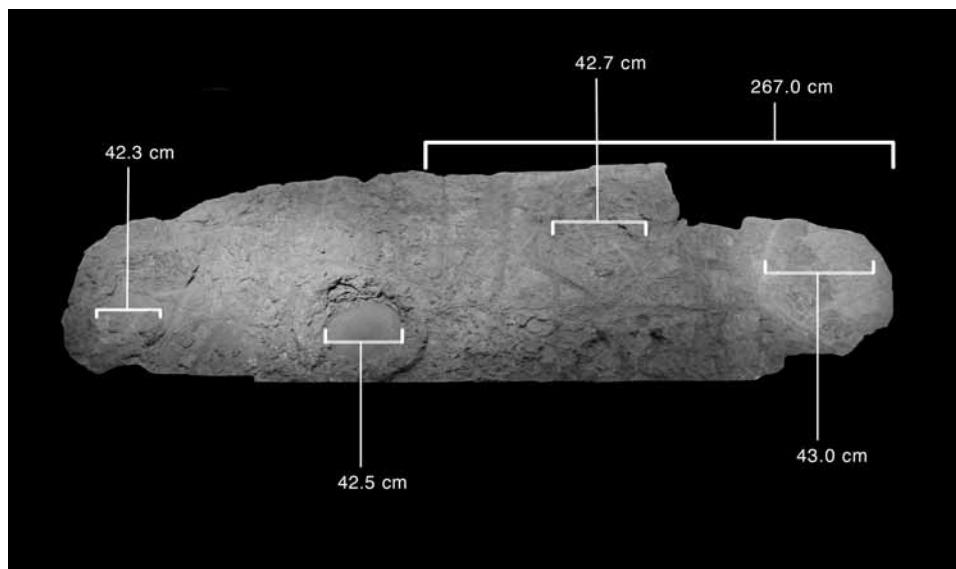


Figure 4: RAM 187, as currently displayed at the RAM (track measured at 42.5 cm is the same one as shown in top center of Figure 3).

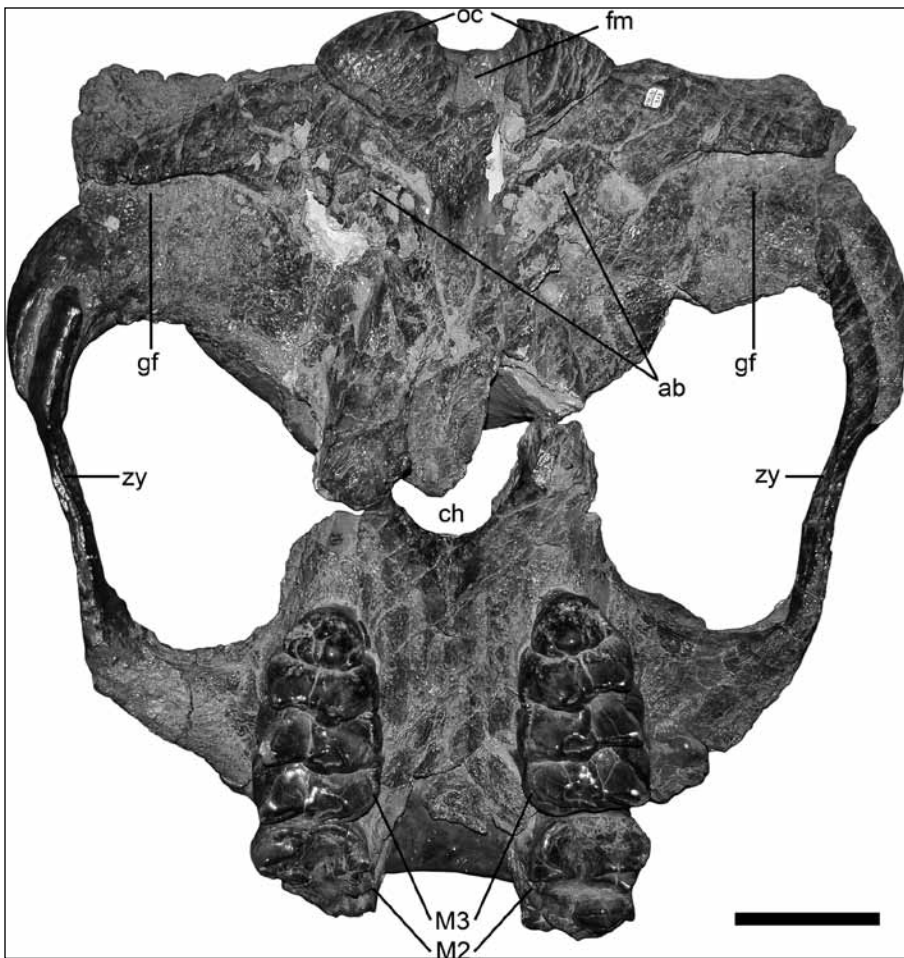


Figure 5: RAM 908, a slightly crushed of partial skull of *Zygodontodon* cf. *Z. proavus*. oc: occipital condyle; fm: foramen magnum; gf: glenoid fossa; ab: auditory bulla; zy: zygomatic arch; ch: choanae. Scale bar equals 10 cm

Discussion: In 1965, Webb faculty member Ken Monroe found RAM 908 from a site described in the RAM locality data base as “about one mile east of Owl Canyon.” Thus, although it’s precise stratigraphic level is unknown, RAM 908 is thought to be from a thick section of the upper member exposed about one mile east of Owl Canyon. RAM 908 is of particular interest due to its rarity and size as it represents the only known skull of *Zygodontodon* from North America (Lofgren and Anand 2011). The M3’s of RAM 908 are smaller than those of *Z. proavus*, which indicates that the skull probably represents a smaller individual of *Z. proavus* whose size may be a



Figure 6: RAM 907, dentary with tusk and m3 of *Zygodontodon* cf. *Z. proavus*. Scale in cm.

reflection of sexual dimorphism in the species (Lofgren and Anand 2011).

Specimen and locality: RAM 907, a damaged right dentary with tusk and m3 of *Zygodontodon* cf. *Z. proavus* (Figure 6), from RAM locality V201205.

Description: RAM 907 has a worn m3 with four lophs and a tusk with a flat lingual face. The length of the m3 is 144.43 mm, and the widths of the lophs are 62.94 mm (first), 59.36 mm (second), 57.50 mm (third), and 52.14 mm (fourth). The maximum diameter of the tusk is 40 mm. The lack of cuspsules between lophs indicates that RAM 907 is a zygodont mammutid. The size of the m3 of RAM 907 is larger but still relatively similar to M3’s of RAM 908, the partial skull of *Zygodontodon* cf. *Z. proavus* also from the Barstow Formation. Thus, RAM 907 is referred to that taxon as well.

Discussion: In 1959, while prospecting outcrops in the Fullers Earth Canyon area, Webb student Al Korber found RAM 907, which remains the only proboscidean jaw ever recovered from the Barstow Formation (Lofgren and Anand 2010). The locality of RAM 907 was not carefully recorded so V201205 represents outcrops in the general area of Fullers Earth Canyon.

Zygodontodon?

Specimen and locality: RAM 6505, a slightly damaged right dp4? (Figure 7), probably of *Zygodontodon*, collected in February 1992 from RAM locality V94042.

Description: RAM 6505 has two lophs both of which exhibit heavy to moderate wear. The first loph is narrower than the second loph and the enamel is broken and absent on the postero-lingual and posterior margin of the second loph. RAM 6505 probably represents *Zygodontodon* as there is no evidence of accessory cuspsules in the valley between lophs. The length of RAM 6505 is 45.2 mm and the width is 31.1 mm.

Specimen and locality: RAM 6504, a left dp4? (Figure 8) probably of *Zygodontodon*, collected in April 1994 from RAM locality V94184.



Figure 7: Occlusal view of RAM 6505, right dp4? of *Zygalophodon*? Scale in cm.



Figure 8: Occlusal view of RAM 6504, left dp4? of *Zygalophodon*? Scale in cm.



Figure 9: Occlusal view of RAM 7626, left dp4? of *Zygalophodon*? Scale in cm.

Description: RAM 6504 has two lophs which are moderately worn, with the anterior loph narrower than the posterior loph. A well-developed valley is present between lophs and accessory cuspsules are absent. RAM 6504 is referred to *Zygalophodon* based on this morphology. This specimen resembles F:AM 20850B (see below) in shape and morphology. The length of RAM 6504 is 32.5 mm and the width is 29.7 mm.

Specimen and locality: RAM 7626, a damaged left dp4? (Figure 9) probably of *Zygalophodon*, collected in May 2006 from RAM locality V200047.

Description: RAM 7626 has two lophs. The first loph is slightly worn and has two distinct cuspsules. The second loph is heavily worn and is missing a significant portion of its posterior and postero-labial margins. The second loph is wider than the first loph. RAM 7626 is referred to *Zygalophodon* because it lacks accessory cuspsules between lophs. The length of RAM 7626 is 48.6 mm and the width is 37.8 mm.

Specimen and locality: F:AM 20850B, maxilla fragment with dp3 identified and described by Frick (1933; figure 33) as one of two holotypes of “*Trilophodon bartonis*” (F:AM 20850A is the other). F:AM 20850B is probably a dp4 and was collected in 1927 from an unrecorded locality (was in Box 80 of the Frick collections from Barstow).

Description—discussion: F:AM 20850B is very slightly worn and has a length of 44.9 mm and a width of 33.6 mm. Two lophs are present, the anterior of which is the narrower one. F:AM 20850B has a well-developed cingulum on its entire margin except for its labial side, with accessory cuspsules developed on its anterior and posterior cingulum. Valleys between lophs lack accessory cuspsules indicating that F:AM 20850B probably represents *Zygalophodon*. Specimens referred to “*Trilophodon bartonis*” by Frick (1933) should now be referred to *Zygalophodon*, the only zygodont proboscidean recognized from the Barstow Formation (Lofgren and Anand 2011) and from Middle Miocene strata in North America (Lambert and Shoshani 1998). The holotypes of “*Trilophodon bartonis*” are inadequate to define a taxon distinct from *Zygalophodon*.

Gomphotherium

Specimen and locality: RAM 10362, a damaged right M2 of *Gomphotherium* (Figure 10), collected in November 2007 from RAM locality V98004, a site about 30 meters below the tuff that underlies the *Hemicyon* Quarry (Lofgren et al. 2011).

Description: RAM 10362 has three slightly worn lophs, all of which are missing parts of their enamel. The first loph is more worn than the others and is also missing its anterior margin due to breakage. RAM 10362 has accessory cuspsules that invade the valleys between lophs, so it is



Figure 10: Occlusal view of RAM 10362, right M2 of *Gomphotherium*. Scale in cm.

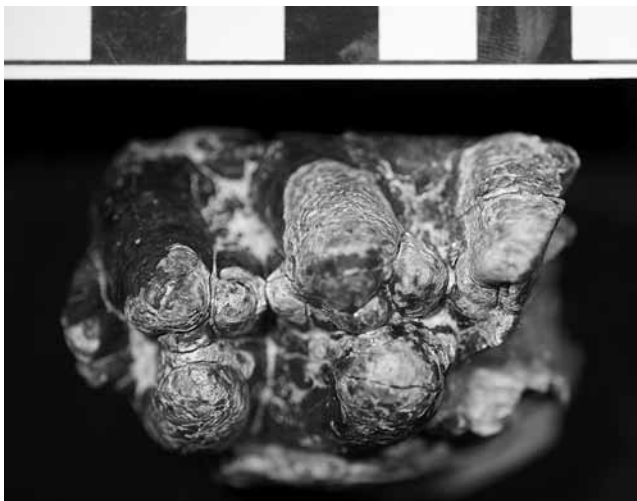


Figure 11: Occlusal view of SBCM A489-200, a dp4? of *Gomphotherium*. Scale in cm.

clearly aligned with *Gomphotherium*. RAM 10362 is 95.9 mm in length and 65.7 mm in width.

Discussion: Previously, the oldest known occurrence of *Gomphotherium* in the Barstow Formation was a tooth (F:AM 20850A) from the *Hemicyon* Quarry, collected by Frick Laboratory crews in 1933. RAM 10362 was collected from strata about 30 meters below the *Hemicyon* Quarry and now represents the oldest well-documented occurrence of *Gomphotherium* from the Barstow Formation (Figure 2).

Specimen and locality: SBCM A489-200, a damaged dp4? (Figure 11) of *Gomphotherium*, from the SW $\frac{1}{4}$, NW $\frac{1}{4}$, NE $\frac{1}{4}$ of Section 15, Township 11 north, Range 2 west (pers. comm.. R. Reynolds 2012), donated to the SBCM in 1967 by a private collector.

Description—discussion: SBCM A489-200 has at least three lophs and an incipient fourth loph consisting of two small low cusps (Figure 11) on the tooth's posterior. The front part of the tooth and half of the first loph are missing due to breakage. The second and third lophs each have two main cusps. Accessory cusps invade the valleys between lophs indicating that SBCM A489-200

is *Gomphotherium*. This is the second well-documented occurrence of *Gomphotherium* in the Barstow Formation (RAM 10362 is the other). SBCM A489-200 has a width of 34.0 mm and the minimum length of this incomplete tooth is 55.1 mm. This specimen was donated to the SBCM in 1967 and was labeled as found in Pierre Canyon. There is no Pierre Canyon in the Mud Hills, but Pirie's Canyon is the informal name of a drainage (Lindsay 1972; figure 1) now labeled Fossil Canyon on the Mud Hills quadrangle topographic map. However, R. Reynolds describes the specimen locality as the canyon north of Fuller's Earth Canyon that contains Rodent Hill. Thus, SBCM A489-200 probably is from section 15 where there is also extensive outcrop of the upper member.

***Proboscidea* sp.**

Specimen and locality: RAM 6905, a damaged left P4 (Figure 12), collected in March 2000 from RAM locality V200009.

Description: RAM 6905 has two heavily worn lophs. The postero-labial corner and most of the posterior margin of RAM 6905 is missing due to breakage. In occlusal view (Figure 12), RAM 6905 is distinctly ovate in outline. The lack of a well-developed valley between the lophs of RAM 6905 precludes its identification to genus. The length of RAM 6905 is 41.1 mm and the width is 39.3 mm.

Specimen and locality: RAM 9347, a slightly damaged P3? (Figure 13), collected before 1990 from RAM locality V94281.

Description: RAM 9347 lacks easily discernible dental landmarks and this makes identification problematic. RAM 9347 appears to have two weakly developed lophs that are slightly worn. The length of RAM 9347 is 29.6

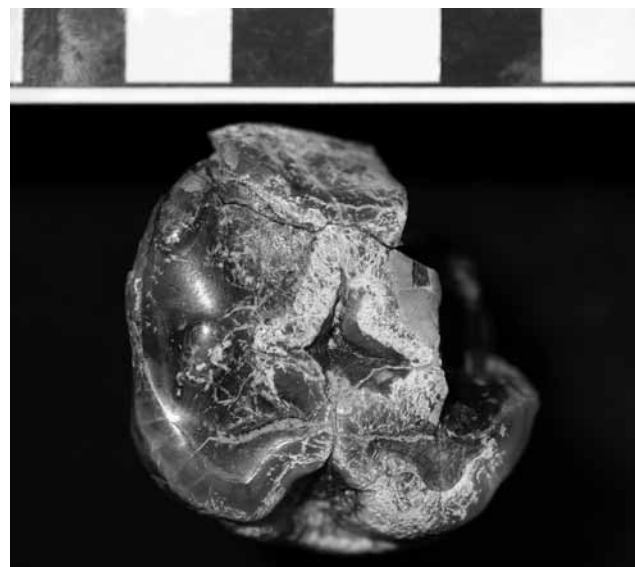


Figure 12: Occlusal view of RAM 6905, left P4. Scale in cm.



Figure 13: Occlusal view of RAM 9347, P3? Scale in cm.

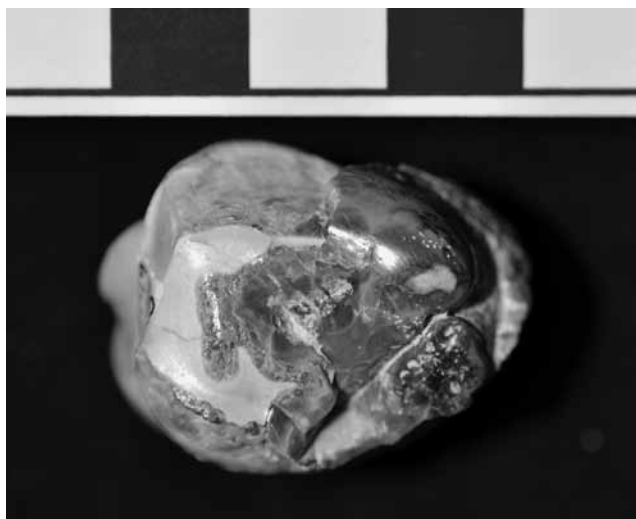


Figure 14: Occlusal view of RAM 7625, P3? Scale in cm.



Figure 15: Occlusal view of RAM 6906, left P4. Scale in cm.

mm and the width is 24.5 mm (if we orientated the tooth properly).

Specimen and locality: RAM 7625, a slightly damaged P3? (Figure 14), collected in October 2005 from RAM locality V200149.

Description: RAM 7625 exhibits heavy wear and some damage due to breakage and lack of enamel. RAM 7625 has a roughly ovate shape but less so than RAM 6905 and RAM 6906 which are P4's. This specimen is too worn to identify to genus and its tooth site is uncertain. The length of RAM 7625 is 29.8 mm and the width is 24.3 mm.

Specimen and locality: RAM 6906, a left P4 (Figure 15), collected in May 2000 from RAM locality V95052.

Description: RAM 6906 has two lophs which have merged into a single wear facet on the labial half of the tooth because of heavy wear. RAM 6906 has a distinct ovate outline in occlusal view (Figure 15) like RAM 6905 (Figure 12). Lack of a well-developed valley between lophs of RAM 6906 precludes its identification to genus. The length of RAM 6906 is 45.2 mm and the width is 32.1 mm.

Specimen and locality: F:AM 20850A, an isolated tooth identified as a left p4 and described by Frick (1933; figure 36) as the second holotype of "*Trilophodon bartonis*" (F:AM 20850B is the other). F:AM 20850A probably is a dp4 and was collected in 1933 from *Hemicyon* Quarry (in box 74 of Frick Barstow field collections).

Description—discussion: F:AM 20850A is 39.3 mm in length and 33.1 mm in width and has two lophs. The anterior loph is slightly worn while the higher posterior loph has moderate wear. The shape and morphology of F:AM 20850A is similar to RAM 6505 and 7626, but F:AM 20850A is smaller. As noted above, the name "*Trilophodon bartonis*" should be abandoned. F:AM 20850A could be *Zygodolophodon* or *Gomphotherium*.

Specimen and locality: LACM 27181, a left P4 (Figure 16), from LACM locality 7133 (Rainbow Basin), collected May 1971.

Description: LACM 27181 is 40.3 mm in length and 35.6 mm in width. The tooth is very heavily worn which has erased most of its occlusal morphology. LACM 27181 is very similar to RAM 6905 and RAM 6906, but is slightly smaller.

Specimen and locality: Uncataloged AMNH left p3?, from crate BAR 99-32, collected in 1928 from north end of formation, layer #3.

Description: This uncataloged tooth is slightly worn and has four cusps arranged in a box pattern. Its length is 29.5 mm and its width is 23.4 mm.

Specimen and locality: Uncataloged AMNH tusk fragment, from crate BAR 439H, collected in 1950 about 300



Figure 16: Occlusal view of LACM 27181, a left P4. Scale in cm.

feet above Chert Ridge Quarry. Specimen is too fragmentary for additional identification.

Specimen and locality: Uncataloged AMNH upper tusk fragments (two), from crate BAR 326-1773, collected in 1935 from miscellaneous localities above Leader Quarry horizon. Specimens are too fragmentary for additional identification.

Specimen and locality: Uncataloged AMNH molar root, from crate BAR 99-32, collected in 1928 from north end of formation, layer #3. Specimen is too fragmentary for additional identification.

Specimens and localities: Proboscidean tooth fragments collected by RAM crews between 1993 and 2011, cataloged as RAM 8413, RAM 7169, RAM 8550, RAM 14272, RAM 11637, RAM 11624, RAM 14271, RAM 14274, RAM 7642, RAM 14601, and RAM 7644, from RAM localities V94028, V94039, V95092, V200154, V200155, V200025, V200206, and V200511. Although not identifiable to taxon, tooth fragments are useful for documenting the stratigraphic occurrence of proboscideans within the formation.

Specimen and Locality: RAM 6862, an unciform, collected in April 1995 from RAM locality V95092.

Specimen and locality: RAM 14273, an unciform, collected before 1990 from RAM locality V94033.

Specimen and locality: RAM 9352, an unciform, collected in November 2004 from RAM locality V200405.

Specimen and locality: RAM 6861, a distal humerus fragment, collected in October 1992 from RAM locality V94049.

Specimen and locality: Uncataloged AMNH sesmoid, from box 162, collected in 1930 from north end of formation, lower strata.

Specimen and locality: Uncataloged AMNH metapodial, from crate BAR 439-J, collected in 1950 from north end of Chert Ridge Quarry horizon, about 150 yards east of quarry, first division.

Specimen and locality: Uncataloged AMNH rib capitulum, from crate BAR 439-L, collected in 1950 from Chert Ridge Quarry, north end.

Specimen and locality: Uncataloged AMNH limb fragments (two), from crate BAR 439-K, collected in 1950 from north end of Chert Ridge Quarry, about 150 yards east of quarry.

Specimen and locality: Uncataloged AMNH patella, from crate BAR 439-I, collected in 1930 from north end of Chert Ridge Quarry, about 150 yards east of Chert Ridge horizon, first division.

Specimen and locality: F:AM 20850C, a femur from an unrecorded locality. Specimen was referred to "*Trilophodon bartonis*" by Frick (1933), but could not be found in the AMNH collections.

Specimen and locality: F:AM 20850C, three carpals and one phalanx (Frick 1933), from an unrecorded locality. Specimens were referred to "*Trilophodon bartonis*" by Frick (1933), but could not be found in the AMNH collections.

Discussion—summary

Cataloged and uncataloged proboscidean fossils from the Barstow Formation housed at the RAM, AMNH, LACM, and SBCM total nearly 50 specimens. The RAM collection is largest (26 specimens) and includes a track way, a dentary with tusk and m3, a partial skull, eight isolated teeth, eleven tooth fragments, three carpals, and a humerus fragment. The AMNH has 16 proboscidean specimens, of which three are isolated teeth, three are tooth fragments, and the others are postcranial elements. The LACM and SBCM each house one isolated tooth.

The most complete specimens are a partial skull referred to *Zygodontodon* cf. *Z. proavus* (Lofgren and Anand 2011) and a dentary we refer to the same taxon. *Zygodontodon* is the only zygodont mammutid genus known from the Barstow Formation and other Middle Miocene strata in North America (Lambert and Shoshani 1998). It is likely *Zygodontodon* cf. *Z. proavus* is also represented by four isolated teeth, but we take a cautious approach and refer them to *Zygodontodon*?

The only other known proboscidean from the Barstow Formation is *Gomphotherium*, whose molars have accessory cusps in the valleys between lophs, unlike *Zygodolophodon*. We only identified two specimens as *Gomphotherium*, suggesting that *Gomphotherium* is less common in the Barstow Formation than *Zygodolophodon*. An m2 (RAM 10362) referred to *Gomphotherium* is from RAM locality V98004, a site 30 meters below the tuff that underlies the *Hemicyon* Quarry. An isolated proboscidean tooth (F:AM 20850A) collected from the *Hemicyon* Quarry in 1933, was described as a holotype of "*Trilophodon bartonis*" (Frick 1933). Later, F:AM 20850A was informally identified as *Gomphotherium* (Woodburne et al. 1990; Pagnac 2005, 2009) which, at that time, indicated that F:AM 20850A represented the oldest record of *Gomphotherium* from the Barstow Formation. We question whether this specimen can be identified to genus. In any case, RAM 10362 is now the oldest occurrence of *Gomphotherium* in the Barstow Formation.

RAM V98004 is an important site because it yields whole elements of large and small mammals as well as birds. The holotype of *Megahippus mckennai* (RAM 910), a partial skull, was collected at V98004 in 1957 and described in 1962 (Tedford and Alf 1962). Recent collections from V98004 include a carapace-plastron with postcranial material of *Xerobates mohavense*, and numerous specimens of *Aepycamelus*, *Protolabis*, and *Scaphohippus*. The elements of small birds and mammals at V98004 are concentrated within a 5cm thick lens of siltstone that is about 2 meters wide. Excavation of this fossil rich siltstone lens has yet to be completed.

Locality data is poor for many proboscidean specimens collected from the Barstow Formation prior to the 1970's. With the exception of some impressions identified as proboscidean tracks in the Calico Mountains (Reynolds and Woodburne 2001), all proboscidean remains with precise locality data were recovered from the unnamed upper member of the Barstow Formation.

The oldest *Zygodolophodon* specimen (F:AM 126896; now lost) is a tooth from Rainbow Quarry Prospect, at the approximate stratigraphic level of the Dated Tuff (Figure 2) or New Years Quarry, low in the upper member (Pagnac 2005, 2009). RAM 10362, the oldest known specimen of *Gomphotherium*, is from strata higher in the upper member. Thus, the proboscidean track way (RAM 187) from strata low in the upper member was probably made by *Zygodolophodon*.

The unnamed upper member of the Barstow Formation is late Barstovian (Ba2 biochron) in age (Woodburne et al. 1990; Tedford et al. 2004; Pagnac 2009). Thus, all proboscidean body fossils from the Barstow Formation are late Barstovian (Ba2). Early Barstovian (Ba1) records of *Zygodolophodon* and *Gomphotherium* are reported from central California, Oregon, and Mexico (Tedford et al. 1987; 2004). These areas are in relatively close proximity to the Barstow depositional basin. Why proboscidean body fossils are not known from early Barstovian strata

of the Barstow Formation after 100 years of prospecting is unclear, but it is likely not a factor of inadequate sampling.

ACKNOWLEDGEMENTS —We thank D. Pagnac., R. Reynolds, and M. Woodburne for helpful discussions, J. Shearer of the California Bureau of Land Management for assistance with permits, J. Meng, R. O'Leary, and J. Galkin of the AMNH for access to specimens, E. Scott and K. Springer of the SBCM and S. McLeod and J. Harris of the LACM for access to and loan of specimens, and the Mary Stuart Rogers Foundation and the David B. Jones Foundation for financial support.

References cited

- Frick, C., 1926. Tooth sequence in certain Trilophodont tetrabelodont mastodons and *Trilophodon* (*Serridentinus*) *pojoaquensis*, new species. Bulletin of the American Museum of Natural History 56:123-178.
- Frick, C., 1933. New remains of trilophodont-tetrabelodont mastodons. Bulletin of the American Museum of Natural History 59:505-652.
- Higgs, W., A. Gardner and M. Beech, 2005. A Fossil Proboscidean Trackway at Mleisa, Western Region of Abu Dhabi, United Arab Emirates. Pp. 21-27, in, P. Hellyer and M. Ziolkowski (eds.), Emirates Heritage Volume 1, Proceedings of the 1st Annual Symposium on Recent Palaeontological and Archaeological Discoveries in the Emirates. Al Ain Zayed Center for Heritage and History.
- Lambert, W. D. and J. Shoshani, 1998. Proboscidea. Pp. 606-621, in C. M. Janis, K. M. Scott, and L. L. Jacobs (eds.), Evolution of Tertiary Mammals, Volume 1: Terrestrial Carnivores, Ungulates, and Ungulate-like Mammals. Cambridge University Press, Cambridge.
- Lindsay, E. H., 1972. Small mammal fossils from the Barstow Formation, California. University of California Publications in Geological Sciences 93:1-104.
- Lofgren, D. L., and R. S. Anand, 2010. 75 years of fieldwork in the Barstow Formation by the Raymond Alf Museum of Paleontology. Pp. 169-176, in Reynolds, R. E. and D. M. Miller (eds.), Overboard in the Mojave, 20 million years of lakes and wetlands. Desert Studies Consortium.
- Lofgren, D. L., and R. S. Anand, 2011. Partial skull of *Zygodolophodon* (Mammalia, Proboscidea) from the Barstow Formation of California. Journal of Vertebrate Paleontology 31:1392-1396.
- Lofgren, D. L., Pagnac D., Hess, A., Liskanich, P. and D. Silver, 2011. Proboscideans from the Middle Miocene Barstow Formation of California. Journal of Vertebrate Paleontology, Supplement to Volume 31, p. 146.
- Merriam, J. C., 1919. Tertiary mammalian faunas of the Mohave Desert. University of California Publications in Geological Sciences 11:437a-437e, 438-585.
- Pagnac, D. C., 2005. A systematic review of the mammalian megafauna of the middle Miocene Barstow Formation, Mojave Desert, California (PhD dissertation). University of California-Riverside. 384 pp.
- Pagnac, D. C., 2009. Revised large mammal biostratigraphy and biochronology of the Barstow Formation (Middle Miocene), California. Paleobios 29:48-59.

- Panin, N. and E. Avram, 1962. Noi urme de vertebrate in Miocenul Subcarpatilor Rominesti. *Studii Cercetari de Geologie* 7:455-484.
- Prothero, D. R., Davis, E. D., and S. B. Hopkins, 2008. Magnetic stratigraphy of the Massacre Lake beds (late Hemingfordian, early Miocene), northwest Nevada, and the age of the "Proboscidean Datum" in North America. Pp. 239-245, in S. D. Lucas and J. Speilman (eds.), *Neogene Mammals*. New Mexico Museum of Natural History and Science Bulletin 44.
- Reynolds, R. E., 1999. Gomphothere tracks in southern California. p. 31-32, in R. E. Reynolds and J. Reynolds (eds.), *Tracks Along the Mojave*. San Bernardino County Museum Association Quarterly 46, number 3.
- Reynolds, R. E., and M. O. Woodburne, 2001. Review of the Proboscidean datum within the Barstow Formation, Mojave Desert, California, *Journal of Vertebrate Paleontology* 21:3 p.93.
- Scrivner, P. J., and D. J. Bottjer, 1986. Neogene avian and mammalian tracks from Death Valley National Monument, California: Their context, classification and preservation. *Palaeogeography, Palaeoclimatology, and Palaeoecology* 57:285-331.
- Steinen, R. P., 1966. Stratigraphy of the middle and upper Miocene, Barstow Formation, California. (m.s. thesis): University of California-Riverside, 150 pp.
- Tedford, R. H., and R. M. Alf, 1962. A new Megahippus from the Barstow Formation San Bernardino County, California. *Bulletin of the Southern California Academy of Sciences* 61:113-122.
- Tedford R. H., Galusha, T., Skinner, M. F., Taylor, B. E., Fields, R. W., MacDonald, J. R., Rensberger, J. M., Webb S. D., and D. P. Whistler, 1987. Faunal succession and biochronology of the Arikareean through Hemphillian interval (late Oligocene through earliest Pliocene epochs) in North America. Pp.153-210, in M. O. Woodburne (ed.), *Cenozoic mammals of North America, Geochronology and Biostratigraphy*. University of California Press, Berkeley.
- Tedford, R. H., Albright III, L. B., Barnosky, A. D., Ferrusquia-Villafranca, I., Hunt Jr., R. M., Storer, J. S., Swisher II, C. C., Voorhies, M. R., Webb S. D., and D. P. Whistler, 2004. Mammalian biochronology of the Arikareean through Hemphillian interval (late Oligocene through early Pliocene epochs). Pp. 169-231, in M. O Woodburne (ed.), *Late Cretaceous and Cenozoic mammals of North America*. Columbia University Press, New York.
- Webb, S. D., 1992. A brief history of New World Proboscidea with emphasis on their adaptations and interactions with man. Pp. 16-34 in J. W. Fox, C. B. Smith and K. T. Wilkins (eds.), *Proboscidean and Paleoindian Interactions*. Baylor University, Waco, Texas.
- Woodburne, M. O., Tedford, R. H. and C. C. Swisher III, 1990. Lithostratigraphy, biostratigraphy, and geochronology of the Barstow Formation, Mojave Desert, southern California. *Geological Society of America Bulletin* 102:459-477.

A near-complete skull of *Castor canadensis* from the badlands of El Golfo de Santa Clara, Sonora, Mexico

Carrie M. Howard¹ and Christopher A. Shaw²

¹Natural History Museum of Los Angeles County

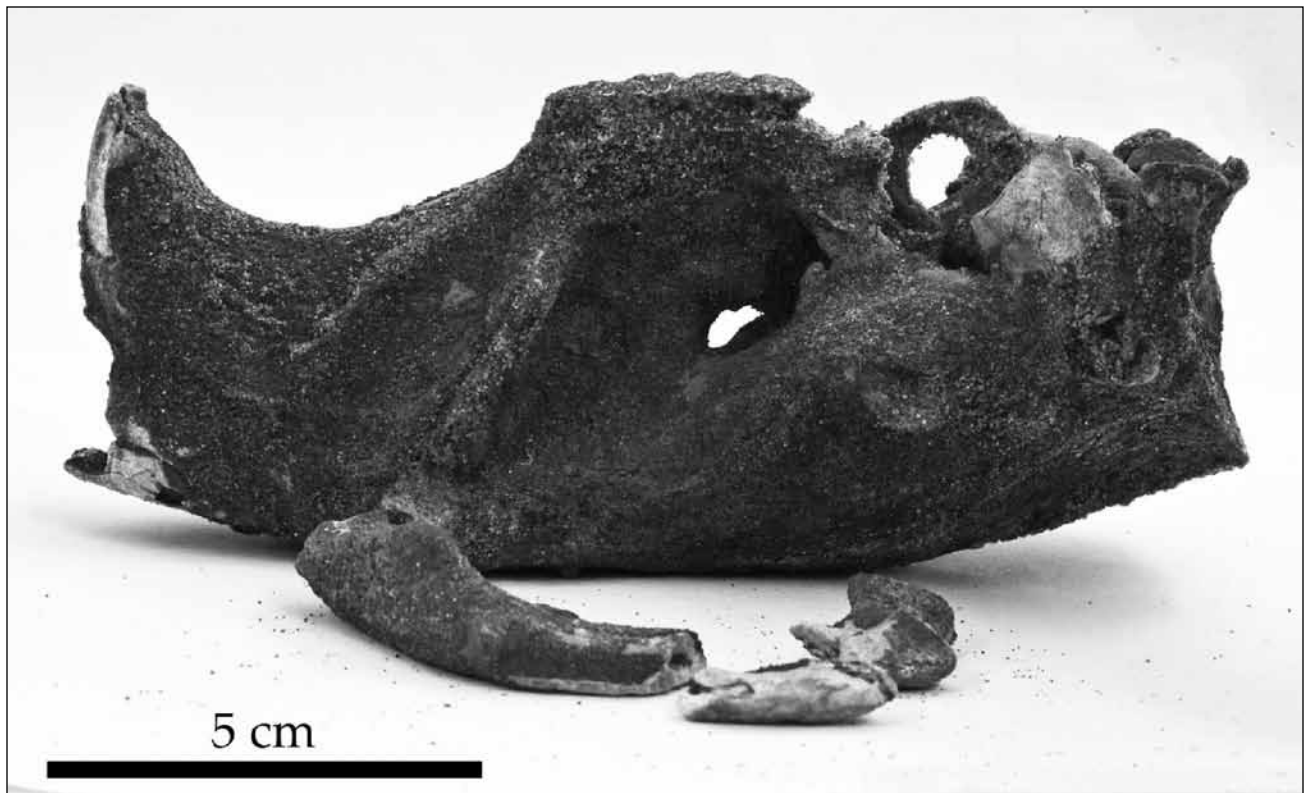
²George C. Page Museum of Rancho La Brea Discoveries

Early to middle Pleistocene Colorado River Delta deposits are exposed in the upper Gulf of California, northwestern Sonora, México and are host to a diverse paleo-fauna and -flora (El Golfo local paleobiota) of Irvingtonian Land Mammal Age. The fossiliferous exposures are found in badlands developed in fluvio-deltaic sediments that have been mildly deformed during late Pleistocene doming along the Cerro Prieto Fault. For the past two decades, the El Golfo Project has been part of a resource inventory for the Upper Gulf of California and Colorado River Delta Biosphere Reserve that has recovered over 6,000 fossils through joint efforts by Arizona Western College, the George C. Page Museum, and the Biosphere Reserve. The preserved paleobiota, now numbering over 120 species, suggests an Irvingtonian tropical to semitropical climate and the existence of four ecologic communities: freshwater aquatic, riparian galleria forest, shrub and brush woodland, and savannah-like grassland.

In 2011, a near-complete skull of *Castor canadensis*, was recovered as part of the ongoing El Golfo Project. The specimen is only missing the the left second molar. Almost the entire surface of the specimen was covered by indurated iron oxide deposits, so that preparation has been slow and difficult. To our knowledge, this is the most complete skull found at any Irvingtonian site in North America.

References

- Croxen III, F. A., C. A. Shaw, and D. R. Sussman. 2007. Pleistocene Geology and Paleontology of the Colorado River Delta at Golfo de Santa Clara, Sonora, Mexico. The 2007 Desert Symposium field guide and abstracts from proceedings, California State University, Desert Studies Consortium and LSA Associates, Inc. April 2007, Robert E. Reynolds, Editor, pp 84-89
- Shaw, C. A. 1981. The Middle Pleistocene El Golfo local fauna from northwestern Sonora, Mexico. Master Thesis, California State University, Long Beach.



Ichnites in the Bouse Formation, Amboy, San Bernardino County, California

Robert E. Reynolds

Redlands, CA, 92373, rreynolds220@verizon.net

ABSTRACT—New vertebrate and invertebrate ichnofossils are reported from the Bristol arm of the Bouse Formation in outcrops north of Amboy, California. Tracks of small wading birds are similar in morphologies to tracks of modern shore birds such as sandpipers, plovers, and sand-erlings. These imprints are referred to ichnogenera *Avipeda*, *Avidactyla*, and *Alaripeda*. A new ichnospecies, *Alaripeda bristolia*, is described. Associated burrows of invertebrates are either parallel with, or diagonal and perpendicular to, bedding planes. Tracks are preserved in water-laid, fine-grained, micaceous sediments stratigraphically higher than the early Pliocene Lawlor Tuff (4.83 Ma) in this section.

Geology and stratigraphy

A far western occurrence of the Bouse Formation crops out north of Amboy in the Bristol arm of the Bouse embayment (Spencer, 2011; Miller and others, this vol). The outcrops are considered to represent the Bouse Formation based on marine and brackish-water ostracodes, phytohermal carbonate mounds, and a spine of the marine fish *Colpichthys* (G. R. Smith, p. c. to RER, 2010; Miller and others, 2012). The Bouse outcrops lie at elevation 290 m, an elevation closely concordant with that of other Bouse outcrops (Spencer, 2008), but approximately 540 m higher than reported Bouse sediments and marine fossils buried in Cadiz Lake ~30 miles southeast (Smith, 1970; Brown, and Rosen, 1992). The Bouse sedimentary section north of Amboy rests unconformably on locally-derived fanglomerate, and consists of basal arkosic sand and white, glass-rich Lawlor Tuff (4.83 Ma) followed by a sequence of thin, platy, sandy limestone?, then by calcareous arkosic sand and gravel, finally giving way to fine-grained, gypsiferous, micaceous, silty sand (Miller et al, this vol). The sedimentary sequence suggests a transgressive marine incursion with a stable depth while large stromatolites formed in shallow, clear water, followed by regression and evaporation of the water body to produce fissile carbonate layers, followed by gypsiferous mud-flats as the body of water evaporated or receded.

Shore bird tracks: abbreviated systematics

Class Aves

Subclass Neornithes

MORPHOFAMILY *Avipedidae* Sarjeant and Langston, 1994. ICHNOGENUS *Alaripeda* Sarjeant and Reynolds, 2001 1986 *Avipeda* sp. D. Scrivner and Bottjer, p. 295, fig. 3D. DIAGNOSIS: Avian footprints showing three or, often, four digits. Central digit (III) is directed forward, but may curve sharply; digit I is short, less than half the length of digit III, often oriented reverse of the axis of digit III, but sometimes deviating up to 20°. The other digits (II

and IV) are directed laterally and may also curve. Digits united or separate proximally. Length of digit III comparable to (or less than 25% greater than) that of digits II and IV. Webbing lacking; no indication of metatarsal pad. TYPE SPECIES: *Alaripeda lofgreni* Sarjeant and Reynolds, 2001, Miocene, California.

Alaripeda bristolia Reynolds, sp. nov.

Figure 1a, RAM14740, Figure 1b. RAM14740

DIAGNOSIS: Avian footprints showing four digits. Central digit (III, 17-18mm) is directed forward; digit I is short (6 mm), one-third the length of digit III, oriented reverse, but deviating 20° from the axis of digit III toward digit II, and opposite of digit IV. The other digits (II, 13-17 mm; and IV, 11-15 mm) are straight, directed laterally. Claws acute, attached to digit. Digits separate proximally. Length of digit III 20% greater than that of digits II and IV. Webbing lacking; no indication of metatarsal pad.

HOLOTYPE: Specimen RAM14740, housed in the Raymond Alf Museum, Claremont, California.

DERIVATION OF NAME: Specimens from Bristol Basin outcrops referred to the early Pliocene Bouse Formation (Miller and others, this vol.) near Amboy in the Bristol-Danby Trough of the southeastern Mojave Desert, California.

LOCALITIES: Early Pliocene Bouse Formation, Amboy, Mojave Desert, California (RAM# V201208).

FIGURED SPECIMENS: (2a) specimen RAM14740/ V201208; (2b) collections of the Raymond M. Alf Museum of Paleontology, Claremont, California.

DISCUSSION: lateral digits (II and IV) of *Alaripeda bristolia* are longer than those in *Alaripeda lofgreni*, *Avidactyla vialovi* and *Avipeda gryponyx*. Digits, including digit I, join in *Alaripeda lofgreni*, but not in *A. bristolia*. Digit I does not leave an impression in *A. vialovi* and *A. gryponyx*. Compared to *A. vialovi* and *A. gryponyx*, Digits II and IV of *A. bristolia* are 78% as long as digit

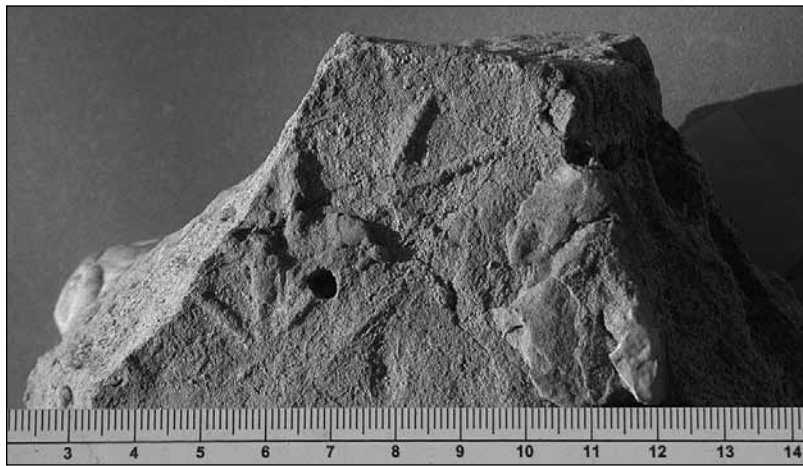


Figure 1a and 1b. Photo and drawing of new species, *Alerapeda bristolii*. RAM14740/V201208. Scale bar 0.6 cm.

digit III; but digit IV is always separate and neither webbing nor a metatarsal pad are present. In specimens from Amboy, the lateral digits are of comparable length (15 mm), with digit III the longest (20 mm). Trackway of moderate width; stride of moderate length.

HOLOTYPE: Specimen V.15276 (Vt 142),

Hungarian National Geological Institute, Budapest.

III. The footprints of *A. bristolii* are similar to those figured for the least sandpiper (Elbroch and Marks, 2001, p. 104, 105). The least sandpiper rarely wades, preferring mudflats near grassy, weedy vegetation.

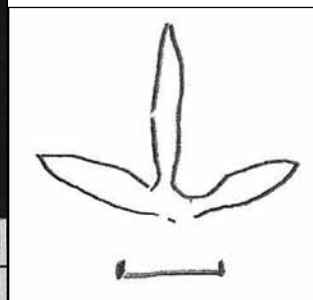
Aviadactyla vialovi (Kordos in Kordos and Prakfalvi, 1990); emended Sarjeant and Reynolds, 2001 Figure 2a, RAM14741. Figure 2b, RAM14741,

LOCALITIES: Miocene (Helvetian), Romania. Miocene (Clarendonian), Avawatz Mountains, San Bernardino County, California; Early Pliocene Bouse Formation, Amboy, Mojave Desert, California (RAM# V201208). The tracks of *A. vialovi* associated with *A. lofgreni* have been recorded from the Bouse Fm. in the Chemehuevi basin, California (Reynolds, 2008)

DIAGNOSIS: *Aviadactyla vialovi* (Sarjeant and Reynolds, 2001). Avian footprints of small to moderate size, having slender and flexible digits (II to IV) with slender claws whose inclination is only slightly divergent from the digit axis. The digits lack interpad spaces. Interdigital span variable according to pace and substrate, ranging from about 80° to over 155°. The interdigital angle between digits II and III is slightly less than between digits III and IV. Claws acute, attached to digit. The digits converge proximally, with digit II sometimes in slight contact with

FIGURED SPECIMENS: (2a) Specimen V94021/272; (2b) Specimen V94021/278 (Sarjeant and Reynolds, 2001, Plates 5, 6; Figs. 6, 7). Collections of the Raymond M. Alf Museum of Paleontology, Claremont, California.

DISCUSSION. Divarication of digits II and IV in *A. vialovi* is broader than in *A. gryponyx* and *A. bristolii*. Digits II and IV of *A. vialovi* are 75% as long as digit III. The footprints of *A. vialovi* are similar to those figured for the killdeer (Elbroch and Marks, 2001, p. 110, 111).



Avipeda gryponyx Sarjeant and Reynolds, 2001 Figure 3a, RAM14742, Figure 3b. RAM14742

DIAGNOSIS. Avian footprints of small size, having three slender digits, the outer ones (II and IV) curving forward, the central digit (III) curving in toward the track axis. Digits acuminate, but claws not distinct; interpad spaces not evident. Claws acute, attached to digit. Digits united proximally, and lack webbing or an intertarsal pad. Interdigital span (at base) around 95°. Length of digits III and IV almost uniform (15 mm); Digit II 10 mm); interdigital angle between II and III less than that between III and IV.

HOLOTYPE: Sarjeant and Reynolds, 2001. (Plates 2, 3, 4; Figures 4, 5) V94021/110 (P. 4, Fig. 4). Raymond M. Alf Museum of Paleontology, Claremont, California.

Figure 2a and 2b. Photo and drawing of *Aviadactyla vialovi*. RAM14741/V201208. Scale bar 1 cm.

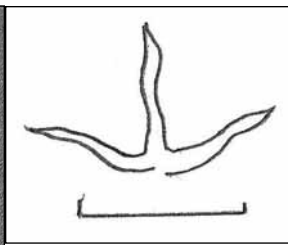
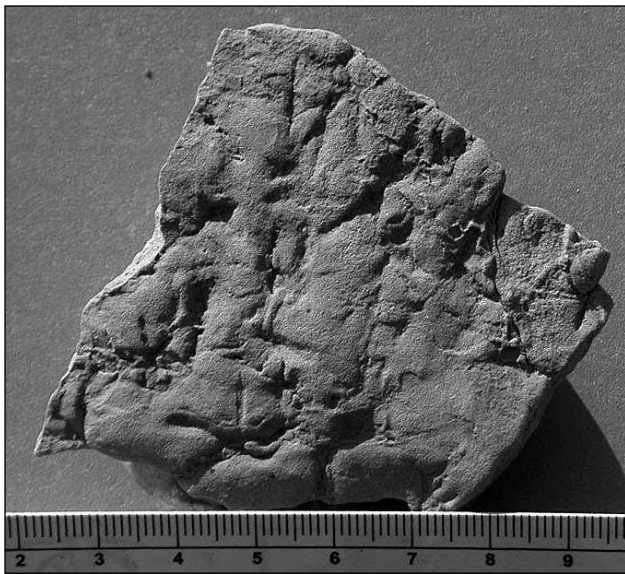


Figure 3a and 3b. Photo and drawing of *Avipeda gryponyx*. RAM14742/V201208. Scale bar 2 cm.

gryponyx from all other ichnospecies of *Avipeda*. Divarication of digits II and IV in *A. gryponyx* is as broad or broader than in *A. vialovi*, and much broader than *A. bristolii*. Digits III and IV of *A. gryponyx* are of approximately equal length, while digit II 60% of their length. *A. gryponyx* is distinguished by its slightly curving digits.

The footprints of *Avipeda gryponyx* are similar to those figured for the sanderling (Elbroch and Marks, 2001, p. 105, 106).

LOCALITIES. Avawatz Formation, Miocene (Clarendonian), Avawatz Mountains, San Bernardino County, California; Bouse Fm., early Pliocene, Amboy, San Bernardino County, California (RAM# V201208).

DISCUSSION. The curvature of the digits, their thinness and their proximal union combine to differentiate *A.*

Paleontology

A marine fish, *Colpicthys* sp., was identified from Bouse Formation outcrops at Amboy (G. R. Smith, p. c. to author, 2010). This fish spine was found in white, platy limestone from a source immediately above the Lawlor Tuff (4.83 Ma). Because this fish requires full marine water, its presence helps document the environment in which the ash fell. A relatively complete skeleton of *Colpicthys* has also been recovered from Bouse Formation marls near Cibola (Todd, 1976).

Associated invertebrate burrows have been located higher in the section, in fine-grained silty micaceous sands associated with the avian tracks. These burrows can be grouped into two types: "horizontal" or parallel to the bedding plane and from 1 to 5 mm in diameter (Figure 4); and "vertical" or inclined, cutting across the bedding plane, ranging from 5 to 15 mm in diameter (Figures 5 and 6). The horizontal burrows probably represent

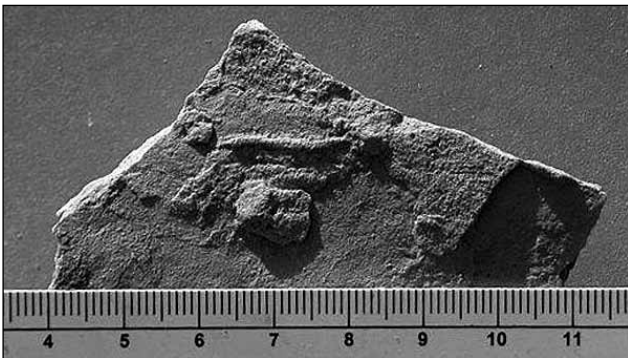


Figure 4. Bedding plane burrows, 2 mm diameter. RAM14745/V201208.

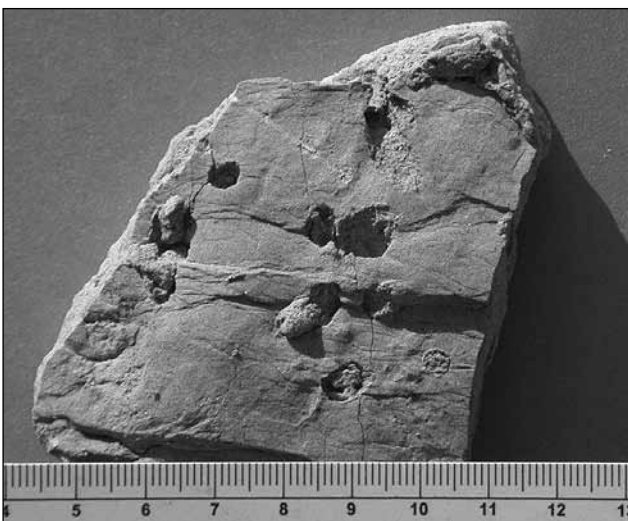


Figure 5. Vertical and inclined burrows, 5 mm diameter. RAM14746/V201208.

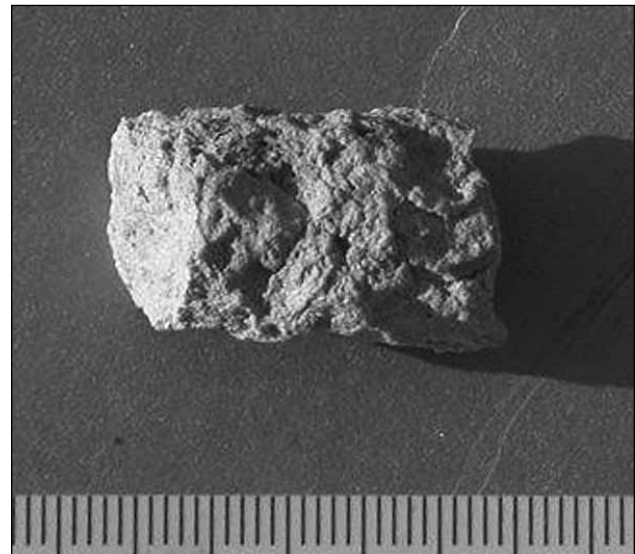


Figure 6. Large vertical burrow cast, 10 mm diameter. RAM14747/V201208.

isopods, small gastropods, midge larvae, rove beetles, and mud-loving beetles. The vertical burrows may be from the fresh or brackish water equivalents of ghost shrimp, mole crabs, and particularly mantis, mud, and snapping shrimp, commonly found on intertidal flats.

If the early Pliocene shorebirds are suspected to have the same habitat as their modern counterparts, their environment can be inferred. Killdeer (representing *Aviadactyla vialovi*) are not confined to lakes and sea like most shorebirds. They nest in meadows, pastures, and dry uplands miles from water. Sanderlings (representing *Avipeda gryponyx*) occur on ocean beaches, feed along the surf line on ocean beaches, and nest in moors and marshes. *Alaripeda bristolia* is represented by the least sandpiper, which frequents beach, tidal flats, marshes, and nests close to a pond or tidal water or in uplands among low bushes or gobs (Sibley, 2000).

Summary

Early Pliocene fossils and impressions (ichnites) from Bouse Formation outcrops near Amboy can help interpret the environmental conditions and biotic habitats at a time when the Bristol arm of the Bouse incursion reached from the vicinity of Parker, Arizona to Amboy, California. A spine of a marine fish spine, *Colpichthys* sp., occurs low but not at the base of the section. The presence of this fish suggests that the platy limestone associated with the Lawlor Tuff was deposited under marine conditions.

Fine-grained, gypsiferous, silty sands high in the section were deposited as shore line or intertidal sand and mud flats. This environment of deposition is supported by the presence of horizontal and vertical burrows made by invertebrates, and three different morphologies of bird tracks. If these early Pliocene bird tracks are representative of modern counterparts, then a habitat of beach and tidal flat is represented. From low to high in the section, fossils and ichnites suggest that the Bouse marine transgression gives way to gypsiferous mudflats as the body of water receded.

ACKNOWLEDGMENTS—I thank David Miller for suggesting that I visit this interesting locality, and Don Lofgrehn for his careful review of and insightful comments about this paper.

References

- Brown, W. J., and M. R. Rosen. 1992. The depositional history of several basins in the Mojave Desert: implications regarding a Death Valley–Colorado River hydrologic connection, in *Old Routes to the Colorado*, J. Reynolds, ed. Redlands, San Bernardino County Museum Association Special Publication 92-2, p. 77-82.
- Elbroch, Mark and E. Marks. 2001. *Bird Tracks and Sign*. Stackpole Books, Mechanicsburg, PA.
- Kordos, Laslo and P. Prakfalvi. 1990. A contribution to the knowledge of Neogene beds with footprint marks in Europe. *Am. All. Foldtani Intezet evi Jelentese az 1988*, vol. 1, pp. 201-212.
- Miller, D. M., R.E. Reynolds, J. Bright, and S.W. Starratt. 2012. Depositional environment of the Pliocene Bouse Formation at Amboy, California, and tectonic implications, California State University Desert Studies Center 2012 Desert Symposium, this volume.
- Reynolds, R. E. 2008. Review of freshwater mollusks from the Bouse Formation, Lake Havasu area, California. California State University Desert Studies Center 2008 Desert Symposium volume and proceedings, p.54-57.
- Sarjeant, W.A.S. and W. Langston Jr. 1994. Vertebrate footprints and invertebrate traces from the Chadronian (Late Eocene) of the Trans-Pecos Texas. *Texas Memorial Museum Bulletin* no. 36, pp 86.
- Sarjeant, W.A.S. and R. E. Reynolds. 2001. Bird footprints from the Miocene of California. California State University Desert Studies Center 2008 Desert Symposium volume and proceedings, p 21-40.
- Sibley, D. A. 2000. *Sibley Guide to Birds*. Alfred A. Knopf, New York.
- Smith, P. B. 1970. New evidence for Pliocene marine embayment along the lower Colorado River, California and Arizona. *Geological Society of America Bulletin*, 81:1411-1420.
- Todd, Thomas N., 1976. Pliocene occurrence of the Recent Antherinid fish *Colpichthys regis* in Arizona. *Journal of Paleontology*, vol. 50, no. 3, p.462-466.

Was it washed in? New evidence for the genesis of Pleistocene fossil vertebrate remains in the Mojave Desert of southern California

J. D. Stewart,^{1,2} Michael Williams,¹ Marjorie Hakel,³ and Scott Musick⁴

¹URS Corporation, 4225 Executive Square, Suite 1600, La Jolla, California 92037

²Natural History Museum of Los Angeles County, 900 Exposition Boulevard, Los Angeles, CA 90007

³107 Cedar Street, Pasadena, California 91103

⁴SWCA Environmental Consultants, 150 South Arroyo Parkway, 2nd floor, Pasadena, California 91105

Introduction

There are divergent theories on genesis of desert pavements (accretion vs. deflation). Likewise, there has been some difference of opinion on the origin and provenance of fragments of Pleistocene bones, particularly tortoise fragments, found on generally flat surfaces in the Mojave Desert. This paper summarizes findings from a paleontological resources survey on the Palo Verde Mesa in southeastern Riverside County that are pertinent to the topic. The fauna will be documented in a separate paper.

In early 2011, URS Corporation was given the responsibility of surveying and assessing the paleontological resources of approximately ten square miles of Palo Verde Mesa between the Imperial County border and Interstate 10 (Figure 1). The entire site, including a proposed power transmission line, lies at the southern edge of Riverside County and extends over 10 miles to the north. There has been no prior geologic mapping of the area at greater detail than 1:100,000 (Stone, 1990, 2006), and even those do not cover the southern part of the project. More than 12 square miles lie outside of the 1:100,000 coverage.

Approach

A paleontological records search from the San Bernardino County Museum indicated that there were no known vertebrate fossil localities for some distance around the site. The URS team initiated its survey by doing east-west

transects along discrete parcels. During the early stages of the survey, numerous Permian marine invertebrate fossils were found in exotic chert gravels and cobbles, but no clearly fossil vertebrate remains were encountered.

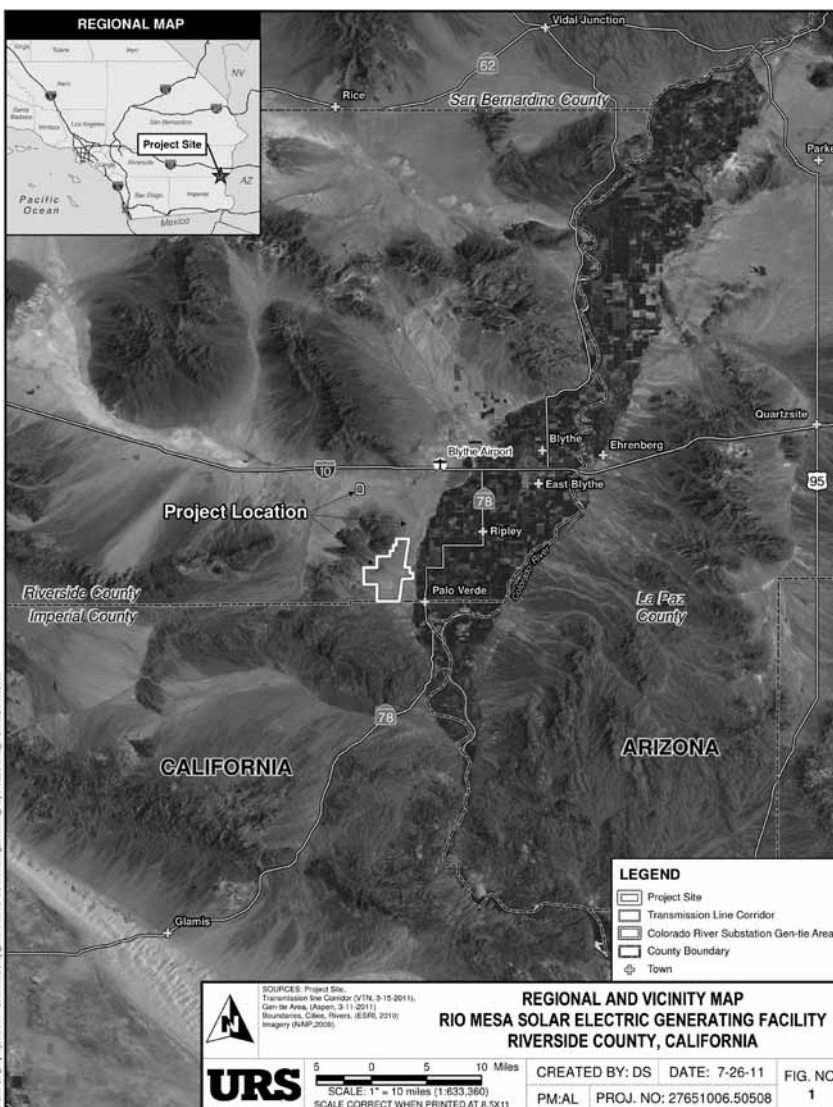


Figure 1. Map of study area.



Figure 2. Outcrop.

In an effort to understand the stratigraphy underlying the mesa we were traversing, we switched to searching natural faces of eroded exposures, which appeared conducive to fossil preservation. Some vertebrate remains were found in the fine-grained sediments traditionally assigned to the Chemehuevi Formation, but these tended to be at a depth not encountered on eroded areas away from the edge of the mesa. A paleosol was recognized over a good deal of the project (Figure 2), and exposed at many places on the desert floor. The reddish-brown color, lithology, and prismatic structure of the paleosol were generally uniform across the project. Weathered horizontal surfaces of the paleosol usually showed a series of



cracks resulting in a polygonal pattern. Where the surface was somewhat covered with sand and gravel, these would concentrate in the cracks, forming a system of polygons outlined by sand and gravel. Its stratigraphic relationship to more elevated desert pavements made of the aforementioned well-rounded exotic gravels and cobbles was unclear. Natural and artificial cuts in the paleosol did not yield any vertebrate fossils. Renewed walking of closely spaced transects across the desert floor began to produce small permineralized bones and bone fragments, some caliche-coated.

Results

The appearance of these permineralized bones was very similar to bones recently arriving on the desert floor, but not showing the flaking and splintering due to subaerial weathering, characteristic of modern bones. In many cases, it was unclear whether the specimens had been moved to the locations where they were discovered or whether they had weathered out of sediments near to where they were discovered. *In situ* fragments of egg shell were also observed on surfaces of the paleosol.

In some cases, multiple bone fragments were encountered in a small area. These sometimes signalled that a partial skeleton was still partially buried (three tortoises and two rabbits), or a partial skeleton completely exhumed (two tortoises). A pre-excavation and post-excavation photo of one tortoise are shown in Figure 3. These specimens were clearly eroding out of the paleosol exposed on the desert floor. In the case of one tortoise, more than 100 associated badly-weathered fragments were found on a slope, but none could have moved downhill more than 22 feet. These do not constitute “an assemblage transported some distance to the present site *post mortem*.” The main erosional agent was water in many cases, but clearly wind in others. There were found many instances of a bone fragment largely encased in caliche and lying on the desert floor. Such finds indicate that the bone was a fragment, probably isolated, when interred, then encased in caliche, and then weathered free of the paleosol. Tortoise eggshell fragments were found in the



Figure 3. Tortoise, pre- and post-excavation.

sediments containing all the associated rabbit remains. These instances and the mixing of numerous small vertebrate taxa in the two limited areas where microfauna can be recovered by screening attest to multiple taxa using the same substrate over time.

In many places where fossil bone fragments were found in an incipient desert pavement on a flat desert floor, test pits revealed the paleosol immediately below the surface. The caliche coating on the majority of these bones and bone fragments indicated that they had weathered from a horizon where caliche had formed, almost certainly the paleosol. The presence of abundant carbonate nodules in the same desert pavement bear witness to their origin in now-deflated paleosol sediments.

The areal limits of the paleosol are not known. It has been confirmed north of Interstate 10 and into northern Imperial County. These points are more than 13 miles apart. Caliche masses in the paleosol are often evident as hard, erosion-resistant in dirt roads and jeep trails. The presence of carbonate nodules in multiple horizons of the paleosol suggest that it was slowly accreting. One possible mechanism could be continuing loess deposition.

Known and deduced dates

The fauna of the paleosol includes at least two taxa that went extinct in the new world at the end of the Pleistocene Epoch (*Equus* and Proboscidea). Thus, one would expect dates for the sediments producing these taxa to be in excess of 10,000 ybp. Retallack (2005) gives rough timing for formation of various calcareous pedogenic phenomena. "Over time, Bk horizons evolve from wisps and filaments of carbonate, which takes 1 – 2 kyr to differentiate. These grow into small nodules, then larger nodules, until nodules coalesce into tabular carbonate (K) horizons after ~ 12 kyr." The only radiocarbon date thus far available for the paleosol was obtained from tortoise eggshell fragments that appeared to be in a silt-filled vacuity within more indurated sediment containing moderate to large caliche nodules. An Accelerator Mass Spectrometry (AMS) radiocarbon dating of the eggshell yielded a 2 sigma (95% confidence interval) result of 13,620 to 13,790 calendar years before present. A partial skeleton of a tortoise was recovered from a burrow in the same relationship to the more indurated sediment at the same locality, and the walls of the burrow contained moderate to large caliche nodules. Thus, the sediment making up the walls of the burrow should be several thousand to ten thousand years older than the tortoise and eggs. In many localities, the base of the paleosol does have a zone of concentrated carbonate nodules, but at only one locality have we observed a tabular carbonate horizon. It persists for no more than 20 feet.

Vertebrate fossils are known to occur in Pleistocene paleosols in the northern and central Great Plains (Burns, 1996; Johnson et al., 2007; Schultz, 1968; Stewart, 1979;

1987; Stewart and Rodgers, 1984; Tobin, 2004, 2005), but we have not found an instance where the phenomenon has been documented in California. In the cited examples, remains of burrowing organisms are much more common than those of non-burrowers. This pattern is shared by the Palo Verde Mesa paleosol. If we assume that all of the chelonian specimens belong to the genus *Gopherus*, more than 80% of the identified vertebrate fossils belong to taxa that inhabit burrows. If rabbits are included, more than 90% are from taxa that can be found in burrows. The fragments of non-burrowing organisms recovered were probably brought below ground by Carnivora or bioturbation.

Significance

There seems to be no prior published account of vertebrate fossils occurring in Pleistocene paleosols in California.

Two natural gas pipeline projects in the 21st century have churned up dozens of vertebrate fossils from this paleosol within the boundaries of this project, and the subsequent paleontological accounts reported nothing from this area. We recovered more than 60 vertebrate fossils within the pipeline scar.

It has been suggested in print that isolated fossil bones or bone fragments on the desert floor may have been washed in from an unknown place of origin and do not constitute significant paleontological resources. "The observations of the taphonomy point to an assemblage transported some distance to the present site post mortem." In most of the instances we observed, there was not a sufficient gradient to allow a small bone to move more than a few meters in years, by which time it might be destroyed by weathering. Multiple elements of a tortoise skeleton cannot be concentrated in a small area on flat desert pavement by transport. The associated and even articulated specimens in the paleosol cannot have been the result of transport. Three localities produced articulated rabbit metapodials cemented together by caliche. These individuals evidently died in burrows or their still-articulated body parts were abandoned in burrows. A pair of exhumed and articulated *Lepus* dentaries could not have been transported even a few feet without separating them. Furthermore, two microfauna localities have yielded specimens indicative of an *in situ* burrowing community that would not have been transported and deposited together by chance.

Reviewers of environmental documents and government officials overseeing the permitting of projects in desert settings should be skeptical of claims that fossil vertebrate bones and teeth lying on the desert floor have been "washed in," especially when there are carbonate nodules intermixed. In some cases, abraded bones are the result of natural sand blasting and specimens that might be regarded as *ex situ* have not moved laterally and only moved a slight amount vertically.

ACKNOWLEDGEMENTS—We benefitted from field visits and conversations with Jay Rehor, Kyle House, Kathleen Springer, Casey Weaver, Paul Marshall, Christopher Dennis, and Abdel-Karim Abdulaban.

References

- Burns, J. A. 1996. Review of Pleistocene zoogeography of prairie dogs (genus *Cynomys*) in western Canada with notes on their burrow architecture. pp. 34-53 In: Stewart, K. M., and K. L. Seymour (Eds.), *Paleoecology and Palaeoenvironments of Late Cenozoic Mammals*. University of Toronto Press, Toronto.
- Johnson, W. C., K. L. Wiley, J. A. Mason, and D. W. May. 2007. Stratigraphy and environmental reconstruction at the middle Wisconsinan Gilman Canyon formation type locality, Buzzard's Roost, southwestern Nebraska, USA. *Quaternary Research* 67:474-486.
- Retallack, G. J. 2005. Pedogenic carbonate proxies for amount and seasonality of precipitation in paleosols. *Geology* 33:333-336.
- Schultz, C. B. 1968. The stratigraphic distribution of vertebrate fossils in the Quaternary eolian deposits in the mid-continent region of North America. p. 115-138 In: Luginbuhl, A. L., and C. B. Schultz (eds.), *Loess and related eolian deposits of the world*. University of Nebraska Press, Lincoln.
- Schultz, C. B., and T. M. Stout. 1945. Pleistocene loess deposits of Nebraska. *American Journal of Science* 243 (5):231-244, 671-689.
- Stewart, J. D. 1979. Paleontology and paleoecology of the Trapshoot local fauna, Rooks County, Kansas. M.A. thesis, University of Kansas, Lawrence. 146 p.
- Stewart, J. D. 1987. Latitudinal effects in Wisconsinan mammalian faunas of the Plains. p. 153-158 in: Johnson, W. C. (ed.) *Quaternary environments of Kansas*. Kansas Geological Survey Guidebook Series 5.
- Stewart, J. D., and R. A. Rogers. 1984. Analysis of pollen from the Trapshoot local fauna quarry (Rancholabrean) of Kansas. *American Midland Naturalist* 112:198-200.
- Stone, P. 1990. Preliminary geologic map of the Blythe 30' by 60' quadrangle, California and Arizona. U.S. Geological Survey Open File Report OF-90-497, scale 1:100,000.
- Stone, P. 2006. Geologic map of the west half of the Blythe 30' x 60' quadrangle, Riverside County, California and La Paz County, Arizona. U.S. Geological Survey Scientific Investigations Map SIM-2922, scale 1:100,000.
- Tobin, R. J. 2004. Taphonomy of ground squirrel remains in a Late Pleistocene ichnofabric, Nebraska, USA. *Palaeogeography, Palaeoclimatology, Palaeoecology* 214:125-134.
- Tobin, R. J. 2005. Ichnology of a late Pleistocene ichnofabric, Nebraska, USA. *Palaeogeography, Palaeoclimatology, Palaeoecology* 215:111-123.

Quaternary offset of the Cady fault, eastern California shear zone, southern California

K. M. Schmidt and V. E. Langenheim

U.S. Geological Survey, 345 Middlefield Rd., Menlo Park, CA, 94025, kschmidt@usgs.gov and zulanger@usgs.gov

ABSTRACT—We interpreted bedrock and surficial geologic mapping in conjunction with gravity and magnetic anomalies to constrain offsets along the east-striking sinistral Cady fault within the Mojave block of the eastern California shear zone. Field mapping of Quaternary deposits and analysis of recently acquired aeromagnetic data indicate that the Cady fault forms a significant structural boundary separating northwest-striking faults to the south, such as the dextral Rodman, Pisgah, and Lavic Lake faults, from east-northeast-striking faults to the north, such as the Manix fault. Both methods indicate that Cady fault strands truncate northwest-striking dextral faults; hence, sinistral offset in this region is likely younger in age and may be more dominant kinematically in the area local to the Cady fault. Earthquakes during the past 50 years, though, demonstrate that both east-striking oblique sinistral and northwest-striking dextral faults to the south remain active. Time-averaged sinistral offset rates, estimated from field mapping of displaced Quaternary alluvial fan deposits and from regional age constraints obtained through luminescence and radiocarbon dating techniques, decrease with older deposit age. Late Pleistocene/Holocene deposits yield rates exceeding 1 mm/yr whereas minimum rates for middle to early Pleistocene deposits are as low as 0.02 mm/yr, assuming the time-averaged fault offset ensued immediately following deposit formation. We estimated a total sinistral offset of ~6 km along the Cady fault based upon reconstruction of displaced bedrock outcrops and magnetic anomalies. Assuming extensional strain in the region began ~10 Ma, as recorded by interbedded sediments and volcanics of the Ricardo Group, the long-term offset rate is ~0.6 mm/yr. Assuming the opening of the Gulf of California to marine incursions by rifting associated with the San Andreas fault system restricts the onset of strain to a more recent time of ~6 Ma, the long-term offset rate is roughly 1 mm/yr.

Introduction

According to kinematic models describing Late Cenozoic deformation in the eastern California shear zone (ECSZ), the Mojave block (Figure 1) is inferred to have evolved in both size and shape as a consequence of varying amounts of coeval north-south shortening and east-west directed extension during progressive deformation of the Pacific–North America plate boundary (Carter et al., 1987; Dokka and Travis, 1990; Garfunkel, 1974; Glazner et al., 2002; Ross, 1995; Unruh et al., 1994). Geologic data (Dokka and Travis, 1990; Walker et al., 2002) and GPS measurements (Miller and Johnson, 2001) are consistent with a significant portion of inter-continental strain being accommodated by the ECSZ. Dokka and Travis (1990), for example, concluded that the individual primary faults of the ECSZ have displacements ranging from 1.5 to 14.4 km and a net total slip of about 65 km across the broader area which accumulated since ~10 Ma. Similarly, using geologic relations, Glazner et al. (2002) bracketed total slip on multiple strands in the larger area surrounding the Cady fault to range from 10 to 33 km.

The overall primary sense of strain in the ECSZ is northwest-oriented dextral shear sub-parallel to, and east

of, the San Andreas fault zone. Deformation, though, in the eastern Mojave domain of the ECSZ is distributed through regional dextral shear on northwest-striking faults, east and northeast-striking sinistral faults, and clockwise rotation of included blocks (Carter et al., 1987; Hillhouse et al., 2010; Ross, 1995). The Cady fault acts as one of the structural block boundaries in the eastern Mojave domain of the ECSZ with an east-west strike and sinistral sense of offset similar to the longer Garlock fault to north and the Pinto Mountain fault to south (Figure 1). It forms a structural boundary separating the east-northeast-striking faults to the north, such as the Manix fault, from the northwest-striking fault domain to the south, which includes the dextral Rodman, Pisgah, and Lavic Lake faults (Figure 2). The northeastern portion of the Mojave block is characterized by east-west striking faults that rotated clockwise since the Miocene (Schermer et al., 1996). Recent notable surface rupture in the ECSZ includes the 1947 Manix (Richter, 1947), 1992 Landers (Unruh et al., 1994), and 1999 Hector Mine (Treiman et al., 2002) earthquakes. In conjunction with the Landers earthquake, the “Newberry fractures” formed at the northern end of this rupture sequence (Unruh et al., 1994), terminating at the latitude of the projection of

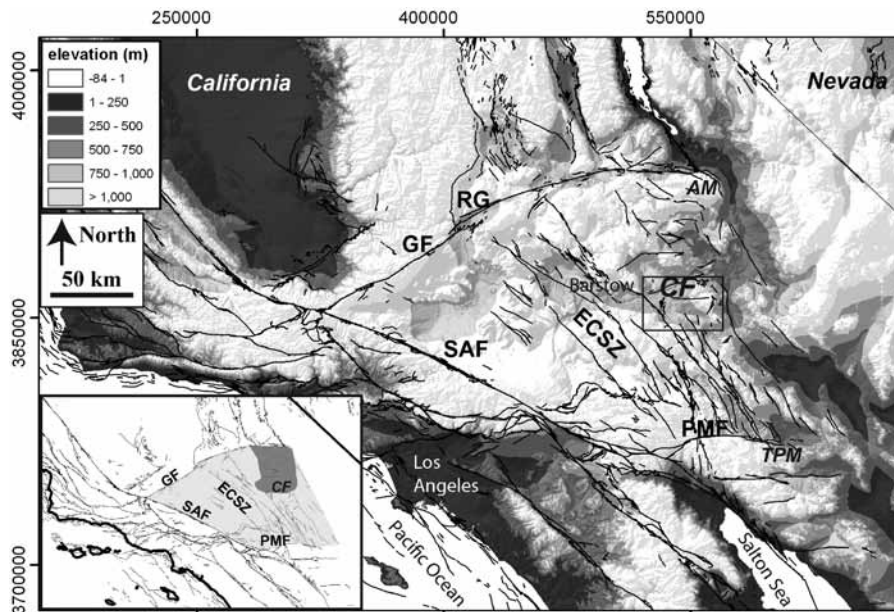


Figure 1. Topographic base depicting regional fault database from U.S. Geological Survey and California Geological Survey, 2006, Quaternary fault and fold database for the United States, accessed October 13, 2011, from USGS web site: <http://earthquake.usgs.gov/hazards/qfaults/>. AM is Avawatz Mountains, CF is Cady fault, ECSZ is eastern California shear zone, GF is Garlock fault, PMF is Pinto Mountain fault, RG is Ricardo Group sediments, SAF is San Andreas fault, and TPM is Twentynine Palms Mountain. Box around CF is study extent depicted in Figures 2 & 3. Inset in lower left depicts Mojave block with ECSZ in light shading and northeast Mojave domain of sinistral faulting in dark shading [after Schermer et al. (1996) and Glazner et al. (2002)]. Grid in UTM NAD83 ZONE11 coordinates.

the Cady fault (Figure 2). Motivation for this study was to determine millennial- to million-year slip rates of the Cady fault in the area characterized by complicated coeval dextral northwest-striking faults and sinistral east-northeast striking faults.

The Cady fault, which transects through the Cady Mountains, is located about 50 km east of Barstow, CA (Figure 1) between Interstates 15 and 40 (Figure 2). The geology of the region, including the Cady fault, was first mapped through field work by Kupfer and Bassett (1962), revised by Dibblee and Bassett (1966), included in a state compilation by Rogers (1967), and incorporated in the California state compilation by Jennings (1994) as well as a compilation specific to the northern Mojave Desert (Walker et al., 2002). Quaternary surficial deposits mantle the underlying Pre-Tertiary granitic basement as well as Miocene volcanic and sedimentary

rocks (Dibblee and Bassett, 1966; Walker et al., 2002). The fault is flanked to the south by the topographically higher part of the Cady Mountains and cumulative displacement has created the presence of the long east-west trending Hidden Valley along the fault. A similar south-side-up relationship exists for older Quaternary units (Qia and Qoa in Table 1a), consistent with oblique slip accommodating uplift to the south. Ford et al. (1990) inferred an additional fault strand bounding the northern extent of Hidden Valley by analysis of Landsat Thematic Mapper images. In most current published depictions (e.g., Figure 2), the eastern end of the Cady fault terminates abruptly on the southern edge of Hidden Valley. The western extent is occluded by pervasive young (decadal to century scale) and active eolian deposits sourced from the nearby Mojave River sink. Here

we combined surficial and crustal structure constraints on faulting by interpreting data collected during a U.S. Geological Survey regional mapping of Quaternary surficial deposits and buried geophysical crustal signatures to

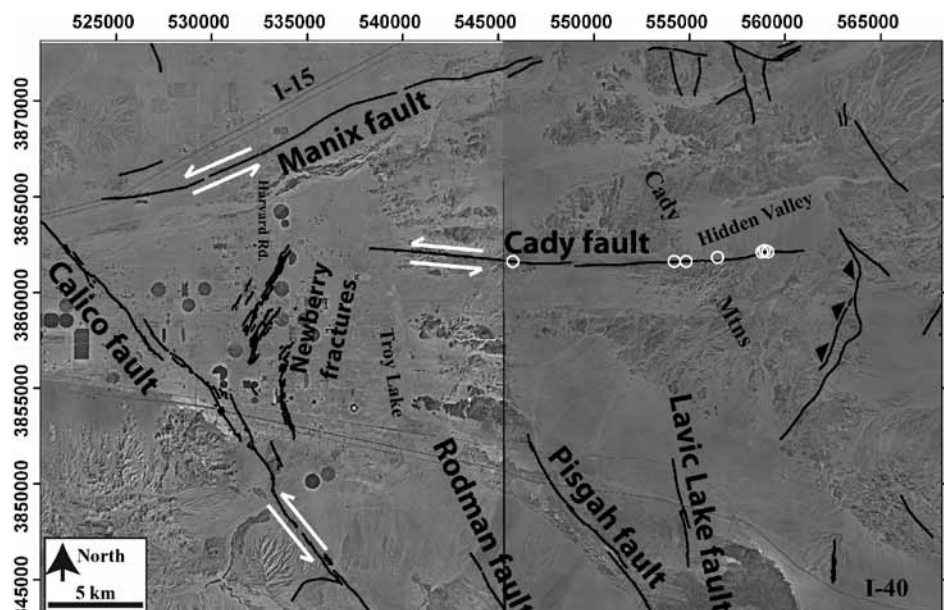


Figure 2. Digital orthophotograph image base with faults in black (<http://earthquake.usgs.gov/hazards/qfaults/>) and white arrows denoting sense of long term offset (not shown for all faults). Open white circles denote locations of offset deposits listed in Table 1a. The Newberry fractures generated by the 1992 Landers earthquake express a northeasterly strike and a northwest-southeast oriented extension direction. Barstow lies ~20 km to west from the western edge of map. Grid in UTM NAD83 ZONE11 coordinates.

map the extent of the Cady fault and constrain its offset rates in the context of the ECSZ.

Results

Extent of Cady fault

Ongoing U.S. Geological Survey mapping efforts have advanced estimates of the spatial extent of the Cady fault, its interactions with neighboring faults, and fault offset rates over a range of time scales (Figures 3 & 4, Tables 1a & 1b). Field observations indicate steeply dipping (70–90° south) fault strands, with up to three sub-parallel components, displaying oblique slickensides. Fault exposures within bedrock are fairly widespread where valleys orthogonally intersect fault traces. Relative age and magnitude of slip on strands within bedrock were estimated by measuring the thickness and maturity of fault gouge. Scarps within the granular Quaternary materials are commonly located near bedrock exposures and they are universally diffused. From field observations, the evidence for lateral offset is more decipherable than vertical offset, hence the oblique component of slip is difficult to estimate. Older Quaternary units offset by the fault are located adjacent to the steep bedrock front of the Cady Mountains with alluvial fan deposits offset in a sinistral sense and beheaded from their sediment sources. Displaced older fans record greater cumulative sinistral slip. In some locales, numerous fault strands with right-stepping segments have resulted in transpressional pop-up structures that have exhumed older, pre-Quaternary basin fill. The youngest units offset by faulting are late Pleistocene to early Holocene in age (Table 1a).

Evidence gleaned through field work indicates that at its eastern termination the Cady fault likely changes orientation abruptly to a more north-northeast strike with deformation spanning a larger number of fault strands that may include more of a thrust offset component (barbs in Figures 2 & 3). Although previous mapping efforts, such as Dibblee and Bassett (1966), represented an

un-named northeast striking fault with a northwest side up that exposed pre-Tertiary granitic basement rocks, prior researchers did not spatially connect this structure to the Cady fault. We found evidence indicating that the two faults are spatially continuous and that the Cady fault changes orientation at its eastern extent, increasing the thrust component of slip with an eastward vergence. This structure is similar to the sinistral Garlock fault generating the impressive Avawatz Mountains front and the eastern termination of the sinistral Pinto Mountain fault, generating Twentynine Palms Mountain (Howard, 2002)(Figure 1). Aeromagnetic data presented in Figure 3 reveal a prominent gradient associated with the eastern edge of the uplifted Cady fault block. Prominent gradients within potential-field geophysical data, such as aeromagnetic data, mark the location of steeply dipping faults juxtaposing rocks with disparate magnetic signatures (Blakely and Simpson, 1986). An accompanying cluster of recent seismicity is located west of the thrust fault and south of the sinistral main Cady fault trace. At the eastern extent of the Cady fault south of Hidden Valley, both the seismicity and the exhumation of basement rocks are consistent with left-slip driving a component of transpression as the primary structure changes orientation (Figures 2 & 3).

At the western end of the Cady fault, aeromagnetic anomalies indicate that the trace of the Cady fault does not coincidentally end under the ample cover of Holocene eolian and fluvial deposits south of the Mojave River that preclude satisfactory surface geologic mapping. Rather, the primary structure continues under the eolian deposits and may change orientation to a more north-westerly strike, may diverge into two strands, and may merge with the Manix fault to the north near Interstate 15 and Harvard Road (Figures 2 & 3). The westward extension of the Cady fault beneath the active eolian deposits is inferred to follow the linear aeromagnetic gradient that separates high magnetic values to the south and low magnetic values to the north (Figure 3).

This gradient results from the juxtaposition of two magnetically different rock packages, and displacement along the Cady fault is consistent with this abrupt juxtaposition. We infer two strands of the Cady fault (Figure 3, heavy dashed lines) that extend westward, close to or possibly intersecting the Manix fault. Preliminary analysis of gravity data, not shown here, revealed moderately strong gradients associated with basin margins, supporting the interpretation that the fault changes orientation to a more west-northwesterly

Table 1a. Sinistral fault slip rates inferred from field-measured offset of unpublished mapped surficial units. Minimum and maximum age brackets from Miller et al. (2009) and Miller et al. (2010). Sinistral offset distances inferred from combination of field observations, measurements on remote sensing imagery, and GPS waypoints.

| Offset Quaternary map unit | Minimum age (ka) | Maximum age (ka) | Sinistral displacement (m) | Maximum rate (mm/yr) | Minimum rate (mm/yr) |
|----------------------------------|---------------------|---------------------|-------------------------------|-------------------------|-------------------------|
| Qya4 | 9 | 14 | 13 | 1.44 | 0.93 |
| Qya4 | 9 | 14 | 7 | 0.78 | 0.50 |
| Qia2 | 40 | 110 | 5 | 0.13 | 0.05 |
| Qoa | 450 | 900 | 20 | 0.04 | 0.02 |
| Qoag | 450 | 900 | 32 | 0.07 | 0.04 |
| Qoag | 450 | 900 | 35 | 0.08 | 0.04 |
| Qoag | 450 | 900 | 20 | 0.04 | 0.02 |
| | | | average | 0.37 | 0.23 |
| | | | standard deviation | ±0.54 | ±0.35 |

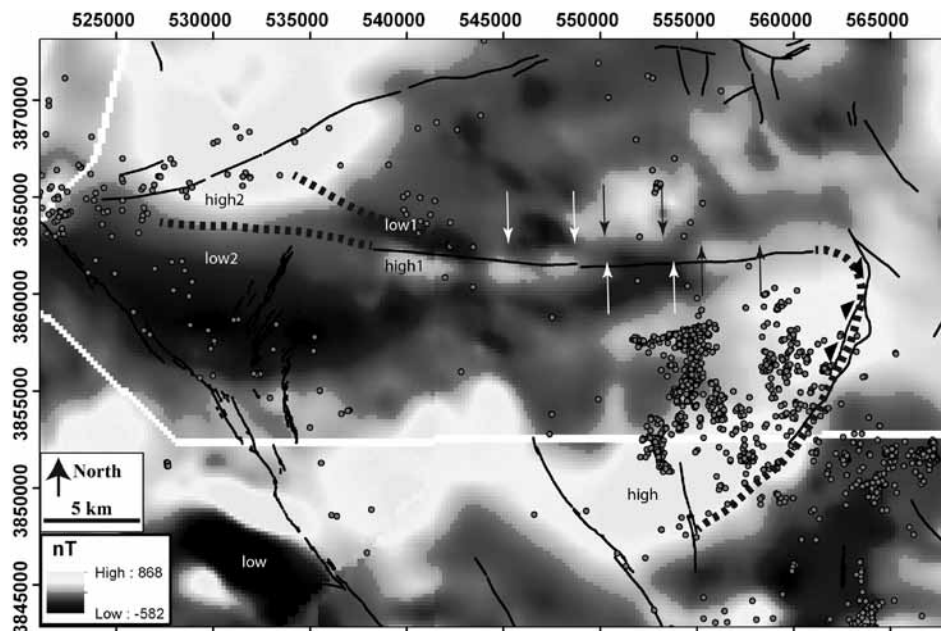


Figure 3. Gridded total field intensity aeromagnetic data includes the combined signal from crystalline basement and Tertiary volcanic rocks. Solid black lines are mapped faults (<http://earthquake.usgs.gov/hazards/qfaults/>), heavy dashed black lines are inferred extensions of the Cady fault, and gray circles are earthquake hypocenters (Yang et al., 2011) (<http://www.data.scec.org/research-tools/alt-2011-yang-hauksson-shearer.html>). Arrows denote boundaries of anomalies (white arrows for low, black arrows for high) used to reconstruct total slip. Anomaly pairs at western terminus used to infer extend strands labeled low1/high1 and low2/high2. Note the hypocenter locations of recent earthquakes plot about 5 km to the south of the surface trace of the Cady fault. The northern extent of the hypocenters form a plane with a steep southward dip. Grid in UTM NAD83 ZONE11 coordinates.

strike extending westward toward the Manix fault for a total length of ~32 km. These western fault extensions are consistent with a structure responsible for the abrupt truncation of the Newberry fractures associated with the Landers earthquake (Figures 2 & 3).

Constraints on cumulative fault slip and ages of units displaced

Sinistral offset rates along the Cady fault were inferred from estimates of total slip recorded by i) displaced Quaternary map units, ii) displaced bedrock map units, and iii) offset aeromagnetic anomalies. Measured fault displacement of Quaternary deposits ranges from 5 to 35 m as determined by tape, GPS, and remote sensing analysis (Table 1a). Displaced deposits have an approximate age span from ~10 ka to almost 1 Ma as documented by recent mapping in the context of a regional soil chronosequence including luminescence and radiocarbon dating techniques (Miller et al., 2009; Miller et al., 2010). Offsets were estimated based upon deformed lateral fan margins, shutter ridges, and uphill-facing scarps oriented parallel to the fault trace. Deposits assigned an apparent 9–14 ka age, based on the regional chronostratigraphic framework, were cut by fault gouge that included clasts rotated parallel to fault traces and gouge projecting into the bed of active washes.

Our long-term constraints are derived from reconstructions of cumulative sinistral slip of displaced

Miocene andesitic and basaltic outcrop bodies represented by Walker et al. (2002). Reconstruction of these displaced volcanic rocks (primarily Miocene andesite, unit Mva of Walker et al., 2002) account for a total offset of ~6 km. Furthermore, this geologic reconstruction is in agreement with reconstructed displacements inferred from correlation of aeromagnetic anomalies (Figure 3). We inferred accumulated slip from displaced aeromagnetic anomalies by aligning moderate value magnetic signatures, likely representative of local andesite sources, and magnetic highs, likely from buried basalt. The lateral boundaries of these magnetically high and low bodies were used as piercing points to reconstruct fault displacement.

The range of total sinistral displacement inferred from displaced aeromagnetic anomalies ranged from 5.7 to 6.1 km. For simplicity, we ignore the amount of Neogene block rotation in this preliminary strain budget. For comparison, Glazner et al. (2002) bracketed total slip in the greater area surrounding the Cady fault to range from 10 to 33 km; hence, the Cady fault alone may account for ~20–60% of the total strain budget in the region.

Timing of the onset of shear across the entire ECSZ, or specifically within the Mojave block, has not been precisely ascertained, but it can be restricted based upon relations deduced in the surrounding region. In order to determine offset rates from the estimates of cumulative slip, we appraised the approximate timing for the onset of displaced Neogene volcanic rocks and buried aeromagnetic anomalies along the Cady fault through the regional controls arising from i) deposition of aerially extensive sedimentary and volcanic units, ii) deposition of rocks along regional faults, and iii) rifting of the Gulf of California in Baja California. We assume that the timing attributed to the onset of deformation associated with primary bounding structures, such as the Garlock and San Andreas faults, can be used as proxies for the initiation of offset along the subsidiary Cady fault. The Peach Spring Tuff, a widespread ignimbrite, has been used as a once continuous regional stratigraphic marker bed extending 350 km from the western Colorado Plateau to Barstow, CA (Nielson et al., 1990). It presumably

blanketed most of the eastern Mojave Desert region and was dated by $^{40}\text{Ar}/^{39}\text{Ar}$ techniques at 18.51 ± 0.10 Ma (Nielson et al., 1990). Because this structural marker bed is disrupted by faulting and rotation (Hillhouse et al., 2010; Hillhouse and Miller, 2011), it can be used as a proxy for dating the onset of ECSZ tectonic strain. Hence, a conservative estimate for the onset of Cady fault slip dates back well into the Miocene. Similarly, Ross (1995) suggested the present pattern of tectonic deformation in the Cady Mountains east of Troy Lake (Figure 2) began post-14 Ma associated with the disruption of the “Barstow formation” in the area. More regionally, from dated deposits of the Ricardo Group, a sequence of Miocene sedimentary and volcanic rocks located 120 km to the northwest of our study area adjacent to the Garlock fault (Figure 1), Loomis and Burbank (1988) inferred that east-west deformation in the Mojave block of the ECSZ began around 10–9 Ma. The Ricardo Group sediments, though, do not directly constrain the beginning of strike-slip motion on the Garlock fault. Rather, Loomis and Burbank (1988) inferred increased sediment accumulation rates to indicate extension and crustal thinning associated with the Garlock fault. Additional regional evidence from the age of the onset for San Andreas fault rifting through the Gulf of California is based on the presence of marine conditions from outcrops of a 5.7 ± 0.2 Ma tuff and sediments containing 6.4–4.0 Ma microfossils (Oskin and Stock, 2003). This age of ~6 Ma represents the inception of the primary continental structure in the region, the San Andreas fault zone, which is thought to be responsible for generation of the ECSZ. Hence, the boundary between the Miocene and Pliocene corresponds with the earliest approximate timing for the onset of deformation on the Cady fault.

Discussion of Cady fault offset rates

Sinistral fault slip rates calculated from field-measured displacements of Quaternary deposits, mapped in the context of a regional pedogenic chronosequence framework (Miller et al., 2009; Miller et al., 2010), exhibit greater than an order of magnitude range from 0.02 to 1.44 mm/yr (Figure 4; Table 1a). Given our interpretation of the geologic mapping of Quaternary materials, rates increase toward the present. A portion of this broad range in values arose because we assumed that fault offset began immediately following unit deposition, hence rates for older units are averaged over longer time periods. Also, our Quaternary age control is not absolute, but relative with respect to the regional framework, with minimum and maximum brackets. That is, absolute dates of the discrete deposits offset by the fault do not exist. Furthermore, the assigned map unit

designation (Qoa) for the oldest units may not be everywhere accurate. Heightened eolian sand input and oblique slip along the fault may have accelerated the generation of high-relief, well-rounded ballena-like deposit surfaces that are actually younger than estimates gleaned from morphologic characteristics.

We inferred total sinistral fault displacement from apparent offset of aeromagnetic anomalies (5.7–6.1 km) and the realignment of volcanic outcrop bodies (~6 km). As no known absolute ages exist for the Tertiary volcanic rocks displaced across the Cady fault, we use the conservative 18.5 Ma age of the Peach Spring tuff to bound the oldest onset of deformation on the Cady fault. Such an assumption leads to time-averaged offset rates of 0.31–0.33 mm/yr (Figure 4; Table 1b). If, however, the onset of the Ricardo Group sedimentation to the north is more indicative of the onset of displacement along the Cady fault, the averaged offset rates increase to 0.57–0.61 mm/yr (Figure 4; Table 1b). Lastly, if the more recent inception of the Gulf of California along the San Andreas fault at ~6 Ma better represents the onset of Cady fault slip, the averaged offset rates are 0.97–1.11 mm/yr (Figure 4; Table 1b). Hence, rates inferred from both the youngest Quaternary deposits displaced and the reconstructions from both Tertiary volcanic rocks and offset aeromagnetic anomalies are as high as ~1 mm/yr.

For comparison, modern strain rates inferred from GPS measurements greatly exceed those measured from geologic observations. For instance, Miller et al. (2001)

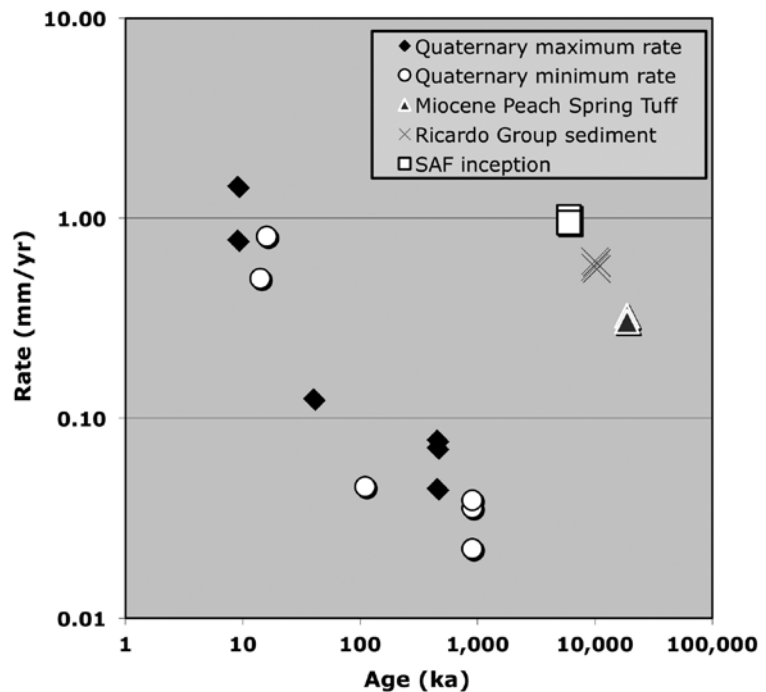


Figure 4. Cady fault offset rates inferred from displaced Quaternary units, Tertiary volcanic bedrock outcrops, and inferred displacements in aeromagnetic anomalies. Ages of displaced Quaternary map units from regional chronostratigraphy. Age constraints for the onset of Cady fault slip include the Miocene Peach Spring tuff, Ricardo Group sedimentation, and rifting within the Gulf of California with the inception of the greater San Andreas fault (SAF) system. Note log-log scale of plot.

Table 1b. Sinistral fault slip rates inferred from aeromagnetic data and regional stratigraphic markers used to infer the inception of offset along the Cady fault within the ECSZ. Sinistral offset distances inferred from reconstruction of gradient boundaries of aeromagnetic boundaries depicted in Figure 3.

| Offset Miocene unit | Age (Ma) | Minimum sinistral displacement (km) | Maximum sinistral displacement (km) | Minimum rate (mm/yr) | Maximum rate (mm/yr) |
|---|------------|-------------------------------------|-------------------------------------|----------------------|----------------------|
| Peach Spring Tuff ^a | 18.51±0.10 | 5.7 | 6.1 | 0.31 | 0.33 |
| Ricardo Group ^b | 10 | 5.7 | 6.1 | 0.57 | 0.61 |
| Gulf of California rifting ^c | 5.7±0.2 | 5.7 | 6.1 | 0.97 | 1.11 |
| | | | average | 0.61 | 0.68 |
| | | | standard deviation | ±0.33 | ±0.39 |

a. Ignimbrite dated by ⁴⁰Ar/³⁹Ar techniques by Nielson et al. (1990)

b. Sequence of sedimentary and volcanic rocks reported by Loomis and Burbank (1988)

c. Marine tuff reported by Oskin and Stock (2003)

report that the station “TROY” located near the Cady fault undergoes -7.75 and 3.47 mm/yr in respective east and north directed velocities relative to stable North America. These high rates may be indicative of time-varying deformation associated with the recent Landers earthquake, although no systematic decrease in rates were observed by Miller et al. (2001) in the 1993–1998 period following the 1992 earthquake. Furthermore, the differential between geologically and geodetically derived rates may be explained by the fact that plate-boundary deformation within the ECSZ is accommodated across numerous fault and fold structures, of which the Cady fault is merely a single structure.

Summary

Recent geologic mapping of Quaternary deposits and interpretation of aeromagnetic anomalies support assertions that the Cady fault zone expresses a greater number of fault strands, a longer total length than previously mapped, and a total cumulative offset of ~6 km. At its western and eastern extents, for instance, the fault changes orientation and may connect with neighboring structures. Displacement rates inferred from offset recorded by Quaternary deposits and Neogene bedrock across the Cady fault range from <0.1 to ~1 mm/yr. Long-term slip rates averaged over the Neogene may be comparable to those for offsets of the most recent Quaternary deposits (~1 mm/yr). Future research opportunities exist to more precisely constrain the timing of Cady fault inception by dating both Quaternary deposits and Miocene volcanic rocks displaced by faulting.

References

Blakely, R.J., and Simpson, R.W., 1986, Approximating edges of source bodies from magnetic or gravity anomalies: *Geophysics*, v. 51, p. 1494-1498.
 Carter, J.N., Luyendyk, B.P., and Terres, R.R., 1987, Neogene clockwise rotation of the eastern Transverse Ranges, California, suggested by paleomagnetic vectors: *Geological Society of America Bulletin*, v. 98, p. 199-206.

Dibblee, T.W., and Bassett, A.M., 1966, Geologic map of the Cady Mountains quadrangle, San Bernardino County, California: U.S. Geological Survey Miscellaneous Geologic Investigations Map I-467, 4 p. pamphlet, 1 sheet, scale 1:62,500.
 Dokka, R.K., and Travis, C.J., 1990, Late Cenozoic strike-slip faulting in the Mojave Desert, California: *Tectonics*, v. 9, no. 2, p. 311-340.
 Ford, J.P., Dokka, R.K., Crippen, R.E., and Blom, R.G., 1990, Faults in the Mojave Desert, California, as revealed on enhanced Landsat images: *Science*, v. 248, p. 1000-1003.
 Garfunkel, Z., 1974, Model for the late Cenozoic tectonic history of the Mojave desert and its relationship to adjacent areas: *Geological Society of America Bulletin*, v. 85, no. 12, p. 1931-1944.
 Glazner, A.F., Walker, J.D., Bartley, J.M., and Fletcher, J.M., 2002, Cenozoic evolution of the Mojave Block of Southern California: *in* Geologic evolution of the Mojave Desert and southwestern Basin and Range, Glazner, A.F., Walker, J.D., and Bartley, J.M., eds., Geological Society of America, Boulder, CO, Memoir 195, p. 19-41.
 Hillhouse, J.W., Miller, D.M., and Turrin, B.D., 2010, Correlation of the Miocene Peach Spring Tuff with the geomagnetic polarity time scale and new constraints on tectonic rotations in the Mojave Desert, California: *in* Overboard in the Mojave; 20 Million Years of Lakes and Wetlands, Reynolds, R.E. and Miller, D.M. eds., 2010 Desert Symposium volume, California State University, Fullerton, California, p. 105-121.
 Hillhouse, J.W. and Miller, D.M., 2011, Magnetostratigraphy and tectonic rotation of the Miocene Spanish Canyon Formation at Alvord Mountain, California: *in* The Incredible Shrinking Pliocene, Reynolds, R.E. ed., 2011 Desert Symposium volume, California State University, Fullerton, California, p. 49-52.
 Howard, K.A., 2002, Geologic map of the Sheep Hole Mountains 30 by 60 quadrangle, San Bernardino and Riverside counties, California: U.S. Geological Survey Miscellaneous Field Studies Map MF-2344, 1:100,000 scale.
 Jennings, C.W., 1994, Fault activity map of California and adjacent areas with location and ages of recent volcanic eruptions: California Geologic Data Map Series, Map No. 6. California Division of Mines and Geology.
 Kupfer, D.H., and Bassett, A.M., 1962, Geologic reconnaissance map of part of the southeastern Mojave Desert, California: U.S. Geological Survey, Mineral Investigations Filed Studies Map MF-205, 1:125,000 scale.

- Loomis, D.P., and Burbank, D.W., 1988, The stratigraphic evolution of the El Paso basin, southern California: Implications for the Miocene development of the Garlock fault and uplift of the Sierra Nevada: *Geological Society of America Bulletin*, v. 100, p. 12-28.
- Miller, M.M., and Johnson, D.J., 2001, Refined kinematics of the Eastern California shear zone from GPS observations, 1993-1998: *Journal of Geophysical Research*, v. 106, no. B2, p. 2245-2263.
- Miller, D.M., Bedford, D.R., Hughson, D.L., McDonald, E.V., Robinson, S.E., and Schmidt, K.M., 2009, Mapping Mojave desert ecosystem properties with surficial geology: *in* The Mojave Desert, Ecosystem Processes and Sustainability, Webb, R.H. Fenstermaker, L.F., Heaton J.S., Hughson, D.L., McDonald, E.V., and Miller, D.M, eds., University of Nevada Press, Reno, NV, p. 225-251.
- Miller, D.M., Schmidt, K.M., Mahan, S.A., McGeehin, J.P., Owen, L.A., Barron, J.A., Lehmkuhl, F., and Löhner, R., 2010, Holocene landscape response to seasonality of storms in the Mojave Desert: *Quaternary International*, v. 215, p. 45-61.
- Nielson, J.E., Lux, D.R., Dalrymple, G.B., and Glazner, A.F., 1990, Age of the Peach Springs Tuff, southeastern California and western Arizona: *Journal of Geophysical Research*, v. 95, p. 571-580.
- Oskin, M., and Stock, J., 2003, Marine incursion synchronous with plate-boundary localization in the Gulf of California: *Geology*, v. 31, no. 1, p. 23-26.
- Richter, C.F., 1947, The Manix (California) earthquake of April 10, 1947: *Bulletin of the Seismological Society of America*, v. 37, no. 3, p. 171-179.
- Rogers, T.H. compiler, 1967, Geologic Map of California, Olaf P. Jenkins edition, San Bernardino Sheet: California Div. Mines and Geology, scale 1:250,000.
- Ross, T.M., 1995, North-south-directed extension, timing of extension, and vertical-axis rotation of the southwest Cady Mountains, Mojave Desert, California: *Geological Society of America Bulletin*, v. 107, no. 7, p. 793-811.
- Schermer, E.R., Luyendyk, B.P., and Cisowski, S., 1996, Late Cenozoic structure and tectonics of the northern Mojave Desert: *Tectonics*, v. 15, no. 5, p. 905-932.
- Treiman, J.A., Kendrick, K.J., Bryant, W.A., Rockwell, T.K., and McGill, S.F., 2002, Primary Surface Rupture Associated with the Mw 7.1 16 October 1999 Hector Mine Earthquake, San Bernardino County, California: *Bulletin of the Seismological Society of America*, v. 92, no. 4, p. 1171-1191.
- Unruh, J.R., Lettis, W.R., and Sowers, J.M., 1994, Kinematic interpretation of the 1992 Landers earthquake: *Bulletin of the Seismological Society of America*, v. 84, no. 3, p. 537-546.
- Walker, J.D., Black, R.A., Berry, A.K., Davis, P.J., Andrew, J.E., and Mitsdarfer, J.M., 2002, Geologic maps of the northern Mojave Desert and southwestern Basin and Range Province, California: Explanation of maps on CD-ROM: *in* Geologic evolution of the Mojave Desert and southwestern Basin and Range, Glazner, A.F., Walker, J.D., and Bartley, J.M., eds., Geological Society of America, Boulder, CO, Memoir 195, p. 297-299.
- Yang, W., Hauksson, E., and Shearer, P.M. (manuscript in preparation), 2011, Computing a large refined catalog of focal mechanisms for southern California (1981 - 2010). (<http://www.data.scec.org/research-tools/alt-2011-yang-hauksson-shearer.html>)

Reynoldsite, a new mineral from the Blue Bell claims, California and the Red Lead mine, Tasmania

Anthony R. Kampf,^{1*} Stuart J. Mills,² Robert M. Housley,³ Ralph S. Bottrill,⁴ and Uwe Kolitsch⁵

¹Mineral Sciences Department, Natural History Museum of Los Angeles County, 900 Exposition Boulevard, Los Angeles, CA 90007, USA (akampf@nhm.org)

²Geosciences, Museum Victoria, GPO Box 666, Melbourne 3001, Australia

³Division of Geological and Planetary Sciences, California Institute of Technology, Pasadena, CA 91125, USA

⁴Mineral Resources Tasmania, P.O. Box 56, Rosny Park, Tasmania 7018, Australia

⁵Mineralogisch-Petrographische Abt., Naturhistorisches Museum, Burgring 7, A-1010 Wien, Austria, and Institut für Mineralogie und Kristallographie, Universität Wien, Geozentrum, Althanstrasse 14, A-1090 Wien, Austria

The new mineral reynoldsite, $\text{Pb}_2\text{Mn}^{4+}_2\text{O}_5(\text{CrO}_4)$, occurs at the Blue Bell claims, near Baker, San Bernardino County, California, U.S.A. and at the Red Lead mine, Dundas, Tasmania, Australia. The Blue Bell claims exploit the oxidation zone of a small Pb–Cu–Zn–Ag deposit. At the Blue Bell claims, reynoldsite was discovered by Joe Marty and Brent Thorne in the C adit, in cracks and very narrow veins in a highly siliceous hornfels. Species observed in direct association include: coronadite, fluorite, goethite, opal, pyromorphite, quartz, and wulfenite. The C adit had previously yielded two other new minerals: plumbophyllite (Kampf et al. 2009) and fluorphosphohedyphane (Kampf and Housley 2011).

The Red Lead mine exploits a supergene mineral assemblage, which has resulted from the superposition of carbonate-altered, Cr-rich, ultramafic rocks (containing stichtite, “fuchsite,” and magnesiochromite) with galena-rich veins, followed by deep weathering by acid groundwater (Bottrill et al. 2006). At the Red Lead mine, reynoldsite occurs coating stalactitic coronadite and lithiophorite, and is locally overgrown by crocoite crystals.

At the Blue Bell claims, reynoldsite occurs in subparallel growths and divergent sprays of thin prisms with a square cross-section. At the Red Lead mine, it occurs as thin rectangular blades. At both occurrences, crystals are small (≤ 0.2 mm), and ubiquitously and multiply twinned. At both deposits, reynoldsite formed as a secondary mineral derived from the weathering of primary minerals including oxides and sulfides in the presence of acidic groundwater.

Reynoldsite is dark orange brown to black in color and has a dark orange-brown streak. Its luster is subadamantine and its Mohs hardness is about 4½. The mineral is brittle with irregular to splintery fracture and a poorly developed {001} cleavage. The calculated density based on the ideal formula is 6.574 g/cm³. The average index of refraction predicted by the Gladstone–Dale relationship is 2.473. Extinction is approximately parallel to the direction of prism elongation for Blue Bell crystals. Very

thin plates exhibit an orange-brown color in transmitted light and are pleochroic from medium brown to dark orange brown. Electron microprobe analyses of Blue Bell reynoldsite provided the empirical formula: $\text{Pb}_{1.97}\text{Mn}_{2.01}\text{O}_5(\text{Cr}_{1.01}\text{O}_4)$.

Reynoldsite is triclinic with space group $P\bar{1}$ and unit-cell parameters (for a Blue Bell crystal): $a = 5.018(1)$, $b = 7.599(2)$, $c = 10.290(3)$ Å, $\alpha = 92.14(2)$, $\beta = 99.54(2)$, $\gamma = 109.15(2)^\circ$, $V = 363.7(2)$ Å³, and $Z = 2$. The crystal structure of reynoldsite contains close-packed layers of edge-sharing Mn^{4+}O_6 octahedra parallel to {001}. These layers are composed of edge-sharing double chains of octahedra extending along [100], which in turn are linked to one another by sharing edges in the [010] direction. The thick interlayer region contains Pb^{2+} cations and CrO_4 tetrahedra. The structure bears strong similarities to those of the phyllosulfates, such as chalcophanite (Post and Appleman 1988) and birnessite (Post and Veblen 1990).

The name is in honor of Robert E. Reynolds (b. 1943), former Curator of Earth Sciences at the San Bernardino County Museum. Influential instructors at Pasadena City College (Pasadena, California) and the University of California, Riverside inspired Mr. Reynolds to pursue mineralogical and paleontological studies of the Mojave Desert and



Multiply twinned crystal of reynoldsite from the Blue Bell claims (0.1 mm tall); plane-polarized light micrograph.

he has maintained this focus for more than four decades. He has written or edited numerous publications and has organized many symposia focused on the Mojave Desert region. Over the course of several years, he coordinated and supported a dedicated group of volunteers from the San Bernardino County Museum in an extensive study of the Blue Bell claims, which culminated in a publication detailing the history and mineralogy of the deposit (Maynard et al. 1984).

The complete description of reynoldsite will appear in an upcoming issue of the *American Mineralogist*.

References

- Bottrill, R.S., Williams, P.A., Dohnt, S., Sorrell, S., and Kemp, N.R. (2006) Crocoite and associated minerals from Tasmania. *Australian Journal of Mineralogy*, 12, 59–90.
- Kampf, A.R. and Housley, R.M. (2011) Fluorophosphohedyphane, the fluorine analogue of phosphohedyphane from the Blue Bell claims near Baker, San Bernardino County, California. *American Mineralogist*, 96, 423–429.
- Kampf, A.R., Rossman, G.R., and Housley, R.M. (2009) Plumbophyllite, a new mineral from the Blue Bell claims near Baker, San Bernardino County, California. *American Mineralogist*, 94, 1198–1204.
- Maynard, M.F., Valenti, A., Jenkins, J., Jenkins, F., Hall, D., Hall, J., White, B., White, S., Mansfield, M., and Mansfield, E. (1984) The Blue Bell Claims. San Bernardino County Museum Special Publication, San Bernardino County Museum, San Bernardino, 61 pp.
- Post, J.E. and Appleman, D.E. (1988) Chalcophanite, $ZnMn_3O_7 \cdot 3H_2O$: new crystal-structure determinations. *American Mineralogist*, 73, 1401–1404.
- Post, J.E. and Veblen, D.R. (1990) Crystal structure determinations of synthetic sodium, magnesium, and potassium birnessite using TEM and the Rietveld method. *American Mineralogist*, 75, 477–489.

Early Neogene cat tracks from California and Utah

Robert E. Reynolds¹ and Andrew R. C. Milner²

¹Redlands, CA, rreynolds220@verizon.net

²St. George Dinosaur Discovery Site at Johnson Farm, 2180 E. Riverside Drive, St. George, UT, 84790, arcmilner@gmail.com

ABSTRACT —Tracks of fossil cats (Felidae) are discussed from Neogene sediments in California and Utah. The sparse record of tracks is compared to the published phylogenetic record developed from body fossils. Tracks discussed span the Miocene late Hemingfordian to Blancan NALMA. Tracks with cat morphology may have been left by Felinae (*Pseudailurus* or *Nimravides*) or by Machairodontinae. Distinction between Felinae and Machairodontinae tracks is attempted based on morphology, and large cats from smaller cats based on both size and morphology. The stratigraphic record of felid fossil tracks apparently differs somewhat from the published temporal range of body fossil occurrences.

Track morphology

Fossil felid footprints are distinguished by size and morphology, and morphometric differences can be placed in a temporal/stratigraphic framework. Nomenclature used in describing digitigrade cat tracks is presented in Figure 1. The term “metapodial pad” denotes the pad on the foot at the base of the metacarpals or metatarsals, located posterior to the pads on the digits (digital pads). If the print is clear enough to distinguish front from hind foot, the terms manus and pes are used, respectively. North American Land Mammal Age is abbreviated as NALMA, and specific land mammal age abbreviations (e.g., He2) follow Tedford and others (2004; see table A).

Background

Phylogenetic relationships between Miocene and Pliocene North American Felidae have been proposed (Martin, 1998a, 1998b, Fig 13.3, 13.4). The fossil record for Felidae in North America originates at the start of the late Hemingfordian (He2) with *Pseudailurus*, a puma-size cat, whose record continues into the early Pliocene (Hh/Bl). *Nimravides*, a bobcat-sized medium felid with transversely flattened upper incisors, is recognized in

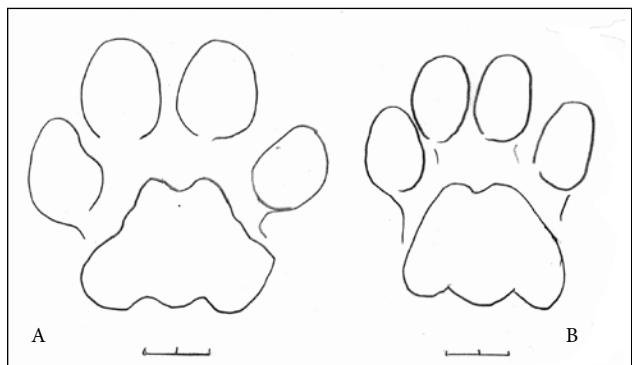


Figure 1. Puma tracks: manus (a), pes (b), showing four oval digital pads and large trilobed metapodial pad on each print. Scale bar=2 cm.

the late Barstovian (Ba2, Tedford et al, 2004; Martin, 1998b, Fig 13.4) and also continues into the early Pliocene (Blancan Bl). In the late Early Hemphillian (Hh2), these early Felidae gave rise to two separate lineages: the Felinae (including *Pseudailurus* and *Nimravides*) with short, conical incisors; and Machairodontinae (including *Meganteron/Smilodon* and *Homotherium*) with enlarged, transversely flattened upper incisors, as well as the derived Felinae (including *Lynx*, *Puma* and *Miracinonyx*) with conical incisors.

The branch of modern Felinae, including *Felis* and *Panthera* (Pantherinae) (Wozencraft, 2005; Johnson and others, 2006), did not reach North America until the Pleistocene. Similarly, the machairodont *Smilodon* did not appear in the North American fossil record until the early Pleistocene (about 2 Ma) near the end of the Blancan (Turner and Antón, 1997; Hulbert, 2010).

There is a five million year interval on the North American continent, Arikarean (Ak2) to mid-Hemingfordian (He2), where no cat-like carnivores, Felidae or Nimravidae, are represented (Martin, 1998a). Nimravidae reappear during the late Tertiary represented exclusively by the genus *Barbourofelis*, which ranges from the early Clarendonian through late Hemphillian (ClI- Hh3). In contrast to the cursorial Felidae, which produce digitigrade tracks (Fig. 1), *Barbourofelis* was somewhat plantigrade (Martin, 1998a), and might have left large tracks with an elongate metapodial pad.

Proposed relationships between late Tertiary groups consisting of nimravids and felids (Martin, 1998a,

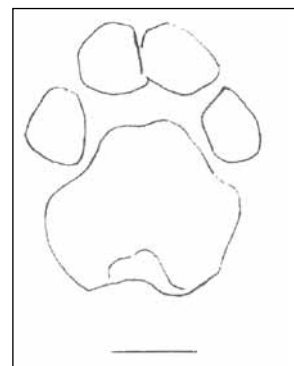


Figure 2. Medium cat track, Barstow, showing circular digital pads and equidimensional bilobed metapodial pad. Scale bar = 2 cm.

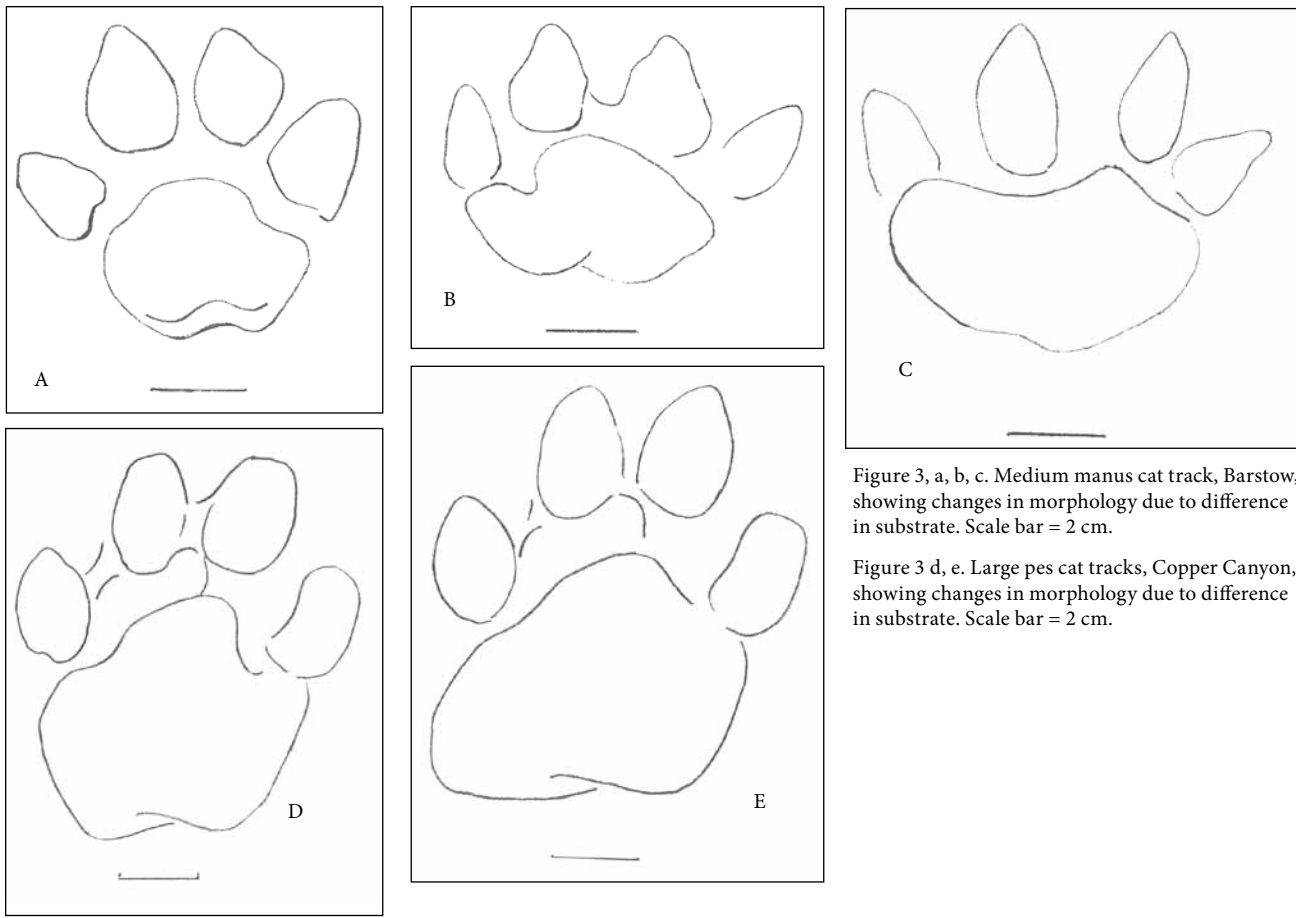


Figure 3, a, b, c. Medium manus cat track, Barstow, showing changes in morphology due to difference in substrate. Scale bar = 2 cm.

Figure 3 d, e. Large pes cat tracks, Copper Canyon, showing changes in morphology due to difference in substrate. Scale bar = 2 cm.

b) suggest that the makers of late Hemingfordian to Hemphillian tracks (He2 through Hh3) might include, from small to large, bobcat-size *Nimravides*, puma-sized *Pseudailurus*, and African lion-sized *Machairodus*. Cat tracks discussed here are from the Hemingfordian and Barstovian Barstow Formation of California, early Clarendonian unnamed strata at Enterprise Reservoir, Utah, the Clarendonian Avawatz Formation of California, the Blancan Olla Formation, Palm Spring Group in Fish Creek Wash, Anza-Borrego Desert State Park, and from the mid-Blancan Copper Canyon Formation in Death Valley, California (Scrivner and Boettjer, 1986; Santucci and Nyborg, 1999; Nyborg and Buchheim, 2005; Nyborg and others, 2012).

Manus cat tracks are usually larger and proportionally wider meso-laterally than those of the associated pes (Murie, 1982). Claw impressions are generally lacking, which helps differentiate them from late Tertiary canid tracks. In the late Tertiary fossils, metapodial pads may be bilobed (Fig 2) or trilobed (Fig 1) and may be equidimensional (Fig. 2) or wider meso-laterally (Fig 3c). Digital pads may be circular (Fig 2), oval or elongate (Fig 3c), and either separate (Fig 3a) or oppressed against the metapodial pad (Fig 3d, 3e). Using manus measurements where possible, this paper employs the following classifications:

- Small-size cat tracks are approximately 3cm long (antero-posterior) and x 3.5cm wide (meso-lateral);
- Medium-size cat tracks range from 6.0-7.5 cm long and 5.5 -7.5 cm wide
- Large-size cat tracks are greater than 8 cm long and 9 cm wide.

Since the combined age of the strata containing the cat tracks spans 14 million years (17–3 Ma), morphologic changes due to evolution and immigration of new species is expected. Changes in track shape also occur due to differences in substrate (Fig. 3a, 3b, 3c; Reynolds, 2002).

Descriptions and locations

Daggett Ridge, Barstow Formation, CA: medium cat tracks (Fig. 4a, 4b)

DESCRIPTION: manus (6 cm length x 7 cm width) and pes (6.5 cm length x 5.5 cm width).

METAPODIAL PAD: manus bilobed, pes trilobed; Digits: manus oval, pes elongate, separate from metapodial pad

AGE: Late Hemingfordian (He 2), 17–16.2 Ma.

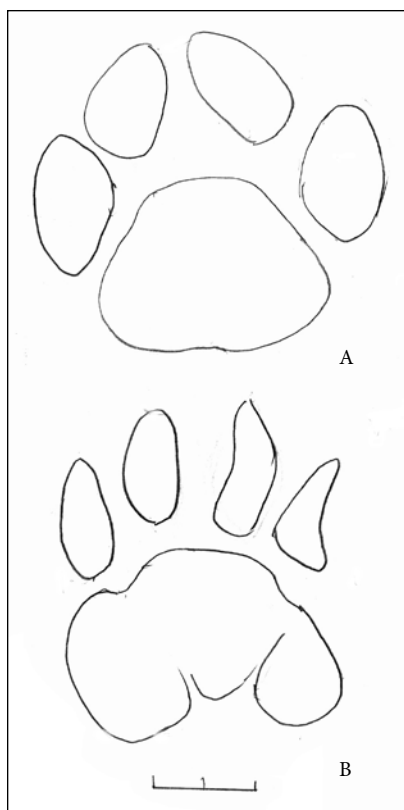


Figure 4a, b. Medium cat track, Daggett Ridge, manus (a) has oval digital pads and equidimensional bilobed metapodial pad. Pes, (b) has elongate digital pads and trilobed metapodial pad. Scale bar = 2 cm.

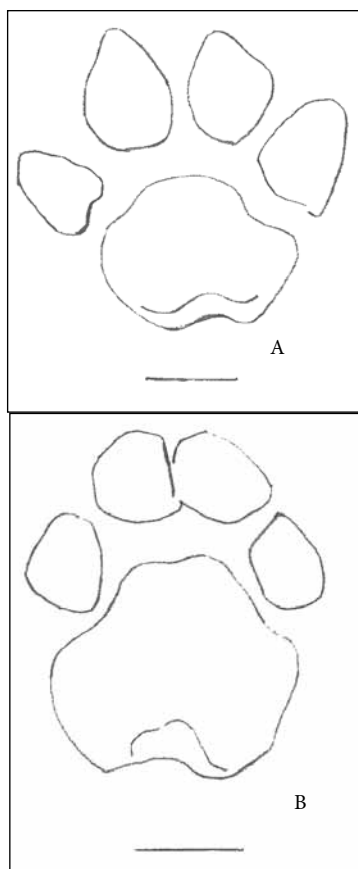


Figure 5a, b. Medium cat track, West Owl Canyon, manus (a) and pes (b) exhibit oval digital pads and equidimensional bilobed metapodial pad. Scale bar = 2 cm.

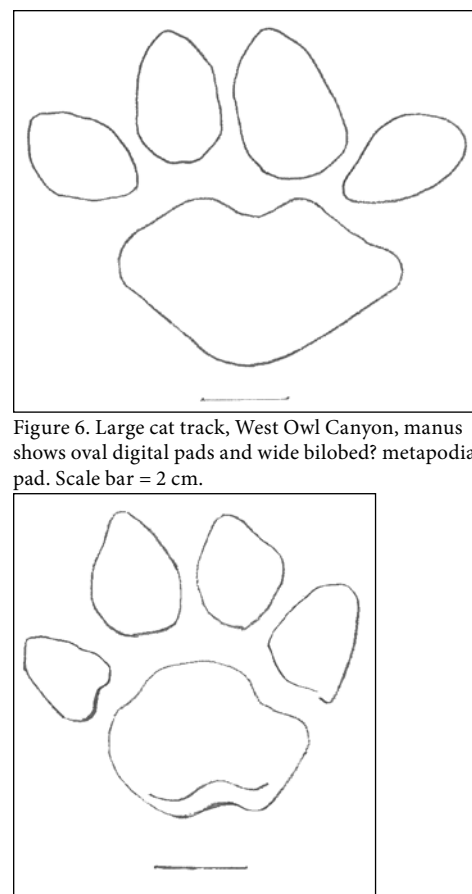


Figure 6. Large cat track, West Owl Canyon, manus shows oval digital pads and wide bilobed? metapodial pad. Scale bar = 2 cm.

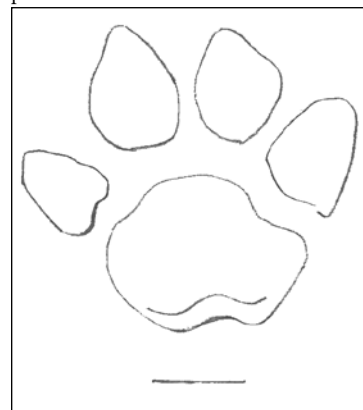


Figure 7. Medium cat track, Barstow Loop Apex, manus has oval digital pads and equidimensional bilobed metapodial pad. Scale bar = 2 cm.

ASSOCIATED FAUNA: Daggett Ridge Powerline locality (Loc. SBCM 1-109-2; Reynolds and others, 2010, 2011), associated medium size camel tracks.

Mud Hills West Owl Canyon, Barstow Formation, CA: medium cat tracks (Fig. 5a, 5b)

DESCRIPTION: manus (6.5 cm length x 7 cm width) and pes (6.5 cm length x 6.0 cm width).

METAPODIAL PAD: manus bilobed, pes trilobed; Digits: manus oval, pes circular, separate from metapodial pad.

AGE: Early Barstovian (Ba 1), 15 Ma.

ASSOCIATED FAUNA: Barstow, Second Division Fauna (Reynolds, 2004; Pagnac, 2009; Woodburne and Reynolds, 2010); associated large cat tracks and medium-size camel tracks.

Mud Hills, West Owl Canyon, Barstow Formation, CA: large cat tracks (Fig 6)

DESCRIPTION: manus (8 cm length x 10 cm width).

METAPODIAL PAD: manus bilobed; Digits: manus oval, separate from metapodial pad.

AGE: Early Barstovian (Ba 1), 15 Ma.

ASSOCIATED FAUNA: Barstow, Second Division Fauna (Reynolds, 2004; Pagnac, 2009; Woodburne and Reynolds, 2010); associated medium cat tracks and medium size camel tracks.

Mud Hills, Rainbow Loop Apex, Barstow Formation, CA: medium cat tracks (Fig. 7)

DESCRIPTION: manus (6.5 cm length x 6.7 cm width).

METAPODIAL PAD: manus bilobed; Digits: manus oval, separate from metapodial pad.

AGE: Middle Barstovian (Ba 2), 14.5 Ma.

ASSOCIATED FAUNA: Barstow Fauna (Reynolds, 2004; Pagnac, 2009; Woodburne and Reynolds, 2010); associated medium size camel tracks.

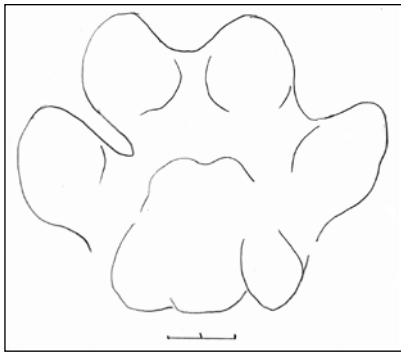


Figure 8. Large cat track, Enterprise Reservoir, manus shows oval digital pads and trilobed metapodial pad. Scale bar = 2 cm.

Figure 9 (right). Enterprise Reservoir large cat tracks paralleled by coyote-size tracks



**Enterprise Reservoir, unnamed strata, UT:
large cat tracks (Figs. 8, and 9)**

DESCRIPTION: manus (9 cm length x 11 cm width).

METAPODIAL PAD: manus bilobed; Digits: manus oval, separate from metapodial pad.

AGE: Early Clarendonian (Cl 1), 12–11? Ma.

ASSOCIATED FAUNA: unnamed fauna (Reynolds and Milner, 2007); associated coyote size tracks, several sizes and morphologies of camel tracks, rabbits, rodent, birds and impressions of grasses and invertebrate trails.

**Avawatz Mountains, Avawatz Formation, CA:
medium cat tracks (Fig. 10a, 10b)**

DESCRIPTION: manus (7.5 cm length x 7.2 cm width) and pes (7.5 cm length x 7.0 cm width).

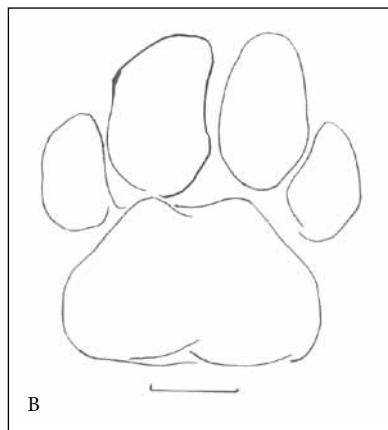
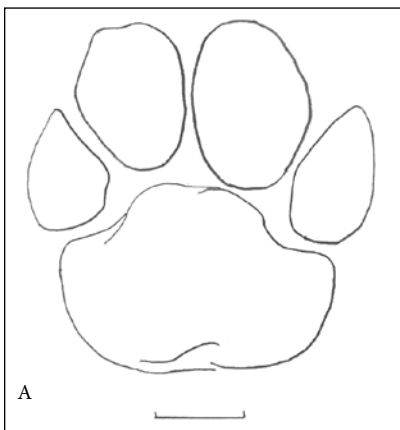


Figure 10a, b. Medium cat track, Avawatz Formation, manus (a) and pes (b) have oval digital pads and equidimensional bilobed metapodial pad. Scale bar = 2 cm.

METAPODIAL PAD: manus bilobed, pes bilobed; Digits: manus oval, separate from metapodial pad; pes oval, digit V oppressed.

AGE: Early Clarendonian (Cl 2), 12–10 Ma.

ASSOCIATED FAUNA: unnamed fauna (Reynolds and Whistler, 1990; Reynolds, 2004); associated camel tracks.

Death Valley, Copper Canyon Formation, CA: small cat tracks (Fig. 11a)

DESCRIPTION: manus (3 cm length x 3.5 cm width).

METAPODIAL PAD: manus bilobed; Digits: manus oval, separate from metapodial pad.

AGE: Middle Blancan (Bl III), 4.1–3.0 Ma.

ASSOCIATED FAUNA: medium size and large-size cat tracks and medium-size camel tracks (Scrivner and Bottjer, 1986; Santucci and Nyborg, 1999; Reynolds, 2004; Nyborg, and others, 2012).

**Death Valley, Copper Canyon Formation, CA:
medium cat tracks (Fig. 11b)**

DESCRIPTION: manus (6.0 cm length x 6.8 cm width); (7 cm x 6.2 cm: RAM v.94276/105; Manus paratype of *Felipeda scrivneri*, Sarjeant and others, 2002). Pes (7.5 cm x 6.0 cm: RAM V.94276/103, Holotype; RAM V.94276/104, paratype of *Felipeda bottjeri*; Sarjeant and others, 2002).

METAPODIAL PAD: manus trilobed; Digits: manus oval, digit V oppressed to metapodial pad.

AGE: Middle Blancan (Bl III), 4.1–3.0 Ma.

ASSOCIATED FAUNA: unnamed fauna (Scrivner and Bottjer, 1986; Santucci and Nyborg, 1999; Sarjeant and others, 2002; Reynolds, 2004; Nyborg, and others, this vol); Paratype of *Felipeda scrivneri* (Sarjeant and others, 2002); associated small and large cat tracks and medium size camel tracks.

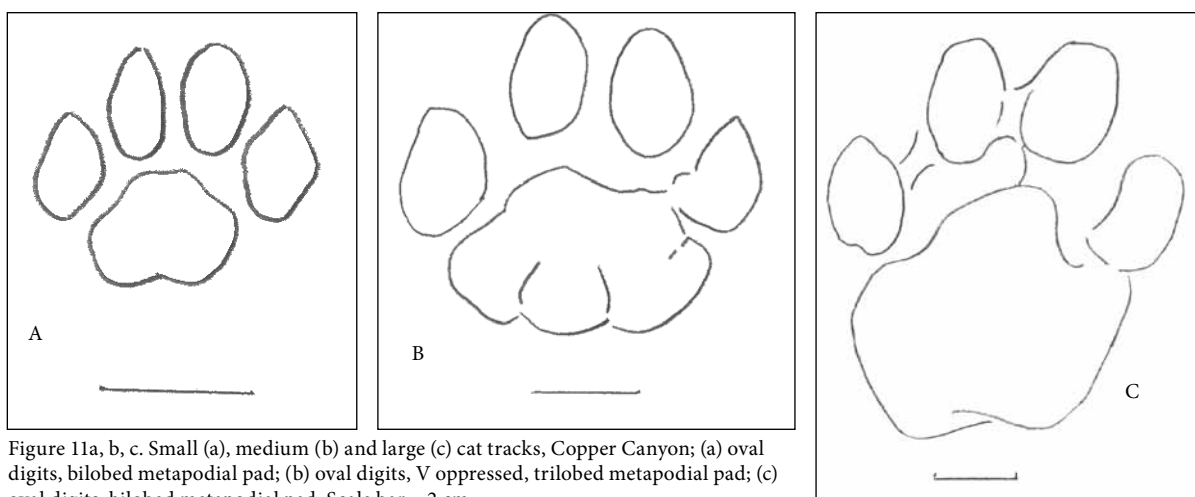


Figure 11a, b, c. Small (a), medium (b) and large (c) cat tracks, Copper Canyon; (a) oval digits, bilobed metapodial pad; (b) oval digits, V oppressed, trilobed metapodial pad; (c) oval digits, bilobed metapodial pad. Scale bar = 2 cm.

Death Valley, Copper Canyon Formation, CA:

large cat tracks (Fig. 11c)

DESCRIPTION: manus (10.6 cm length x 9.6 cm width; holotype: *Felipeda scrivneri*; Sarjeant and others, 2002); pes (Fig. 11c: 9.5 cm length x 8.5 cm width).

METAPODIAL PAD: manus trilobed?; Pes bilobed; Digits: manus and pes oval, digit V of manus and pes oppressed to metapodial pad.

AGE: Middle Blancan (Bl III), 4.1–3.0 Ma.

ASSOCIATED FAUNA: unnamed fauna (Scrivner and Bottjer, 1986; Santucci and Nyborg, 1999; Sarjeant and others, 2002; Reynolds, 2004; Nyborg, and others, 2012); these may represent large specimens of *Felipeda scrivneri* (Sarjeant and others, 2002); associated medium and small cat tracks and medium size camel tracks.

Fish Creek Wash, Olla Formation, CA: medium cat tracks (Fig. 7 in Remeika, 1999)

DESCRIPTION: manus (5.3 cm length x 6.1 cm width; holotype: *Pumaeichnium milleri*, Figs. 6, 7 in Remeika, 1999); pes (5.8 cm length x 6.3 cm width).

METAPODIAL PAD: manus trilobed; digital pads of manus oval.

AGE: Late Blancan (Bl IV), 2.8 Ma.

ASSOCIATED FAUNA: unnamed (Remeika, 1999); associated tracks of small canid, camel, horse and bird tracks.

Discussion

The stratigraphic distribution in correlation to size range of cat tracks through early Neogene time (Table A) suggests that medium size cats are persistent through time in the environment where cat tracks are preserved, presumably damp playa or riparian environments (Nyborg and others, 2012). Large cats that left tracks may be less dependent on such environments, or food procurement strategies caused them to visit these kinds of

Table A Temporal range of small, medium and large cat tracks

| Age (Ma) | Locality | Small Cat | Medium Cat | Large Cat |
|--------------------|----------------------|-------------------|-----------------------|------------------------|
| He1: 18.8–17.5 Ma | | | | |
| He2: 17.5–16.0 Ma | Daggett Ridge | | 6 cm l. x 7 cm w. | |
| Ba1: 16–14.8 Ma | West Owl Canyon | | 6.5 cm l. x 7cm w. | 8 cm l. x 10 cm w. |
| Ba2: 14.8–12.5 Ma | Loop Apex | | 6.5 cm l. x 6.7cm w. | |
| Cl1: 12.5–12 Ma | Enterprise Reservoir | | | 9 cm l. x 11 cm w. |
| Cl2: 12–10 Ma | Avawatz Fm | | 7.5 cm l. x 7.2 cm w. | |
| Cl 3: 10–9 Ma | | | | |
| Hh1: 9.0–8.6 Ma | | | | |
| Hh2: 8.6–7.6 Ma | | | | |
| Hh3: 7.6–5.9 Ma | | | | |
| Hh4: 5.9–4.9 Ma | | | | |
| Bl I: 4.9–4.62 Ma | | | | |
| Bl II: 4.62–4.1 Ma | | | | |
| Bl III: 4.1–3.0 Ma | Copper Canyon | 3cm l. x 3.5cm w. | 6.0 cm l. x 6.8 cm w. | 10.6 cm l. x 9.6 cm w. |
| Bl IV: 3.0–2.5 Ma | Fish Creek Wash | | 5.3 cm l. x 6.1 cm w. | |
| Pleistocene | | | | |

environments less frequently. The stratigraphic record for small cats suggests that they evolved recently to fill empty habitat niches that became available due to climatic and structural changes at the end of the Neogene (Martin, 1998b, Fig. 13.4). These trends, however, are subject to revision as more cat tracks are discovered and reported.

The somewhat plantigrade *Barbourofelis* (Cl1–Hh3; Martin, 1998a) may have left large tracks with an elongate metapodial pad (R. Tedford, pers. comm. to R. Reynolds, 2002). Such an impression might appear similar to the feloid(?) track morphology of *Quiritipes impendens*, a possible late Eocene Nimravinae (Sarjeant and others, 2002; fig. 4). No early Neogene tracks with this description have been located and are not discussed herein.

Generic names of the makers of cat tracks can be suggested by reviewing the available literature. The only generic choice for Barstovian medium cats is the puma-size cat *Pseudailurus* (Martin, 1998b). In the middle to late Blancan, the best choice for a large cat is one of the Machairodontinae, since *Barbourofelis* is extinct and *Pseudailurus* probably is also (Martin, 1998a, 1998b).

The small cat from the Blancan of Copper Canyon in Death Valley, California was slightly larger than an average-sized living domestic cat, and warrants interest since small cat skeletal remains are absent in the fossil record until latest Blancan time. Skeletal remains of felids smaller than *Lynx rufus* have been recovered from the Hueso Formation at Anza Borrego Desert State Park between 9–1.5 Ma (L. Murray, pers. comm. to R. Reynolds, 2012).

The medium-size cat print is the size of a modern bobcat (*Lynx rufus*; Murie, 1982). The earliest fossil record of *Lynx* sp. is from the late Hemphillian (Martin, 1998b). However, a similar size genus, *Nimravides* sp. (Felinae, not Nimravinae) is known from skeletal remains in the late Barstovian (Martin, 1998b). In the Barstow Formation of the Mojave Desert, *Nimravides* sp. occurs at the level of the Hemicyon Tuff (14.09 Ma) (Reynolds, 2004; Browne, 2005; Pagnac, 2009).

The medium cat tracks increase slightly in size (15%) through time from latest Hemingfordian to Blancan, but do not appear to change in morphology (Figs. 4, 5, 7, 11b). Since body fossils of small cats are not recorded from the start of the late Hemingfordian (He2) to the late Barstovian (Ba2), a period of 3.5 mya, the tracks probably indicate that *Nimravides* sp. was present in western North America in latest Hemingfordian time, two million years before skeletal remains have been reported.

The Blancan Copper Canyon medium cat track (Santucci and Nyborg, 1999, Appendix A, p. 25; Reynolds, 2004) has a trilobed metatarsal pad in the manus, different from the Barstovian and Clarendonian medium cat tracks. The Blancan medium cat tracks do not necessarily extend the range of *Nimravides* sp., but might represent another felid with similar locomotory habits. A similar size cat, *Lynx rufus*, is present as body fossils at this time.

By late Blancan time, there were a number of genera that could have made the medium size tracks in Fish Creek Wash at Anza-Borrego. These include *Puma*, *Miracinonyx*, *Dinofelis*, *Meganteron/Smilodon* and *Homotherium*.

ACKNOWLEDGEMENTS—The authors thank reviewers Don Lofgren, George Jefferson, and Lyn Murray for guidance with article preparation.

Volunteers from San Bernardino, the Riverside Metropolitan Museum, and the Mojave River Valley Museum, and L. Leggitt of Loma Linda University documented and replicated tracks from multiple Barstow Formation outcrops under the technical direction of Reynolds and Bob Hilburn.

The Enterprise Utah track site was discovered by Gary Hunt and Jared Brinton. Under NFS permit, thorough documentation was encouraged by Jim Kirkland, state paleontologist, and accomplished by volunteers from Utah Friends of Paleontology (Jerry Harris, B. and L. Baldazzi, T. Birthisel, D. Slauf,) and the Mojave River Valley Museum (R. Hilburn, D. Romero, J. Walkup). Site transect was performed by Utah Geologic Survey members J. Cavin, D. DeBlieux and S. Masters. St. George Dinosaur Discovery Site at Johnson Farm (SGDS) volunteers (B. Baldazzi, J. Brinton, S. Gibson, D. Whalen) helped with excavation of the felid/canid trackway.

Documentation of the Copper Canyon tracks was encouraged by Vince Santucci, NPS, and accomplished by volunteers under the direction of Torrey Nyborg, LLU.

Paul Remeika shared his recordation of cat tracks from Fish Creek Wash, Anza-Borrego Desert State Park.

Literature cited

- Browne, I. 2005. A case for reassignment the reassignment of the Barstovian Felid *Pseudaelurus marshi* to the genus *Nimravides*. *Journal of Vertebrate Paleontology*, Abstracts Vol. 25, (3 Suppl), p. 40A.
- Hulbert, R. C. 2010. A new early Pleistocene tapir (Mammalia: Perissodactyla) from Florida, with a review of Blancan tapirs from around the state. *Bulletin of the Florida Museum of Natural History* 49(3), p. 67-126
- Johnson, W.E., E. Eizirik, J. Pecon-Slattery, W. J. Murphy, A. Antunes, E. Teeling, and S. J. O'Brien. 2006. The Late Miocene radiation of modern Felidae: A genetic assessment (abstract). *Science* 311 (5757), p. 73–77.
- Martin, L. D., 1998a. Nimravidae, Chapter 12, p. in *Evolution of Tertiary Mammals of North America*, C. M. Janis, K. M. Scott, and L. L. Jacobs, ed. Cambridge University Press, N. Y., Vol. I, p. 228-236.
- Martin, L. D., 1998b. Felidae, Chapter 13, in *Evolution of Tertiary Mammals of North America*, C. M. Janis, K. M. Scott, and L. L. Jacobs, ed. Cambridge University Press, N. Y., Vol. I, p. 236-242.
- Murie, O. J., 1982. *A Field Guide to Animal Tracks*. Peterson Series, Houghton Mifflin Co. New York. 375p.
- Nyborg, T., and H. P. Buchheim. 2005. Age constraints of the Copper Canyon Formation, Death Valley, California.

- California State University Desert Symposium volume, 2005, p. 79-81
- Nyborg, T., P. Buchheim and K. E. Nick. 2012. Age, stratigraphy, depositional environment and vertebrate ichnology of the Pliocene Copper Canyon Formation, Death Valley, California. California State University Desert Symposium, this volume.
- Pagnac, D. 2009. Revised large mammal biostratigraphy and biochronology of the Barstow Formation (Middle Miocene), California. University of California Museum of Paleontology, *PaleoBios* 29(2), p. 48-59.
- Remeika, P. 1999. Identification, stratigraphy, and age of Neogene vertebrate footprints from the Vallecito-Fish Creek Basin, Anza-Borrego Desert State Park, California. SBCM Association *Quarterly* vol. 46(2) p. 37-45.
- Reynolds, R. E. 2002. Impressions: Late Tertiary mammalian footprints in various substrates. Abstract, *Jour. Vert. Paleontology*, vol. 22, (3 Suppl), p. 99A.
- Reynolds, R. E. 2004. Miocene cat tracks from the Mojave Desert of California. Abstract, *Jour. Vert. Paleontology*, vol. 24, (3 Suppl), p. 103A.
- Reynolds, R. E., D. M. Miller, M. O. Woodburne and L. B. Albright. 2010. Extending the boundaries of the Barstow Formation in the central Mojave Desert. California State University Desert Symposium Proceedings, p. 148-161
- Reynolds, R. E., D. M. Miller, M. O. Woodburne and L. B. Albright. 2011. Geographic extent of the Barstow Formation: central Mojave Desert. Abstract, *Jour. Vert. Paleontology*, vol. 31, (6 Suppl): p. 107A.
- Reynolds, R. E., and D. P. Whistler. 1990. Early Clarendonian faunas of the eastern Mojave Desert, San Bernardino County, California. SBCMA *Special Publication* 90-1, p. 105-107.
- Reynolds, R. E., and A. R. C. Milner. 2007. Preliminary description of mammal trackways from middle Miocene (Late Barstovian NALMA) Enterprise Reservoir sediments in southwestern Utah. In *Cenozoic Vertebrate Tracks and Traces*, S. Lucas, J. Spielmann and M. Lockley, ed.. New Mexico Museum of Natural History and Science, Bull 42. p. 261-266.
- Sarjeant, W.A.S., R. E. Reynolds and M. M. Kissell-Jones. 2002. Fossil creodont and carnivore footprints from California, Nevada, and Wyoming. CSU Fullerton Desert Symposium Volume and Proceedings, p. 37-50.
- Santucci, V. L., and T. G. Nyborg. 1999. Paleontological resource management, systematic recording, and preservation of vertebrate tracks within Death Valley National Park, California. San Bernardino County Museum Association *Quarterly*, vol. 46(2), p. 21-26.
- Scrivner, P. J. and D. J. Bottjer. 1986. Neogene avian and mammalian tracks from Death Valley National Monument, California: their context, classification and preservation. *Palaeogeography, Palaeoclimatology, Palaeoecology*, vol. 56, p. 285-331.
- Tedford, R. H., L. B. Albright, A. D. Barnosky, I. Ferrusquia-Villafranca, R. M. Hunt, Jr., J. E. Storer, C. C. Swisher III, M. R. Voorhies, S. D. Webb, and D. P. Whistler. 2004. Mammalian biochronology of the Arikareean through Hemphillian interval (late Oligocene through early Pliocene epochs). In *Late Cretaceous and Cenozoic Mammals of North America: Biostratigraphy and Biochronology*, M.O.Woodburne, ed. New York, Columbia University Press, p. 169-231
- Turner, A., and M. Antón. 1997. *The Big Cats and their Fossil Relatives*. Columbia University Press, New York, 234 p.
- Woodburne, M. O. and R. E. Reynolds. 2010. The mammalian litho- and biochronology of the Mojave Desert Province. CSU Fullerton Desert Studies Symposium, Proceedings, p. 124-147.
- Wozencraft, W. C. 2005. Order Carnivora. In *Mammal Species of the World: A Taxonomic and Geographic Reference* (3rd ed.), D. E. Wilson and D. M. Reeder, ed. Baltimore, Johns Hopkins University Press, p. 545-548

Fumaroles exposed by the dropping Salton Sea level

David K. Lynch,¹ Kenneth W. Hudnut,¹ and Paul M. Adams²

¹USGS ²Thule Scientific

ABSTRACT—New field observations, aerial surveys, lidar measurements and laboratory studies of mud samples (2006 to 2011) are reported of several fumarole complexes that have recently or are currently being exposed as the Salton Sea level drops. The main NE striking field is irregular in outline and is roughly 400 meters long and 120 meters wide. It consists of hundreds of warm to boiling hot gryphons (mud volcanoes), salses (mud pots), and countless active gas vents. Unusual shaped mud volcanoes in the form of vertical tubes with central vents were observed in many places. Since being exposed, the surface morphology has changed dramatically, the trend being towards growing gryphons, enlarging mud pots and the development of sulfur vents in 2011. Mud from several gryphons was analyzed and contained the ammoniated sulfate minerals boussingaultite and lecontite as well as other more common sulfates. With other geothermal features, the fumaroles fall along a well-defined northwest-striking lineament marking the probable trace of the Calipatria fault. A model for the development of gryphons is presented.

I. Introduction

Mud volcanoes are dynamic, topographically positive structures formed by the upward migration of fluidized sediment driven by subsurface over-pressure gas that forces viscous mud upward through a narrow vent (Ives 1951; Jakubov et al. 1971; McDonald 1982; Hovland et al. 1997; Delisle et al. 2002; Etiopie et al. 2005; Kopf 2008; Mazzini et al. 2009a&b, 2011; Planke et al. 2003; Martinelli and Panahi 2003; Bonini 2008, 2009; Svensen et al. 2009; Onderdonk et al. 2011). Mud is extruded

or ejected and accumulates around the vent creating a conical feature, mechanically analogous to igneous volcanoes. Though some can be hundreds of meters high, mud volcanoes on land smaller than about 2 m in height are called *gryphons*. On the earth's surface where water is abundant, bubbling water sometimes stands in the calderas of gryphons, where they are termed *salses*. Gryphons and salses may be "hot" (steaming) or "cold" (not steaming).

Geothermal gryphons and salses are associated with fumaroles and large geothermal gradients caused by relatively shallow magma bodies. The most common gasses emitted by fumaroles are CO₂, H₂O, SO₂, H₂S, NH₃, and CH₄ (Dimitrov 2002). Mud volcanoes are relatively rare geological structures and tend to occur at active plate margins (Martinelli and Panahi 2003; Dimitrov (2002).

The Salton Sea Geothermal Field of Imperial County, California (Figure 1) has a large geothermal gradient (Younker et al. 1982) and is well known for its gryphons and salses, particularly those at the northeast corner of Davis and Schrimpf roads (DS). These have been extensively studied (Helgeson 1968; Sturz et al. 1992, 1997; Svensen et al. 2007, 2009; Mazzini et al. 2009a&b, 2011; Manga and Rudolph 2009; Rudolph and Manga 2010; Onderdonk et al. 2011) and are representative of the mud and gas extrusions in the area. There are other nearby gryphons and salses (Lynch and Hudnut 2008) and recently, the Salton Sea's dropping water level has exposed several more fumarole fields that are the subject of this paper. Table 1 lists the locations

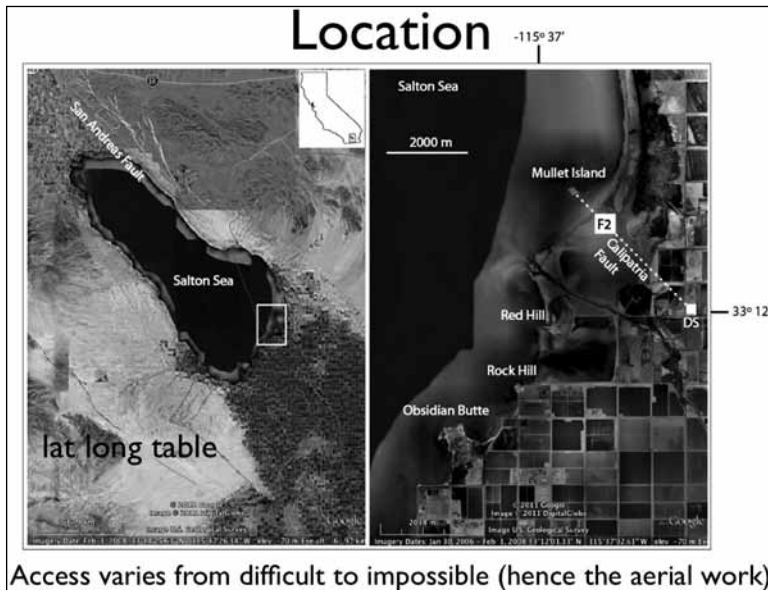


Figure 1. Maps of the region of study, in extreme southeastern California. The left hand part of the figure shows a Google Earth map with the Qfaults data overlaid. The long straight red line across the southeastern part of the Salton Sea is the approximate centerline of the Brawley Seismic Zone and defines the axis of the Salton Sea Geothermal Field. The white rectangle outlines the right hand figure, which shows the Salton Buttes, Calipatria Fault and the Davis-Schrimpf fumarole field (DS) along with the location of F2, the largest fumarole field discussed in this paper.

Table 1. Locations of known vent fields in the area.

| Name | Latitude | Longitude | ~ Size (m) | Comment (13 Oct 2011) |
|------|-----------|------------|------------|--|
| F1 | N 33.2210 | W 115.6036 | 25 x 50 | Hot, exposed, surroundings dry |
| F2 | N 33.2184 | W 115.6011 | 120 x 400 | Hot, exposed, surroundings dry |
| F3 | N 33.2135 | W115.5931 | 30 x 50 | Hot, exposed, many salses, surroundings wet, muddy |
| F4 | N 33.2150 | W 115.5937 | 50 x 60 | Partially exposed, many salses, a few gryphons, not steaming |
| F5 | N33. 2122 | W115.5951 | 100 x 100 | Underwater, many vents flowing mud, not steaming |
| F3N | N 33.2141 | W 115.5935 | | Possible vent field, under water, not steaming |
| F3S | N 33.2126 | W115.5931 | | Possible vent field, under water, not steaming |

Figure 2 (below). Aerial (top) and ground (bottom) photographs of F1 and F2.

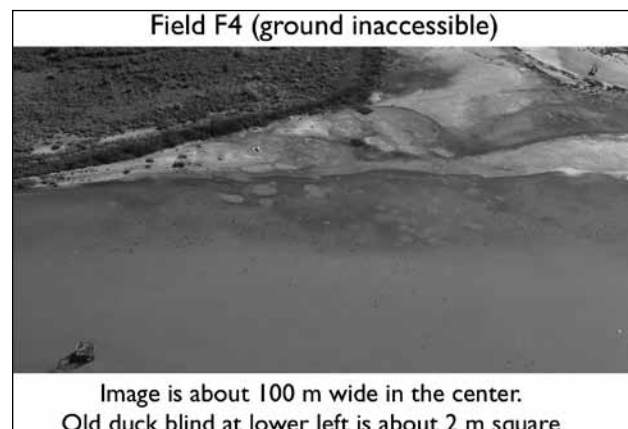
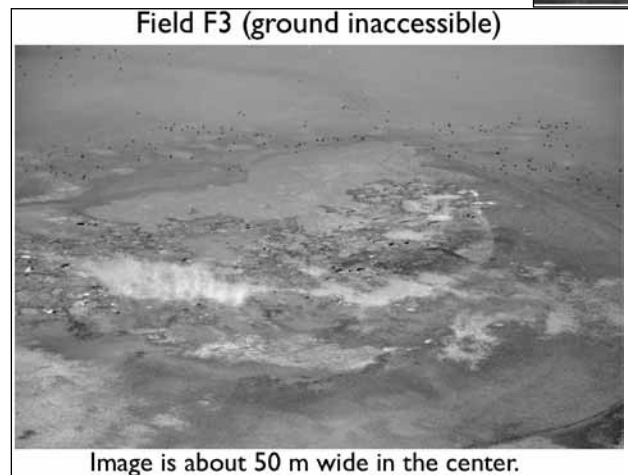
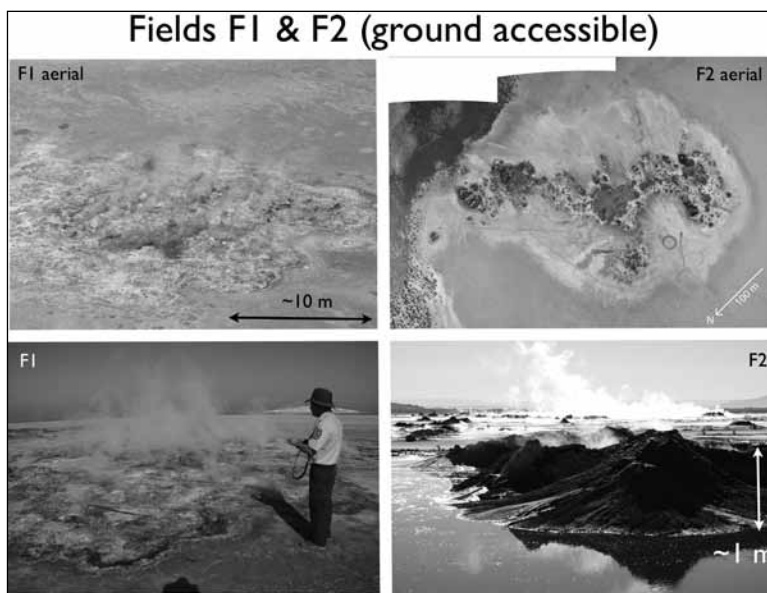
and properties of the larger fumaroles fields, labeled F1 through F5.

2. Ground and aerial images

Two of the fumarole fields, F1 and F2 (Figure 2), are accessible on foot, though with significant difficulty. Both are boiling hot, contain gryphons and salses, sulfur vents and emit noxious gasses. Owing to mud and water, F3, F4 and F5 are inaccessible by foot (Figures 3, 4, 5) respectively.

3. Results

F1 and F2 sit on a nearly flat, slightly elevated sand spit roughly 1000 m x 1200 m oriented with the long axis striking ~N45E. This



mound was probably produced by mud extruded from below the surface by rising CO₂ and then deposited more or less uniformly in all directions. During Nov 2010, a lidar survey of the Salton Sea shoreline and environs was carried out by Dewberry, Inc (2011) from an elevation of 800 m AGL (nominal). At this time the highest part of the F2 grade was less than 0.5 m above the Salton Sea

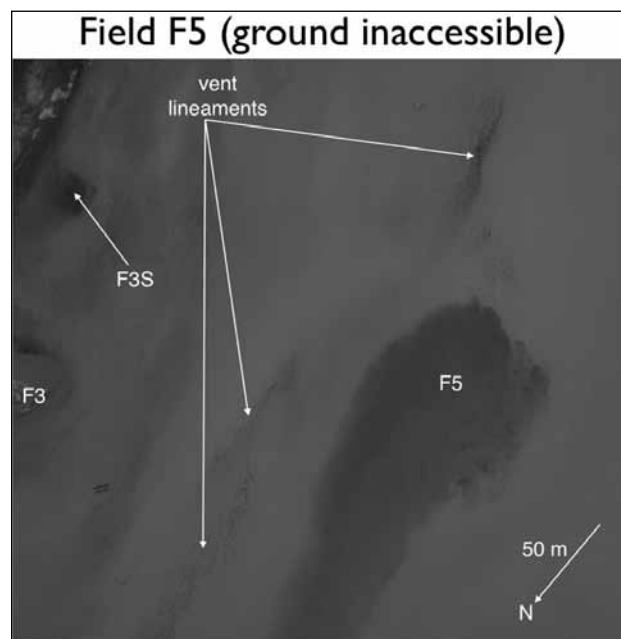


Table 2 – Samples from September 2011

| Name | Setting | Composition |
|---------------|-------------------|--|
| F2-1 | sulfur vent | sulfur, quartz, calcite |
| F2-2 | sulfur vent | sulfur, gypsum |
| F1-1 | sulfur vent | sulfur, quartz |
| F2 Background | 33.2172 -115.6028 | halite, quartz, glauberite Na ₂ Ca(SO ₄) ₂ |
| F2 Rind | 33.2174 -115.6026 | halite, quartz, gypsum, calcite |

Table 3 – Samples from October 2011

| Name | Location | Composition |
|-------------------|--------------------------------------|--|
| S1-1 | Salse S1 in F2 33.217-115.60124 | gypsum, quartz, minor bassinite 2CaSO ₄ •(H ₂ O) & halite |
| S1-2 | " | halite, gypsum, anhydrite CaSO ₄ , quartz |
| S1-3 | " | sulfur, minor quartz & gypsum |
| S1-4 | " | boussingaultite (NH ₄) ₂ Mg(SO ₄) ₂ •6(H ₂ O), thenardite Na ₂ (SO ₄), minor quartz & lecontite (NH ₄ ,K)Na(SO ₄)•2(H ₂ O) |
| S1-5 | " | Sulfur, minor quartz & gypsum |
| S5-1 | Salse S5 in F2 33.21954-115.59950 | quartz, halite, calcite |
| S5-2 | Salse S5 33.21954 -115.59950 | quartz, halite, minor calcite & bloedite Na ₂ Mg(SO ₄) ₂ •4(H ₂ O) |
| S vent rind | Sulfur vent in F1 | gypsum, quartz, minor bassinite & halite |
| S vent background | Near sulfur vent in F1 | quartz, glauberite Na ₂ Ca(SO ₄) ₂ , halite, minor calcite & dolomite |

water level and fell off gradually in all directions. This surface represents the naturally-exposed Salton Sea floor. Neither lidar nor field inspection revealed any evidence of tectonic features such as scarps, ridges or offset channels.

F2 is by far the most extensive fumarole field in the region. The country sediment of the sand spit (Tables 2 and 3) was medium brown and soft, consisting of crusty quartz sand and feldspar cemented by evaporates that

overlaid very fine grained dark gray mud. Immediately surrounding F2 is a “rind” of lighter colored material 30–100 m wide that is rich in evaporite effluent from the gryphons. This region showed flow patterns indicative of aqueous material flowing radially away from the elevated gryphon field, primarily to the NE where the surface slope is largest. Assuming

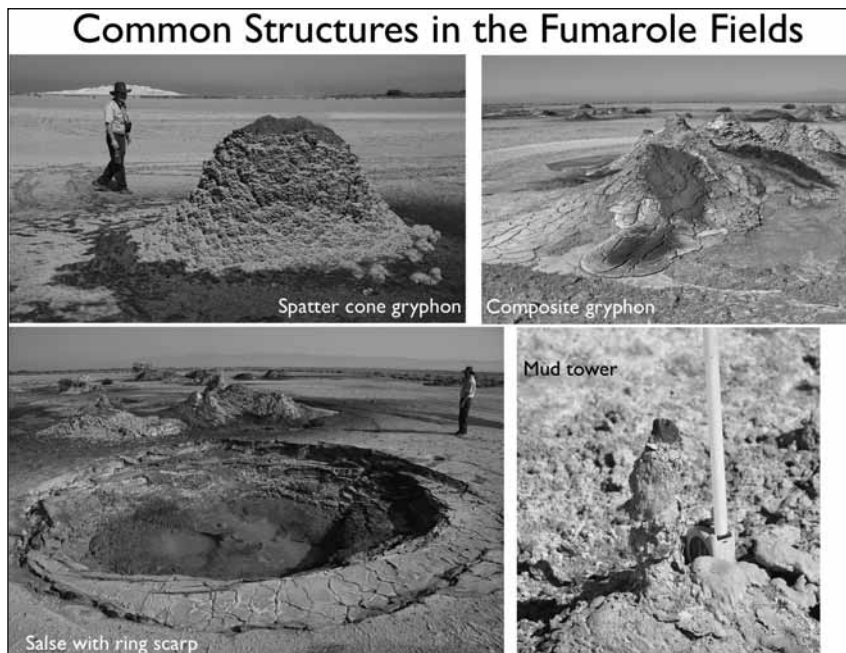
that the rind represents surface deposits from evaporates extruded from the gryphons, its slight elevation is strongly suggestive of a net upward mass transport of subsurface material.

Near the gryphons, the ground was warm or hot to the touch, and caution was necessary to prevent breaking through the surface. In many places, hot mud (~100° C) was only a few cm below the surface. Owing to the shallow water table, the region was muddy and wet, making walking difficult and in some

cases impossible. As a result, few if any of the gryphons could be approached for hands-on examination.

The gryphons’ morphologies are almost completely analogous to those of igneous volcanoes and we will adopt the corresponding terminology. Gryphons showed a range of shapes including steep-sided “spatter cones”, and less steeply sided “composite” gryphons (Figure

6). Their eruption mechanisms also appeared to be analogous to conventional volcanoes. Strombolian-like eruptions produced spatter cones. Effusive eruptions formed composite gryphons of mud extruded from the central and side vents that flowed down the flanks. Somma gryphons were common (caldera within a caldera). Owing to time-variations in the gas and water content of the mud, or differences in subsurface conduits, some gryphons showed both spatter cones and composite surfaces. Large gryphons of both types were usually surrounded by a roughly circular, depressed area filled with water, a moat-like structure. In every case, composite gryphons had smaller flank slopes than spatter cones.





Composite gryphons ranged in size from a few cm to up to 10 m across. Some were single structures, others were composed of several gryphons that grew and merged with other composites. Spatter cone gryphons were numerous, some exceeding 1.8 m in height and almost invariably symmetric about a single central vent. Explosive release of gas propelled viscous mud clasts from the vent that fell onto the flanks or onto the surrounding ground where a dark ejecta blanket was evident. The largest spatter cones were steep sided, some exceeding 45°. Smaller and presumably younger spatter cones had smaller flank slopes. Many older spatter cones displayed Gaussian-like profiles (Figure 6).

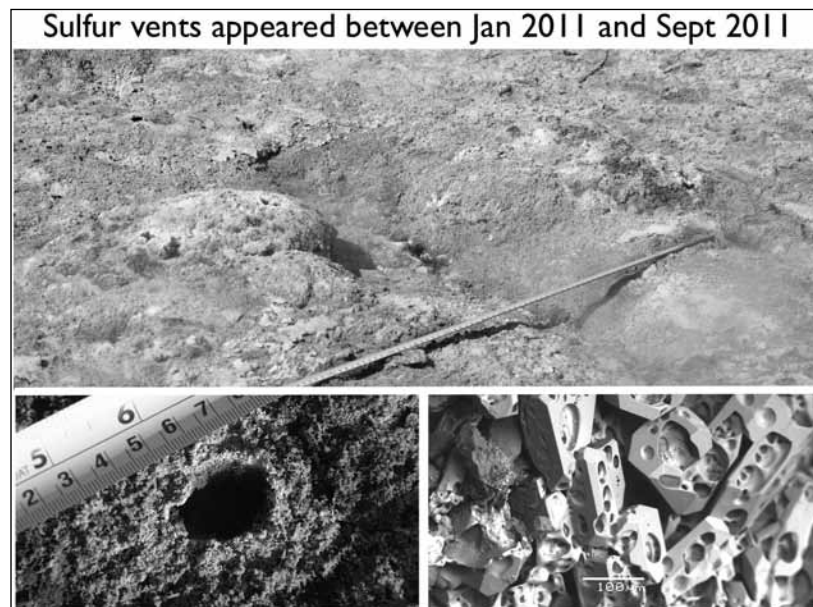
F2 showed hundreds of unusual gryphons that we called *mud towers*, tall, slender tubes with vertical sides and central vents emitting hot gas and relatively inviscid mud (Figure 6). They ranged in height from a few cm to over 0.5 m, and were between 3 and 20 cm thick. Isolated mud towers were the most common, but many were also formed inside or atop composite gryphons. To our knowledge these mud towers are unique to this fumarole field; we are unaware of similar structures being reported anywhere in the world. Such mud towers were reported at what we believe to be at the same location in 1857 by Veatch (1860).

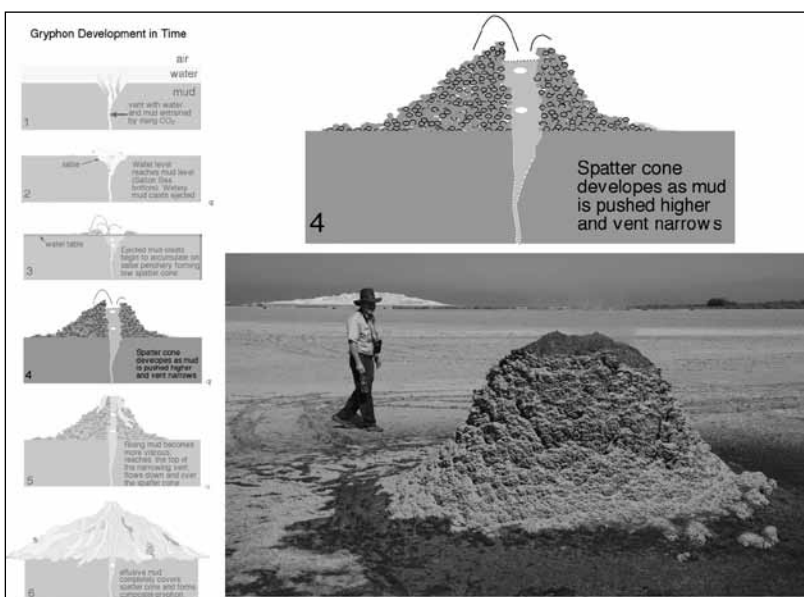
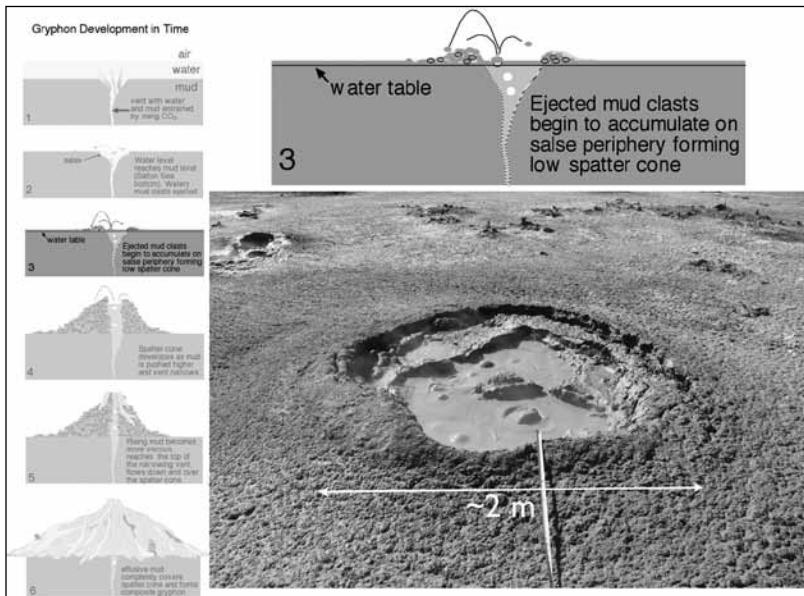
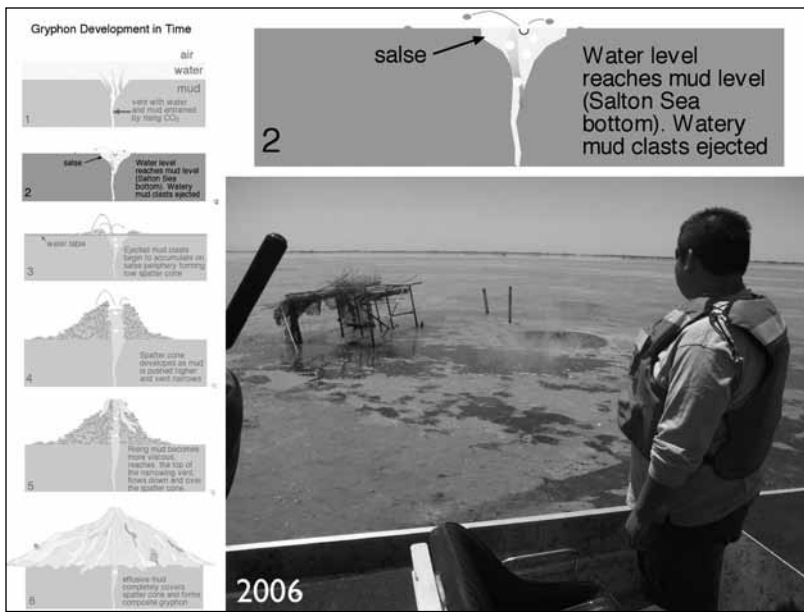
Salses were common and most contained bubbling water and dark gray mud (Figure 6). Their sizes ranged from a few cm to over 20 m. Many were circular, others were irregular in shape owing to merging with nearby mud pots. Most were steaming. A few were sufficiently wet and active that bursting bubbles threw mud clasts beyond their edges.

4. Time evolution

The formation and growth of gryphons was observed episodically for five years. We visited F2 on 8 June 2007 when most of it was still beneath a few cm of water. At this time the Salton Sea water diluted the upwelling mud, making it relatively inviscid. As a result, the mud had little compressive strength and could not sustain significant vertical growth. Currents in the Salton Sea washed away newly emergent mud, thereby further preventing any upward advancement. We also visited F1 and F3 when they were still under water and neither of them showed steam clouds. Presuming that they were hot in 2007, the absence of steam clouds suggests that the hot gas was cooled and/or absorbed by the overlying water. It is therefore possible that F5, F3N, F3S and perhaps others will begin to show steam clouds when the water level has dropped enough.

After exposure, the fumarole fields evolved rapidly. Between April and Aug 2010, the surface coloration and mud flow patterns showed significant changes. Even between Jan 18 and 26, 2011, there were marked visual alterations in F1, notably the amount of algae, and the color and shape of surface deposits. Pictures taken in 2011 documented marked growth of gryphons and salses. The evident trend was to larger, more massive gryphons and larger salses (Figure 7). Such development suggests that there was a net upward flux of mud, rather than continuous recycling of mud like what seems to be happening at DS (Onderdonk et al. 2011). Indeed, recent plant growth in the immediate vicinity of the fumaroles – especially evident at F1 – is compelling evidence that water





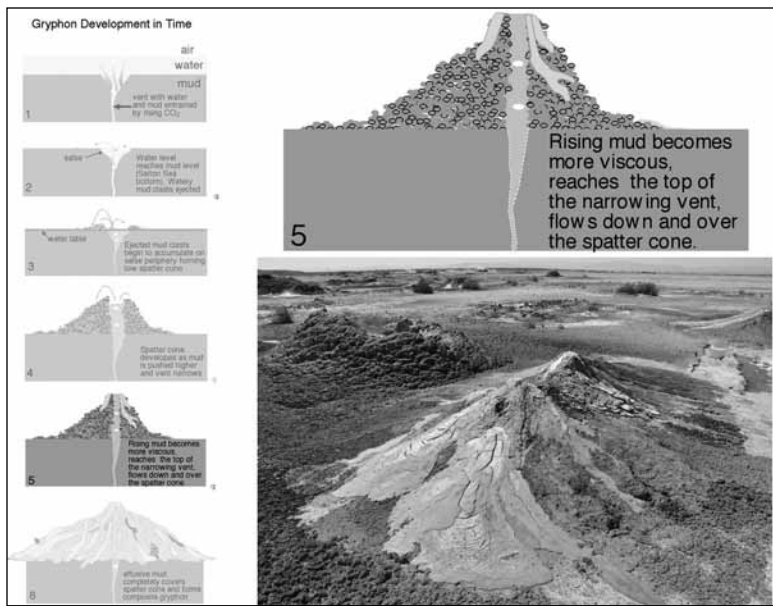
and mud are being raised to the surface. Owing to the impossibility of directly approaching and measuring F2's gryphons, we cannot quantify the amount of growth in most cases.

In September 2011, Schoneman (private communication) reported what he believed to be a sulfur vent at F2. Subsequent inspection by the authors a few days later confirmed Schoneman's observations, and further revealed dozens of such vents in F1 and F2 (Figure 8). The vents were discrete and found in groups on slightly elevated structures, some on gryphons, others being more or less isolated. They were typically a few cm across and with a periphery of yellow or greenish-yellow opaque, bladed or acicular sulfur crystals less than two mm long. In most cases the vents were expelling hot gas, some audibly. In view of the evident greenish tinge to the sulfur, we surmised that they were primarily orthorhombic α - S_8 crystals, a result later confirmed by laboratory analyses.

We did not notice sulfur vents in F1 and F2 in January 2011, although upon reviewing our photographs, a small number might have been present. In view of the large number of such vents observed in September 2011, it is clear is that a great many of them formed during the eight month period. The relatively sudden appearance or rapid increase in the number of sulfur vents could mean one of two things: 1) There was a fundamental change in the subsurface plumbing, chemistry or both, or 2) Sulfur vent development is a normal occurrence as gryphons and salses develop after emergence water, somehow mediated or controlled by a combination of temperature, water level and subsurface chemistry.

5. Model of gryphon time evolution

Based on observations at F2 and F3 and the Davis-Schrimpf fields, we believe that gryphons near the Salton Sea develop progressively through several stages as the water table drops, the above-grade vent narrows, and the entrained mud becomes more viscous. We have sketched this development in Figures 9–12. The gryphons shown as examples are not the same gryphon evolving over time, but rather



6. Tectonic implications

The locations of the Davis-Schrimpf field, F1, F2, F3 and Mullet Island fall on or cluster about a virtually straight line (Figure 14), an almost certain indication of a fault. This is probably the Calipatria fault, a feature that has been previously discussed (Lynch and Hudnut 2008). This and other putative faults in the area strike N45W, more or less parallel to the controlling San Andreas and Imperial faults. The Salton Buttes clearly volcanic in origin and therefore likely to originate at a spreading center fall along a curved arc that strikes ~N25E. The line of volcanoes meets the fumarole fields (Calipatria Fault) at a 50 degree angle, far from the expected >90 degrees for a spreading center-transform fault angle (Atwater and Macdonald 1977). While we may be seeing evidence of the junction of a spreading center and its associated transform

different ones that we interpreted to be at various stages of development.

The time-sequence suggested here is based on observations of hundreds of gryphons and salses in the Salton Sea fields. Every stage has been observed many times, and no other type of gryphon was seen. The most telling stage of development (stage 5) has been observed on many gryphons where effusive flow is observed at the top of a spatter cone or beginning to slide down the flank. In no case was a spatter cone ever observed atop an effusive composite gryphon.

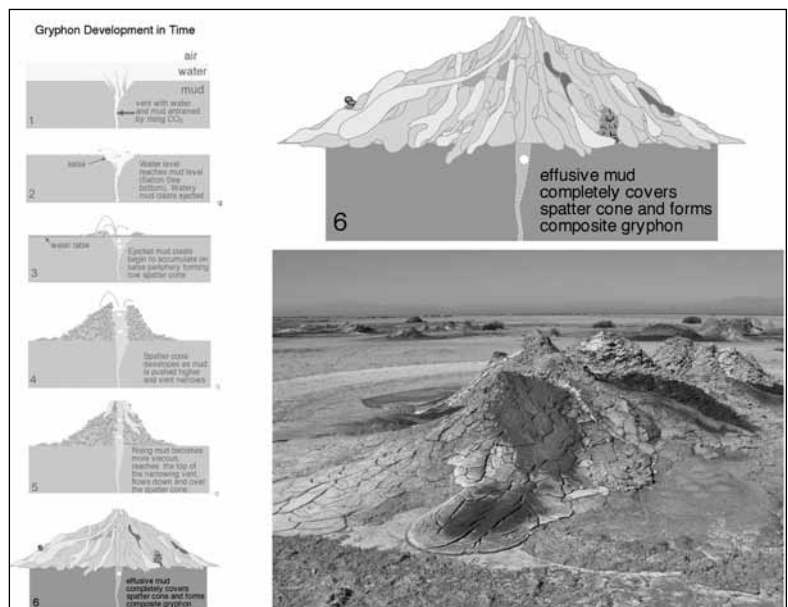
The presence of gryphons at F2 in every level of development is almost certainly a result of different gas/water/mud ratios. Although the development we have outlined is for a monotonically lowering water table level, variations from place to place can produce gryphons at different stages within the same fumarole field. Some gryphons may never evolve to stage 6; the underground plumbing may pinch off and render the gryphon extinct. Or the mud/water ratio may change, as it apparently did at several spatter cones at F1, which is presently just emitting gas, its mud growth having stopped some time ago. And not all salses will become gryphons; if the vent is particularly rich in water and poor in sediment, it can remain relatively unchanged. Indeed, Onderdonk et al. (2011) and others have noted the persistence of several salses at DS over many years.

As the Salton Sea level drops, we will have a good opportunity to watch gryphons form and see them at every stage of their growth. As of October 2011, F2 gryphons were at stage 1-6, while those at F3 are at stages 1 & 2. The gryphons at DS are all composite and in stage 6, where they have been for many years.

fault, the situation is clearly more complicated.

The fumaroles fall in the Salton Sea Geothermal Field and the Brawley Seismic Zone, the step over region between the SE end of the San Andreas fault and the NW end of the Imperial Fault, clearly an extensional structure of some sort (Muffler and White 1968, 1969; Robinson, Elders and Muffler 1976). Being at nearly the lowest part of the Salton Trough, it is not unreasonable to suppose that they are also nearest to the top of the magma body that is responsible for the large geothermal gradients in the area. In this regard, their high temperatures and extrusive activity is no surprise.

Yet the tectonic significance of the fumarole fields is unclear. On one hand, they represent the hottest, extrusive geothermal features in the Salton Trough and would seem to be related to the Salton Buttes that are only a few km away. On the other hand, they are very small compared to



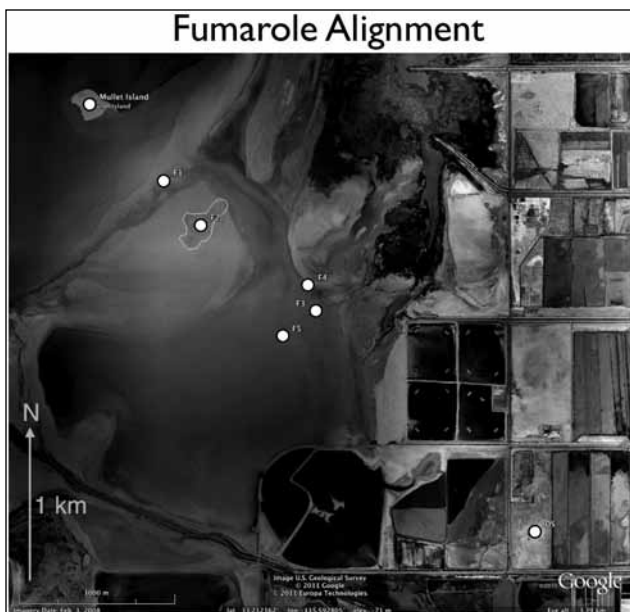


Figure 14. Google Earth image (2009) showing the locations F1, F2, F3 and the Davis-Schrimpf field (DS) as circles (from upper left to lower right, respectively) and the Salton Buttes as triangles. The fumarole fields fall along a straight line that intersects Mullet Island (upper triangle) and is indicative of a fault, probably the Calipatria fault.

the much larger Salton Trough (~150 by 30 km), a well-studied region that extends from Riverside County, CA USA into northern Baja & Sonora, Mexico. The trough contains the transition between the right lateral San Andreas transform fault system and the extensional basins of the East Pacific Rise.

If pull apart basins consist of alternating transform faults and spreading centers that are roughly perpendicular to each other, one might expect to find chains of NE and NW striking structures. NE striking features include the Salton Buttes, the 2005 Obsidian Butte swarm (Lohman and McGuire 2007), the Elmore Ranch faults and Kane Springs fault (Hudnut et al. 1989), the Holocene faults found by Brothers et al. (2009) beneath the Salton Sea and the long axis of F2. Mud pot lineaments (Lynch and Hudnut 2008), seismicity lineaments (Lin et al. 2007), Superstition Hills fault and Superstition Mountain fault (Hudnut et al. 1989) strike NW. In contrast, some seismic lineaments fall at oblique angles relative to NE and NW (Lohman and McGuire 2007). And the long axis of the BSZ strikes N22W (e.g. Lin et al. 2007 Figure 2) with a short segment striking N62E. Together these features indicate a complex region of transform faults and spreading centers, but do not portray a clear and coherent picture of the region's tectonics. The alignment of the fumaroles reported here adds further evidence for the existence of a fault overlying the shallow magma body, but adds little tectonic information to what is already known about the area.

7. Summary and conclusions

We have presented preliminary results on fumarole fields that have recently been exposed by the dropping Salton Sea level between 2006 and 2011. The interaction between mud, water and gas in a desert environment, coupled with a high geothermal gradient has produced large variety of structures and phenomenology, including unusual chemistry and mineralogy. This work began before any gryphons at F1, F2, F3 and F4 were present and ended during an intermediate development stage, before most of them reached a steady state configuration like the mature gryphons and salses at the Davis-Schrimpf field. Of particular interest are the large number of spatter cones and the relatively sudden appearance of sulfur vents in 2011.

A number of sulfate minerals were found in and around the fumaroles, something not unexpected in view of the abundant sulfur vents. The presence of ammoniated sulfates such as boussingaultite and lecontite, however, is highly unusual in fumaroles, and is the result of agriculture in the area. Fertilizer run off and bacterial activity in the eutrophic waters of the undrained Salton Sea have caused high levels of ammonia to accumulate in the water and lake bottom sediments (Holdren and Montaño 2002). Ammonia is highly soluble in water and the aqueous environment affords an opportune setting for sulfur-ammonia chemistry.

Slow, secular changes in the vent fields over time could be altered by earthquakes. Many mud volcanoes' behavior is triggered by seismic activity (Mellors et al. 2007), including perhaps those in the Salton Sea Area (Rudolph and Manga 2010). Clearly, gryphons and salses are dynamic structures and their properties change over times, a challenging yet promising opportunity for researchers in the future.

The work reported here is only a first look at the fumaroles, and many questions remain. What is the composition of dissolved minerals in the water and emitted gas? How do they vary in space and time? What is the total gas flux and is it a significant contribution to greenhouse gases? What is the isotopic composition of the gas and can it be used to determine if the CO₂ is meteoric or originates from the mantle? Is the model we set forth for gryphon development applicable to those in other parts of the world? As the Salton Sea water level continues to drop as it surely will (Quantification Settlement Agreement 2003), how will the gryphons and salses change? With known vent fields still under water, we are presently in a good position to monitor them and watch gryphon development. Such observations would tell us more about how gryphons are formed and help refine the model set forth in Section 4.

ACKNOWLEDGEMENTS—We would like to thank Christian Schoneman of the US Fish and Wildlife Service for logistic support on various occasions. We are indebted to Brad Busch of Aspen helicopters for expert piloting and to John

R. Bayless of First Point Scientific for assistance during the July 2011 imaging flights. Howard Hall of Howard Hall Productions rendered valuable service in obtaining the October 2011 aerial photographs. Lee Case of the USGS provided the recent lidar data and M. Bonini made many valuable comments on an earlier draft of the paper. Danny Brothers and Kate Scharer of the USGS made many valuable comments on an early version of this paper. This work was supported in part by the Southern California Earthquake Center (SCEC).

References

- Atwater, Tanya and Ken C. Macdonald, 1977, Are spreading centers perpendicular to their transform faults? *Nature*, v. 270, 715-719.
- Bonini, M., 2008. Elliptical mud volcano caldera as stress indicator in an active compressional setting (Nirano, Pedemontane margin, northern Italy). *Geology* 36, 131-134.
- Bonini, M., 2009. Mud volcano eruptions and earthquakes in the Northern Apennines and Sicily, Italy. *Tectonophysics* 474, 723-735.
- Brothers, D., Driscoll, N., Kent, G., Harding, A., Babcock, J., Baskin, R., 2009. Tectonic evolution of the Salton Sea inferred from seismic reflection data. *Nature Geoscience* 2, 581 - 584 (2009) doi:10.1038/NGEO590.
- Delisle, G., von Rad, U., Andruleit, H., von Daniels, C.H., Tabrez, A.R., Inam, A., 2002. Active mud volcanoes on- and offshore eastern Makran, Pakistan. *Intl. J. Earth Sci.* 91, 93-110.
- Dewberry, Inc. 2011 "USGS Salton Sea LiDAR Project" USGS Contract: G10PC00013 Dewberry, 8401 Arlington Blvd. Fairfax, VA 22031-4666
- Dimitrov, L., 2002. Mud volcanoes- the most important pathway for degassing deeply buried sediments. *Earth Sci. Rev.* 59, 49-76.
- Etiopie, G., Feizullayev, A.A., Baciuc, C.L., Milkov, A., 2004. Methane emission from mud volcanoes in eastern Azerbaijan. *Geology* 32, 465-468.
- Helgeson, H., 1968. Geologic and thermodynamic characteristics of the Salton Sea geothermal system. *Am. J. Sci.* 266, 129-166.
- Holdren, G. C., and A. Montaño (2002), Chemical and physical characteristics of the Salton Sea, California, *Hydrobiologia*, 473(1-3), 1-21, doi:10.1023/A:1016582128235.
- Hovland, M., Hill, A., Stokes, D., 1997. The structure and geomorphology of the Dashgil mud volcano, Azerbaijan. *Geomorphology* 21, 1-15.
- Hudnut, K.W., Seeber, L. and Pacheco, J. (1989). Cross-fault triggering in the November 1987 Superstition Hills earthquake sequence, Southern California. *Geophysical Research Letters* 16(2): doi: 10.1029/88GL04147. issn: 0094-8276.
- Ives, R., 1951. Mud volcanoes of the Salton depression. *Rocks Miner.* 26, 227-235.
- Jakubov, A.A., AliZade, A.A., Zeinalov, M.M., 1971. Mud volcanoes of the Azerbaijan SSR. Atlas (in Russian). Azerbaijan Academy of Sciences, Baku.
- Kopf, A., 2002. Significance of mud volcanism. *Rev. Geophys.* 40, 1-52.
- Lin, G., P. Shearer, and E. Hauksson (2007). Applying a three-dimensional velocity model, waveform cross correlation, and cluster analysis to locate southern California seismicity from 1981 to 2005, *J. Geophys. Res.* 112, B12309.
- Lohman, R. B. and J.J. McGuire, Earthquake swarms driven by aseismic creep in the Salton Trough, California, *J. Geophys. Res.* 112, B04405, 10.1029/2006JB004596, (2007).
- Lynch, D., Hudnut, K., 2008. The Wister Mud Pot Lineament: Southeastward Extension of Abandoned Strand of the San Andreas Fault? *Bull. Seismol. Soc. Am.* 98, 1720-1729.
- Macdonald, K.C., 1982, Mid-ocean ridges: Fine scale tectonic, volcanic and hydrothermal processes within the plate boundary zone: *Annual Review of Earth and Planetary Sciences*, v. 10, p. 155-190.
- Manga, M., Brumm, M., Rudolph, M., 2009. Earthquake triggering of mud volcanoes. *Mar. Petrol. Geol.* 26, 1785-1798.
- Martinelli, Giovanni; Panahi, Behrouz (Eds.) Mud Volcanoes, Geodynamics and Seismicity. Proceedings of the NATO Advanced Research Workshop on Mud Volcanism, Geodynamics and Seismicity, Baku, Azerbaijan, 20-22 May 2003, NATO Science Series: IV: Earth and Environmental Sciences, Vol. 51
- Mazzini, A., Nermon, A., Krotkiewski, M., Podladchikov, Y., Planke, S., Svensen, H., 2009b. Strike-slip faulting as a trigger mechanism for overpressure release through piercement structures. Implications for the Lusi mud volcano, Indonesia. *Mar. Petrol. Geol.* 26, 1751-1765.
- Mazzini, A., Svensen, H., Planke, S., Guliyev, I., Akhmanov, G., Fallik, T., Banks, D., 2009a. When mud volcanoes sleep: Insights from seep geochemistry at the Dashgil mud volcano, Azerbaijan. *Mar. Petrol. Geol.* 26, 1704-1715.
- Mazzini, A., Henrik Svensen, Giuseppe Etiopie, Nathan Onderdonk and David Banks, 2011 "Fluid origin, gas fluxes and plumbing system in the sediment-hosted Salton Sea Geothermal System (California, USA), *J. Volcanology and Geothermal Research*, 205 67-83.
- Mellors, R., Kilb, D., Aliyev, A., Gasanov, A., Yetirmishli, G., 2007. Correlations between earthquakes and large mud volcano eruptions. *J. Geophys. Res.* 112 (B04), 304.
- Muffler, J., White, D., 1968. Origin of CO₂ in the Salton Sea geothermal system, southeastern California, U.S.A. *Proc. Intl. Geol. Congress* 97, 185-194.
- Muffler, J., White, D., 1969. Active metamorphism of the upper Cenozoic sediments in the Salton Sea geothermal field and the Salton trough, southern California. *Geol. Soc. Am. Bull.* 80, 157-182.
- Onderdonk, Nathan, Luke Shafer, Adriano Mazzini, Henrik Svensen, 2011 Controls on the geomorphic expression and evolution of gryphons, mud pots, and caldera features at hydrothermal seeps in the Salton Sea Geothermal Field, southern California. *Geomorphology* (in press)
- Planke, S., Svensen, H., Hovland, M., Banks, D., Jamtveit, B., 2003. Mud and fluid migration in active mud volcanoes in Azerbaijan. *Geo Mar. Lett.* 23, 258-268.
- Quantification Settlement Agreement (2003). <http://bondaccountability.resources.ca.gov/plevel1.aspx?id=20&pid=4www.fgc.ca.gov/.../Quantification%20Settlement%20Agreement.pdf>
- Robinson, P.T., W. A. Elders & L. J. P. Muffler 1976 Quaternary volcanism in the Salton Sea geothermal field, Imperial Valley, California, *GSA Bulletin* 87, p.347-360, March
- Rudolph, M., Manga, M., 2010. Mud Volcano response to the 4 April 2010 El Mayor-Cucapah earthquake. *J. Geophys. Res.* 115, B12211. doi:10.1029/2010JB007737.
- Schoneman, C. 2011 (private communication, September)

- Sturz, A., Itoh, M., Earley, P., Otero, M., 1997. Mud volcanoes and mud pots, Salton Sea geothermal area, Imperial Valley, California. In: Deen, P., Metzler, C., Trujillo, A. (Eds.), *Geology and Paleontology of the Anza-Borrego Region, California. Field trip guidebook for the National Association of Geoscience Teachers Far Western Section, 1997 Spring Field Conference.*
- Sturz, A., Kamps, R., Earley, P., 1992. Temporal changes in mud volcanoes, Salton Sea geothermal area. In: Kharaka, Y., Maest, A. (Eds.), *Water-Rock Interaction. Balkema, Rotterdam, Netherlands*, pp. 1363–1366.
- Svensen, H., Karlsen, D., Sturz, A., Backer-Owe, K., Banks, D., Planke, S., 2007. Processes controlling water and hydrocarbon composition in seeps from the Salton Sea geothermal system, California, USA. *Geology* 35, 85–88.
- Svensen, H., Ø. Hammer, A. Mazzini, N. Onderdonk, S. Polteau, S. Planke, and Y. Y. Podladchikov (2009), Dynamics of hydrothermal seeps from the Salton Sea geothermal system (California, USA) constrained by temperature monitoring and time series analysis, *J. Geophys. Res.*, 114(B9), B09201, doi:10.1029/2008JB006247.
- Veatch, J., 1860. Salses or mud volcanoes of the Colorado Desert. *Hesperian* 3, 481–489.
- Yunker, L. W., P. W. Kasameyer, and J. D. Tewhey (1982). Geological, geophysical and thermal characteristics of the Salton Sea geothermal field, California, *J. Volcanol. Geotherm. Res.* 12, no. 3–4, 221–258.

The Oro Copia Mine, Orocopia Mountains, Riverside County, California

Larry Vredenburg

Bureau of Land Management, 3801 Pegasus Dr., Bakersfield, CA 93308

Dos Palmas Spring, located 15 miles southeast of Mecca, in the early 1860s was an important stop on the Bradshaw Trail—the road to the La Paz, Arizona gold diggings. Just to the north of the spring are the Orocopia Mountains and the location of a long forgotten gold mine, variously known as the Sommerville, Fish, Dos Palmas, Gold Canyon, or Oro Copia.

Edward G. Fish and his son G. B. Fish of San Bernardino and C. O. Barker of Banning began working the Sommerville gold mine in the Orocopia Mountains around 1892. The mine made news in 1894 when large specimens of quartz, laced with gold, were brought into San Bernardino. At that time a “few men” were working the mine but apparently they had accomplished a lot they had driven two adits, 90 and 300 feet long. (Could it be that this was an old mine that was being reactivated?) One 1895 newspaper article stated that this mine “is one of the most promising prospects in Southern California, and conservative mining men estimate that the present developments put \$160,000 in sight in the property.” Yet operations remained relatively modest. It was reported in 1896 that Fish and son were processing 3 tons of ore a day at a 2-stamp gasoline powered mill located at Dos Palmas Spring. This mine is often referred to as the Fish Mine because of their early ownership of the property.

In December 1897 it was announced that the Gold Canyon Mining Company had been organized to work the mine. Company executives included D. E. Mitchell, president; E. B. Fish, vice-president, and C. C. Doran, secretary. In the same press release, it was stated that a 10-stamp mill would be built. The *Riverside Press and Horticulturist* in February 1899 related that the company had completed a wagon road to the mine, had graded the mill site, graded a 400-foot long mine rail line to connect the mine to the mill, and were constructing a tramway. Edward Fish pronounced, “the ledge being opened to be the largest and best in this southern country, barring the Gold Cross at Hedges.” A 5-stamp mill was running by June, 1899, but they found the nature of the gold was too fine to be recovered, and in September indicated they would install a cyanide plant.

On August 25, 1902 the Oro Copia Mining and Milling Company was incorporated in Arizona for \$3 million to develop the mine,

with Charles Foreman, president; Richard Mercer and J.L. Johnston vice presidents; W.F. Winnie, secretary; and G.L.A. Richter, superintendent. Apparently east coast (in one report, “old Comstock”) men were the principle investors.

In 1904 the Oro Copia company announced the intention to spend \$100,000 developing the property. A well was sunk near Dos Palmas Spring and a 9-mile long 2-inch pipeline was laid to the mine and mill. The stamp mill was replaced with three roller mills with a combined capacity of 40-tons per day. A cyanide plant was also constructed, and by 1905 it was planned to increase the capacity of the mine to 200 tons.

According to a 1912 article, litigation brought work at the mine to a halt around 1905. The general manager, C. C. Doran, showed a reporter from the *Indio Date Palm* around the place. In the 1912 article the following improvements were noted: the well, 9-mile pipeline, a roller mill, a cyanide plant, a tramway, and 400 feet of mine rail track. Doran indicated he hoped to be producing bullion in a few weeks.

Finally, in 1915, the *Date Palm* reported Mr. Doran, of Long Beach, present lessee of the Oro Copia Mining Company, expected to open up the Oro Copia in a few weeks.

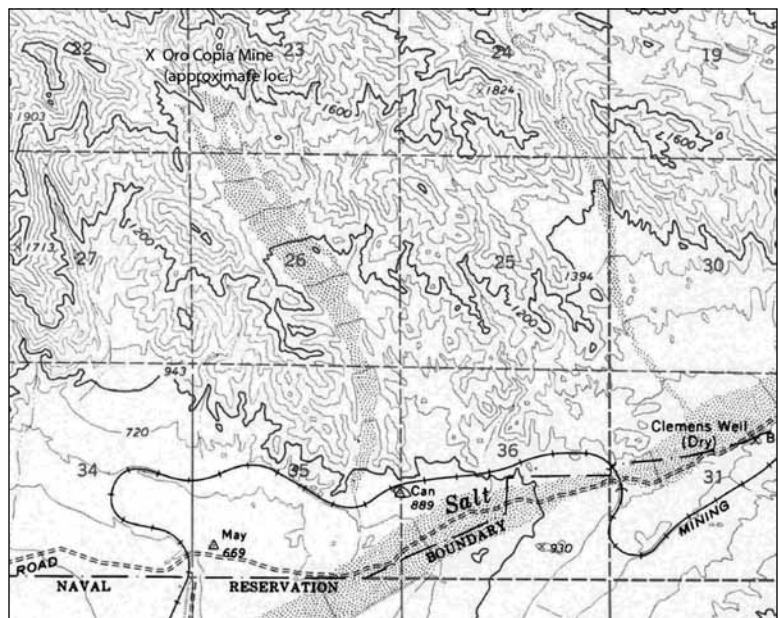


Figure 1. Approximate location of the Oro Copia mine.

John Hilton, in his 1940 article in *Desert Magazine* describing an onyx location in the Orocochia Mountains, stated this mine was said to have produced a fortune. He also stated, "the old mine camp is about demolished. The tool house and blacksmith shop which survived many years of weather and vandalism were blown down in recent times by a desert twister. Some tunnels, inhabited by bats, the tailings and the foundation of the mill are all that remain."



Figure 2. Mill ruins, 1981.

1960 Description of the Dos Palmas Mine by R. B. Saul (Saul, Gray, Evans, 1961)

Location: Sec. 16?, T. 7S., R. 12 E. SBM., [note: this map did not have the public land survey grid shown on it.] U.S. Army Corps of Engineers Canyon Spring quadrangle, 15' 1944, 3 1/2 miles northwest of Clemens Well, on the south slope of the Orocochia Mountains. The mine is reached by an unimproved dirt road up a wash which leaves the range near the triangulation station marked Can 890 on the topographic map.

Ownership: Undetermined. The claims were held in 1955 by John C. Brinton, Eileen Brinton and George W. Robinson, under the name Black Jack Claims.

Geology: The country rock is gneiss. A quartz vein lies in the plane of a fault: which strikes N. 55° E., and dips 50° -55° NW. The fault zone is as much as 5 feet wide and contains a soft gouge of chlorite schist. It is well exposed for several thousand feet across several ridges and intervening canyons. The full northeasterly extent of the fault was not determined but to the southwest it is truncated by a wide, northwest-trending fault zone which probably is part of the San Andreas system.



Figure 3. Bed of mine railroad, 1981.

The quartz vein pinches and swells, ranging from 0 to 4 feet in thickness. It is fractured. Contained pyrite is altered almost completely to iron oxides which have filled fissures and cavities. Small amounts of secondary copper minerals and calcite are present. Several samples of ore contain visible traces of gold but no assay data were found.

Development: The vein was explored by means of adits driven northeast on 3 levels in the southwest slope of a ridge immediately north of a mill and camp site. The

adits are driven northeast and are joined by stopes which appear to be as much as 30 feet wide. The ground stands well, being only slightly caved at the portal. The adits are untimbered. The stopes are timbered with stulls. Ore was milled at the mine but water was probably in short supply.

My visit

I visited this mine on October 1, 1981 and placed the location of this mine (on the Hayfield 15 minute quad) as in T. 7 S., R. 12 E. Sec. 22 NE1/4 NE1/4 SE1/4 SBM. While there I noted the bed of a 400-foot long mine rail track, the trace of the tramway, and ruins of the cyanide plant referred to above as well as the 3 adits that Saul noted.

References

- Crawford, J. J., 1894, "Riverside County," *California Mining Bureau Report 12*, 1894, p. 221
- Crawford, J. J., 1896, "Riverside County," *California Mining Bureau Report 13*, 1896, p. 371
- F. J. H Merrill and Clarence A. Waring, 1917, *Report of the State Mineralogist*, Vol. 15, Part IV, Chapter III, p. 541.
- Saul, R. B., Gray, C. H. and J. E. Evans, 1961, Mineral Resources of Riverside County, California, California Division of Mines and Geology, unpublished manuscript.
- Tucker, W. B., 1929, "Riverside County," *California Mining Bureau Report 25*, p. 477
- Vredenburg, Larry M., Shumway, Gary L., Hartill, Russell D., 1981, *Desert Fever*, (Canoga Park: Living West Press) p. 27, 28.

Periodicals and newspapers

- Redlands *Citrograph* 23 Jun 1894
- Indio *Date Palm*: 7 Feb 1912, 22 Jan 1915
- John W. Hilton, "Bloodstone in the Orocopias," *Desert*, March, 1938, p. 14, 15, 31.
- John W. Hilton, "Petrified Bacon," *Desert*, November, 1940, pp. 13-16.
- Engineering and Mining Journal*: 21 Nov 1903, 28 Nov 1903
- Los Angeles *Herald* 10 Jun 1896
- Mining And Metallurgical Journal*, 1 Apr 1897; June 15, 1899, p. 13-14
- Mining and Scientific Press*: 17 Mar 1894, p. 173; 9 Feb 1895, p.90; 11 Dec 1897, p. 554; 3 Dec 1898, p. 557; 4 Feb 1899, p. 127; 4 Mar 1899, p.239; 24 June 1899, p. 671; 16 Apr 1904, p. 272
- Los Angeles *Mining Review*: 18 Feb 1899, p. 4; 25 Feb 1899, p. 8; 1 April 1899 p. 4
- Pacific Coast Miner*: February 28, 1903
- Riverside Press and Horticulturist*: 2 Feb 1895, 11 Feb 1899, 29 May 1903
- The Mining World* 23 Jan 1904; 27 Feb 1904; 28 Jan 1905

Sites I would like to see: moonshine still sites in the California Desert

Frederick W. Lange, PhD/RPA

LSA Associates, Riverside, California 92507, fred.lange@lsa-assoc.co

Introduction

Archaeologists have questioned whether or not all vestiges of human social, economic, and technical behavior are preserved in the archaeological record. The first step in the present discussion of the lack of moonshine still sites on the archaeological landscape, despite frequent references to these sites in the historical literature (Walker 1999), is to open the door to the vault of traditional anthropological/archaeological terminology that will assist us in answering this question.

Lewis Binford (1931–2011) is known for his contributions to archaeological theory and his promotion of ethnoarchaeological research (the integration of ethnographic and archaeological research). He promoted a systemic view of culture (Binford 1962) and divided the assemblage of material culture (artifacts) left by ancient peoples into three categories: (1) the technomic (artifacts developed to cope with the physical environment), (2) the socio-technic (artifacts that function in the social sub-system of human adaptation), and (3) the ideo-technic artifacts that deal with beliefs of the cultural system. Binford also thought that, with the assistance of ethnographic comparisons (cf. Binford 1980), all types of behavior could be identified from archaeological patterns.

Other archaeologists, such as Michael Schiffer (1983), have emphasized the extent to which the archaeological context is often (always?) altered between deposition and investigation by cultural behavior (“c-transforms”), natural forces (“n-transforms”), or both. Binford agreed with Schiffer that sites were transformed by both natural and cultural actions, but he disagreed that such transformations interfered with the potential for the archaeological interpretation of the site.

Central to this discussion has been the role of the so-called “Pompeii premise” (Binford 1981); this premise states that the patterns that the archaeologist uncovers are found exactly in the way that the person or persons responsible for their deposit left them, and that they have not been subject to post-depositional c- or n- transformation, as characterized by Schiffer (1985).

This paper has resulted from research experiences during various stages of my professional career (which is still ongoing) in which I have addressed the concepts of ethnographic analogy, both c- and n-transforms (although I never referred to them as such), the Pompeii premise (although I never referred to a site context as such), and when I have needed to assess whether or not

all behaviors are in fact detectable in the archaeological record.

My first foray into this line of inquiry resulted from research in Barbados during the 1970s (Handler and Lange 1978). As a result of this research, I questioned whether the socio-economic practice of slavery, in its many different degrees and forms, was archaeologically identifiable without documentary support, or whether strictly archaeological evidence for slavery might always run the risk of being confused with prisoners or other captive populations. In this case, Handler and I concluded (1978) that the institution of slavery could not be identified with certainty only from archaeological traces.

Subsequent research in southern California has led me to consider another historic behavior pattern that may not be discernible based purely on archaeological data: that of the moonshine still and the moonshiner.

When I was doing background research on the National Old Trails Road for a project in the Barstow–Ludlow area, two persons familiar with Edwin Q. Sullivan had directed me to the memoirs that he had prepared for Caltrans. Sullivan was the first Caltrans highway engineer for District VIII of Caltrans, which at its inception in 1923 encompassed Imperial, Riverside, and San Bernardino counties, all three counties bounded on the east by the Colorado River. Sullivan stated (ms:3) that he was instructed to focus on establishing roads to the Nevada and Arizona state borders. The challenges were many: the route to Las Vegas had not yet been defined, the road to Blythe was nothing more than a trail, and the road to Yuma, beyond the edge of the cultivated part of the Imperial Valley to the Sand Hills, consisted of nothing more than tracks in the sand with an 8-foot wide plank road across the Sand Hills and two deep ruts east from the Sand Hills to Yuma. Sullivan was also the principal engineer for the National Old Trails Road segment in California. It was in this role that I first became acquainted with him.

I was looking for written details on construction and maintenance activities to attempt to support our interpretations of and speculations about the construction methods we had observed in the field, but was side-tracked when I came across the sentence (Edwin Q. Sullivan, n.d.: 3)

In the early period of District VIII, there were a number of moonshine stills throughout the desert region. The product was usually

referred to as ‘turtle juice,’” but much of it was probably made from cactus.

To me, part of the joy of archival research in association with archaeological investigation is that the side streets are almost inevitably more interesting than the main avenues!

Sullivan’s account described where “turtle juice” was usually manufactured: the moonshiner’s shack would be found near a spring or well-hidden in a distant, isolated canyon, beside a desert trail that passed for a road. The dwelling might be a lean-to shack but often was only a tent, usually remote from the sedentary population and the prying eyes of the law. While the production of turtle juice was hidden from view, the sale and consumption was much more open; the two loci were functionally and economically linked. C. Walker’s 1999 volume entitled *One Eye Closed and the Other Red: The California Bootlegging Years* is perhaps the most comprehensive single source on the Prohibition period in California.

Here, I thought, as I had many years before in Barbados, was an archaeological-style description that integrates the natural setting, a physical feature, cultural actors, and an economic activity. Survey archaeologists have almost always looked carefully around natural springs or other water sources, since they were a focus for settlement by Native Americans and early pioneers, especially in the desert; had they possibly overlooked one or more historic stills? A prehistoric millstone site is characterized by grinding slicks, metates, bedrock mortars, and an occasional handstone or *mano* what would characterize an historic moonshine still site?

The interactive methodology of ethno-historic research in archaeology

Having framed the outline for my research, I returned to the documentary record. Had a moonshine still site ever been recorded as such in the California Department of Parks and Recreation (DPR) annals of California archaeology? Would we be capable of recognizing one if we came across it in the midst of a survey? For much of my professional career I have made the case, in projects as far apart as Wisconsin (Lange 1969), Barbados (Lange 1972, 1974, 1976; Handler and Lange 1978, 1979; Handler, Orser, and Lange 1979; Corrucini, Handler, Mutaw, and Lange 1982; Lange and Handler 1977, 1980a, 1980b, 1985, 2006; Lange and Carlson 1985), Nicaragua (Lange 2004) and now California (Lange 2006), for the value of the ethnohistorical approach to archaeological research.

As in the study of slavery in the Barbados, the step-by-step articulation of the historical and archaeological data “mined” the historical data for details that were not initially being sought, and likewise a more careful perusal of the same historical data suggested different approaches to the archaeological data. Furthermore, this articulation of history and archaeology produced interpretations that would have been difficult or impossible on the basis

of historical data alone and probably impossible if only archaeological data had been available.

In the present study, the historical evidence has alerted us to the potential of identifying the sites of a specialized manufacturing activity, the illegal production of “turtle juice” or “moonshine” even though no such “stills” have apparently even been reported in the archaeological literature or officially recorded on State of California Department of Parks and Recreation (DPR) 523 forms (4). The historical documentation from Sullivan’s unpublished memoirs and a return to Walker’s magnum opus with a fresh archaeological perspective may help some of us to redirect our field recording and to be sensitive to the possibility of moonshine still sites in our survey areas (5).

The probable frequency of moonshine sites on the landscape

While no moonshine still sites have ever been officially recorded as historic resources in California, Sullivan’s memoir and Walker’s documentation suggest that they were not an uncommon occurrence, nor were they particularly difficult to find. In recounting a tour of District VIII with an out-of-state engineer, Sullivan mentioned that the visitor sampled the wares of several of the moonshiners that they passed; as he stated (Sullivan n.d.) there are indications that many of the early gas stations were distribution points for the sale of illegal alcohol (these sales locations were known as “blind pigs”). The available products ranged from home-made brew that was shared with customers to whiskey made by more professional moonshiners who sold their product to the station owners for re-sale to passing customers; Sullivan added that from many accounts the results were often the same for the consumers of the stronger-than-beer products, and he concluded his telling of the out-of-state engineer’s visit and excessive consumption by stating that the engineer woke up the next morning to discover he was blind and that he required many weeks of medical care to at least partially recover his vision!

Additional documentary evidence for southern California is contained in Richard Thompson’s “Sagebrush Annie and the Sagebrush Route” (<http://mojavehistory.com/sagebrush1.html>). This history covers a nine mile stretch of Route 66 between Oro Grande and Helendale from 1925 to the mid-1940s, encompassing the years of Prohibition, the Depression, and World War II. Another link to Edwin Q. Sullivan is that prior to being re-named US Route 66, this highway was the original National Old Trails Road. Thompson notes that driving through the region one can imagine “blind pigs” and moonshiners and their stills hidden off in the nearby canyons. The chief bootlegger for the Oro Grande–Helendale area was one Guy Wadsworth; he also was a builder who constructed many of the stone buildings along the nine mile route (some, it is said, with “hidey holes” for illegal

liquor built into the stone walls) (Thompson(<http://moja-vehistory.com/sagebrush1.html>))

Many Guy Wadsworth buildings are still standing, but to the best of my knowledge no one has confirmed the presence of these architectural details.

David Caterino, coordinator of the South Coastal Information Center at San Diego State University, informed me that, while he was unaware of any moonshine still sites having been recorded with the SCIC, he had a friend who had knowledge of stills in the Julian area, but the locations, naturally, were secret. He also shared the information that a now-deceased acquaintance, who has been the caretaker at the Descanso Cemetery had identified a cave on the hill behind the cemetery where her father had had his still. As with the oral history from the Julian area, this location has not been confirmed.

The material culture of moonshine sites in the context of historical archaeology

If none have been found, then what are we looking for to be able to identify and record historic moonshine stills? Walker described many stills throughout the state that were disguised as houses, as haystacks, and other ingenious ruses. One of his photos (Walker 1999:424) shows the remains of a still on the Sandoz Ranch in Hinckley, northwest of Barstow, where a trash littered hole is all that is left of a new dairy; men from L.A. rented the ranch, ostensibly to start a dairy, but used the operation to hide the largest distillery in that part of the desert. A basic list of necessities might include: technomic, socio-technic, and perhaps ideo-technic artifacts (Figure 1).

(1) Half-pint whiskey bottles. These classically shaped and sized bottles were filled with moonshine whiskey as gifts or for sale.

(2) Mason jars and lids. These jars, which are still in use today as canning and preserving containers and have never really disappeared from the American scene, are ubiquitous at 20th century historic sites throughout North America. They are also frequently seen in historic photographs of stills and would have been a common container around the house to be used for purposes of liquid storage and transport, in addition to putting up fruits and vegetables. More recently, Mason jars have become fashionable in root beer and lemonade stands.

(3) Barrels (hoops and slats). Fragment of barrels and the hoops are often found on historic sites. As far as stills are concerned, they could represent larger scale, commercial production. We seldom if ever find whole barrels, but we do frequently record barrel parts (the hoops obviously last longer than the slats) without stopping to consider what the barrels might have been used for out in remote locations, re-cycled from their original use.

4) Hearths. Heating the fruit (including cactus) or the grain “mash” is the first step in distilling. During survey, we often encounter hearths in isolated locations. There is usually some initial question as to whether they are prehistoric or historic; if the decision is made that the hearth most likely is historic, then it is often attributed to hunters, off-roaders, or Boy Scouts. On the other hand, if a moonshiner really cleaned out a still area to avoid raising suspicion, then the hearth and perhaps a few broken Mason jars and barrel hoops and slats might be the only artifacts left behind.

(5) Boiling pots. In most illustrations, a boiling pot was the focal point of the still. The boiling pot sat on the hearth, stove, or fireplace, and created the vapor that was subsequently distilled into alcohol.

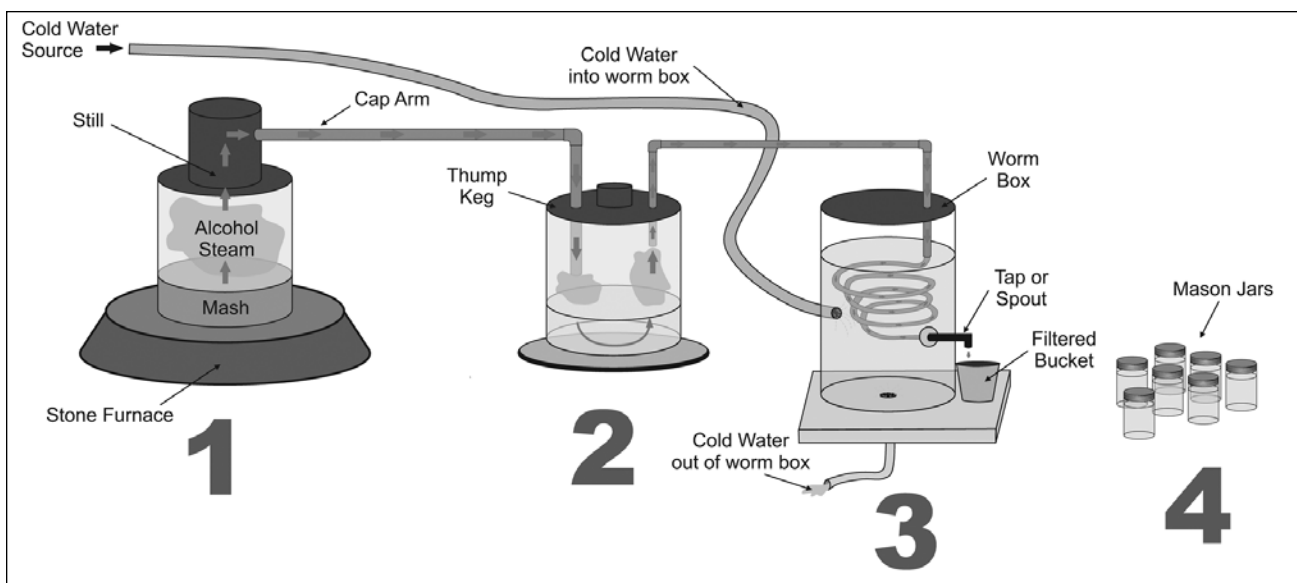


Figure 1. Generalized still apparatus. Drawing by David Cisneros.

Two Southern California case studies

Following the background studies on moonshine in the Mojave, I had selected two case studies from my California experience with the intent of visiting the locations prior to completion of this paper: the Moore house still site near Lockhart, California and the Ord Mountain still site southeast of Barstow known to have been moonshine still sites. I had the documentary information, but I hoped to examine both sites using archaeological methods to determine whether or not they could be classified as moonshine still sites on their own. The following section describes the two case study locations and discusses the reported archaeological characteristics of the sites.

15563 Lockhart Road: This is the former site of the Frank Luster Moore homestead and chicken ranch; the ranch was a cover for his notorious bootlegging business (Hampson and Swanson 1989). Moore built two chicken coops on the property, one made from stucco and the other made from adobe.

Moore's original residence at the address burned (date unknown) and he converted the stucco chicken house into a residence, where he lived until 1939. Moore's sister, Hazel Dupue, and her husband Earl moved their family into the house in 1939 and lived there until 1942. Hampson and Swanson (1989) noted that the stucco chicken coop might still be standing. Several buildings are currently present on the parcel that may date to the 1940s and 19650s, Lockhart's apogee as a community. The AECOM Mojave Solar Project Cultural Resources Technical Report (Wilson et al. 2010:148) stated that although the farmstead is potentially significant as the location of Moore's original homestead, no features were directly related with the Moore farmstead during the Prohibition era.

Ord Mountain: Willis Well on the northeast side of Ord Mountain was previously identified as a still site with a possible copper cap and copper tubing were identified "away from the domestic structure" (Robert E. Reynolds, personal communication 12-2011).

Unfortunately, it was not possible to visit these site locations as planning prior to the 2012 symposium. They are still on the list for the future.

Possible confusion with other historic resources

Fermented beverages have been made since the earliest recorded history, and became the stuff of folklore and movies during Prohibition in the United States. Home brews continue to be a hobby for many connoisseurs who would rather make and drink their own.

Since moonshine stills are historic sites, let us note other types of historic sites that have been recorded in the southern California desert that might be confused with a still. Those in the same general area where we might expect to find moonshine stills (although not an exhaustive list) are (a) Desert Training Center sites, (b) historic trash scatters, (c) USGS survey sites, (d) farm houses,

and (e) wagon trails. Small Desert Training Center sites such bivouac sites are usually identified by fox holes, fuel and oil cans, tracked vehicle trails on desert pavement, ordnance casings, and clearings for tents. Historic trash scatters are identified by quantities of cans, construction debris, broken glass, and bundles of baling wire and may or may not be associated with the remains of a structure. USGS survey sites are initially identified by survey buttons; within a short distance there are indications of a briefly occupied camp, with the occasional hip-pocket flask size liquor bottle, foods containers, Prince Albert tobacco cans, and often construction by-products from building the marker (6). Old farm houses are usually identified by foundations with associated trash scatters, outhouses and other outbuildings, window glass, fruit, nut, and shade trees, wells and pumps, and stone or puddle cement or concrete blocks. Wagon trails are usually identified by parallel ruts and may also show tracks of motorized vehicles since many dirt trails were converted into early highways in southern California (Robinson 2005).

Summary

Why is it so difficult to locate and describe still sites, when milling slicks and bedrock mortars have been identified all over the hillsides of southern California?

We might posit a general disdain for historic sites and debris on the part of many archaeologists. The presence of historic materials, and a sub-set representing illegal alcohol production, does not fit with some of the major research foci of California archaeologists such as hunters-gatherers, Channel Islands adaptation, obsidian exploitation and trade, Pacific Coast to Colorado River transhumance and trade, acorn and piñon exploitation, and others (cf. Jones and Klar 2008).

We might also lack a frame of reference for what we might expect a moonshine still to look like, or what might distinguish it from any other historic feature, scatter, or trash from the contemporary time period. Finally, even before and after Prohibition, tax evasion from the production and sale of moonshine continue to be an issue, even when the consumption of alcoholic beverages was legal. The State of California was not completely dry and had what was called the county option; this made both manufacture and distribution of illegal alcohol a patchwork affair.

A moonshine still site might be confused with the traces of other activities in remote and mountainous areas. The behaviors in the area of the National Old Trails Road/U.S. Route 66 would include mining, hunting, transmission line construction, informal gravel mining, house construction, service station operation, highway construction, and railroad construction and maintenance. Many men, of whom Guy Wadsworth is perhaps the best known in that area, were both builders and moonshiners.

The boiling pot and copper coil are the only distinctive components of a still whose form and function are suitable for no other function. They are the elements most likely to be conveyed from place to place by the moonshiner, since unlike the other elements listed above, the pot and coil would be relatively difficult to replace (and might also be the most difficult to explain away if the “revenueurs” paid an unexpected visit). The other elements that are listed above are less diagnostic of a still, since they had many other functions and uses in daily life and merged, without difficulty, into the mosaic of either urban or rural life. The pot and the coil are also the most likely to be picked up by historic artifact collectors (their removal would constitute c-transform behavior, according to Schiffer’s terminology).

Can the manufacture of moonshine be interpreted strictly from archaeological evidence? As discussed above, the archaeological characterization of a site as having been a moonshine still is possible if the boiling pot or copper coil are preserved in situ. If not, documentary evidence is necessary to be sure. However, the descriptions above have provided some hints as to what other traces we might look for: (1) a remote canyon location near a source of water; (2) scatters of Mason jar shards and other glass containers to the exclusion of more typical domestic artifacts; and (3) in terms of gender, lack of evidence of female presence in the living site (while there is no practical reason that women could not have been involved with the production of “shine”, the historical descriptions strongly suggest that most of the production activity was carried out by men (possibly because of the remoteness and danger of the still locations).

This is a site I would like to see. Let me know when you submit the form to the information center.

ACKNOWLEDGMENTS—I thank Deborah Cismowski (History Librarian, Caltrans Headquarters, Sacramento), and Gene Heck (Principal Architectural Historian, Caltrans 8) for guiding me to the Edwin Q. Sullivan data. Robin Laska of the CHRIS Information Center at the San Bernardino County Museum led me to Cliff Walker’s volume. I am thankful to Elizabeth Davidson in LSA’s Carlsbad office for pointing out the correlation between USGS “buttons” and the frequent presence of adjacent concentrations of camp debris.

References cited

- Binford, Lewis R.
1962. Archaeology as Anthropology. *American Antiquity* 28 (2): 217–225.
- 1980 Willow smoke and dog’s tails: Hunter gatherer settlement systems and archaeological site formation. *American Antiquity* 45(1):4–20.
- 1981 Behavioral archaeology and the “Pompeii premise”. *Journal of Anthropological Research* 37(3):195–208.
- Corruccini, Robert., Jerome S. Handler, Robert. Mutaw, and Frederick W. Lange.
1982 “A Slave Skeletal Population from Barbados, West Indies: Implication for the Biological History of American Blacks,” *American Journal of Physical Anthropology* (12):443–459.
- Hampson, R. Paul and Mark T. Swanson
1989 Cultural Resource Investigation: Five Sections West of Harper Lake, San Bernardino County. Greenwood and Associates. Submitted to Luz Development and Finance Corporation. Unpublished report on file at San Bernardino County Museum.
- Handler, Jerome.S. and Frederick.W. Lange
1978 Plantation Slavery in Barbados: An Archaeological and Historical Investigation. Cambridge: Harvard University Press.
- Handler, Jerome S. and Frederick W. Lange
1979 “Plantation Slavery on Barbados, West Indies,” *Archaeology* 32:45–52.
- Handler, Jerome S., Charles.E. Orser, Jr., and FrederickW. Lange
1979 “Two Necklaces and Carnelian Beads from a Slave Cemetery in Barbados, West Indies,” *Ornament* 4:15–18.
- Jones, Terry and Katherine Klar (editors)
2008 California Prehistory. New York: Alta Mira Press.
- Lange, Frederick W.
1969 “The Bigelow Site (47-Pt-29): An Ethnohistoric Analysis of the Historic Artifacts,” *Wisconsin Archeologist* 50:215–255.
- 1972 “An Archaeological Investigation of the Domestic Life of Plantation Slaves in Barbados, West Indies,” 37th annual meeting, Society for American Archaeology, Miami.
- 2004a “Slave Mortuary Practices, Barbados, West Indies,” 41st International Congress of Americanists, Mexico.
- 2004b “Slave Mortuary Practices, Barbados, West Indies,” Actas, XLI Congreso Internacional de Americanistas (Mexico) 2:477–483.
- 2004c Planteamientos Iniciales Sobre El Impacto Indirecto de Las Enfermedades de los españoles, y la Falta de Identificación de Sitios Protohistóricos e Históricos en Nicaragua y Centroamérica. Ponencia preparada para el Ciclo de Conferencias “Leyendo el Pasado” organizado para celebrar el 107 aniversario del Museo Nacional de Nicaragua, y Rendir Homenaje a Doña Leonor Martínez de Rocha al Cumplirse 5 años de su Fallecimiento. Palacio Nacional de la Cultura, Museo Nacional de Nicaragua, Instituto Nicaragüense de Cultura, 26 Agosto.
- 2006 Ethnographic Analogy and the Mesquite Regional Landfill Project. 20th Annual Desert Studies Symposium, Desert Studies Center, Zzyzx, California.
- Lange, Frederick W. and Jerome S. Handler
1977 Mortuary Patterns of Plantation Slaves in Barbados, 9th Conference of the Association of Caribbean Historians, Cave Hill, Barbados.
- 1980a “The Newton (Barbados) Slave Cemetery: Patterns, People, When and Where the Twain do Meet,” in symposium, “Every Man’s Proper House and Home: Archaeological Perspectives on the Mentalite of Earlier

- Generations,” 13th annual meeting, Society for Historical Archaeology, Albuquerque.
- 1980b “The Application of the South Ceramic Formula on Barbados, West Indies,” 13th annual meeting, Society for Historical Archaeology, Albuquerque.
- 1985 “The Ethnohistorical Approach to Slavery” in *The Archaeology of Slavery and Plantation Life*. T. Singleton (ed.). New York: Academic Press, pp. 15–29.
- 2006 “On Interpreting Slave Status from Archaeological Remains.” The African Diaspora Archaeology Network, June 2006 Newsletter. <http://www.diaspora.uiuc.edu/news0606/news0606.html>.
- Lange, Frederick W. and Shawn B. Carlson,
1985 “The Distribution of European Earthenware on Barbadian Plantations” in *The Archaeology of Slavery and Plantation Life*. T. Singleton (ed.). New York: Academic Press, pp. 97–111.
- Robinson, John W.
2005 *Gateways to Southern California. City of Industry, California: The Big Santa Anita Historical Society.*
- Schiffer, Michael B.
1982 “Toward the identification of formation processes.” *American Antiquity* 48:675-706.
1985 “Schiffer, Michael B. 1985 Is there a ‘Pompeii premise in archaeology?’ *Journal of Anthropological Research* 41:18-41.
- Edwin Q. Sullivan
n.d. “The Federal Writer’s Project of the Works Progress Administration, Guide to San Bernardino County. California Department of Transportation (Caltrans) District 8 Archives.
- Thompson, Richard
n.d. “Sagebrush Annie and the Sagebrush Route” (<http://mojavehistory.com/sagebrush1.html>)
- Walker, Clifford James
1999 *One Eye closed and the Other Red: The California Bootlegging Years*. Barstow, CA Back Door Press.
- Wilson, S., M. K. Meiser, and T. Cooley
2010 *Cultural Resources Class III Survey Report for the Proposed Mojave Solar Project and Lockhart Substation Connection and Communication Facilities, San Bernardino County, California*. AECOM (San Diego, California).

Abstracts of proceedings— the 2012 Desert Studies Symposium

Robert E. Reynolds, compiler

Redlands, California 92373 • rreynolds220@verizon.net

Climatic variation predictably affects clutch phenology in Agassiz's Desert Tortoise (*Gopherus agassizii*)

Mickey Agha,¹ Meaghan Liszewski,¹ Jeff Lovich,¹ Kathie Meyer,² Josh Ennen,^{1,3} Caleb Loughran,¹ Sheila Madrak,⁴ and Curtis Bjurlin⁵

¹U.S. Geological Survey, Southwest Biological Science Center, MS-9394, Flagstaff, Arizona 86011, USA e-mail and phone: magha@usgs.gov (425)445-8431; mliszewski@usgs.gov (928)310-8808; jeffrey_lovich@usgs.gov (928)556-7358; jennen@usgs.gov (928)523-7766; cloughran@usgs.gov (928)853-4351

²U.S. Forest Service, Front Country Ranger District, San Bernardino National Forest, 1209 Lytle Creek Road, California 92358, USA, e-mail: kpmeyer@fs.fed.us

³Department of Biology, Maryville College, 502 E. Lamar Alexander Parkway, Maryville, Tennessee 37804, USA, e-mail: josh.ennen@maryvillecollege.edu

⁴San Diego State University/UC-Davis, Department of Biology, 5500 Campanile Drive, San Diego, California 92180, USA, e-mail: svmadrak@gmail.com

⁵Wind Capital Group, 2617 Chamberlain Ave, Madison, Wisconsin 53705, USA, e-mail: curtbjurlin@gmail.com

Phenology is the study of the timing and environmental causes both biotic and abiotic of biological events and life cycles. We studied clutch phenology of an Agassiz's Desert Tortoise (*Gopherus agassizii*) population at a wind energy generation facility near Palm Springs, California for seven field seasons from 1997-2011, and at Joshua Tree National Park in 1998. Using radiotelemetry and X-radiography we quantified the following phenophases based on the number of calendar days since 1 January: appearance and disappearance of first and second clutches, and interclutch intervals between first and second clutches. Third clutches were only observed in five of seven years, produced by seven different females, none of which produced more than one triple clutch during the entire period of study, so they were not included in some statistical analyses. During the course of the study, shelled eggs were visible from as early as 11 April to as late as 28 July, and the total length of time that eggs were visible differed among years. Appearance of first clutches in cool years was later than in warm years. After controlling for maternal effects, we observed statistically significant interannual variation in all phenophases except for interclutch intervals. Based on known and inferred

oviposition dates in 2011, females dropped their eggs 1-12 days ($x = 6.4$) after they were last visible in X-radiographs. Using degree day methodology we calculated heat unit accumulation (HUA) during the post-hibernation and nesting season for each year. After setting our biofix to the approximate date of emergence from hibernation (March 1) at a minimum threshold temperature of 17.80 C we calculated HUA to various clutch phenological events. We then used minimum HUA during two time periods to predict the mean date of first clutch appearance in subsequent years, with 1-6 day accuracy. We also tested the broader application of HUA against reproduction data collected at Joshua Tree National Park, and predicted first clutch appearance within one day. HUA, as it relates to clutch phenology, has important management and climate modeling implications for predicting phenophases in the reproductive cycle of the federally threatened Desert Tortoise.

Long-runout rock avalanche (sturzstrom) deposits in the Baker, California area

Kim M. Bishop

Department of Geosciences and Environment, California State University, Los Angeles

Long-runout rock avalanches, also called sturzstroms, are large volume catastrophic landslides that can travel long distances across gently sloping to flat surfaces. Velocities are generally 100 km/hr or more. Run-out distances are often greater than 1 km and can be as much as 10's of km. Long runout rock avalanche deposits are common features intercalated within Miocene terrestrial basins of southwest North America.

Nickel Hill, at the west side of city of Baker, and Hank's Mountain, 4 km southeast of the city, are hills with relief greater than 100 meters. Both hills consist of brecciated Paleozoic carbonate interpreted to be long-runout rock avalanche landslides. Additionally, the eastern part of an unnamed hill just west of Hank's Mountain consists of similar material.

Although much of the rock comprising the hills is non-brecciated, significant volumes consist of thoroughly brecciated material with characteristics found in relatively thick rock avalanche deposits. At some locations, clasts have been separated from one another with little or

no rotation, a geometry sometimes referred to as “jigsaw texture”. In other places clasts are rotated relative to one another. The zones of brecciation tend to have irregular boundaries, a condition that argues against tectonic faulting as the origin of the brecciation. It is interpreted that brecciation resulted from strong vibration and localized differential stresses during rapid landslide emplacement.

The ages of the Nickel Hill and Hank’s Mountain rock avalanche landslides are unknown, but the fact that the deposits are gullied and surrounded by alluvium built up around their edges suggests an age of tens of thousands of years or more. Probably, the hills represent hummocks embedded in thinner sheet-like masses that are common to most rock avalanche deposits. If so, the sheet-like areas are likely buried beneath the alluvium surrounding the hills. Possibly, the outcrops of the two hills belong to the same landslide.

The source of the landslide is not known, but it may have been the Soda Mountains to the west. Although no large masses of carbonate are currently present in the Soda Mountains, evidence suggests the mountains were once capped by an extensive allochthon of Paleozoic carbonate that could have served as the source. A remnant of the allochthon consisting of Mississippian age carbonate rests on top of the Soda Mountains above Zzyzx Desert Studies Center and another remnant containing Bird Springs Formation is located in the northern Soda Mountains. The Nickel Hill landslide deposit consists of Bird Spring Formation and the Hank’s Hill deposit is in part Mississippian. Thus, the age correspondence between the landslide carbonates and those in the Soda Mountains is consistent with a Soda Mountain origin for the landslides.

The Amargosa Region Flow Sustainability Project

Brian Brown

Amargosa Conservancy, dates@chinaranch.com

In 2011 the Amargosa Conservancy presented the results of the phase I of an ongoing study to determine the basic hydrology of the Southern Amargosa region. Although there is a significant amount of free-flowing groundwater in the Shoshone and Tecopa area, the sources and sustainability of this water are not well understood.

Phase II of the study is now complete, and this paper will be a summary of the results. Geochemical data suggest a different flow pattern for groundwater than was expected, and an apparent different flow pattern in the southern part of the Amargosa watershed from the northern part. The preliminary results of phase II will be discussed, as well as the continuing parts of the study,

in which we hope to get a good idea of the inflow and outflow of the Southern Amargosa region. The information learned will be used to help the BLM construct a meaningful Wild and Scenic River Management Plan. The results of Phase I and II will also be made available to the public. The project may also serve as a good example of a productive collaboration between public, private, and non-profit entities to accomplish meaningful and long term conservation goals. The structure of this unique collaboration will be explained, as well as the goals of the phase III portion of the project.

Stratigraphy of the possible Peach Spring Tuff in the Alvord Mountain area, California

David C. Buesch

U.S. Geological Survey, 345 Middlefield Road, Menlo Park, California 94025

The 80 to 115 m thick Spanish Canyon Formation in the Alvord Mountain area, California, consists of tuffaceous deposits (redeposited tuffs, fallout tephra, and ignimbrite) interstratified with arkosic sandstone and conglomerate with two olivine basalt flows at the top. An ignimbrite near the middle of the formation is possibly the 18.7 Ma Peach Spring Tuff (PST), and if this ignimbrite can be correlated to the PST, then a valuable stratigraphic marker can be used to evaluate the depositional environments and structural history of this area within the eastern Mojave Desert. The Spanish Canyon Formation, including the possible PST, can be discontinuously traced for approximately 9 km around the northward plunging Spanish Canyon anticline. In most areas, the possible PST was deposited on medium to coarse-grained sandstones and conglomerates (probably medial to distal alluvial fan deposits); however, locally it was deposited on fine-grained sandstone and mudstone that might represent lacustrine deposits. In northern exposures, the possible PST is approximately 1-m thick, in eastern exposures it is as much as 3.3-m thick, and in a south-eastern exposure it probably as much as 7- to 12-m thick (although the top has been covered by alluvium). Most ignimbrite exposures are nonwelded; however, the south-eastern deposit is partially welded and was probably crystallized at high temperature. Minerals in this ignimbrite include sanidine >> plagioclase ± quartz with hornblende > biotite and minor amounts of sphene (which is typically visible in hand specimens) and perrierite; however in some deposits, crystal clasts were probably locally derived. Many exposures have a partially to well-developed, lithic-rich, basal ground layer (BGL) that is overlain by the nonwelded to partially welded ignimbrite with 2 to 5 percent lithic clasts. Where the top of the ignimbrite is exposed, there is no evidence of paleosol development or

erosion prior to deposition of the overlying deposits (typically thinly bedded sandstone).

Based on size and abundance of lithic clasts (less than 5 to 30 mm and 5 to 25 percent, respectively), locally there are as many as four pulses represented in the BGL. Locally, the upper part of the BGL (the upper 30 cm in the best developed sections) contains about 2 to 5 percent lithic clasts, but there are lithic clasts 30 to 55 cm in diameter. Most lithic clasts (and some crystal clasts) in the BGL are consistent with being eroded from locally exposed bedrock or incorporated from materials that had been on the paleogeomorphic surfaces across which the pyroclastic flow traversed. Ground layers can be attributed to a variety of processes including (1) instabilities in the head of a pyroclastic flow or local decoupling of the transporting and depositing processes near the base of the flow, or (2) localized inclusion of fragments near the base of the flow resulting in turbulent boundary conditions and an increase in the bulk density of the lower part that then decouples from the over riding flow. Deposits from the first processes would contain materials primarily from the eruption and vent areas. In contrast, deposits from the inclusion of fragments at the base of the flow would contain the original magmatic material with fragments that occur locally. The abundance of locally derived, and in some cases large, lithic clasts is a good indication that the BGL was derived from incorporation of lithic material into the base of the flow as it traversed surfaces strewn with lithic clasts such as alluvial fan deposits.

The ignimbrite in the middle part of the Spanish Canyon Formation is thinner than most Peach Spring Tuff exposures, many of which are closer to the eruptive source; however, there are many characteristics consistent with it being the Peach Spring Tuff such as the (1) mineral assemblage, (2) development of welding and high-temperature crystallization in deposits less than 15 m thick, and (3) apparent high energy of the pyroclastic flow inferred from the well-developed BGL deposits. Additionally, in some BGL deposits the lithic and pumice clasts are imbricated and locally the pyroclastic flow eroded into the substrate to create elongated furrows and similar furrows also occur in some BGL deposits. Imbrication of clasts and the furrows are consistent with an easterly to westerly transport direction. Petrographic, paleomagnetic, and geochronologic studies will continue to test the correlations with the Peach Spring Tuff, but based on field relations and general characteristics, the exposures in the Spanish Canyon Formation appear to be one of the most distal and northwesterly exposures of Peach Spring Tuff.

Tectonic analyses using geomorphic parameters of the Black Mountains in Death Valley, California

Thomas Feistel

Department of Geological Sciences, California State University-Fullerton

The Black Mountains make up the eastern border of southern Death Valley in the Mojave Desert, California. The mountains are bounded by three fault zones, the strike slip Furnace Creek fault zone (FCFZ), the strike slip Southern Death Valley fault zone (SDVFZ), and the normal Death Valley fault zone (DVFZ). Previously, Denny (1965), Knott (1998), and Bull and McFadden (1977) evaluated the tectonic geomorphology of the mountain range using the geomorphic indices of basin area vs. fan area, mountain front sinuosity, and stream concavity index. This project will use previously unavailable Geographic Information Systems (GIS) to evaluate the aforementioned geomorphic indices and compare these new findings to the previous findings of Denny (1965), Knott (1998), and Bull and McFadden (1977).

Each parameter being re-evaluated will be examined in greater detail than previously. Mountain front sinuosity will be taken over five different segments as defined by Knott (1998), instead of just one value for the entire 80 kilometer mountain range. Similarly, more drainages, fans, and streams will be evaluated to find basin area vs. fan area and stream concavity index than were previously evaluated.

References Cited

- Bull, W.B., and McFadden, L.D., 1977, Tectonic geomorphology north and south of the Garlock fault, California, in, Doehring, D.O., ed., *Geomorphology in Arid Regions; Proceeding of the 8th annual Geomorphology Symposium*, Bingham, NY, p. 115-138
- Denny, C.S., 1965 *Alluvial fans in the Death Valley region, California and Nevada: U S Geological Survey Professional Paper 466*, 62 p..
- Knott, R. J. , 1998, *Late Cenozoic, stratigraphy, geomorphology, and neotectonics of the western Black Mountains Piedmont, Death Valley, California: Implications for the spatial and temporal evolution of the Death Valley Fault Zone: Ph.D. Dissertation, University of California Riverside*, 406, p.

The Salton Basin Living Laboratory— a science and social studies curriculum for 4th through 6th grade students in the Imperial Valley

Pat Flanagan

Grass Roots Educators, Author and Project Designer

It is well-documented that children build their lifelong love of the land and the active stewardship of it through experiences in nature. This prompted the Desert Protective Council (DPC) to provide geology and natural history field trips for Imperial Valley California elementary school students. These excursions were popular and after a couple of years DPC decided to support development of science curriculum and provide teacher training to help students think like scientists before going out to explore their desert home like naturalists.

Students in the Salton Basin inhabit a living laboratory with active geology, badlands and fossil beds, geothermal fields, and the largest lake—the Salton Sea—in California, with a maximum depth of 227 feet below sea level. With habitats including the sea, the valley agricultural fields, and the twisting riparian New and Alamo Rivers, 400 species of birds call the area home for some part of the year. The Salton Basin is in the hottest, driest part of California and contains the largest year-round irrigated agricultural area in North America. It is a land of contradictions—a basin full of superlatives.

The Salton Basin Living Laboratory is a science curriculum that supports 4th through 6th grade science standards. Students are shown how to explore the ecology of their environment in an interactive way that triggers insight and discovery. They use the unique EcoMap to visualize the feedback between the living and non-living ecosystem elements. All the elements are defined and referenced to the Colorado Desert and the Salton Basin, grounding students in the geography and natural history of their home.

Field trips include day long explorations to the New River Wetlands (4th grade), the Anza Borrego Desert State Park (5th grade), and the Salton Sea (6th grade). As part of their classroom and field explorations students also learn about the early explorers to the region, including Juan Bautista de Anza (1776), the Williamson Expedition of the Pacific Railroad Survey (1853), and Godfrey Sykes (1891-1935). The maps, diaries, and reports of these explorers and scientists help develop the human story in the Imperial Valley.

A PowerPoint presentation will explain the program and a poster presentation will display the materials that students use in the classroom and in the field.

Implications of adding a fossil record to ecologically endangered/threatened fish species: The deep history of tui/arroyo chubs (*Siphateles mohavensis*, *S. bicolor snyderi*, and *S. bicolor orcutti*) of the Mojave and southwestern Great Basin, eastern California, USA

W. BrittLeatham¹ and Debbie A. Kunath².

¹ *bleatham@csusb.edu. Departments of Geological Sciences and Science, Math, Technology Education, CSU San Bernardino.*

² *debbie_kunath@ymail.com*

Discovery and analysis of fossil fish remains from several localities in eastern California indicates that endangered/threatened (ET) tui/arroyo chub species (i.e. *Siphateles mohavensis*, *S. bicolor snyderi*, and *S. bicolor orcutti*) may have a significant paleontological history. Fossil specimens of *S. bicolor* have been recovered from Pliocene lacustrine limestone of the Coso Formation near Haiwee Reservoir on the western flanks of the Coso Range, southern Owens Valley. Potassium-argon dating of tuff (Bacon and others, 1982) stratigraphically above the fossil horizon suggests that chub species were present in aquatic ecosystems of the region soon after development of the aquatic isolation of the western Great Basin and Mojave provinces, definitively no younger than 3.0 Ma. Fossil *S. mohavensis* pharyngeal teeth recovered from a gravel quarry on the northwestern flank of Silver Lake, north of Baker, California, occur in unionid bivalve/gastropod/ostracode-rich siliciclastics associated with tufa-coated boulders and cobbles. Those specimens based on carbon-dated bivalves are Pleistocene/Holocene, i.e. no older than 13.7 Ka and no younger than 8.3 Ka (Wells and others, 2003). Additionally, isolated bones of *S. mohavensis* from Pleistocene Lake Manix beds reported by Smith and others (2002), as well as bones assignable to *S. mohavensis?* have been reported from several Lake Mojave drainages (Reynolds and Reynolds, 1985; Roeder, 1985; Jefferson, 1985). Based on those occurrences, at the provincial scale, the fossil record closely mimics the modern distribution of extant chub species. Furthermore, fossil occurrences suggest that chub niches and associated aquatic ecosystems have been comparatively stable within the past 3.0 Ma of fluctuating regional climate patterns affecting this area, and that chub species have profoundly survived in this time-averaged environment. Conservation efforts to mitigate survival and to produce sustainable populations of ET chub may benefit from enhanced paleoecologic study of aquatic conditions recorded in deposits containing fossil chubs.

Color and Light in Nature

David K. Lynch

Thule Scientific

What is a rainbow? How many are there? Why is the sky blue? Why is the setting sun red and flattened? What is a mirage? Why are there rays or spokes coming from the setting sun? What is the green flash? Can it be photographed? Why does the moon look so big on the horizon? Why do stars twinkle? What is an aurora borealis? Is it really darkest before dawn? Why are wet spots dark? What is that ring around the Sun? Why can water appear so many different colors? These and dozens of other questions about naturally occurring optical effects are explained with pictures and diagrams, along with tips on how to see and photograph them.

Depositional environment of the Pliocene Bouse Formation at Amboy, California, and tectonic implications

D.M. Miller,¹ R.E. Reynolds,² J. Bright,³ and S.W. Starratt¹

¹U.S Geological Survey, 345 Middlefield Road, Menlo Park CA 94025 (dmiller@usgs.gov)

²220 South Buena Vista St, Redlands, CA, 92373

³Dept. of Geosciences, University of Arizona, 1040 E 4th St, Tucson, AZ 85721

Limestone beds bracketed by alluvial fan gravels near Amboy, California, are correlated to the Pliocene Bouse Formation on the basis of lithology and age (Lawlor Tuff, 4.83 Ma), indicating that a large arm of the Bouse water body extended across part of the southern Mojave Desert. The deposits consist of white, distinctly bedded, limestone and calcareous sandstone as well as stromatolitic "tufa" mounds. The Bouse beds exposed near Amboy contain ostracodes, diatoms, and trace fossils that indicate saline lake or estuarine environments. The spine of an atherinid fish, possibly *Colpichthys*, indicates marine conditions during the deposition of lower part of the sequence. The limestone crops out at an elevation of 290 m, and dips ~20° southward toward Bristol dry lake, where similar age sediments are known in boreholes at depths below sea level (elev. -157 m). These relations indicate significant faulting and folding in this part of the Eastern California Shear Zone during the last few million years. Confirmation of the Bouse Formation near Amboy and other identifications of ancient waterlain deposits in the Bristol arm of the Bouse water body indicate a much greater surface area for the water body than has been assumed previously. The Bristol arm northwest of the Kilbeck Hills had an area of about 2000 km², which increases the area of the Bouse

water body by about 25%. This area would have large evaporative yield, and probably could not be supported as a terminal lake that was fed by the ancestral Colorado River. This conclusion along with the fish bone lead us to argue that the Bouse beds represent estuarine deposits. A marine origin for the water body requires significant Pliocene and Quaternary tectonic adjustments of the southeastern Mojave Desert, because the Bouse deposits are found at depths well below sea level and also draped on the flanks of mountains as high as 330 m elevation. Rise in Pliocene sea level was less than 50 meters, and alone cannot account for this distribution of the Bouse. The Bouse estuarine embayment may have been aided by climatic factors, but the primary cause of Bouse sediment covering diverse topography is tectonic folding and uplift of much of the region since the early Pliocene.

Discovery of dinosaur tracks and arthropod tracks in the Aztec Sandstone (Lower Jurassic), Red Rock Canyon National Conservation Area, Las Vegas, Nevada

Stephen M. Rowland,¹ Marvin (Nick) Saines,² and Heather Stoller¹

¹Department of Geoscience, University of Nevada, Las Vegas, Las Vegas, NV 89154-4010, steve.rowland@unlv.edu, stollerh@unlv.nevada.edu

²Red Rock Canyon Interpretive Association, HCR Box 5500, Las Vegas, NV 89161, nicksaines@rrcia.com

Tracks of dinosaurs and other animals are well known in the Lower Jurassic Navajo Sandstone of Utah, and a diverse assemblage of dinosaur and synapsid tracks is also known from the correlative Aztec Sandstone in the Mescal Range of eastern California. Curiously, however, such tracks have not been reported in the Aztec Sandstone of Southern Nevada—until now. Tracks of dinosaurs and arthropods were recently discovered in the Aztec Sandstone in the Red Rock Canyon National Conservation Area (RRCNCA), twenty miles west of Las Vegas. This is the first documented occurrence of dinosaur tracks in the state of Nevada.

The newly discovered dinosaur tracks have been tentatively assigned to the ichnogenus *Grallator*, the trackmaker of which was a small, bipedal, carnivorous, theropod dinosaur. Occurring on a different bedding plane is a distinctive trackway that we assign to the well-known Permian and Mesozoic ichnogenus *Octopodichnus*, which is generally interpreted to be the track of a large arachnid. A third type of track, apparently made by a small quadruped, does not match any previously described Mesozoic ichnogenus.

The Aztec/Navajo Sandstone was deposited as sand dunes and interdune basins in a vast, low-latitude,

Pangaeian desert that stretched from eastern California through southern Nevada, northern Arizona, Utah, and into the Rocky Mountain States. The climate was monsoonal, with distinct wet and dry seasons. Detailed analysis of the newly discovered tracks is just beginning, but our working hypothesis is that the tracks were formed when animals stepped into sand that was moist after a rain. One especially-well-preserved dinosaur track displays concentric rings around it; we interpret these to be differential compaction rings that formed when the dinosaur stepped in moist sand. The tracks occur most commonly on desert-varnished bedding planes. The varnish helps protect the exposed layers of sandstone from rapid erosion.

If runoff in a small wash is cut off in the desert, do the plants feel it?

Darren R. Sandquist,¹ David R. Bedford,² Miguel Macias,¹ David M. Miller,² April R. Newlander,¹ and Susan Schwinning³

¹*Department of Biological Science, California State University, Fullerton, 800 N State College Blvd, Fullerton, CA 92834*

²*U.S. Geological Survey, 345 Middlefield Road, MS-973, Menlo Park, CA 94025*

³*Biology Department, Texas State University, San Marcos, TX*

Small washes and channels create a complex hydrological network across desert bajadas, but represent only a small proportion of the bajada's spatial area and are usually devoid of vegetation. Nonetheless, these channels may be the most important geomorphic feature influencing local vegetation properties and processes. We examined the functional influence of small channels on the vegetation of a Mojave Desert bajada by conducting a series of studies that contrast an undisturbed area versus that influenced by a ~100 year old linear disturbance (railroad and parallel road). In areas below the disturbance, where flow has been either increased due to channel coalescence into culverts, or cut off due to diversion, plant community structure and cover has changed relative to the undisturbed area. Plant physiological responses to simulated runoff experiments, conducted in active (undisturbed) and inactive (cut-off) channels, revealed subtle but consistent differences that, when compounded through time, are likely to contribute to changes in vegetation. In both channel types, creosote bush (*Larrea tridentata*) within 3 m of a channel, and white bursage (*Ambrosia dumosa*) within 2 m of the channel had access water from the channel, however, the pulse responses were less pronounced, shorter in duration and more variable for plants adjacent to inactive channels than for those near active channels. Stomatal conductance and sap-flow measurements on *Larrea* corroborated these findings, suggesting that root patterns and functions

associated with channels are altered when water flow is reduced or eliminated over extended periods of time. These findings indicate that disturbance of small desert washes can lead to vegetation shifts through time with consequences that are not yet fully realized. Small desert washes may represent a minor spatial component of the vast bajada landscape, but runoff and higher infiltration rates, coupled with the breadth of their spatial influence on adjacent plants, suggests that these modest geomorphic features may have a disproportionate impact on plant function and community properties in arid ecosystems.

Pebble counts from the Pliocene Furnace Creek Formation, Death Valley, California

Coral Shaw

Department of Geological Sciences, California State University, Fullerton

The upper Furnace Creek Formation crops out in the modern Furnace Creek basin between the Funeral Mountains to the north, composed mainly of Paleozoic sedimentary rocks, and the Black Mountains to the south, composed mainly of Tertiary volcanic and sedimentary rocks. The source of sediments in the 4.18~3.22 Ma upper Furnace Creek Formation is not clearly understood because previous studies did not have the benefit of geochronology. I counted clasts in a measured section of the upper Furnace Creek Formation to determine clast provenance. Understanding the clast provenance is important because it may give insight into the uplift of the surrounding mountains. I counted clasts at three locations in the Furnace Creek Formation in the Zabriskie Wash in Death Valley, California, which is closer to the Black Mountains. I found an accessible surface and divided the clasts located there into Sedimentary Clasts, Volcanic Clasts and Granitoid Clasts, but also noted the specific types of clasts in those three groups. I counted at least 100 assorted-size clasts at each location and recorded the rock type. There is a change in the percentage of volcanic clasts from 57-58% in the Lower Furnace Creek Formation to 80% volcanic in the overlying Funeral Formation. I interpret this to suggest a period of uplift of the volcanic terrain of the Black Mountains.

Tortoise time: lessons learned in three decades with *Gopherus agassizii*

Tim Shields

P.O. Box 362, Haines, AK 99827, herpetologic@gmail.com

Gopherus is a genus of tortoise that has been successful in the Mojave Desert for 15 million years. *Gopherus agassizii*, the Pleistocene and recent species from the Mojave

Desert, is now a federally listed threatened species. Thirty years of field research on aspects of biology and ecology show populations of the species have declined between 90 and 95%. Numerous facets of the ecological collision between humans and the desert tortoise are described—the constellation of anthropogenic effects has resulted in the steep declines seen since the 1970s. Implications of the near disappearance of the desert tortoise will be discussed as will the author's prescription for addressing the continuing decline of the species.

Clast composition of Cenozoic deposits on the west flank of the Last Chance Range, Death Valley National Park, CA

Eric Smith

Department of Geological Sciences, California State University, Fullerton

Eureka Valley gives potential evidence of a biologically and geologically unique situation. This is because it is hypothesized as a pathway for the dispersal of pupfish between 6 and 3 million years ago. By describing the sedimentary deposits in the Last Chance Range, I will test whether the Owens River ran through Eureka Valley during this time period. By describing and noting the type of clasts found in the sedimentary deposits, I will test the direction of flow through Eureka Valley 6-3 million years ago. If the study area only show clasts found in the immediate area, it can be inferred that drainage was only local for the time period. But if the sedimentary rocks in the study area show evidence of granitic clast which are not found in the area, it can be inferred that they were transported some distance; perhaps by the Owens River into Eureka Valley. By studying the clast type, clast angularity and imbrication of the clasts within the rocks in the study area, we can provide evidence that shows flow of water through Eureka Valley from 6-3 million years ago. This is significant because flow of the Owens River through Eureka Valley could help to explain the dispersal of pupfish as well as the uplift rate of the Last Chance Range.

Fossil vertebrate tracks and associated sedimentary structures of Death Valley National Park: a Cenozoic record of animal activity within lacustrine systems

Rod Spencer¹ and Torrey Nyborg²

¹*PMB 25, PO Box 5011 Ferndale, WA 98248*

²*Department of Earth and Biological Sciences, Loma Linda University, Loma Linda, CA, 92350, tnyborg06g@llu.edu*

Fossil mammal and bird tracks are numerous within Cenozoic lacustrine deposits of Death Valley. Documentation and an understanding of track abundance/distribution and potential trackmaker have been limited in the past. There are four main track sites within Death Valley National Park: within the Copper Canyon Formation; an unnamed formation at Salt Creek; an unnamed formation near Cow Creek; and at Twenty Mule Canyon within the Funeral Formation. The Copper Canyon track site is the only site that has seen limited research. Ongoing work at the other localities is revealing a much large track record covering much of the Neogene. The depositional environment for all of the localities appears to be a quiet lake margin mudflat that has undergone sheetwash and post-sheetwash deposition. Sheetwash deposition within the mudflat depositional environment is recorded as planar bedding, ripple marks, and soft sediment deformation structures. A typical sequence deposited on the mudflat consists of an upward set of beds: planar laminated sandstone and siltstone, ripple cross-laminated siltstone (showing undulatory and linguoid ripple marks on bedding surfaces), and finally symmetrical or wave ripple cross-lamination and bedding features. Soft sediment deformation (load structures) are common. Load structures occur both as load casts and flame structures. These structures form in response to unstable density contrasts (density loading) or lateral variations in load (uneven loading) when sediment becomes liquidized at the time of deposition or shortly after, during the first stages of the sediments consolidation. In this case, soft sediment deformation indicates denser material, like sand, transported onto the mudflat during sheetwash storm events. Post-sheetwash deposition record a regressive, subaerial exposure phase of the lake margin. Many of the bed surfaces exhibit animal tracks, raindrop impressions, and mudcracks. Preservation of these features indicates: subaerial exposure of the mudflat environment that is saturated with water; followed by a period of drying/evaporation; and subsequent burial by overlying sediments (sheetwash deposits). Limestone beds (interpreted as spring deposits) are numerous within the Copper Canyon Formation but are lacking at the other track localities. Their preservation is consistent with rapid deposition of mudstone/siltstone by sheetwash, probably within hours to days of raindrop formation. The Copper Canyon Formation has twenty-six ichnospecies of cat, camel, horse, mastodon, and bird tracks that have been identified from 60+ localities. The Salt Creek and Twenty Mule Canyon localities are limited to only a few outcrops. The Cow Creek locality was previously believed to also be a limited outcrop however recent work in the area has revealed a track record similar to the Copper Canyon Formation. Mammal and bird tracks of Death Valley are abundant and distributed over a large area representing one of the worlds' best record for Neogene animal tracks.

Quantification of the old highway erosion between Desolation Canyon and the Village Fan, Death Valley, CA

Leonor Thomas

CSUF Dept of Geology; Leonor@csu.fullerton.edu

In the 1960s, Charles Hunt of the U.S. Geological Survey made qualitative observations of the erosion of abandoned roads, trails and other features. From one-half mile north of Golden Canyon south to Desolation Canyon he estimated that 27% of the road had eroded in the 20 years since the road was abandoned. I am revisiting this stretch of abandoned road to document the amount of erosion. I am using a GPS, Google Earth images, and photography. My initial findings are that 75% of the road has been destroyed in the last ~50 years. The greatest amount of destruction is the northernmost portion of the old road. The least amount of destruction is the southernmost portion of the old road. Erosion rates in arid lands are very slow and alluvial fans are frequently thought to have isolated active and inactive areas. This study shows that the majority of the alluvial-fan area is active. I interpret the greater destruction of the northern area to the man-made divergence of Furnace Creek into Gower Gulch.

— NOTES —